

Supporting information for

Light-Driven Reduction of Aromatic Olefins in Aqueous Media Catalyzed by Aminopyridine Cobalt Complexes.

Carla Casadevall,¹ David Pascual,¹ Jordi Aragón,¹ Arnau Call,¹ Alicia Casitas,¹ Irene Casademont-Reig,² and Julio Lloret-Fillol^{1,3*}

¹Institute of Chemical Research of Catalonia (ICIQ), The Barcelona Institute of Science and Technology, Avinguda Països Catalans 16, 43007 Tarragona, Spain.

²Donostia International Physics Center (DIPC) Donostia, Euskadi, Spain. Polimero eta Material Aurreratuak: Fisika, Kimika eta Teknologia, Kimika Fakultatea, Euskal Herriko Unibertsitatea UPV/EHU P.K. 1072, 20080 Donostia, Euskadi, Spain.

³Catalan Institution for Research and Advanced Studies (ICREA), Passeig Lluís Companys, 23, 08010, Barcelona, Spain.

Corresponding author: jlloret@iciq.es

Table of Contents

1. Materials and Reagents	3
2. Instrumentation.....	3
3. Experimental Procedures	5
4. Electrochemistry of selected Co catalysts.....	7
5. Synthesis of ligands and iridium and copper PC and characterization	8
6. Synthesis of substrates.....	221
7. Control experiments in the photoreduction of styrene (16)	24
8. Screening of photoredox catalysts and cobalt catalysts in the reduction of styrene (16) to ethylbenzene (16a).....	27
9. Effect of the temperature in the photoreduction of styrene (16) and α -methylstyrene (28) to ethylbenzene (16a) and cumene (28a) respectively.	31
10. Optimization of aromatic 1,1-disubstituted olefins	332
11. Catalytic assays of the photoreduction of aromatic 1,2-disubstituted olefins	33
12. Oxygen tolerance	36
13. Mechanistic experiments	36
14. Selectivity: competition experiments.....	36
15. Computational studies of the reduction potential of selected aromatic olefins.....	47
16. NMR full characterization of the deuterium labelling mechanistic studies	50
17. NMR of the radical clock ring-opening products	66
18. NMR spectra of synthesized substrates and isolated products.....	71
19. NMR data of the isolated products	113
20. Selected chromatograms for the reduction reactions.....	116
21. References.....	121

EXPERIMENTAL SECTION

1. Materials and Reagents

Reagents and solvents were purchased from commercial sources and used as received unless otherwise stated. Triethylamine and di-isopropylethylamine were distilled over potassium hydroxide and stored under argon. Ascorbic acid (AscH) ($\geq 99\%$) was purchased from Sigma-Aldrich® and used without further purification. Photoredox catalyst [Cu(bathocuproine)(Xantphos)](PF₆) (**PC_{Cu}**),^[1] and [Ir(ppy)₂(bpy)](PF₆) (**HPC_{Ir}**),^[2] and complexes [Co(OTf)(Py₂Tstacn)](OTf) (1)^[3] and [Co(OTf)₂(TPA)] (6),^[4] and ligands N4Py,^[5] DPA-Bpy,^[6] BpcMe,^[7] H-CDPy3^[8] and (S,S)-PDP^[8] were synthesized according to the literature procedures. Photoredox catalysts [Ir(ppy)₂(dmab)](PF₆) (**NMe₂PC_{Ir}**) and [Ir(ppy)₂(dcbpy)](PF₆) (**CO₂HPC_{Ir}**) were synthesized from a modified procedure from the literature.^[9] Anhydrous acetonitrile was purchased from Sigma-Aldrich® Water (18.2 MΩ·cm) was purified with a Milli-Q Millipore Gradient AIS system. All solvents were degassed by the freeze-pump-thaw method and stored under argon.

2. Instrumentation

Nuclear magnetic resonance (NMR). NMR spectra were recorded on Bruker Fourier300, AV400, AV500 and AVIII500 spectrometers using standard conditions (300 K). All ¹H chemical shifts are reported in ppm and have been internally calibrated to the residual protons of the deuterated solvent. The ¹³C chemical shifts have been internally calibrated to the carbon atoms of the deuterated solvent. The coupling constants were measured in Hz.

Microanalyses. Elemental analyses were performed using a CHNS-O EA-1108 elemental analyzer from Fisons. Mass Spectrometry. Electrospray ionization mass spectrometry (ESI-MS) experiments were performed on a Bruker Daltonics Esquire 3000 Spectrometer using a 1 mM solution of the analysed compound, by introducing the sample directly into the ESI-source using a syringe.

Mass Spectrometry. Electrospray ionization mass spectrometry (ESI-MS) experiments were performed on a Bruker Daltonics Esquire 3000 Spectrometer using a 1 mM solution of the analyzed compound, by introducing the sample directly into the ESI-source using a syringe. High resolution mass spectra (HRMS) were recorded on a Bruker MicroTOF-Q IITM instrument with an ESI source at Serveis Tècnics of the University of Girona. Samples were introduced into the mass spectrometer ion source by direct infusion through a syringe pump and were externally calibrated using sodium formate.

Electrochemistry. All the electrochemical experiments were performed with a VSP potentiostat from BioLogic, equipped of the EC-Lab software. CV measurements were carried out under Ar atmosphere by using 1 mM solutions of cobalt complexes or Ir photoredox catalysts in CH₃CN, with tetrabutylammonium tetrfluoroaborate (TBAPF₆) as supporting electrolyte (0.1 M). A single-compartment cell was employed, with glassy carbon (GC) working electrodes (3 mm and 1 mm diameter). Additionally, a Pt wire was used as a counter electrode and a Ag/AgCl wire as pseudo-reference, immersed in a bridge tube containing the same electrolyte solution (0.1 M TBAPF₆/CH₃CN) and separated from the working solution by a porous tip. Ferrocene (Fc) was added to the solution as an internal standard and all the potentials are first referenced vs. the Fc⁺⁰ redox couple and then vs. SCE. The working electrodes were polished by using 0.05 μm alumina powder (CHI Instruments) on a polishing pad wet with distilled H₂O, followed by rinsing with distilled water/acetone and sonication to remove the residues of alumina over the electrode.

UV-Vis spectroscopy. UV-vis spectra were recorded on an Agilent 8453 diode array spectrophotometer (190-1100 nm range) in 1 cm quartz cells. A cryostat from Unisoku Scientific Instruments was used for the temperature control.

Fluorescence spectroscopy. Fluorescence measurements were carried out on a Fluorolog Horiba Jobin Yvon spectrofluorimeter equipped with photomultiplier [or InGaAs if using the nitrogen cooled detector] detector, double monochromator and Xenon light source. Sample preparation was same as that of absorption experiments in 1 cm quartz cells.

Gas chromatography analysis. The analysis and quantification of the starting materials and products were carried out on an Agilent 7820A gas chromatograph (HP5 column, 30m or Cyclosil-B column, 30m) and a flame ionization detector. The enantioselectivity was determined by comparison with the pure samples synthesized by the reported procedures.^[10]

Gas chromatography – mass spectrometry (GC-MS). GC-MS spectral analyses were performed on an Agilent 7890A gas chromatograph interfaced with an Agilent 5975c MS mass spectrometer.

Parallel Pressure Transducer Hardware. The parallel pressure transducer sensors that we used for these studies is the same that was previously reported for the water oxidation studies in our group.^[11] This is composed by 8 differential pressure transducers (Honeywell-ASCX15DN, ± 15 psi) connected to a hardware data-acquisition system (base on Atmega microcontroller) controlled by a home-developed software program. The differential pressure transducer Honeywell-ASCX15DN is a 100 microseconds response, signal-conditioned (high level span, 4.5 V) output, calibrated and temperature compensated (0 °C to 70 °C) sensor. The differential sensor has two sensing ports that can be used for differential pressure measurements. The pressure calibrated devices to within ± 0.5 matm was offset and span calibrated *via* software with a high precision pressure transducer (PX409-030GUSB, 0.08 % Accuracy). Each of the 8 differential pressure transducers (Honeywell-ASCX15DN, ± 15 psi) produce voltage outputs that can be directly transformed to a pressure difference between the two measuring ports. The voltage outputs were digitalized with a resolution of 0.25 matm from 0 to 175 matm and 1 matm from 176 to 1000 matm using an Atmega microcontroller with an independent voltage auto-calibration. Firmware Atmega microcontroller and control software were home-developed. The sensitivity of H₂ analytics allows for quantification of the gas formed when low H₂ volumes are generated. However, it could not be discarded that small amount of H₂ were produced by inactive complexes.

Gas chromatography identification and quantification of gases. Gases at the headspace were analyzed with an Agilent 7820A GC System equipped with columns Washed Molecular Sieve 5A, 2m x 1/8" OD, Mesh 60/80 SS and Porapak Q, 4m x 1/8" OD, SS. Mesh: 80/100 SS and a Thermal Conductivity Detector. The quantification of the H₂ obtained was measured through the interpolation of a previous calibration using different H₂/N₂ mixtures.

In-house developed parallel photoreactor:

An in-house developed parallel blue LED ($\lambda = 447 \pm 20$ nm, 1030 mW @ 700mA) photoreactor with 25 equivalent positions was used to perform the photocatalytic reactions, allowing for strict reaction temperature control by a high precision thermoregulation Hubber K6 cryostat (more information reported elsewhere).^[12] The reactor is made of two modules - a reaction module and an irradiation module – which are independently maintained at constant temperature thanks to independent liquid circuits enabling the heating/cooling of the reaction module and the cooling of the irradiation module. The modules consist of anodized aluminum blocks and are separated by a thermal insulating layer. The photoreactor is typically powered with a power supply of 80 V and current of 0.7 A (2.1 W per LED). Light intensity can be easily change by modifying the current. The LEDs are fixed onto five different printed circuits (one for each row) all connected in series. Actinometry in combination with photodiode measurements were used to measure the quantity of photons at given electrical current source.^[12-14]



Figure S. 1. In-house developed parallel photoreactor.

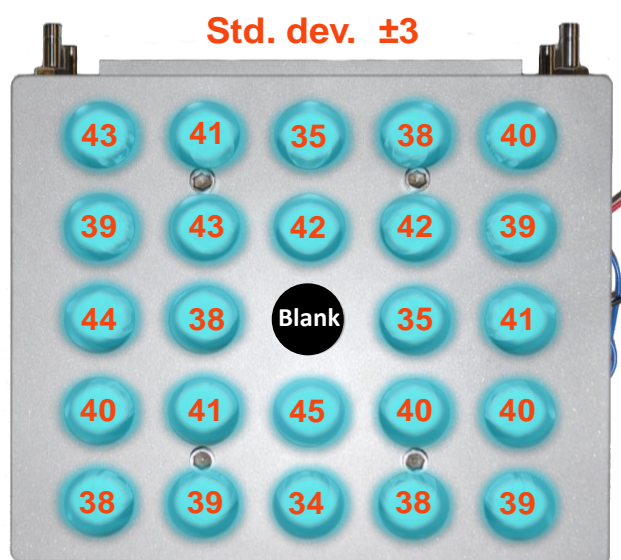
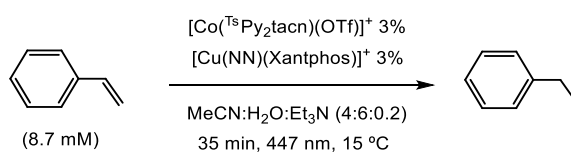


Figure S. 2. Reproducibility test at short reaction time of the 25-well photoreactor in the photoreduction of styrene (**16**) as model substrate. The reaction was stopped after only 35 min to better test the dispersion in speed of the reaction depending of the position in the photoreactor. Conditions A: Co-Cat (261 μM , 3% mol), **PC**_{Cu} (261 μM , 3% mol), **16** (8.7 mM) in H₂O:CH₃CN:Et₃N (6:4:0.2 mL) irradiation (447 nm) for 35 min at 15 °C under N₂. Yields determined by GC analysis after workup relative to a calibrated internal standard. Values were average of triplicates. Values are ethylbenzene (**16a**) GC-FID yields.

3. Experimental Procedures

General procedure employed in reaction screening conditions for the light-driven reduction of monosubstituted aromatic alkenes (16-27). All catalytic reactions were conducted in a 20 mL septum-capped vial under vigorous stirring using an orbital stirrer and irradiating at 447 nm for 5h under nitrogen atmosphere at 15 °C, unless otherwise indicated. Catalytic assays were performed using **PC**_{Cu} as photoredox catalyst (261 μM , 3% mol) in H₂O:CH₃CN:Et₃N (6:4:0.2 mL) reaction solvent mixture, together with the corresponding

substrate (8.7 mM), and complex **1** (261 μ M, 3% mol). After reaction completion, biphenyl was added as internal standard and the crude was quenched by adding 2 mL of AcOEt. The crude was purified by extraction with AcOEt (1 x 3 mL), an aliquote of the organic phase was passed through a plug of MgSO₄ which was eluted with AcOEt. This sample was subjected to GC analysis to determine the conversion of **13a-m** and the yield of the desired product **a-m**. All GC yields reported are an average of at least two runs.

General procedure for the reduction of 1,1-disubstituted aromatic olefins (28-36). All catalytic reactions were conducted in a 20 mL septum-capped vial under vigorous stirring using an orbital stirrer and irradiating at 447 nm for 24h under nitrogen atmosphere at -3 °C, unless otherwise indicated. Catalytic photoreductions were performed in H₂O:CH₃CN:Pr₂EtN (6:4:0.2 mL) reaction solvent mixture, substrate (4.4 mM), **PC_{Cu}** (261 μ M, 6% mol), **1** (261 μ M, 6% mol), unless otherwise indicated. A 447 nm LED was employed as light source. Biphenyl was added as internal standard after the reaction and the reaction was quenched by adding 2 mL of AcOEt. The crude reaction mixtures were purified by extraction with AcOEt (1 x 3 mL), the organic layer was passed through a MgSO₄ plug which was eluted with more AcOEt. The resulting organic solution was subjected to GC analysis to determine the conversion of **15a-h** and the yield of the desired products **16a-h** respectively. All GC yields reported are an average of at least two runs.

General procedure for product isolation. The light-driven photocatalytic reductions of a targeted substrate were carried out under the optimized conditions described above. The crude mixtures of at least 16 independent reactions (equally prepared) for each compound were combined and extracted with CH₂Cl₂ (3 x 40 mL). Organic fractions were combined, dried over MgSO₄ and the solvent removed under reduced pressure. The resulting crude oil was purified by silica gel column chromatography with Hexane/AcOEt (9:1) to obtain the desired reduced product and the isolated yields reported are an average of at least 16 reactions.

Gas-evolution monitoring studies. Each experiment was conducted in a 20 mL volume-calibrated-vial capped with a septum equipped with stir-bars and containing the solvent mixture and reagents. Each reaction vial was connected to one of the ports of a differential pressure transducer sensor (Honeywell-ASCX15DN) and the other port to a reference reaction. Reference reactions, have all components of the reaction except the catalyst. The reaction and reference vials are kept under the same experimental conditions to compensate the noise due to temperature-pressure fluctuations. To ensure a constant and stable irradiation, the LED sources were equipped with a water refrigeration system. This is composed for a refrigerated aluminum block by a Huber cryothermostat (refrigeration system, Minichiller -40°C-20°C). This block is shaken by an Orbital Shaker (IKA KS 260 Basic Package) which provides the agitation of the reaction vessels during the irradiation time. The aluminum block accommodates 16 vials (20 mL) capped with septum in which the reaction takes place. Each vial is submitted and located over a LED irradiation source (Royal-Blue Rebel LEDs ($\lambda = 447 \pm 20$ nm)). The reaction began when the LEDs were turned on. At this point, the hydrogen evolved from the reactions was monitored by recording the increase in pressure of the headspace (1 second interval). The pressure increment is the result of the difference in pressure between the reaction and reference vials. After the hydrogen evolution reached a plateau the amount of the gas formed was measured equilibrating the pressure between reaction and reference vials. The gases at the headspace of the reaction vials and references in each of the reactions were quantified by the analysis of an aliquot of gas at the headspace (0.2 mL) by gas chromatography.

Poisoning studies with Hg⁰. Catalytic reactions were performed in the presence of Hg(0) in a 10 mL septum-capped vials. Each experiment was conducted following the general procedure described above for the light-driven reduction of compounds **16-27**. Hg(0) was added in large excess (>2000 equiv. with respect to catalyst) before starting the reaction by weighting it directly in the reaction vial prior addition of the stock solutions of all the other components. The solution was vigorously stirred for 5 minutes with an orbital stirrer and then the kinetics were performed by irradiating with a LED at 447 nm for 2h. The yield of **16a** was determined at several points during the kinetic study by taking aliquots of the reaction at different times. The LEDs were switched off and a new argon-purged syringe was used to take each aliquot. The yield at each time was determined by GC-FID by the ratio between the area of the substrate and the area of the reduced product.

Kinetic studies under H₂ atmosphere. Catalytic reactions were performed in the presence of H₂ in a 10 mL septum-capped vials. Each experiment was conducted following the general procedure described above for the

light-driven reduction of compounds **16-27**. The reaction vials were then purged with pure H₂ before starting the reaction. Then, kinetic experiments were performed by irradiating with a LED at 447 nm for 2h. The yield of **16a** was determined at several points during the kinetic study by taking aliquots of the reaction at different times. The LEDs were switched off and a new argon-purged syringe was used to take each aliquot. The yield at each time was determined by GC-FID by the ratio between the area of the substrate and the area of the reduced product.

General procedure employed for the deuterium studies with olefins 17, 18, 23, 28, 35 and 41. All catalytic reactions were conducted in a 10 mL septum-capped vial under vigorous stirring using an orbital stirrer and irradiating at 447 nm for 5h under nitrogen atmosphere at 15°C, unless otherwise indicated. At least 16 identical reactions were used for each olefin to be able to isolate the deuterated products and analyse them. Catalytic assays were performed using **PC_{Cu}** as photoredox catalyst (261 μM, 3% mol) in D₂O:CH₃CN:Et₃N (6:4:0.2 mL) reaction solvent mixture, together with the corresponding substrate (8.7 mM), and complex **1** (261 μM, 3% mol). After reaction completion, the crude mixtures of the independent reactions (equally prepared) for each compound were combined and extracted with CH₂Cl₂ (3 x 40 mL). Organic fractions were combined, dried over MgSO₄ and the solvent removed under reduced pressure. The resulting crude oil was purified by silica gel column chromatography with Hexane/AcOEt (9:1) to obtain the desired reduced product and the isolated yields reported as the average of the 16 reactions. Modifications to the standard conditions: i) to obtain deuterated products **[D]-28a** and **[D]-35a** 6 mol % **1** and **PC_{Cu}** (6 mol%), as well as 4.4 mM substrate in D₂O:CH₃CN:Pr₂EtN (6:4:0.2 mL) irradiated (447 nm) for 24 h at -3 °C under N₂ were used; ii) to obtain the deuterated dimeric product **[D]-28b**, standard conditions were used but modifying the substrate concentration to 16 mM and irradiation 5 h at 30 °C; for olefin **41** standard conditions were used changing the substrate concentration down to 4.4 mM and irradiation at 25 °C for 24 h.

4. Electrochemistry of selected Co catalysts

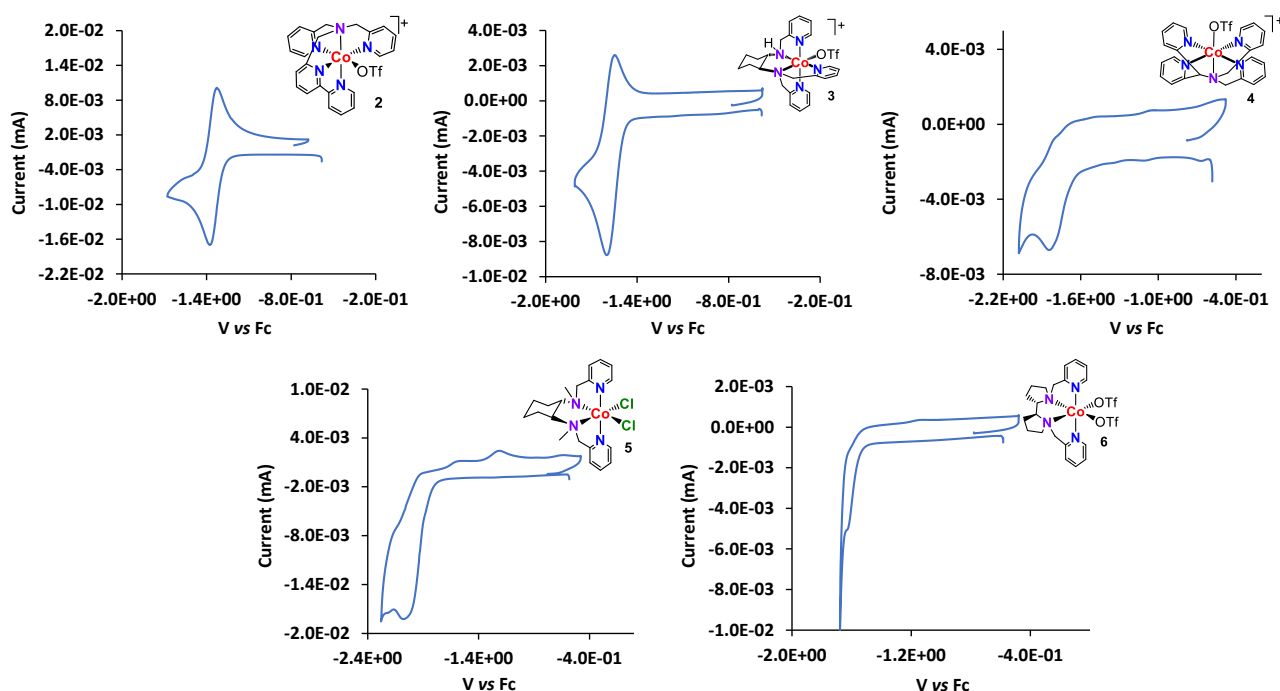


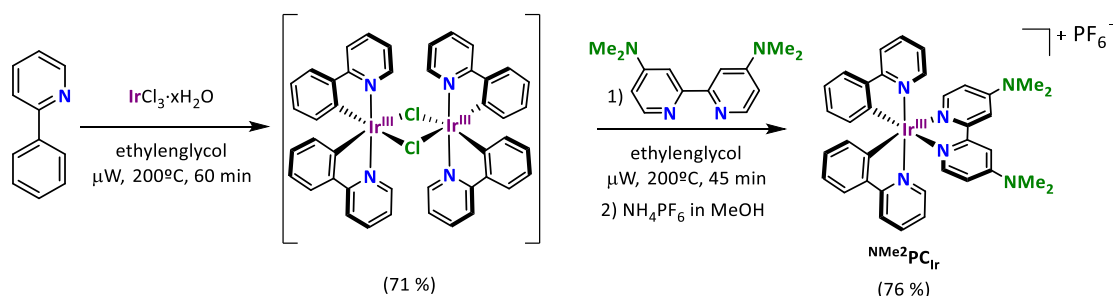
Figure S. 3. Cyclic voltammetry (CV) of cobalt complexes **2, 3, 4, 5** and **6** (1 mM concentration) measured in dry acetonitrile and tetrabutylammonium tetrafluoroborate (TBAPF₆) as supporting electrolyte using a three-electrode configuration under nitrogen atmosphere (see above for set-up details). Scan rate = 100 mV/s, glassy carbon working electrode. Potentials are referenced versus Ferrocene.

5. Synthesis of ligands and iridium and copper PC and characterization

Synthesis of iridium photoredox catalysts and characterization

dmab (2,2'-bipyridine-4,4'-bis(dimethylamino)) ligand was synthesised as previously reported literature.^[9, 15]

Synthesis of [Ir(ppy)₂(dmab)](PF₆), (^{NMe₂}PC_{Ir}). IrCl₃·xH₂O (405 mg, 1.356 mmol), phenylpyridine (1.55 ml, 10.85 mmol, 8eq), and ethylene glycol (15 mL). The reaction mixture was sonicated before microwave irradiation to increase homogeneity of the solution. The reaction was set in the microwave at 200 °C for 60 min. A bright yellow solution with a pale-yellow solid was obtained. Then, **dmab** (493 mg, 2.035 mmol, 1.5 eq) was added and the reaction vessel was set again in the microwave reactor for 45 min at 200 °C at normal power to afford an orange solution. The reaction mixture was cooled to r.t. and diluted with DI H₂O (15 mL) and extracted with DCM (3 × 150 mL) (4 × 150 mL). The organic layers were combined and dried with anhydrous MgSO₄, filtered and the solvent removed in vacuo to afford a yellow solid. The solid was dissolved in some mL of MeOH and, to this concentrated solution, ammonium hexafluorophosphate in MeOH (10.0 g in 100 mL of MeOH) was added. A yellow precipitate rapidly appeared, was filtered and dried to afford ^{NMe₂}PC_{Ir} in 76% yield (0.915 g, 1.03 mmol). ¹H NMR (400 MHz, Acetone-*d*₆) δ 8.19 (d, *J* = 8.1 Hz, 2H), 7.96 – 7.87 (m, 4H), 7.85 (d, *J* = 6.8 Hz, 2H), 7.44 (d, *J* = 6.7 Hz, 2H), 7.20 (t, *J* = 6.6 Hz, 1H), 6.97 (t, *J* = 7.5 Hz, 2H), 6.80 (td, *J* = 7.5 Hz, 2H), 6.73 (dd, *J* = 6.7, 2.8 Hz, 1H), 6.35 (d, *J* = 8.3 Hz, 2H), 3.19 (s, 12H). ¹³C NMR (101 MHz, Acetone-*d*₆) δ 169.18, 156.98, 155.99, 153.72, 149.70, 149.55, 145.15, 138.86, 132.69, 130.93, 125.61, 124.00, 122.55, 120.38, 110.32, 106.61, 39.65. ¹⁹F NMR (376 MHz, Acetone-*d*₆) δ -72.71 (d, *J* = 707.4 Hz). ³²P NMR (162 MHz, Acetone-*d*₆) δ -141.15 (hept, *J* = 707.4 Hz).

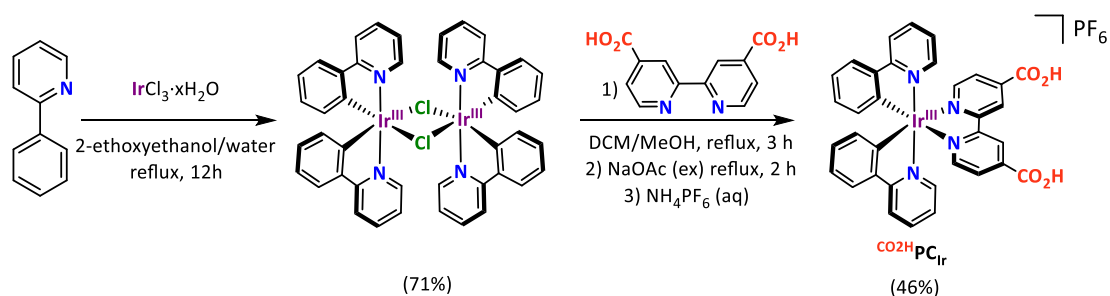


Scheme S. 1. Synthetic route for ^{NMe₂}PC_{Ir}.

Synthesis of [Ir(ppy)₂(dcbpy)](PF₆), (^{CO₂H}PC_{Ir}). This photoredox catalyst was synthesized following a previously modified procedure.^[16] [Ir(ppy)₂(μ-Cl)]₂ (50.0 mg, 0.047 mmol) as a solution in dichloromethane (6 mL) was added to a suspension of 4,4'-dicarboxy-2,2'-bipyridine (22.78 mg, 0.093 mmol) in methanol (6 mL). The reaction mixture was heated to reflux with stirring for 3 h under N₂ atmosphere, and then sodium acetate (excess) in methanol (1.5 mL) was added. The mixture was heated for further 2 h and then cooled to room temperature.

The solvent was removed under reduced pressure, hexafluorophosphoric acid (1 M, 5 mL) was added, and the suspension was stirred for 1 hour. The product was then filtered, washed with water (2 × 10 mL), and extracted into methanol. A saturated solution of ammonium hexafluorophosphate in methanol (2 mL) was added, and the mixture was stirred for further 30 min. The solvent was removed under reduced pressure, and the residue was extracted into dichloromethane and filtered. The mixture was condensed and purified through a short silica path using CH₂Cl₂ for the elution. The solvent was removed under reduced pressure to give iridium [bis(C,N-phenylpyridine)-N,N-4,4'-carboxy-2,2'-bipyridine] hexafluorophosphate as a dark-red powder (39.0 mg, 46%). ¹H-NMR (acetone-*d*₆, 400 MHz, 300 K) δ, ppm: 9.34 (s, 1H), 8.33 (d, 2H, *J* = 5.6 Hz), 8.25 (d, 2H, *J* = 8.0 Hz), 8.17 (dd, 2H, *J* = 5.6, 1.6 Hz), 7.97 (td, 2H, *J* = 7.9, 1.5 Hz), 7.94-7.88 (m, 4H), 7.14 (ddd, 2H, *J* = 7.3, 5.9, 1.4 Hz), 7.06 (td, 2H, *J* = 7.6, 1.2 Hz), 6.94 (td, 2H, *J* = 7.4, 1.3 Hz), 6.34 (dd, 2H, *J* = 7.5, 0.9 Hz). ¹³C{¹H}-NMR

(acetone-d₆, 100.6 MHz, 300 K) δ , ppm: 168.4, 164.8, 157.6, 152.7, 150.6, 150.4, 144.9, 141.6, 139.8, 132.4, 131.4, 129.2, 125.9, 125.6, 124.6, 123.7, 120.9. MS (GC): 745.0 [M].



Scheme S. 2. Synthetic route for $\text{CO}_2\text{HPC}_{\text{Ir}}$.

Mass spectrometry characterization of PC_{Ir} photoredox catalysts

Table S. 1. Measured m/z : 743.2442 for $\text{NMe}_2\text{PC}_{\text{Ir}}$ (expected: 743.2469).

Meas. m/z	Ion Formula	m/z	err [ppm]	err [mDa]	mSigma	e ⁻ Conf	z
741.2433	C36H34N6 ⁺ 191Ir	741.2445	1.7	1.3	547.5	even	1+
	C33H36N5O3 ⁺ 191Ir	741.2419	1.9	-1.4	548.3	odd	1+
743.2441	C36H34N6 ⁺ 193Ir	743.2469	3.8	2.8	2.3	even	1+
	C33H36N5O3 ⁺ 193Ir	743.2442	0.1	-0.1	16.4	odd	1+

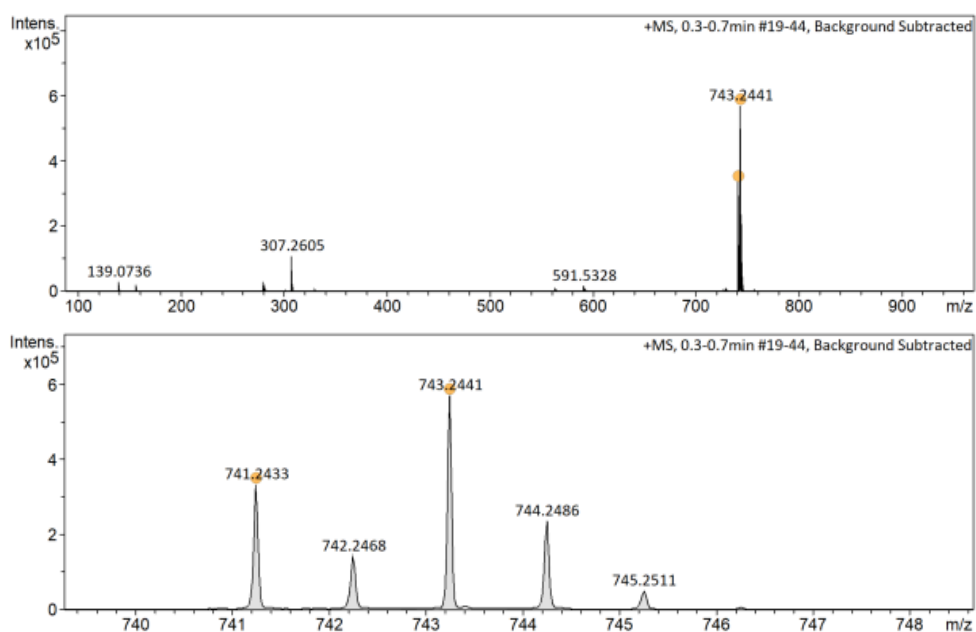


Figure S. 4. HR-MS spectrum (*top*: full range, and *bottom*: zoom in the peak) for complex $\text{NMe}_2\text{PC}_{\text{Ir}}$.

Table S. 2. Measured m/z : 745.1448 for $\text{CO}_2\text{HPC}_{\text{Ir}}$ (expected: 745.1408).

Meas. m/z	Ion Formula	m/z	err [ppm]	err [mDa]	mSigma	e ⁻ Conf	z
743.1393	C34H24N4O4 ⁺ 191Ir	743.1398	0.6	-0.5	550.1	even	1+
	C31H26N3O7 ⁺ 191Ir	743.1371	3.0	-2.2	550.4	odd	1+
	C32H22N7O3 ⁺ 191Ir	743.1385	1.2	-0.9	552.1	odd	1+
745.1435	C32H22N7O3 ⁺ 193Ir	745.1408	3.7	-2.7	1.3	odd	1+
	C34H24N4O4 ⁺ 193Ir	745.1421	1.8	1.4	7.4	even	1+
	C37H22N5O ⁺ 193Ir	745.1448	1.7	1.3	24.9	odd	1+

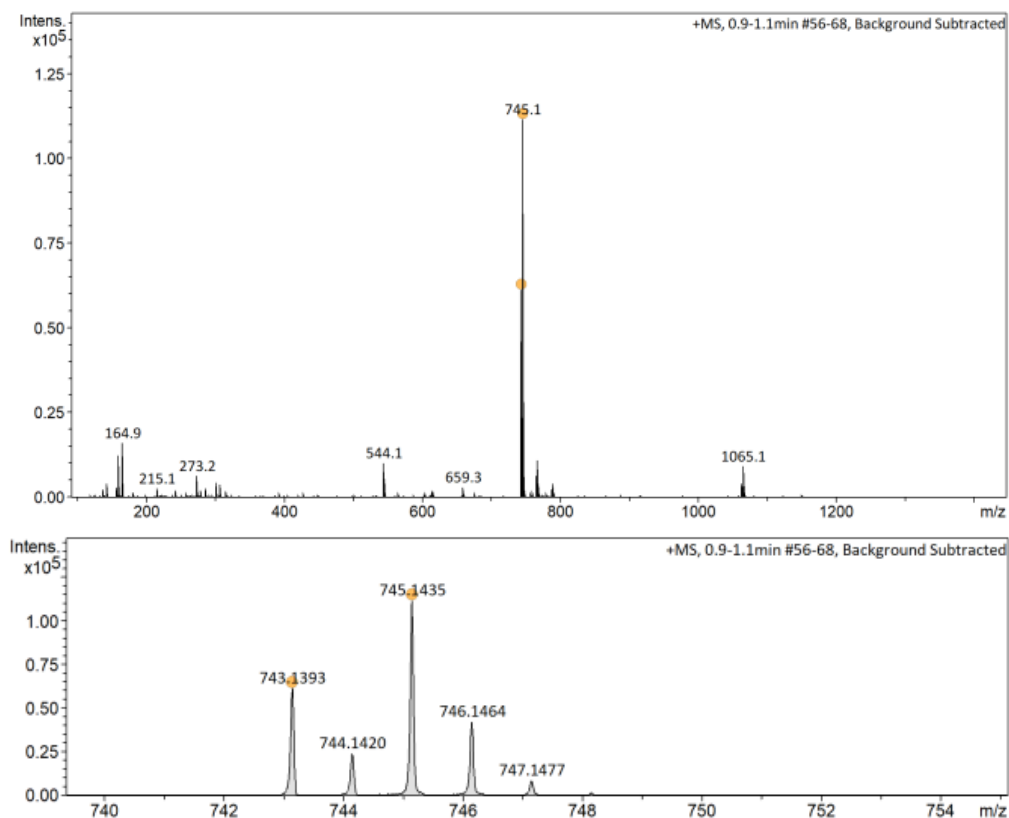


Figure S. 5. HR-MS spectrum (*top*: full range, and *bottom*: zoom in the peak) for complex CO_2HPCIr .

- **Electrochemical characterization of PCIr photoredox catalysts**

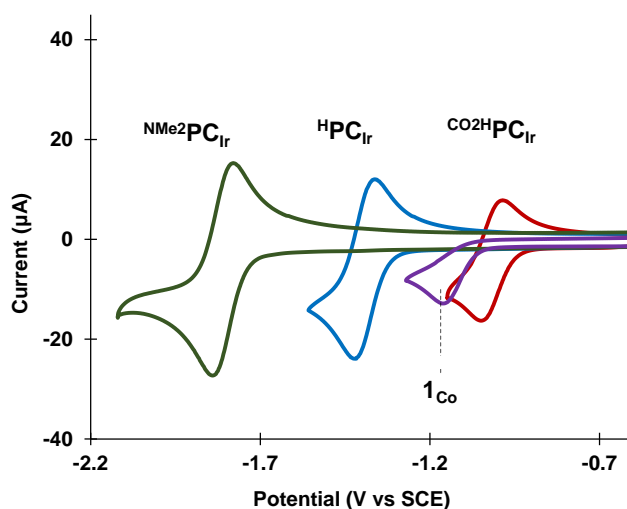


Figure S. 6. Cyclic voltammograms of NMe_2PCIr (1 mM, green), HPCIr (1 mM, blue), CO_2HPCIr (1 mM, red) and **1** (1 mM, purple). CVs were recorded using TBAPF_6 (0.1 M) as a supporting electrolyte in dry acetonitrile. Scan rate = 100 mV/s, glassy carbon working electrode. Potentials are referenced *versus* SCE. $E_{\text{ox}}(\text{NMe}_2\text{PCIr}) = 1.09$ V; $E_{\text{ox}}(\text{HPCIr}) = 1.25$ V; $E_{\text{ox}}(\text{CO}_2\text{HPCIr}) = 1.31$ V; $E_{\text{red}}(\text{NMe}_2\text{PCIr}) = -1.81$ V; $E_{\text{red}}(\text{HPCIr}) = -1.40$ V; $E_{\text{red}}(\text{CO}_2\text{HPCIr}) = -1.01$ V.

Table S. 3. Summary of reduction potentials measured for the PC_{Ir} series and the calculated for the excited state.

	$E^{\circ}(\text{Ir}^{\text{III/II}})$ (V vs SCE)	$E^{\circ}(\text{Ir}^{\text{IV/III}})$ (V vs SCE)	$\lambda_{(E_{00})}$ ^[17-18] (nm)	E_{00} (V vs SCE)	$E^{\circ}(\text{Ir}^{\text{III/II}})$ (V vs SCE)	$E^{\circ}(\text{Ir}^{\text{IV/III}})$ (V vs SCE)
NMe ₂ PC _{Ir}	-1.81	1.09	500	2.48	0.67	-1.39
^H PC _{Ir}	-1.40	1.25	600	2.07	0.67	-0.82
CO ₂ HPC _{Ir}	-1.01	1.31	670	1.85	0.84	-0.54

[17] J. I. Goldsmith, W. R. Hudson, M. S. Lowry, T. H. Anderson, S. Bernhard, *J. Am. Chem. Soc.* **2005**, *127*, 7502;

[18] W. E. Jones Jr.; M. A. Fox *J. Phys. Chem.* **1994**, *98*, 5095.

The energy E_{00} was calculated from Planck's equation: $E_{00} = hv = hc/\lambda$. E_{00} was calculated in Joules taking the Planck constant as $h = 6.62607015 \cdot 10^{-34}$ J·s, the speed of light constant as $c = 2.99792 \cdot 10^{17}$ nm·s⁻¹ and the corresponding wavelength λ in nm. The obtained E_{00} (J) was converted to Volts dividing by the elementary electric charge (electron) in Coulombs ($1.60217733 \cdot 10^{-19}$ C). The value of λ for each complex was taken at the first peak of the emission spectra as an approximation to the 0-0 transition (energy gap between the zeroth vibrational level of the ground and excited states of the PC). The corresponding λ and E_{00} values are included in table S1 in the supporting information.

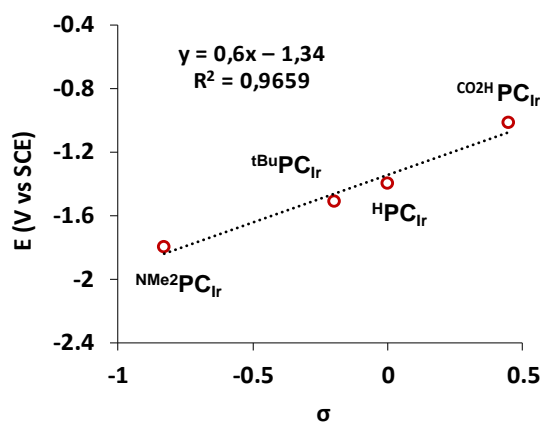


Figure S. 7. Linear correlation of the experimental $E_{1/2}(\text{Ir}^{\text{III/II}})$ vs σ . *the redox potential of ^tBuPC_{Ir} has not been measured but has been taken from literature for comparative reasons.

-Absorption and emission spectra of of PC_{Ir} photoredox catalysts

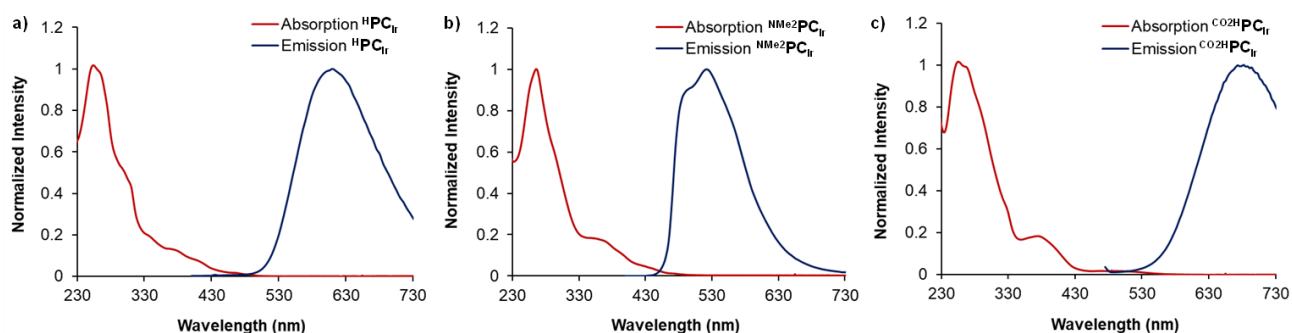


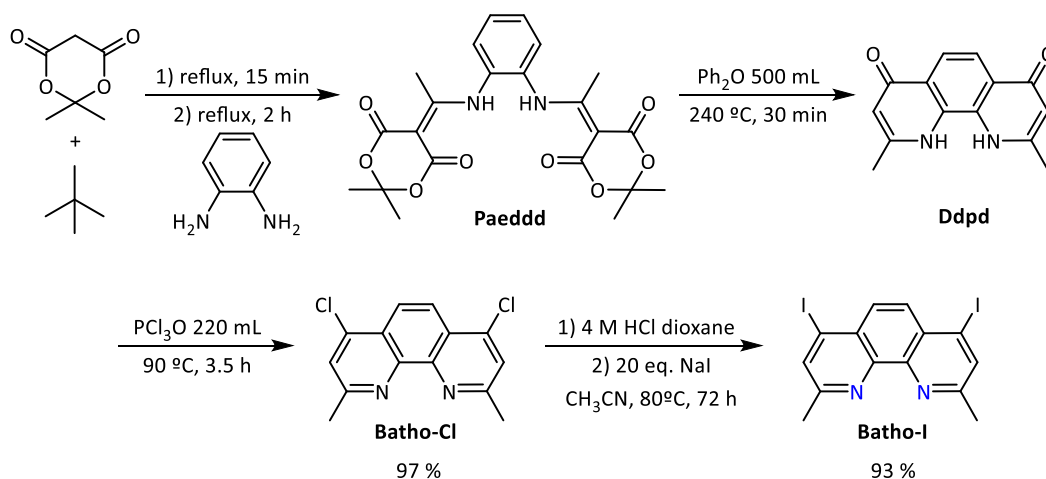
Figure S. 8. Normalized absorption and emission spectra of a) ^HPC_{Ir}, b) NMe₂PC_{Ir}, and c) CO₂HPC_{Ir} at 10 μM concentration in CH₃CN, (V = 2 mL); cell path length = 1 cm; T = 25 $^{\circ}\text{C}$.

- Synthesis of copper photoredox catalysts and characterization

Xantphos, Batho-H and Batho-SO₃⁻ ligands were used as obtain from commercial sources.

Batho-Cl ligand was synthesized according to previously reported procedures following scheme S1.^[19] ¹H-NMR (400 MHz, CDCl₃) δ (ppm): 8.24 (s, 2H), 7.63 (s, 2H), 2.93 (s, 6H).

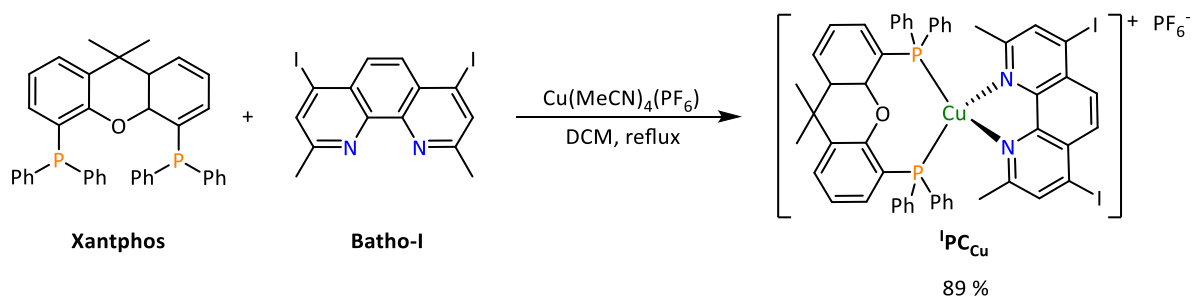
Synthesis of Batho-I ligand: batho-I was synthesized from a modified procedure from literature.^[20] Briefly, batho-Cl (0.15 g, 0.54 mmol) was dissolved in DCM (2 mL). Then, HCl 4M (0.5 mL) in 1,4-dioxane were added and a purple precipitate formed the solution. After 5 min the reaction was cannulated, and the purple precipitate dried under vacuum. Then, the solid was mixed with dried NaI (1.62 g, 20 eq) in anhydrous MeCN (6 mL) and refluxed for 72 h, after which time the reaction had turned yellow. After cooling to rt, NaOH (10%, 5 mL) was added and the crude was extracted with DCM (3 x 30 mL). Organic phases were dried using anhydrous MgSO₄ and the solvent removed under reduced pressure. The oil was purified by silica column chromatography using AcOEt:hexanes:MeOH (16:3:1) mixture and 1 % NH₃ as eluent, obtaining a yellow solid in 93 % yield. ¹H-NMR (400MHz, CDCl₃) δ (ppm): 8.11 (s, 2H), 8.03 (s, 2H), 2.88 (s, 6H).



Scheme S. 3. Synthetic procedure for the synthesis of batho-I ligand.

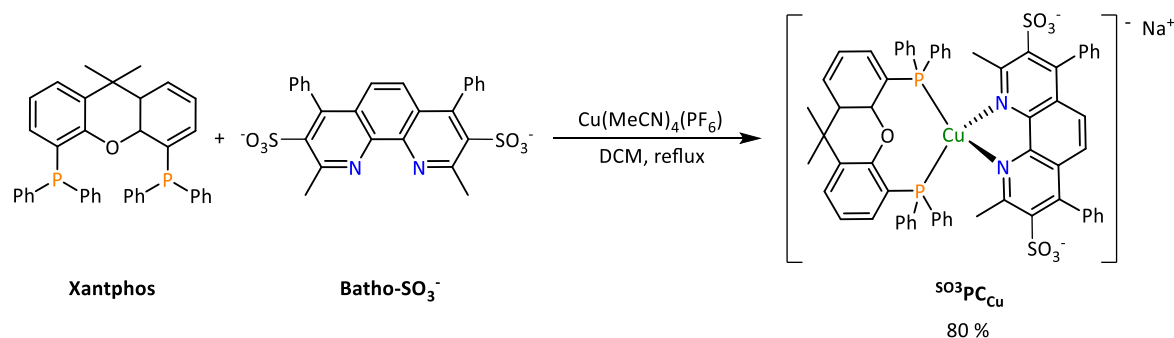
Copper derived photoredox catalysts **PC_{Cu}**, **¹PC_{Cu}** and **^{SO3}PC_{Cu}** were synthesised from a modified procedure from the literature.^[1]

Synthesis of ¹PC_{Cu}: In an oven-dried Schlenk tube, [Cu(MeCN)₄]PF₆ (0.17 g, 0.44 mmol, 1 equiv.) and Xantphos (0.26 g, 0.44 mmol, 1 equiv.) are dissolved in dry DCM (to give a final concentration around 0.05M) at rt. The resulting solution is stirred at reflux overnight. The reaction mixture was then allowed to cool to room temperature and batho-I ligand (0.20 g, 0.44 mmol, 1 equiv.) was added at room temperature dissolved in a minimal amount of DCM. The reaction mixture turned yellow, orange and red while adding the diamine ligand and was left stirring at rt for 3 h until no further color change was observed (at this point a pale orange solution was observed). The reaction mixture was then filtered and the filter cake washed with DCM. The organic solvent was removed under reduced pressure. The resulting solid was purified by recrystallization in a DCM/Et₂O mixture at rt yielding a dark yellow solid in 89 % yield. ¹H-NMR (400MHz, CDCl₃) δ (ppm): 8.14 (s, 2H), 8.02 (s, 2H), 7.22-7.18 (m, 6H), 7.05-6.98 (m, 20H), 2.23 (s, 6H), 1.67 (s, 6H). ¹³C NMR (101 MHz, CDCl₃) δ (ppm): 160 (C_q), 145 (C_q), 136 (C_q), 133.9 (Ph-C), 132.9 (Ph-C), 130.9 (Ph-C), 130.3 (Py-C), 129.9 (Ph-C), 128.9 (Ph-C), 128.7 (Ph-C/Py-C), 35.5 (C_q), 28.5 (-CH₃), 26.7 (-CH₃).



Scheme S. 4. Synthetic route for ¹PCu.

Synthesis of ^{SO3}PCu: In an oven-dried Schlenk tube, [Cu(MeCN)₄]PF₆ (0.16 g, 0.43 mmol, 1 equiv.) and Xantphos (0.25 g, 0.43 mmol, 1 equiv.) are dissolved in dry DCM (to give a final concentration around 0.05M) at rt. The resulting solution is stirred at reflux overnight. The reaction mixture was then allowed to cool to room temperature and batho-SO₃⁻ ligand (0.24 g, 0.43 mmol, 1 equiv.) was added at room temperature dissolved in a minimal amount of MeCN to guarantee its complete solubility. The reaction mixture turned orange and was then heated at 50 °C for 24 h to enable complete solubility and reactivity of the batho-SO₃⁻ ligand. The reaction mixture was then allowed to cool to room temperature and filtered and the filter cake washed with DCM. The organic solvent was removed under reduced pressure yielding a dark yellow solid in 80 % yield. ¹H-NMR (400MHz, CDCl₃) δ (ppm): 7.82-7.78 (m, 2H), 7.66-7.60 (m, 6H), 7.32-7.25 (m, 10H), 7.17-7.09 (m, 20H), 2.40 (s, 6H), 1.75 (s, 6H). ¹³C NMR (101 MHz, CD₃CN:D₂O (2:1)) δ 160 (Cq), 145 (Cq), 133.6 (Ph-C/Py-C), 132.4 (Ph-C), 130.9 (Ph-C), 130.6 (Cq), 130.2(), 129.4 (Py-C), 128.9, 127.1 (Ph-C), 126.9 (Ph-C), 126.4 (Ph-C), 126.2 (Ph-C), 124.1 (Py-Cq), 28.6 (-CH₃), 27.6 (-CH₃).



Scheme S. 5. Synthetic route for ^{SO3}PCu.

- NMR Characterization of PC_{Cu} photoredox catalysts

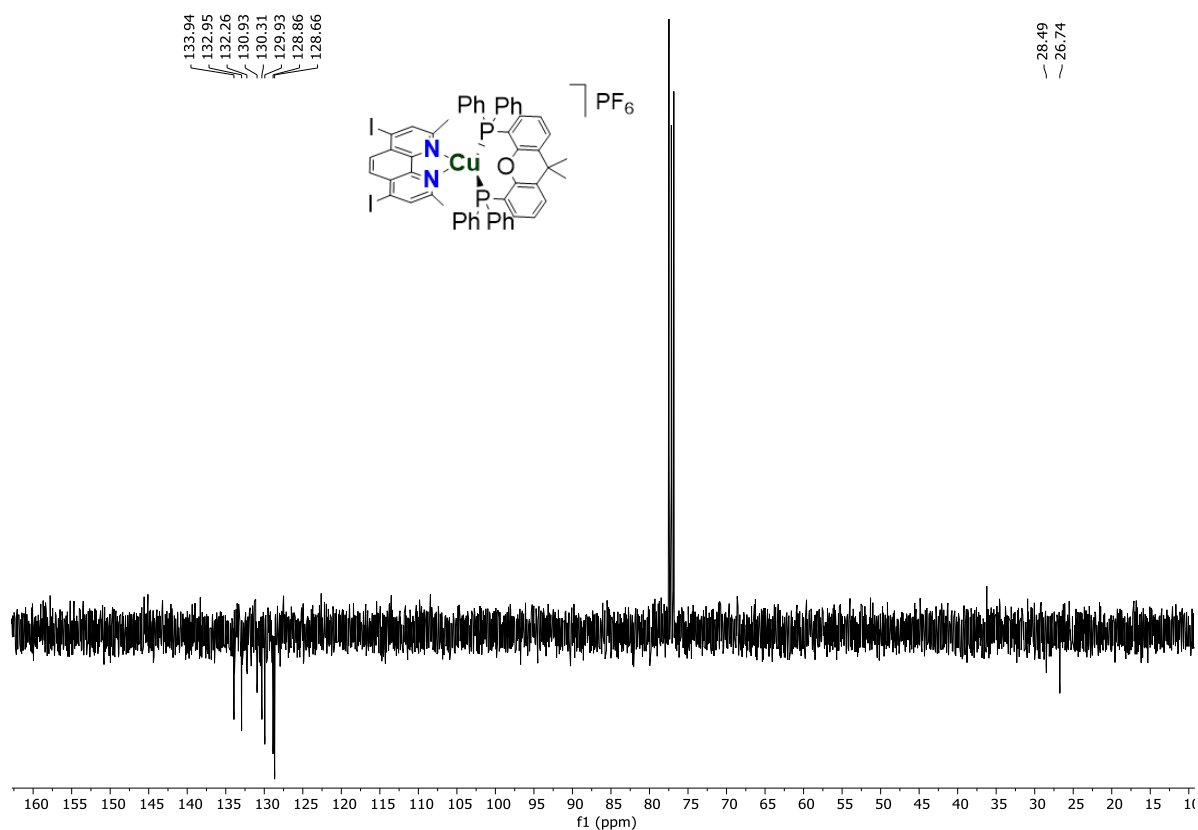


Figure S. 9. APT-¹³C spectra of PC_{Cu} in CDCl₃. ATP: Attached proton test. The compound presented very low solubility in CDCl₃.

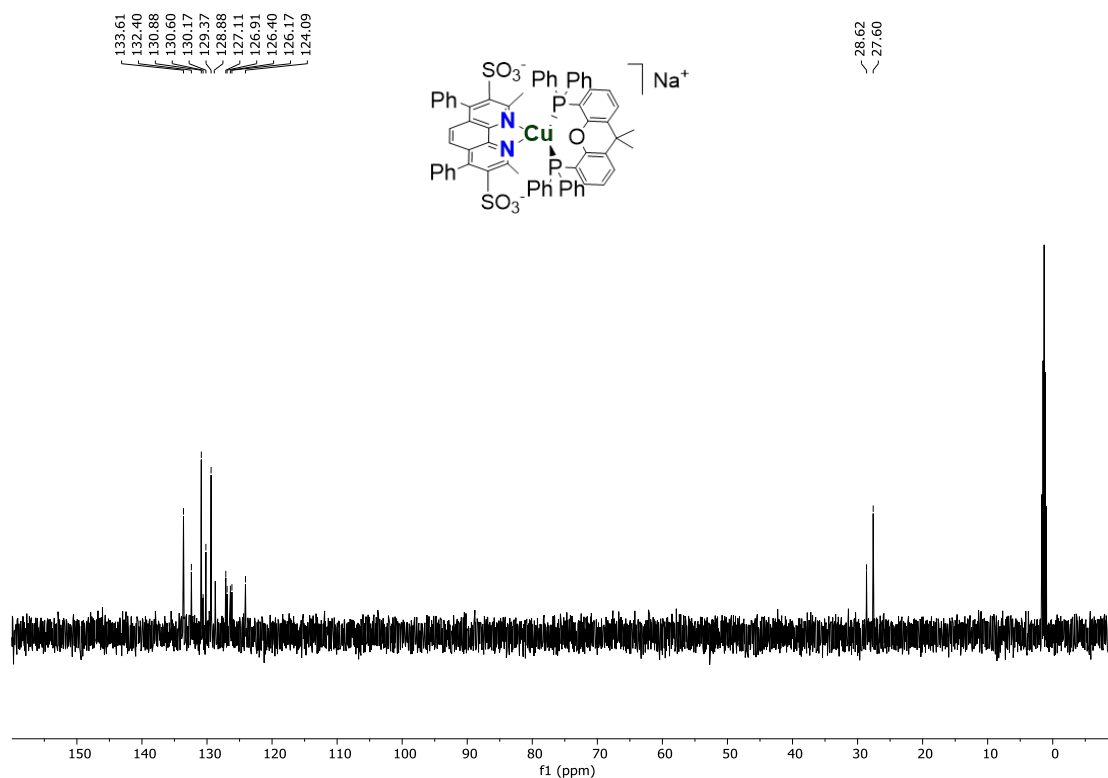


Figure S. 10. DEPT-¹³C spectra of SO₃PC_{Cu} in CD₃CN:D₂O mixture. The compound presented very low solubility.

- **Mass spectrometry characterization of PC_{Cu} photoredox catalysts**

Table S. 4. Measured m/z: 1101.0122 for ¹PC_{Cu} (expected 1101.0152).

Meas. m/z	Ion Formula	m/z	err [ppm]	err [mDa]	mSigma	e ⁻ Conf	z
1101.0106	C ₅₄ H ₄₁ CuI ₂ O ₄ P	1101.0122	1.5	1.7	18.0	even	1+
	C ₅₃ H ₄₂ CuI ₂ N ₂ O ₄ P ₂	1101.0152	4.2	-4.6	22.4	even	1+
	C ₅₀ H ₄₄ CuI ₂ NO ₄ P ₂	1101.0126	1.8	-2.0	39.2	odd	1+

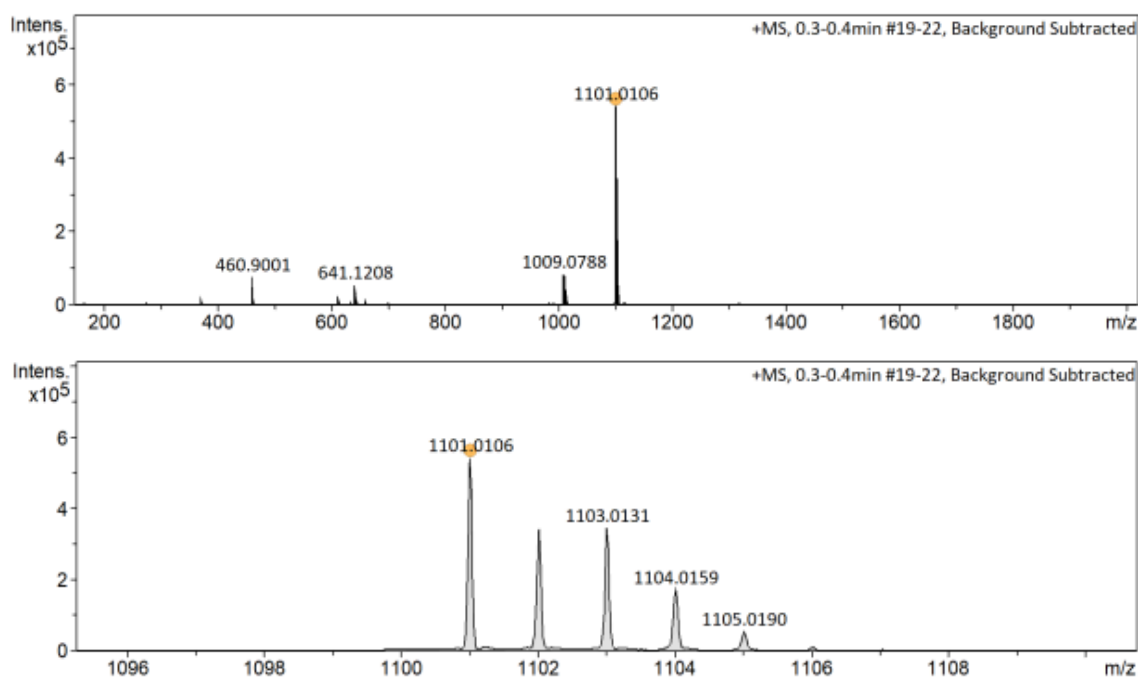


Figure S. 11. HR-MS spectrum (*top*: full range, and *bottom*: zoom in the peak) for complex ¹PC_{Cu}.

Table S. 5. Measured m/z: 1159.1836 for ³PC_{Cu} (expected: 1159.1836).

Meas. m/z	Ion Formula	m/z	err [ppm]	err [mDa]	mSigma	e ⁻ Conf	z
1159.1829	C ₆₅ H ₅₀ CuN ₂ O ₇ P ₂ S ₂	1159.1836	0.6	0.7	32.9	even	1-

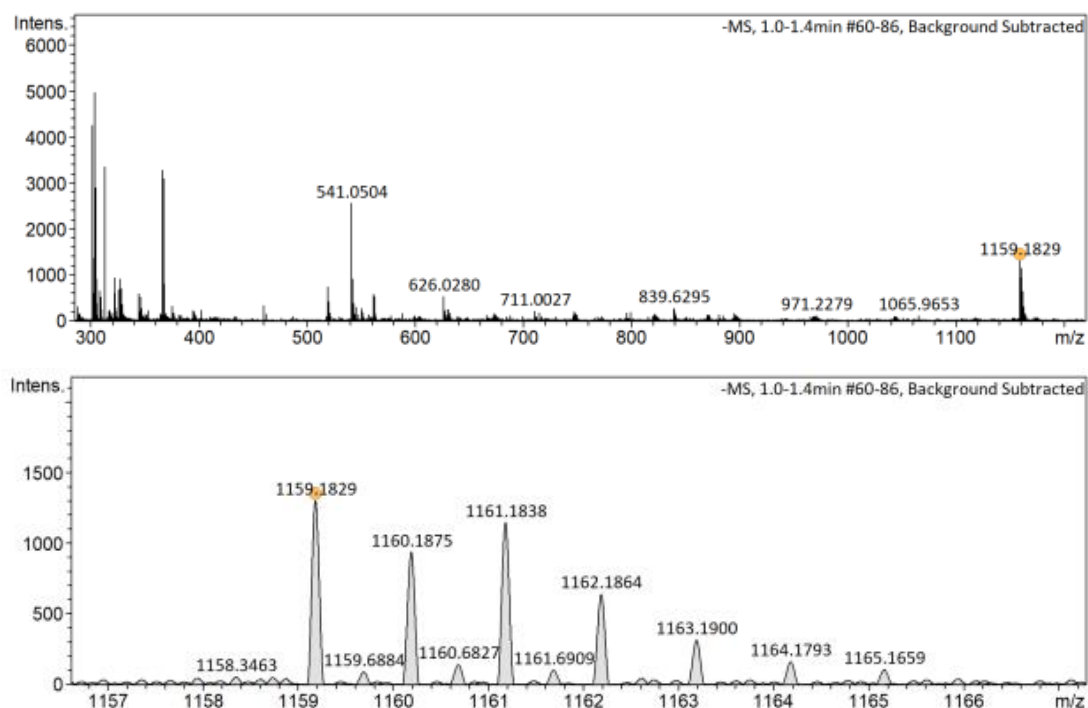
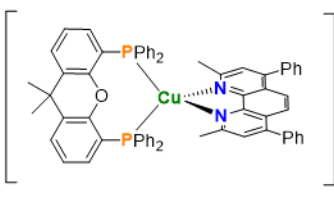
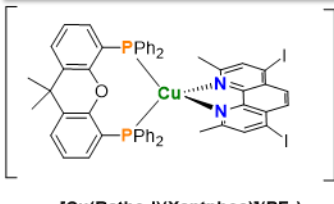
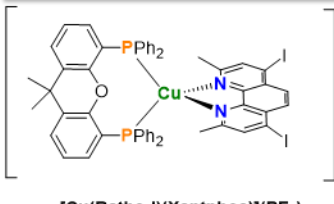
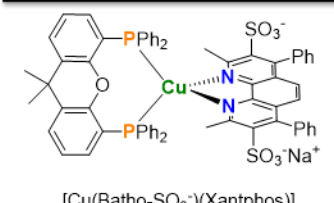


Figure S. 12. HR-MS spectrum (*top*: full range, and *bottom*: zoom in the peak) for complex $^{3\text{SO}_3}\text{PCu}$.

- Electrochemical characterization of PCu

Table S. 6. Summary of reduction potentials measured for the PCu series.

PCu	Conc. (mM)	Solvent	Electrolyte	Potential (V vs SCE)
 $[\text{Cu}(\text{Bathocuproine})(\text{Xantphos})](\text{PF}_6)$	0.25	MeCN:H ₂ O (4:6)	KNO_3 (100 mM)	-1.51
 $[\text{Cu}(\text{Batho-I})(\text{Xantphos})](\text{PF}_6)$	1	MeCN	Bu_4NPF_6 (100 mM)	-1.60
 $[\text{Cu}(\text{Batho-I})(\text{Xantphos})](\text{PF}_6)$	1	MeCN	Bu_4NPF_6 (100 mM)	-1.47
 $[\text{Cu}(\text{Batho-SO}_3^-)(\text{Xantphos})]$	1	MeCN	Bu_4NPF_6 (100 mM)	-1.66

- Spectroscopic characterization of PC_{Cu}

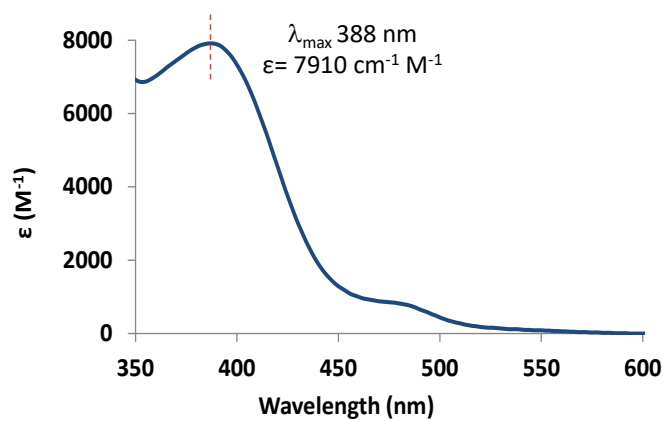


Figure S. 13. UV-vis absorption spectrum of PC_{Cu} (0.1 mM) in MeCN.

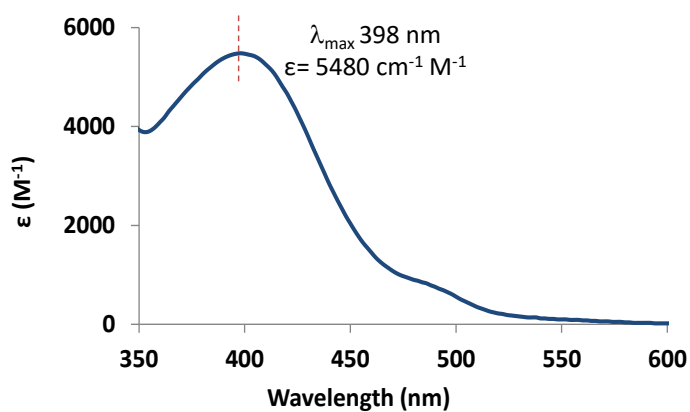


Figure S. 14. UV-vis absorption spectrum of ¹PC_{Cu} (0.1 mM) in MeCN.

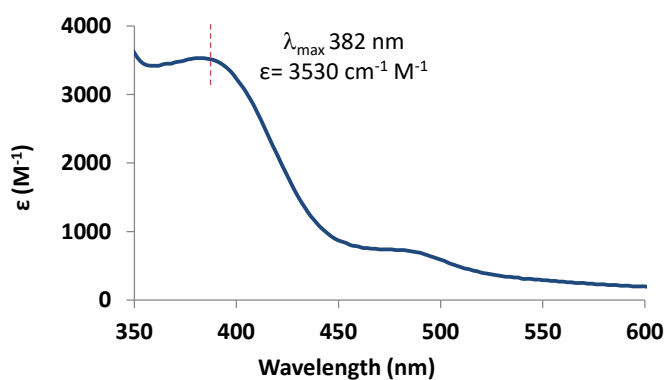


Figure S. 15. UV-vis absorption spectrum of ³SO₃PC_{Cu} (0.1 mM) in MeCN.

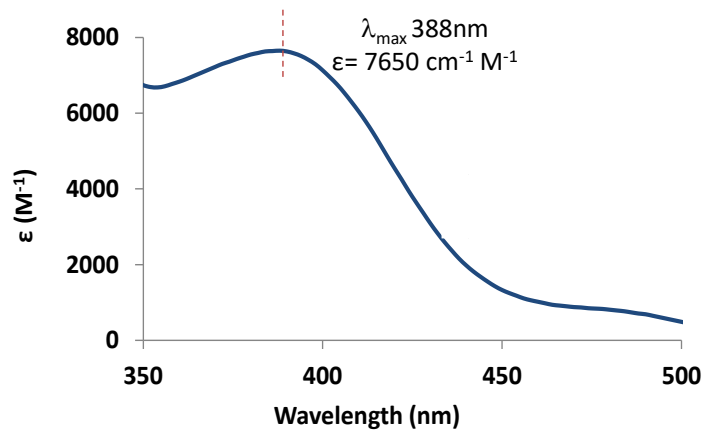


Figure S. 16. UV-vis absorption spectrum of PCu (0.1 mM) in $\text{H}_2\text{O}:\text{MeCN}$ (3:2).

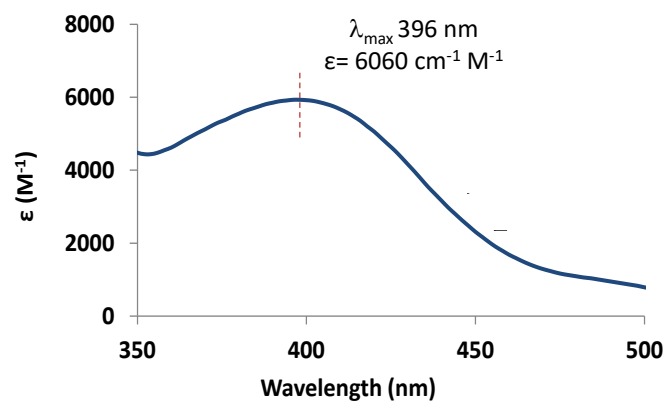


Figure S. 17. UV-vis absorption spectrum of ^1PCu (0.1 mM) in $\text{H}_2\text{O}:\text{MeCN}$ (3:2).

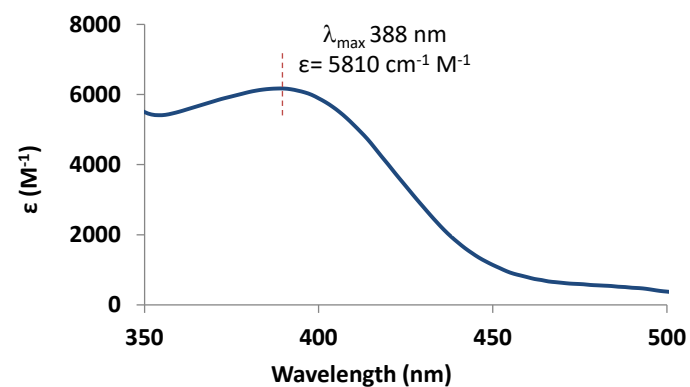


Figure S. 18. UV-vis absorption spectrum of ^{333}PCu (0.1 mM) in $\text{H}_2\text{O}:\text{MeCN}$ (3:2).

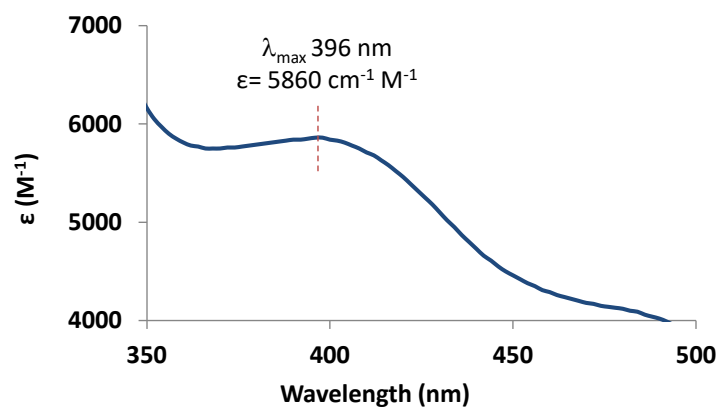


Figure S. 19. UV-vis absorption spectrum of ^{303}PCu (0.1 mM) in H_2O .

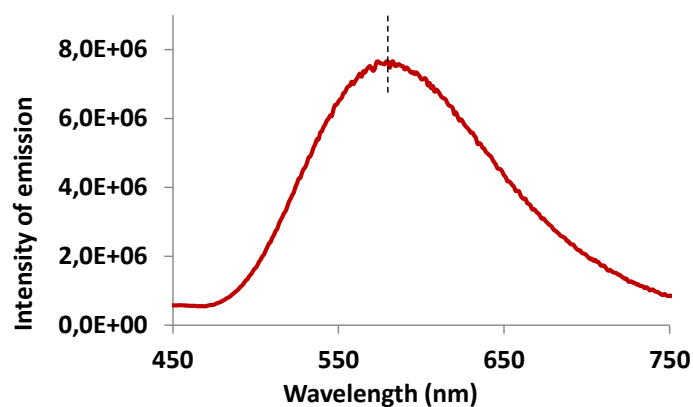


Figure S. 20. Emission spectrum ($\lambda_{\text{ex}} = 388 \text{ nm}$ and $\lambda_{\text{em max}}$ is 581 nm) of PCu (0.1 mM) in MeCN.

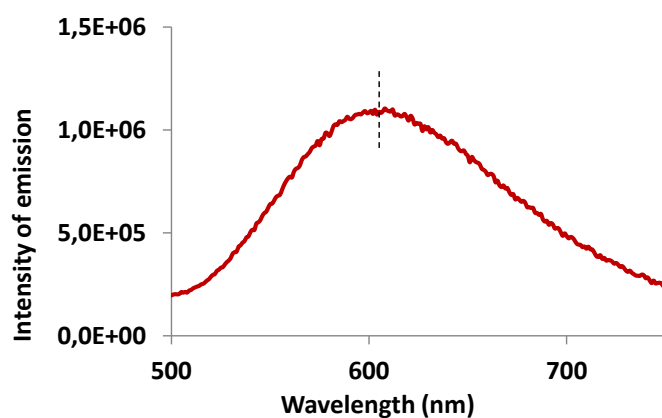


Figure S. 21. Emission spectrum ($\lambda_{\text{ex}} = 398 \text{ nm}$ and $\lambda_{\text{em max}}$ is 601 nm) of ^1PCu (0.1 mM) in MeCN.

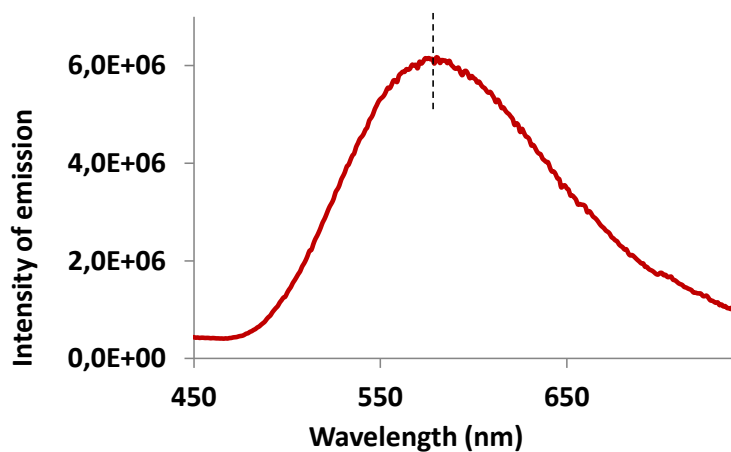


Figure S. 22. Emission spectrum ($\lambda_{\text{ex}} = 382$ nm and $\lambda_{\text{em}} \text{ max}$ is 560 nm) of ^{503}PCu (0.1 mM) in MeCN.

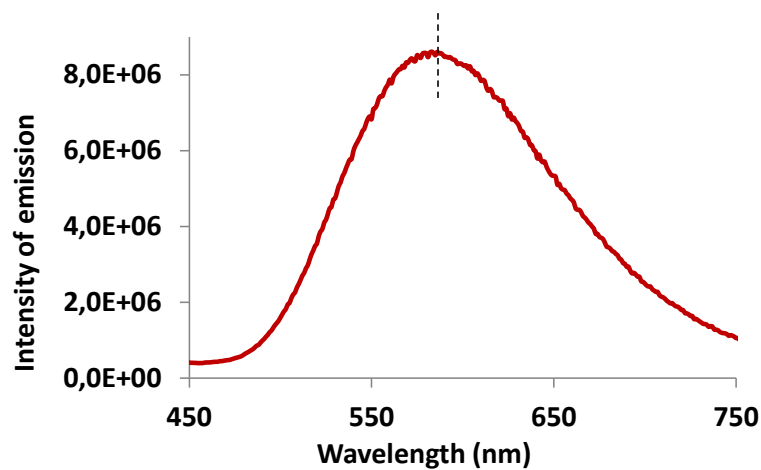


Figure S. 23. Emission spectrum ($\lambda_{\text{ex}} = 388$ nm and $\lambda_{\text{em}} \text{ max}$ is 583 nm) of PCu (0.1 mM) in $\text{H}_2\text{O}:\text{MeCN}$ (3:2).

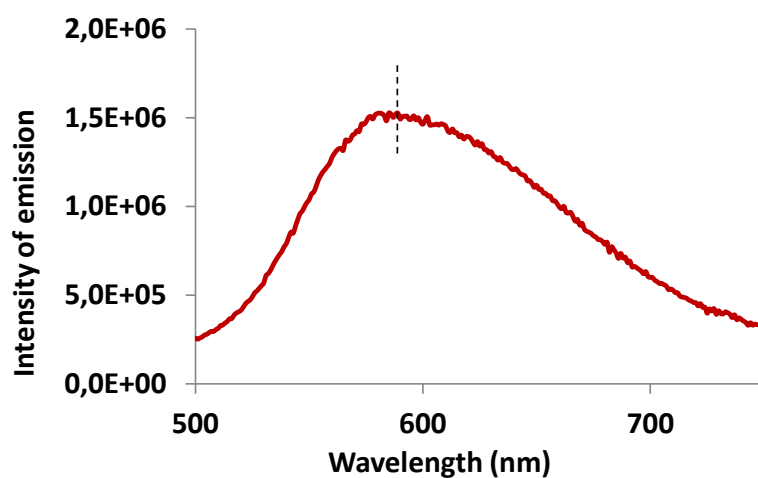


Figure S. 24. Emission spectrum ($\lambda_{\text{ex}} = 396$ nm and $\lambda_{\text{em}} \text{ max}$ is 587 nm) of ^1PCu (0.1 mM) in $\text{H}_2\text{O}:\text{MeCN}$ (3:2).

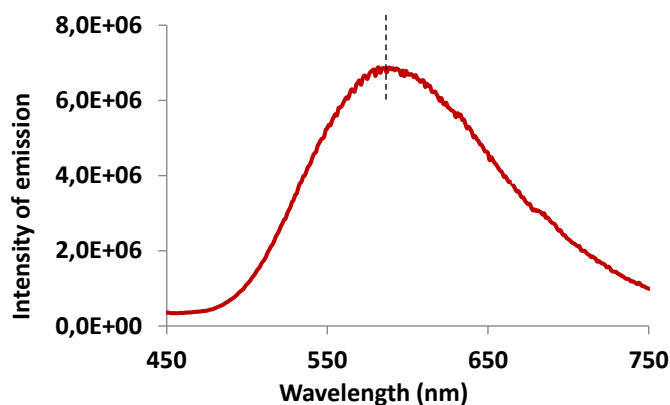


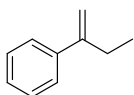
Figure S. 25. Emission spectrum ($\lambda_{\text{ex}} = 388$ nm and $\lambda_{\text{em max}}$ is 586 nm) of ^{503}PCu (0.1 mM) in $\text{H}_2\text{O}:\text{MeCN}$ (3:2).

Table S. 7. Summary of the spectroscopic data and redox potential of the excited state for the copper photoredox catalysts.

PCu	Solvent	λ_{abs} (max) /nm	$\epsilon_{\text{labs}} (\lambda_{\text{max}})$ / $\text{cm}^{-1}\cdot\text{M}^{-1}$	λ_{em} (max)/nm	Stokes shift $\Delta\bar{\nu}_{(\text{abs-em})}$ / cm^{-1}	$E(\text{Cu}^{\text{I}/\text{O}})$ / V vs SCE	E_{00}/nm	E_{00}/eV	$E_{\text{red}}(\text{PS}^*/\text{PS}^-)$
PCu	$\text{MeCN}:\text{H}_2\text{O}$ (2:3)	388	7650	583	8621	-1.51	490	2.53	1.02
	MeCN	388	7910	581	8561	-1.6	490	2.53	0.93
$^{\text{I}}\text{PCu}$	$\text{MeCN}:\text{H}_2\text{O}$ (2:3)	396	6060	587	8217		532	2.33	
	MeCN	398	5480	601	8487	-1.47	521	2.37	0.91
^{503}PCu	$\text{MeCN}:\text{H}_2\text{O}$ (2:3)	388	5810	586	8708		492	2.52	
	MeCN	382	3530	560	8321	-1.66	490	2.53	0.87

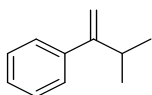
6. Synthesis of substrates

-Synthesis of but-1-en-2-ylbenzene (29)



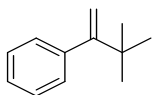
But-1-en-2-ylbenzene (29) was prepared by a Wittig olefination according to previously reported procedure.^[21] $^1\text{H-NMR}$ (CDCl_3 , 400 MHz, 300 K) δ , ppm: 7.46-7.43 (m, 2H), 7.38-7.33 (m, 2H), 7.31-7.27 (m, 1H), 5.31-5.29 (m, 1H), 5.09-5.08 (m, 1H), 2.55 (m, 2H), 1.14 (t, $J = 7.6$ Hz, 3H). MS (GC): 132.1 [M].

-Synthesis of (3-methylbut-1-en-2-yl)benzene (30)



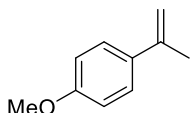
(3-methylbut-1-en-2-yl)benzene (30) was prepared by a Wittig olefination according to previously reported procedure.^[21] $^1\text{H-NMR}$ (CDCl_3 , 400 MHz, 300 K) δ , ppm: 7.39-7.33 (m, 4H), 7.31-7.28 (m, 1H), 5.18-5.17 (m, 1H), 5.07-5.06 (m, 1H), 2.92-2.82 (m, 1H), 1.13 (d, $J = 6.8$ Hz, 6H). $^{13}\text{C}\{^1\text{H}\}\text{-NMR}$ (CDCl_3 , 100.6 MHz, 300 K) δ , ppm: 155.81, 142.85, 128.11, 127.02, 126.62, 109.97, 32.35, 22.05. MS (GC): 146.1 [M].

-Synthesis of (3,3-dimethylbut-1-en-2-yl)benzene (32)



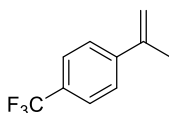
(3,3-dimethylbut-1-en-2-yl)benzene (32) was prepared by a Wittig olefination according to previously reported procedures.^[21] ¹H-NMR (CDCl₃, 400 MHz, 300 K) δ, ppm: 7.35-7.28 (m, 3H), 7.20-7.18 (m, 2H), 5.22 (d, *J* = 1.6 Hz, 1H), 4.82 (d, *J* = 1.6 Hz), 1.17 (s, 9H). ¹³C{¹H}-NMR (CDCl₃, 100.6 MHz, 300 K) δ, ppm: 159.85, 143.50, 129.01, 127.28, 126.24, 111.51, 36.13, 29.68. MS (GC): 160.1 [M].

-Synthesis of 1-methoxy-4-(prop-1-en-2-yl)benzene (33)



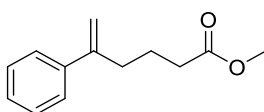
1-methoxy-4-(prop-1-en-2-yl)benzene (33) was prepared by a Wittig olefination according to previously reported procedures.^[21] ¹H-NMR (CDCl₃, 400 MHz, 300 K) δ, ppm: 7.44-7.41 (m, 2H), 6.89-6.86 (m, 2H), 5.30-5.29 (m, 1H), 5.00-4.99 (m, 1H), 3.82 (s, 3H), 2.14-2.13 (m, 3H). ¹³C{¹H}-NMR (CDCl₃, 100.6 MHz, 300 K) δ, ppm: 159.07, 142.56, 133.76, 126.59, 113.54, 110.66, 55.29, 21.92. MS (GC): 148.1 [M].

-Synthesis of 1-(prop-1-en-2-yl)-4-(trifluoromethyl)benzene (34)



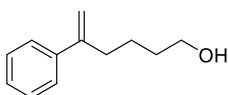
1-(prop-1-en-2-yl)-4-(trifluoromethyl)benzene (34) was prepared by a Wittig olefination according to previously reported procedures.^[21] ¹H-NMR (CDCl₃, 400 MHz, 300 K) δ, ppm: 7.60-7.54 (m, 4H), 5.45-5.44 (m, 1H), 5.20-5.19 (m, 1H), 2.17-2.16 (m, 3H). ¹³C{¹H}-NMR (CDCl₃, 100.6 MHz, 300 K) δ, ppm: 144.76, 142.21, 133.74 (d, *J* = 19.5 Hz), 132.11 (d, *J* = 9.96 Hz), 128.56 (q, *J* = 14.28 Hz), 125.77, 125.17 (q, *J* = 3.8 Hz), 114.55, 21.66. MS (GC): 186.1 [M].

-Synthesis of methyl-5-phenylhex-5-enoate (35)



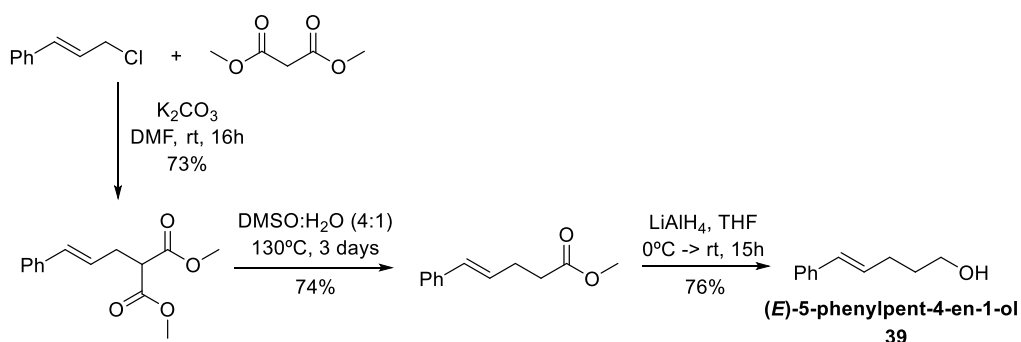
Methyl-5-phenylhex-5-enoate (35) was prepared by Wittig olefination of the corresponding commercially available ketone according to previously reported procedure.^[22] ¹H-NMR (CDCl₃, 500 MHz, 300 K) δ, ppm: 7.42-7.38 (m, 2H), 7.35-7.30 (m, 2H), 7.29-7.24 (m, 1H), 5.30 (d, *J* = 1.4 Hz, 1H), 5.07 (q, *J* = 1.3 Hz, 1H), 3.66 (s, 3H), 2.55 (td, *J* = 7.7, 1.2 Hz, 2H), 2.34 (t, *J* = 7.5 Hz, 2H), 1.79 (quint, *J* = 7.5 Hz, 2H). ¹³C{¹H}-NMR (CDCl₃, 100.6 MHz, 300 K) δ, ppm: 174.17, 147.73, 141.07, 128.57, 127.69, 126.34, 113.16, 51.72, 34.82, 33.61, 23.61. MS (GC): 204.0 [M].

-Synthesis of 5-phenylhex-5-en-1-ol (36)



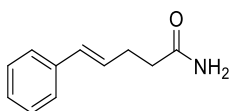
An oven-dried 50 mL two-necked round-bottomed flask equipped with a stirring bar and a dropping funnel and connected to an argon inlet was charged with dry CH_2Cl_2 (10 mL) and substrate **S1** (604 mg, 2.96 mmol). The flask was immersed in dry-ice/acetone bath. Then, a solution of DIBAL-H 1M (5.8 mL, 5.92 mmol) in THF was slowly added via the dropping funnel. After being stirred for 2h at dry ice temperature, the cooling bath was removed and the mixture allowed to warm to room temperature. The reaction was quenched with saturated ammonium chloride solution, the mixture was extracted two times with diethyl ether and the combined organic layers were washed with brine, dried over magnesium sulfate and concentrated under reduced pressure. Then, pure product was obtained in 70% (363 mg) by flash chromatography in silica gel (hexanes/ethyl acetate (80:20)). $^1\text{H-NMR}$ (CDCl_3 , 400 MHz, 300 K) δ , ppm: 7.43-7.37 (m, 2H), 7.36-7.30 (m, 2H), 7.29-7.23 (m, 1H), 5.27 (d, $J = 1.5$ Hz, 1H), 5.07 (q, $J = 1.4$ Hz, 1H), 3.64 (q, $J = 5.5$ Hz, 2H), 2.54 (td, $J = 7.4, 1.3$ Hz, 2H), 1.66-1.47 (m, 4H), 1.22-1.16 (m, 1H). $^{13}\text{C}\{^1\text{H}\}$ -NMR (CDCl_3 , 100.6 MHz, 300 K) δ , ppm: 148.5, 141.4, 128.4, 127.5, 126.3, 112.6, 63.0, 35.2, 32.5, 24.5.

-Synthesis of (*E*)-5-phenylpent-4-en-1-ol (**39**)



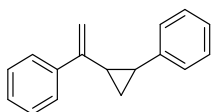
(E)-5-phenylpent-4-en-1-ol (39) was prepared according to previously reported procedures.^[23] $^1\text{H-NMR}$ (CDCl_3 , 400 MHz, 300 K) δ , ppm: 7.37-7.26 (m, 4H), 7.23-7.16 (m, 1H), 6.42 (dt, $J = 15.8, 1.5$ Hz, 1H), 6.23 (dt, $J = 15.8, 6.9$ Hz, 2H), 3.71 (t, $J = 6.5$ Hz, 2H), 2.36- 2.27 (m, 2H), 1.81-1.71 (m, 2H), 1.44 (s br, 1H). $^{13}\text{C}\{^1\text{H}\}$ -NMR (CDCl_3 , 100.6 MHz, 300 K) δ , ppm: 137.8, 130.6, 130.2, 128.7, 127.1, 126.1, 62.6, 32.4, 29.5.

-Synthesis of (*E*)-5-phenylpent-4-enamide (**41**)



(E)-5-phenylpent-4-enamide (41) was prepared according to previously reported procedures.^[24] $^1\text{H-NMR}$ (CDCl_3 , 400 MHz, 300 K) δ , ppm: 7.37-7.35 (m, 2H), 7.34-7.30 (m, 2H), 7.25-7.22 (m, 1H), 6.50-6.45 (m, 1.5 Hz, 1H), 6.28-6.22 (m, 2H), 5.56-5.51 (br m, 2H), 2.61-2.56 (m, 2H), 2.44- 2.41 (m, 2H). $^{13}\text{C}\{^1\text{H}\}$ -NMR (CDCl_3 , 100.6 MHz, 300 K) δ , ppm: 174.51, 137.26, 131.16, 128.53, 128.51, 127.22, 126.06, 35.48, 28.68. MS (GC): 175.1 [M].

-Synthesis of (1-(2-phenylcyclopropyl)vinyl)benzene (**42**)



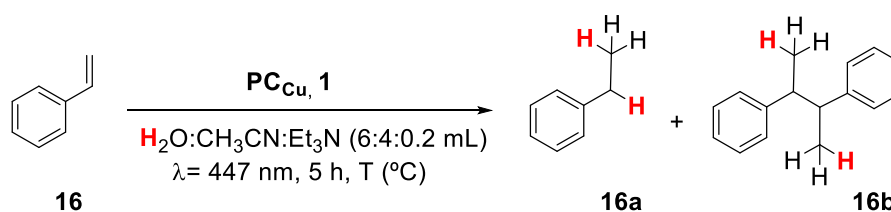
(1-(2-phenylcyclopropyl)vinyl)benzene (42) was prepared according to previously reported procedures through a Corey-Chaykovsky reaction^[25] and further Wittig olefination gave the targeted olefin.^[21] ¹H-NMR (CDCl₃, 400 MHz, 300 K) δ , ppm: 7.53-7.47 (m, 1H), 7.31-7.22 (m, 5H), 7.21-7.15 (m, 1H), 7.15-7.11 (m, 2H), 5.36 (s, 1H), 5.05-5.02 (m, 1H), 2.03-1.91 (m, 2H), 1.42-1.35 (m, 1H), 1.30-1.22 (m, 2H). ¹³C{¹H}-NMR (CDCl₃, 100.6 MHz, 300 K) δ , ppm: 148.5, 142.7, 141.2, 128.6, 128.4, 127.7, 126.2, 125.9, 109.5, 28.0, 26.6, 16.0. MS (GC): 220.1 [M].

7. Control experiments in the photoreduction of styrene (16)

Styrene (**16**) was used as a model substrate for the optimization of the catalytic conditions when using **PC_{Cu}** as photoredox catalyst and **1** as catalyst.

- Optimization of the catalytic system

Table S. 8. Optimization of the catalytic conditions for the reduction of **16** using **PC_{Cu}** as photoredox catalyst and **1** as catalyst.

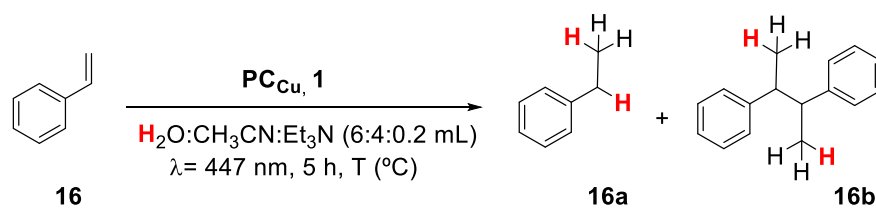


Entry	[Substrate] (mM)	Temp. (°C)	[1] (mol %)	[PC _{Cu}] (mol %)	% Yield 16a	% Yield 16b
1	16.5	35	1	1.5	67	11
2	32	35	3	3	64	11
3	16.5	35	3	3	81	6
4	8.7	35	3	3	86	4
5	8.7	35	3	1.5	92	4
6	8.7	35	3	0.75	83	7
7	8.7	15	3	3	91	0
8	8.7	15	3	3 ^[a]	10	0
9	8.7	15	3	3 ^[b]	78	0

Conditions: **1** (% mol), **PC_{Cu}** (% mol), substrate (mM) as indicated in the table in H₂O:CH₃CN:Et₃N (6:4:0.2 mL) irradiation at $\lambda=447$ nm for 5 h at 35 or 15 °C under N₂. Yields were determined by GC analysis after workup of the reaction and they are relative to a calibrated internal standard. Values are average of triplicates. ^[a] **¹PC_{Cu}** was used instead of **PC_{Cu}**. ^[b] **³PC_{Cu}** was used instead of **PC_{Cu}**.

- Control experiments

Table S. 9. Blank experiments for styrene (**16**) reduction when using **PC_{Cu}** as photoredox catalyst and **1** as catalyst.

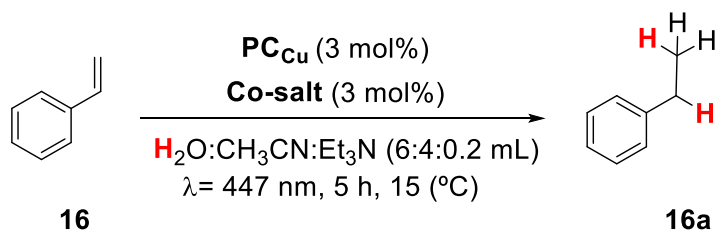


Entry	[Substrate] (mM)	[PC _{Cu}] (mol%)	[1] (mol%)	Temperature (°C)	% Conv.	% 16a	% 16b
1	16.5	1	0	35	2	n.d.	n.d.
2	16.5	0	1.5	35	2	n.d.	n.d.
3	32	3	0	35	3	n.d.	n.d.
4	32	0	3	35	4	n.d.	n.d.
5	16.5	3	0	35	2	n.d.	n.d.
6	16.5	0	3	35	3	n.d.	n.d.
7	8.7	3	0	35	4	n.d.	n.d.
8	8.7	0	3	35	2	n.d.	n.d.
9	8.7	1.5	0	35	4	n.d.	n.d.
10	8.7	0	3	35	3	n.d.	n.d.
11	8.7	0.75	0	35	1	n.d.	n.d.
12	8.7	0	3	35	2	n.d.	n.d.
13	8.7	3	0	15	2	n.d.	n.d.
14	8.7	0	3	15	3	n.d.	n.d.
15	8.7	3	0	25	2	n.d.	n.d.
16	8.7	0	3	25	3	n.d.	n.d.
17	8.7	3	0	45	1	n.d.	n.d.
18	8.7	0	3	45	2	n.d.	n.d.
19	8.7	3	0	55	1	n.d.	n.d.
20	8.7	0	3	55	3	n.d.	n.d.
21	8.7	3	0	80	2	n.d.	n.d.
22	8.7	0	3	80	3	n.d.	n.d.
23	32	10	0	55	4	n.d.	n.d.
24	8.7	10	0	55	2	n.d.	n.d.
25	32	10	0	45	4	n.d.	n.d.
26	8.7	10	0	45	3	n.d.	n.d.
27	32	10	0	35	2	n.d.	n.d.
28	8.7	10	0	35	1	n.d.	n.d.
29	32	10	0	15	1	n.d.	n.d.
30	8.7	10	0	15	2	n.d.	n.d.

Conditions: **1** (% mol), **PC_{Cu}** (% mol), substrate (mM) as indicated in the table in H₂O:CH₃CN:Et₃N (6:4:0.2 mL) irradiated at λ = 447 nm for 5 h at each temperature under N₂. Yields were determined by GC analysis after workup and they are relative to a calibrated internal standard. Values are average of triplicates.

- Screening of cobalt salts

Table S. 10. Control experiments for **16** reduction when using **PC_{Cu}** as photoredox catalyst and different cobalt salts.



Entry	Co-Salt	% Conv. 16	% Yield 16a
1	Co(SO ₄) x 7H ₂ O	0	0
2	Co(AcO) x 4H ₂ O	0	0
3	Co(NO ₃) x 6H ₂ O	0	0
4	Co(acac)	0	0
5	CoCl ₂	0	0
6	Co(OTf) ₂ (MeCN) ₂	0	0
7	1 (synthesized)	100	91
8	1 (<i>in situ</i> generation)	100	90

Conditions: **Co-salt** (261 μM, 3% mol), (**PC_{Cu}** (261 μmol, 3% mol), substrate (0.087 mmol, 8.7 mM) in H₂O:CH₃CN:Et₃N (6:4:0.2 mL) irradiated at λ= 447 nm for 5 h at 15 °C under N₂. [b] **PC_{Cu}** (2.5 μmol, 1.5% mol), substrate (0.16 mmol, 16.5 mM) in H₂O:CH₃CN:Et₃N (6:4:0.2 mL) irradiation at λ= 447 nm for 5 h at 30 °C under N₂. Yields were determined by GC analysis after workup of the reaction and they were relative to a calibrated internal standard. Values are average of triplicates.

8. Screening of photoredox catalysts and cobalt catalysts in the reduction of styrene (16) to ethylbenzene (16a)

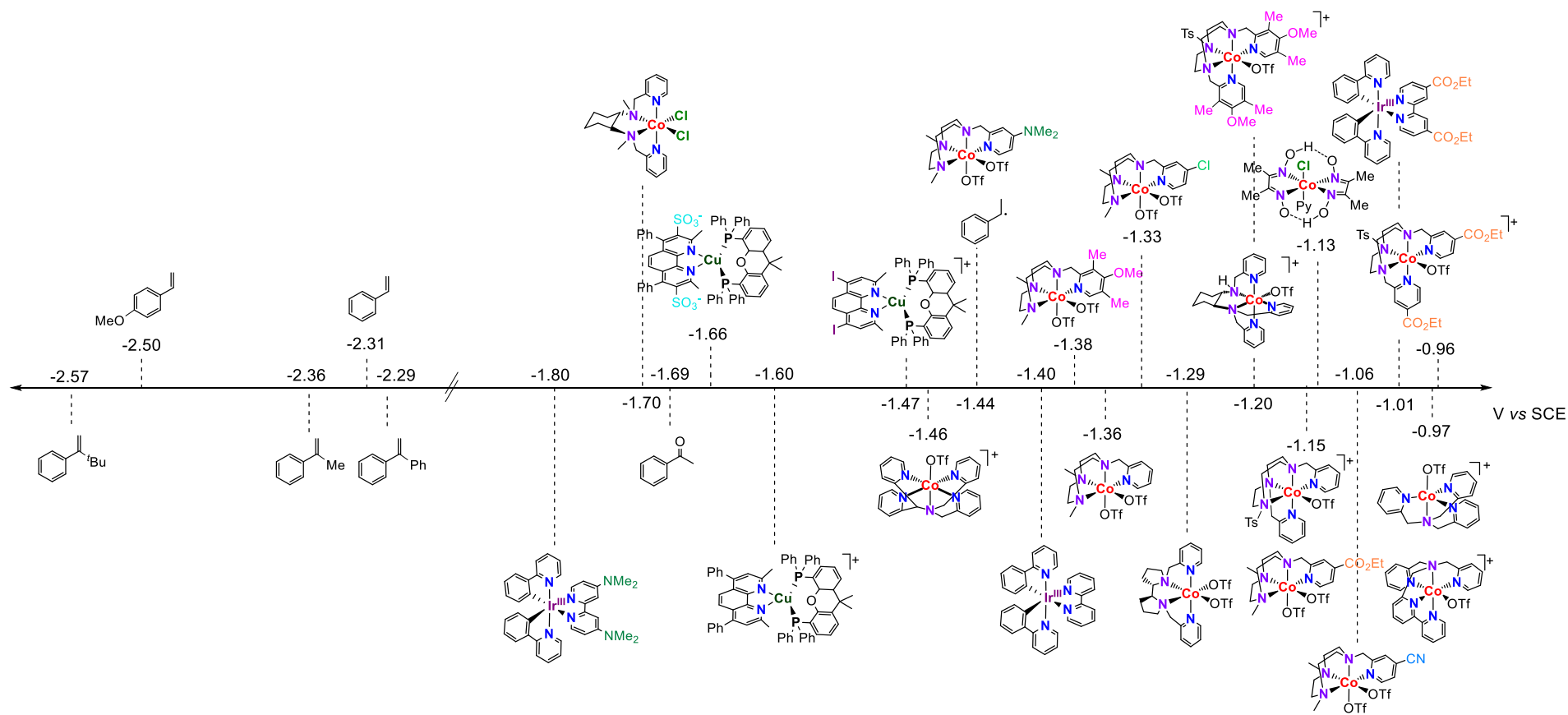


Figure S. 26. Comparison between the reduction potential of selected substrates, photoredox catalysts, and cobalt catalysts used in this study.

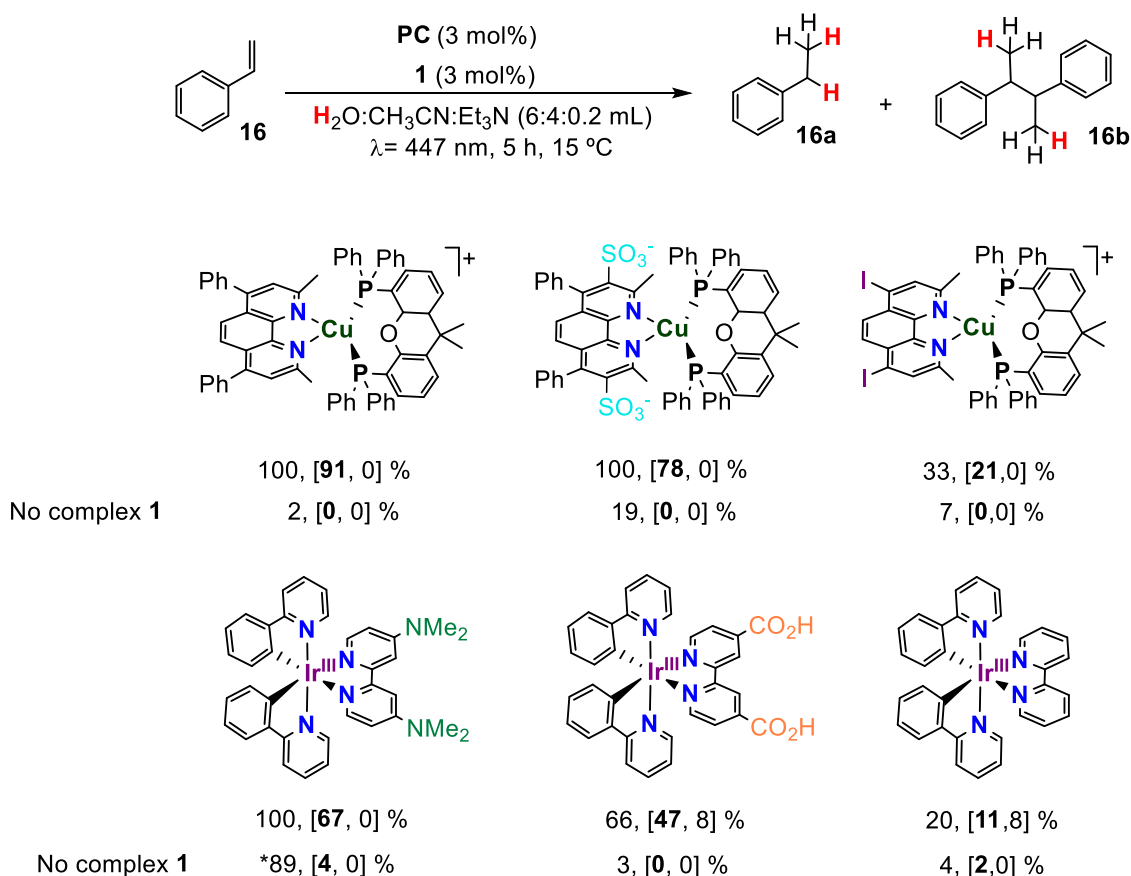


Figure S. 27. Photocatalytic reduction of styrene (**16**) to ethylbenzene (**16a**) by the selected photoredox catalysts. Catalytic conditions **A**: **1** (261 μ M, 3%), **PC**_{Cu} (261 μ M, 3% mol), **16** (0.087 mmol, 8.7 mM) in H₂O:CH₃CN:Et₃N (6:4:0.2 mL) irradiation at λ = 447 nm for 5 h at 15 °C under N₂. Yields determined by GC analysis after workup relative to a calibrated internal standard. Values were average of triplicates. Represented values are as follows: Conv %, % yield **16a**, % yield **16b**. Values from the blank reactions without complex **1** are also represented. *Formation of an adduct with the electron donor (see GC-FID chromatogram Figure S. 109).

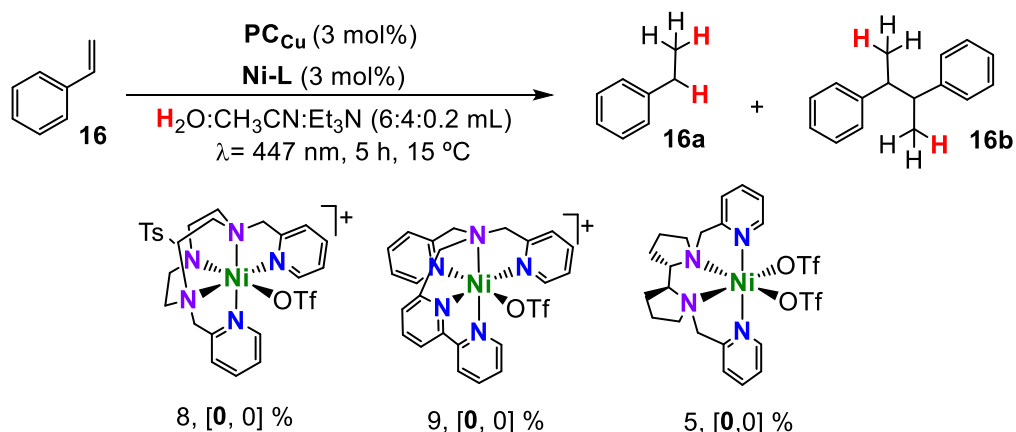


Figure S. 28. Photocatalytic reduction of styrene (**16**) to ethylbenzene (**16a**) by the selected nickel complexes. Catalytic conditions **A**: **Catalyst** (261 μ M, 3% mol), **PC**_{Cu} (261 μ M, 3% mol), **16** (0.087 mmol, 8.7 mM) in H₂O:CH₃CN:Et₃N (6:4:0.2 mL) irradiation at λ = 447 nm for 5 h at 15 °C under N₂. Yields determined by GC analysis after workup relative to a calibrated internal standard. Values were average of triplicates. Represented values are as follows: Conv %, % yield **16a**, % yield **16b**.

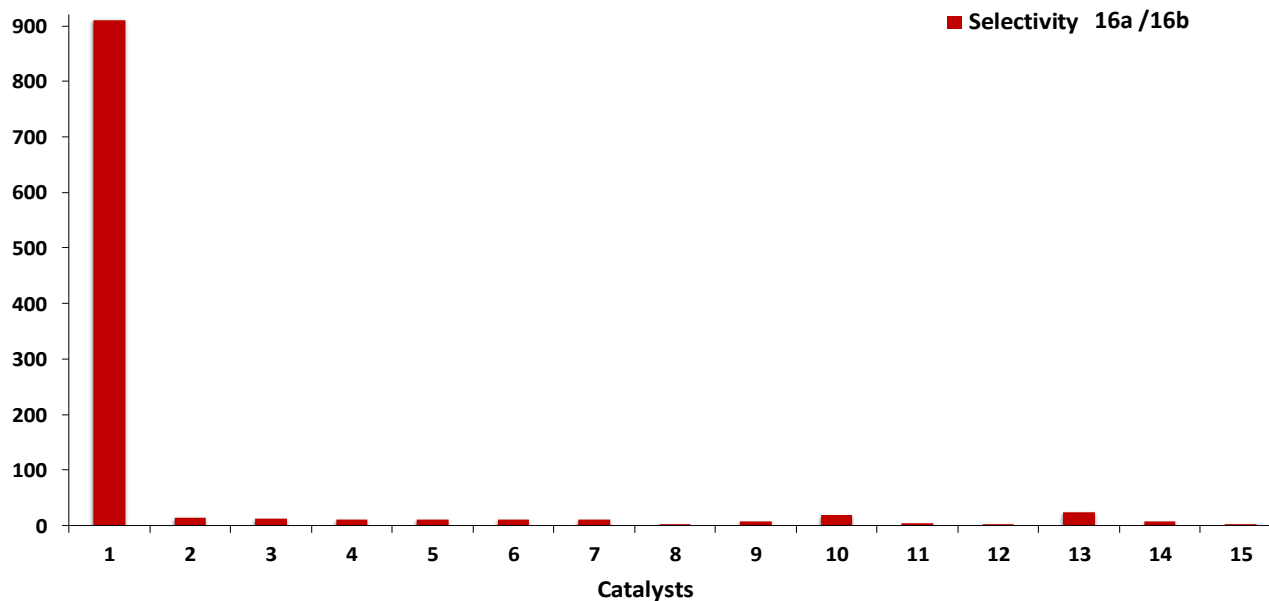
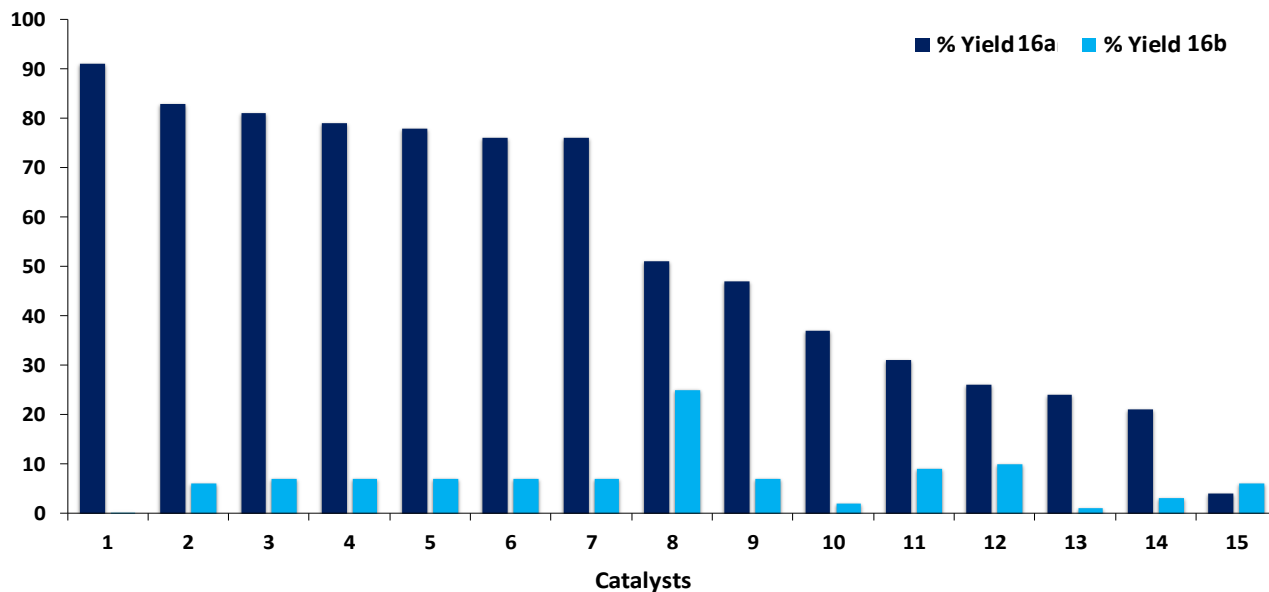
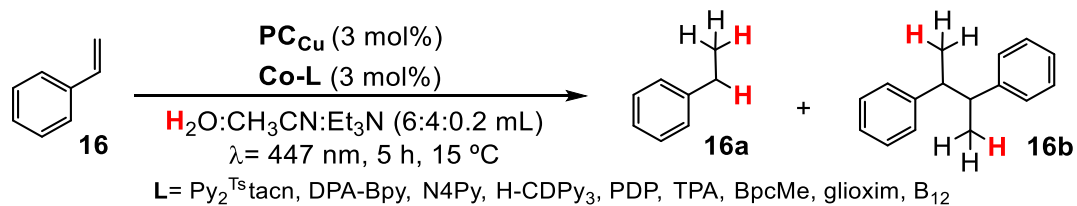


Figure S. 29. Photocatalytic activities of different cobalt-based complexes in **16a** and **16b** formation. *Top:* **16a** and **16b** formation activity. *Bottom:* selectivity of **16a** vs **16b**. Conditions **A:** **Co-Cat** (261 μM , 3% mol), **PCu** (261 μM , 3% mol), **16** (8.7 mM) in $\text{H}_2\text{O}:\text{CH}_3\text{CN}:\text{Et}_3\text{N}$ (6:4:0.2 mL) irradiation (447 nm) for 5h at 15 °C under N_2 . Yields determined by GC analysis after workup relative to a calibrated internal standard. Values were average of triplicates.

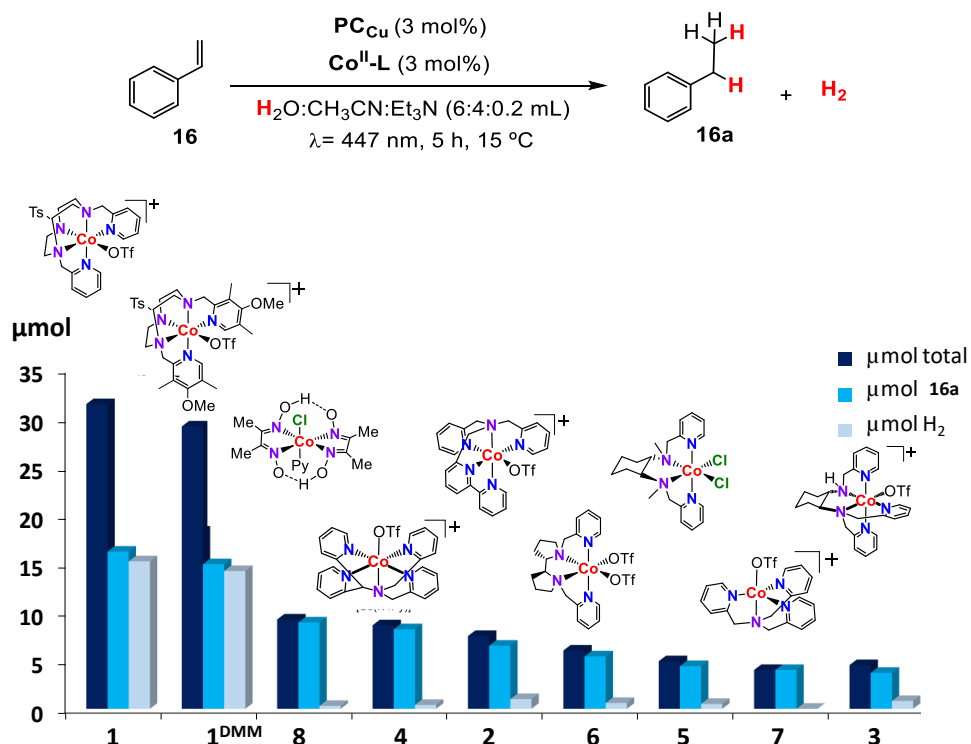


Figure S. 30. Photocatalytic activities of different pentadentate cobalt-based complexes in H_2 and **16a** formation. ^[a]Conditions **A**: $\text{Co}^{\text{II}}\text{-cat}$ (3 mol%), PC_{Cu} (3 mol%), Substrate (8.7 mM) in $\text{H}_2\text{O}:\text{CH}_3\text{CN}:\text{Et}_3\text{N}$ (6:4:0.2 mL) irradiated 5 h (447 nm) at 15 °C under N_2 . Quantity of reduced product (μmol **16a**) determined by GC analysis after workup relative to a calibrated internal standard. H_2 was quantified by GC-TCD analysis of an aliquot of the head-space of the reaction. Values were average of triplicates.

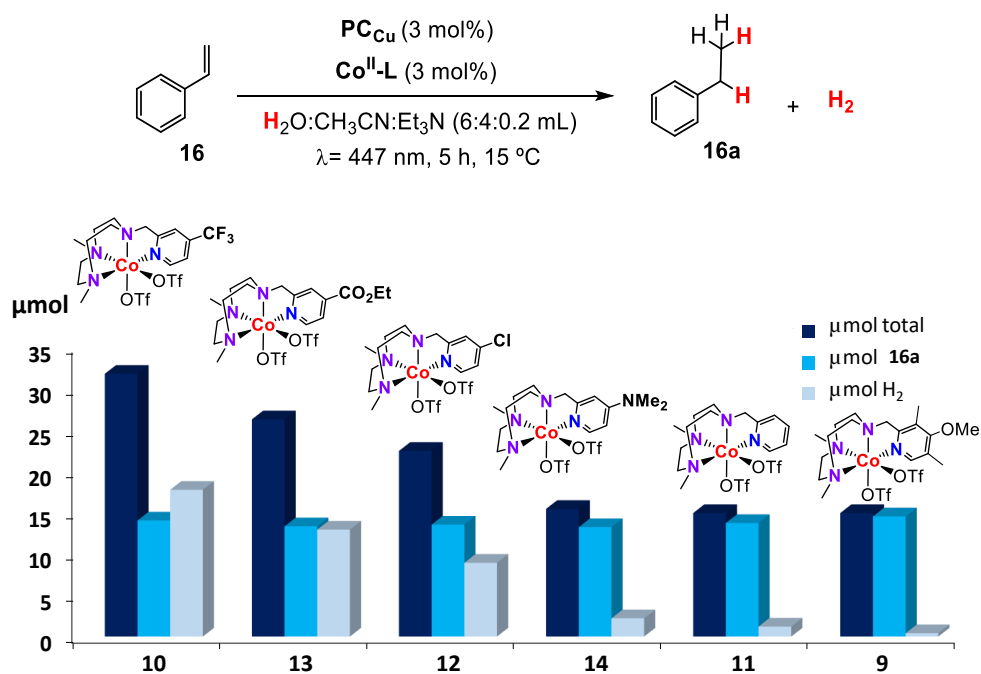


Figure S. 31. Photocatalytic activities of a family of tetradentate cobalt complexes based on the $\text{Py}^{\text{Me}_2}\text{tacn}$ ligand with different electronic effects in H_2 and **16a** formation. ^[a]Conditions **A**: $\text{Co}^{\text{II}}\text{-cat}$ (3 mol%), PC_{Cu} (3 mol%), Substrate (8.7 mM) in $\text{H}_2\text{O}:\text{CH}_3\text{CN}:\text{Et}_3\text{N}$ (6:4:0.2 mL) irradiated 5 h (447 nm) at 15 °C under N_2 . Quantity of reduced product (μmol **16a**) determined by GC analysis after workup relative to a calibrated internal standard. H_2 was quantified by GC-TCD analysis of an aliquot of the head-space of the reaction. Values were average of triplicates.

9. Effect of the temperature in the photoreduction of styrene (**16**) and α -methylstyrene (**28**) to ethylbenzene (**16a**) and cumene (**28a**) respectively.

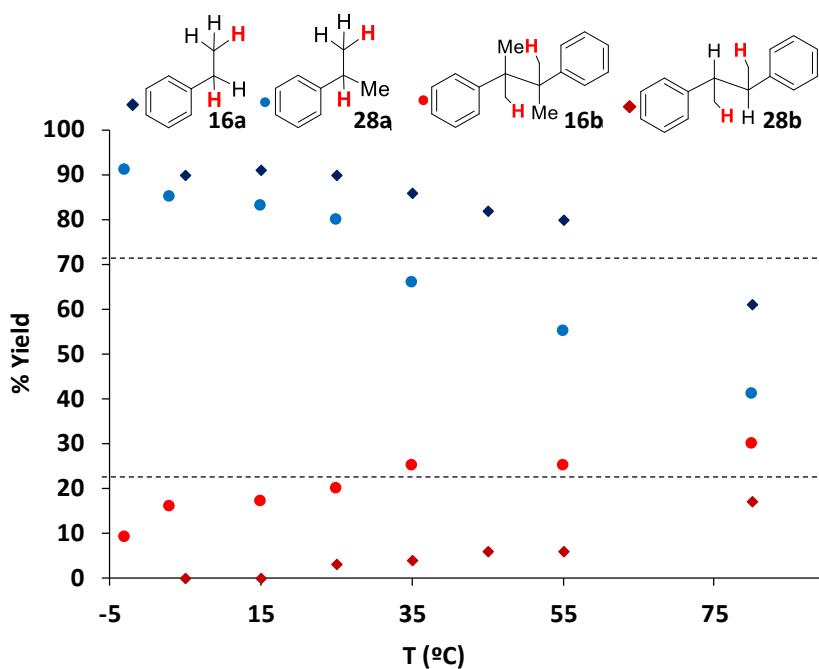
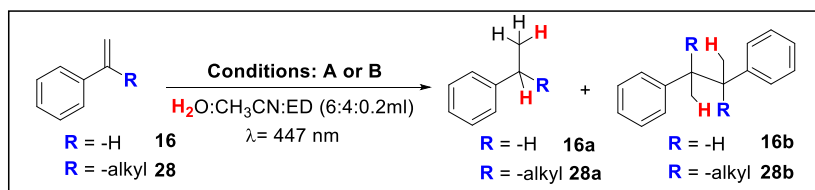


Figure S. 32. Plot of the yield of reduced products **16a** and **28a** and their dimers **16b** and **28b** versus the reaction temperature. Catalytic conditions: **A**: **1** (261 μM , 3% mol), PC_{Cu} (261 μM , 3% mol), substrate **16** (0.087 mmol, 8 mM) in $\text{H}_2\text{O}:\text{CH}_3\text{CN}:\text{Et}_3\text{N}$ (6:4:0.2 mL) irradiation at $\lambda = 447$ nm from 2h to 24h (depending on the temperature) at a given temperature under N_2 . **B**: **1** (261 μM , 6% mol), PC_{Cu} (261 μM , 6% mol), substrate **28** (9 μmol , 4.4 mM) in $\text{H}_2\text{O}:\text{MeCN}:\text{iPr}_2\text{EtN}$ (6:4:0.2 mL) irradiation at $\lambda = 447$ nm from 2h to 24h (depending on the temperature) at a given temperature under N_2 . Yields were determined by GC analysis after workup of the reaction and they were relative to a calibrated internal standard. Values are averages of triplicates. Dotted line indicates product yield in the photoreduction of **16** when the reaction is not thermostated (~ 45 $^{\circ}\text{C}$).

10. Optimization of aromatic 1,1-disubstituted olefins

α -methylstyrene (**28**) was used as a model substrate for the optimization of the catalytic conditions when using PC_{Cu} as photoredox catalyst and **1** as catalyst.

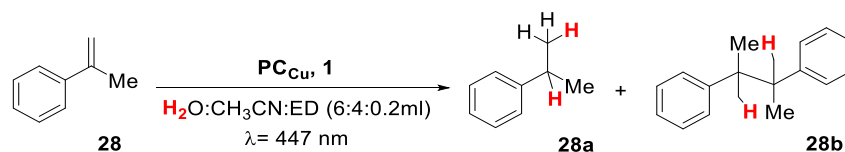


Table S. 11. Variation of the substrate concentration using the optimized conditions for styrene derivatives (**16-27**, see table 4 main text) photoreduction.

Entry	[Substrate] (mM)	[PC_{Cu}] (mol%)	[1] (mol%)	ED	T (°C)	% Conv.	% 28a	% 28b	Mass loss
1	8.7	3	3	TEA	15	100	40	45	15
2	8.7	3	0	TEA	15	9	4	0	5
3	4.4	3	3	TEA	15	100	45	38	17

Table S. 12. Variation of the electron donor (ED) using the best substrate concentration from table **SI.1.10**. (4.4 mM) and the optimized conditions for styrene derivatives (**16-27**, see table 4 main text) photoreduction.

Entry	[Substrate] (mM)	[PC_{Cu}] (mol%)	[1] (mol%)	ED	T (°C)	% Conv.	% 28a	% 28b	Mass loss
1	4.4	3	3	TEA	15	100	45	38	17
2	4.4	3	3	DIPEA	15	100	56	26	18
3	4.4	6	6	TEA	15	100	47	34	19
4	4.4	6	6	DIPEA	15	100	61	15	24

Table S. 13. Variation of the dual catalytic system loading using the best ED (DIPEA) and substrate concentration (4.4 mM).

Entry	[Substrate] (mM)	[PC_{Cu}] (mol%)	[1] (mol%)	ED	T (°C)	% Conv.	% 28a	% 28b	Mass loss
1	4.4	3	3	DIPEA	15	100	56	26	18
2	4.4	3	6	DIPEA	15	100	58	19	23
3	4.4	3	12	DIPEA	15	100	60	16	24
4	4.4	6	3	DIPEA	15	100	57	20	23
5	4.4	6	6	DIPEA	15	100	61	15	24
6	4.4	6	12	DIPEA	15	100	61	13	26

Table S. 14. Variation of the temperature ED (DIPEA), substrate concentration (4.4 mM) and 6 mol% loading of the dual catalytic system.

Entry	[Substrate] (mM)	[PC_{Cu}] (mol%)	[1] (mol%)	ED	T (°C)	% Conv.	% 28a	% 28b	Mass loss
1	4.4	6	6	DIPEA	15	100	61	15	24
2	4.4	6	6	DIPEA	3	100	85	15	0
3	4.4	6	6	DIPEA	-3	100	91	9	0

Conditions: **1** (% mol), PC_{Cu} (% mol), substrate (mM) in $\text{H}_2\text{O}:\text{CH}_3\text{CN}:\text{Et}_3\text{N}$ or $\text{H}_2\text{O}:\text{CH}_3\text{CN}:\text{Pr}_2\text{EtN}$ (6:4:0.2 mL) irradiation at $\lambda = 447 \text{ nm}$ for 5 h at 15 °C or 24 h at 3 and -3 °C under N_2 . Yields were determined by GC analysis after workup of the reaction and they were relative to a calibrated internal standard. Values are averages by triplicates.

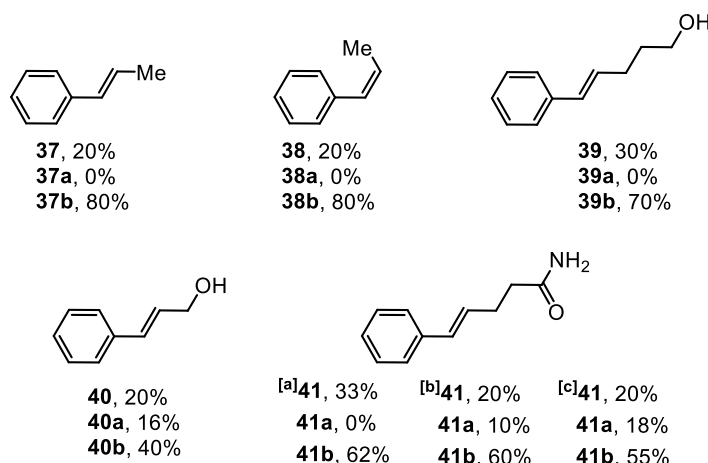
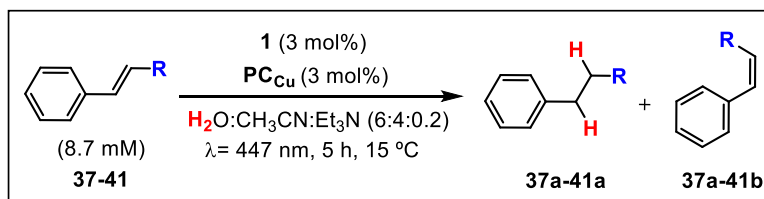
Table S. 15. Control studies with selected 1,1-disubstituted olefins (**28 – 31**).

Entry	Substrate	[PC _{Cu}] (mol%)	[1] (mol%)	% Conv.	% Yield alkane	% Yield dimer
1	28	3	3	100	40	45
2		3	0	9	4	0
3	29	3	3	100	71	11
4		3	0	8	3	0
5	30	3	3	59	58	1
6		3	0	13	3	0
7	31	3	3	83	83	0
8		3	0	10	4	0
9	32	3	3	5	0	0
10		3	0	6	0	0

Conditions: **1** (1% mol), PC_{Cu} (% mol), substrate (8.7 mM) in H₂O:CH₃CN:Et₃N (6:4:0.2 mL) irradiation at λ = 447 nm for 5 h at 15 °C under N₂. Yields were determined by GC analysis after workup of the reaction and they were relative to a calibrated internal standard. Values are averages by triplicates

11. Catalytic assays of the photoreduction of aromatic 1,2-disubstituted olefins

Table S. 16. Light-driven reduction of selected aromatic 1,2-disubstituted olefins (**28-36**).



Catalytic conditions **A**: **1** (261 μM, 3% mol), PC_{Cu} (261 μM, 3% mol), substrate (0.087 mmol, 8.7 mM) in H₂O:CH₃CN:Et₃N (6:4:0.2 mL) irradiation at λ = 447 nm for 5 h at 15 °C under N₂. ^[a]Catalytic conditions **B**: **1** (261 μM, 6% mol), PC_{Cu} (261 μM, 6% mol), substrate **18** (0.044 mmol, 4.4 mM) in H₂O:CH₃CN:Pr₂EtN (6:4:0.2 mL) irradiation at λ = 447 nm for 5 h at 15 °C under N₂. ^[b]Catalytic conditions **B** at 50 °C. ^[c]Catalytic conditions **B** at 80 °C. Yields were determined by GC analysis after workup of the reaction and they are relative to a calibrated internal standard. Values are averages of triplicates.

12. Oxygen tolerance

Table S. 17. Effect on oxygen in the reaction outcome.

Entry	[Substrate] (mM)	[PC _{Cu}] (mol%)	[1] (mol%)	ED	T (°C)	% Conv.	% yield	% dimer
1	(16) 8	3	3	TEA	15	100	91	0
2	(28) 4.4	6	6	DIPEA	-3	90	81	8

Conditions: **1** (% mol), PC_{Cu} (% mol), substrate (mM) in non-deoxygenated H₂O:CH₃CN:Et₃N or H₂O:CH₃CN:Pr₂EtN mixtures (6:4:0.2 mL) were mixed under air and irradiated at λ= 447 nm for 5 h at 15 °C or 24 h at 3 and -3 °C. Yields were determined by GC analysis after workup of the reaction and they were relative to a calibrated internal standard. Values are averages by triplicates.

13. Mechanistic studies

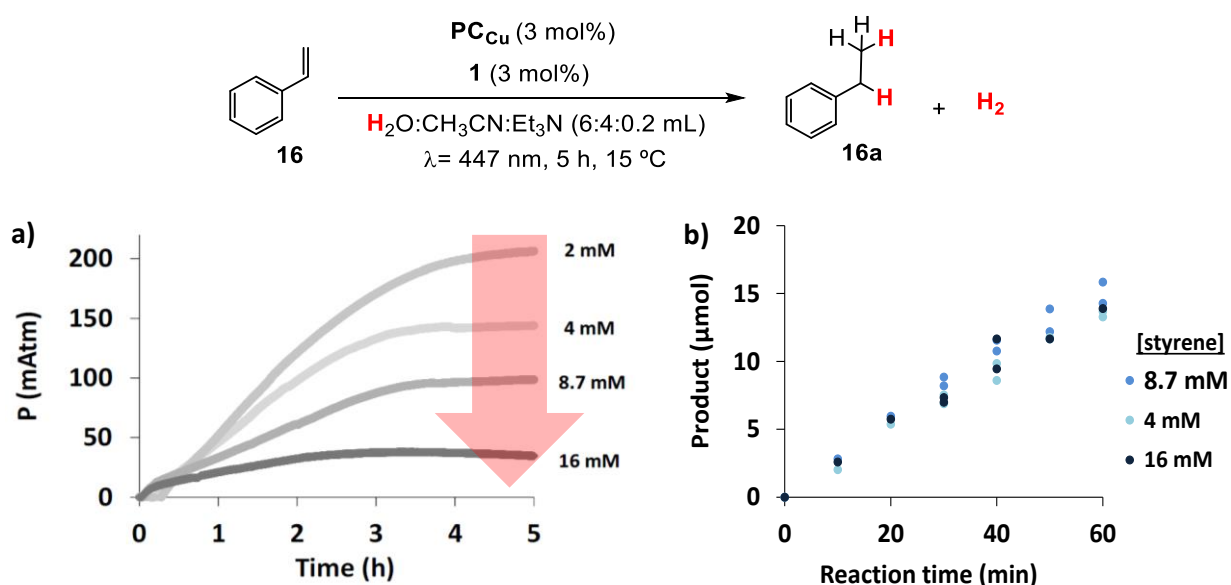


Figure S. 33. a) On-line monitoring of the photochemical H₂ production in the presence of increasing concentrations of **16**. b) Monitoring of the formation **16a** at increasing concentrations of **16**. Conditions **A**: **1** (3 mol%), PC_{Cu} (3 mol%), Substrate (2, 4, 8.7 and 16 mM, unless otherwise noticed) in H₂O:CH₃CN:Et₃N (6:4:0.2 mL) irradiated 5 h (447 nm) at 15 °C under N₂. The yield of **16a** was determined at several points during the kinetic study by taking aliquots of the reaction at different times. The LEDs were switched off and a new argon-purged syringe was used to take each aliquot.

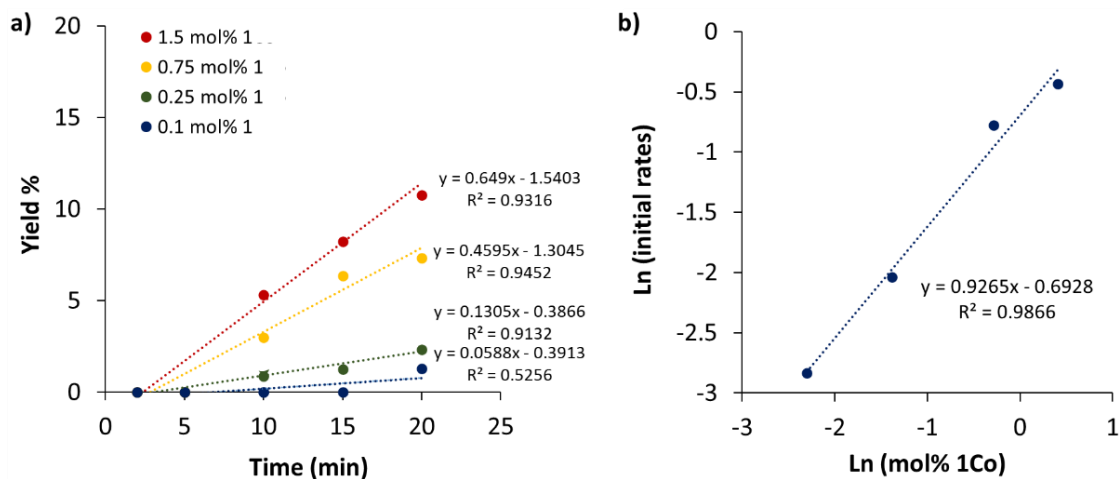
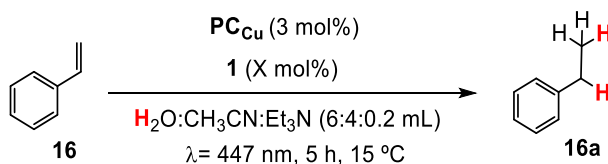


Figure S. 34. a) Initial rates of the formation of product **16a** under optimized catalytic conditions varying the cobalt catalyst (**1**) concentration, and b) the respective double Ln-plot initial rates (mol **16a**·s⁻¹) vs **1** (mol). Conditions **A**: **1** (0.1 to 1.5 mol%), **PC**_{Cu} (3 mol%), Substrate (8.7 mM) in H₂O:CH₃CN: Et₃N (6:4:0.2 mL) irradiated 20 min (447 nm) at 15 °C under N₂. The yield of **16a** was determined at several points during the kinetic study by taking aliquots of the reaction at different times. The LEDs were switched off and a new argon-purged syringe was used to take each aliquot.

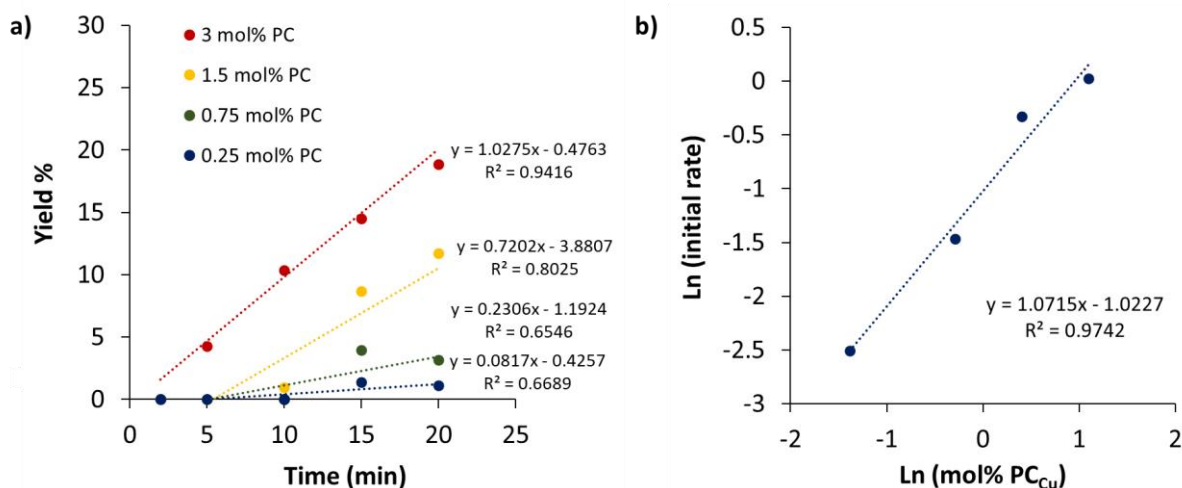
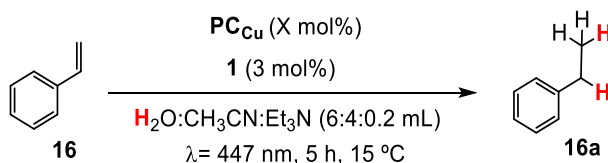


Figure S. 35. a) Initial rates of the formation of product **16a** under optimized catalytic conditions varying the copper photoredox catalyst (**PC**_{Cu}) concentration, and b) the respective double Ln-plot initial rates (mol **16a**·s⁻¹) vs **PC**_{Cu} (mol). Conditions **A**: **1** (3 mol%), **PC**_{Cu} (0.25 to 3 mol%), Substrate (8.7 mM) in H₂O:CH₃CN: Et₃N (6:4:0.2 mL) irradiated 20 min (447 nm) at 15 °C under N₂. The yield of **16a** was determined at several points during the kinetic study by taking aliquots of the reaction at different times. The LEDs were switched off and a new argon-purged syringe was used to take each aliquot.

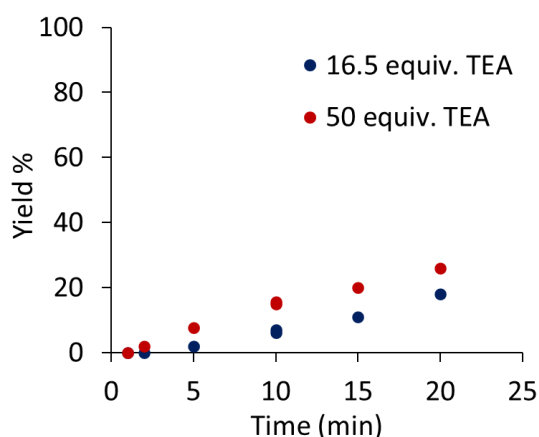


Figure S. 36. Initial rates of the formation of product **16a** under optimized catalytic conditions varying the equivalents of triethylamine (TEA). Conditions **A**: **1** (3 mol%), **PC**_{Cu} (3 mol%), Substrate (2, 4, 8.7 and 16 mM, unless otherwise noticed) in H₂O:CH₃CN (6:4 mL), Et₃N (16.5 equiv. and 50 equiv., respectively), irradiated 20 min (447 nm) at 15 °C under N₂. The yield of **16a** was determined at several points during the kinetic study by taking aliquots of the reaction at different times. The LEDs were switched off and a new argon-purged syringe was used to take each aliquot.

14. Selectivity: competition experiments

Table S. 18. Optimization conditions towards ketone reduction (**43**) in presence of styrene (**16**).

Entry	N ^o LEDs	Light intensity (mmol·hv·s ⁻¹ photons) ^[13]	PC	Mol % PC	Mol % 1	Ratio % 43a / % 16a	Selectivity for the ketone (% 43a / (% 43a +% 16a))
1	1	2.05·10 ⁻³	PC _{Cu}	1.5	1	1.9	65
2	1	2.05·10 ⁻³	NMe ₂ PC _{Ir}	1.5	1	2.6	72
3	3	6.16·10 ⁻³	NMe ₂ PC _{Ir}	1.5	1	7.1	88
4	3	6.16·10 ⁻³	NMe ₂ PC _{Ir}	1.5	0.5	9.1	90
5	3	6.16·10 ⁻³	NMe ₂ PC _{Ir}	3	0.5	15.4	94
6	3	6.16·10 ⁻³	NMe ₂ PC _{Ir}	3	0.25	24.7	96
7	7	1.44·10 ⁻²	NMe ₂ PC _{Ir}	3	0.25	> 100	100

General catalytic conditions: **1** (mol%), **PC** (mol%), Substrate A + B (16.5 mM), A:B (1:1), in H₂O:CH₃CN:Et₃N (6:4:0.2 mL) irradiated (447 nm) for 4 h at 25 °C under N₂.

Table S. 19. Optimization conditions towards olefin reduction (**16**) in presence of ketone (**43**).

Entry	N ^o LEDs	Light intensity (mmol·hv·s ⁻¹ photons) ^[13]	PC	Mol % PC	Co-cat	Mol % Co-cat	Ratio % 16a / % 43a	Selectivity for the olefin (% 16a / (% 43a +% 16a))
1	1	2.05·10 ⁻³	PC _{Cu}	1.5	1	1	0.5	35
2	1	2.05·10 ⁻³	CO ₂ HPC _{Ir}	1.5	1	1	1.2	54
3	1	2.05·10 ⁻³	CO ₂ HPC _{Ir}	1.5	CO ₂ Et ₁	1	2.2	68
4	1	2.05·10 ⁻³	CO ₂ HPC _{Ir}	1.5	CO ₂ Et ₁	3	3.1	76
5	1	1.67·10 ⁻⁴	CO ₂ HPC _{Ir}	1.5	CO ₂ Et ₁	3	>100	100

General catalytic conditions: **Co-Cat** (mol%), **PC** (mol%), Substrate A + B (16.5 mM), A:B (1:1), in H₂O:CH₃CN:Et₃N (6:4:0.2 mL) irradiated (447 nm) for 4 h at 25 °C under N₂

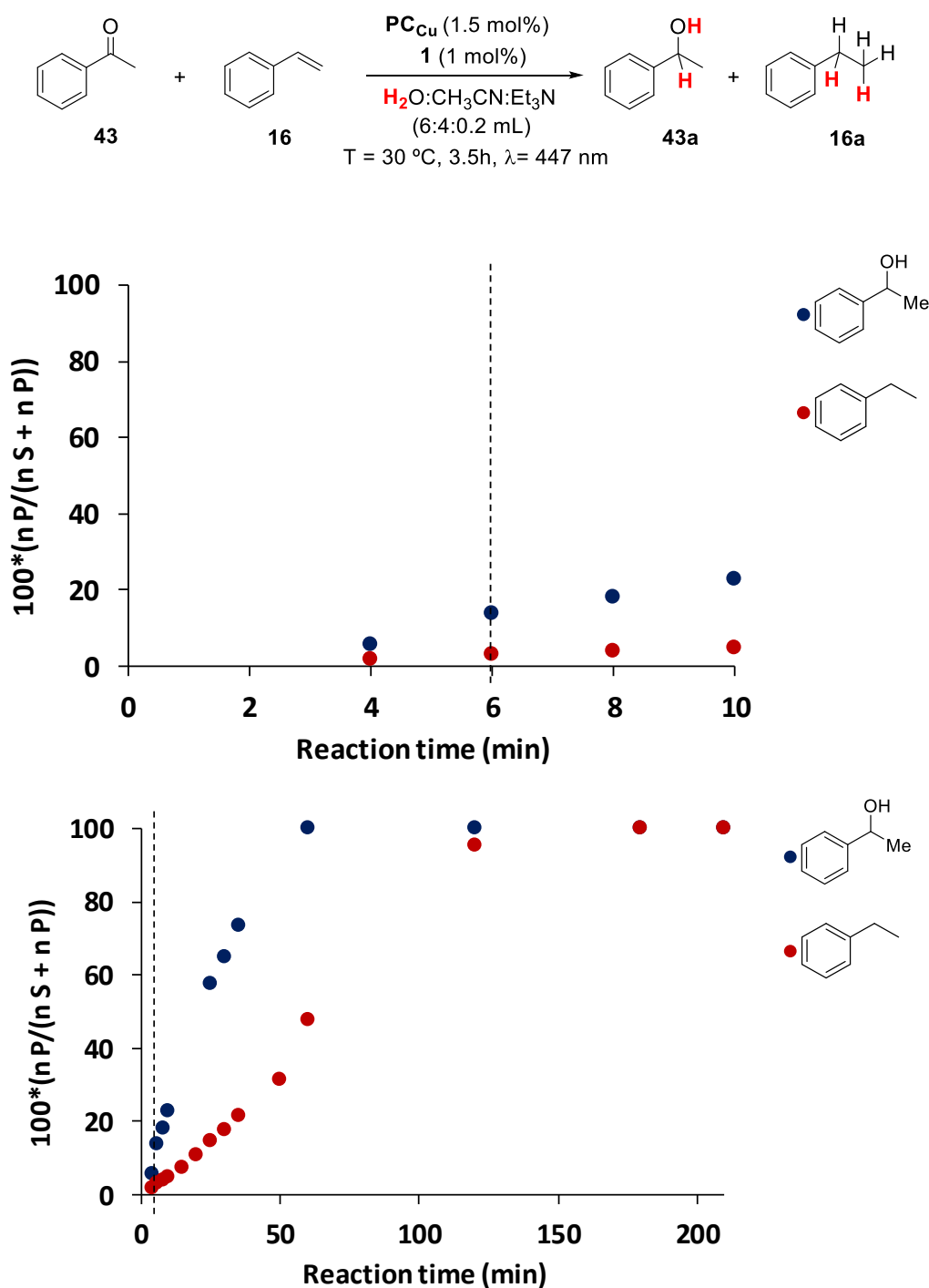


Figure S. 37. Monitoring of the competition between substrates **43** and **16** under catalytic conditions. Top: yield during the first 10 minutes of irradiation, it can be seen that the reduction of substrate **16** starts when **43** has not been totally reduced; bottom, all the reaction time monitorization (3.5 hours). ^[a]Conditions: **1** (1 mol%), PCu (1.5 mol%), Substrate A + B (16.5 mM), A:B (1:1), in $\text{H}_2\text{O}:\text{CH}_3\text{CN}:\text{Et}_3\text{N}$ (6:4:0.2 mL) irradiated (1 LED, 447 nm, $2.05 \cdot 10^{-3}$ mmol·hv·s⁻¹ photons) for 4 h at 25 °C under N_2 . ^[b]The plotted data is the ratio between the amount of the reduced product formed and the sum of the amount of the reduced product formed and the unconverted starting material. ^[c]The black dotted line indicates the point where substrate **16** starts reacting. Selectivity for ketone reduction 65% and for olefin reduction 35%.

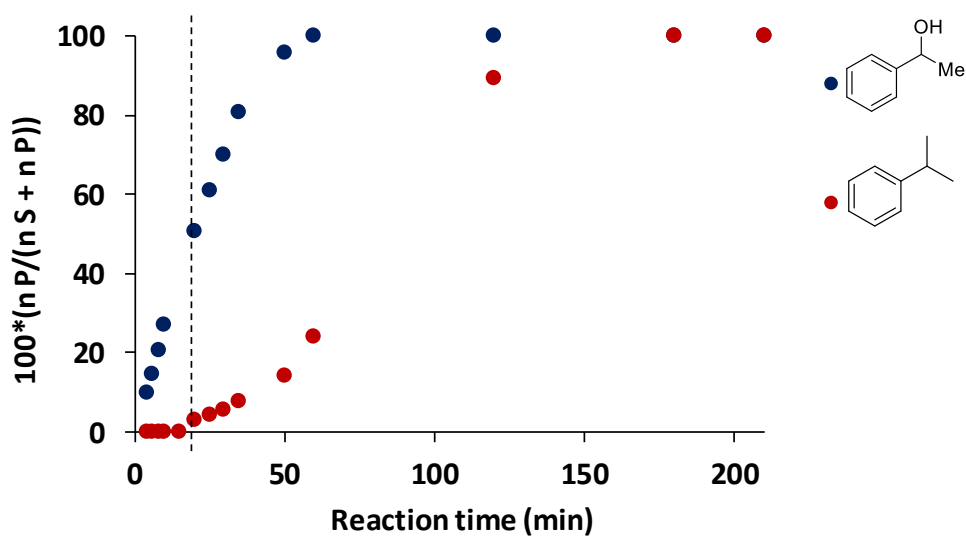
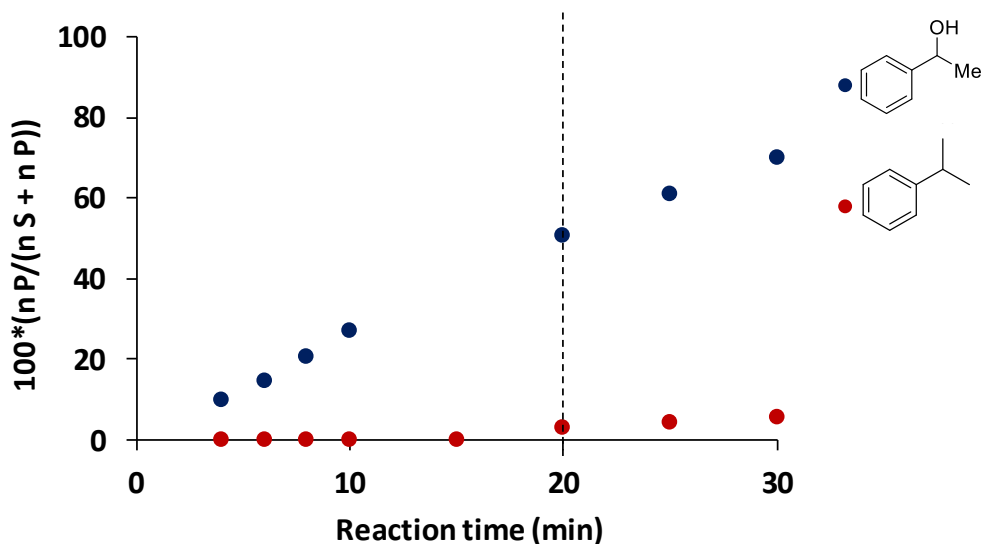
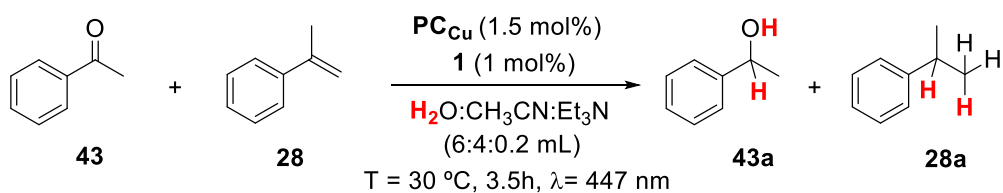


Figure S. 38. Monitoring of the competition between substrates **43** and **28** in the catalytic conditions. Top: yield during the first 30 minutes of irradiation, it can be seen that the reduction of substrate **28** starts even when **43** has not been totally reduced; bottom, all the reaction time monitorization (3.5 hours). ^[a]Conditions: **1** (1 mol%), PCu (1.5mol%), Substrate A + B (16.5 mM), A:B (1:1), in $\text{H}_2\text{O}:\text{CH}_3\text{CN}:\text{Et}_3\text{N}$ (6:4:0.2 mL) irradiated (1 LED, 447 nm, $2.05 \cdot 10^{-3} \text{ mmol} \cdot \text{h} \cdot \text{v} \cdot \text{s}^{-1}$ photons) for 4 h at 25 °C under N_2 . ^[b] The plotted data is the ratio between the amount of the reduced product formed and the sum of the amount of the reduced product formed and the unconverted starting material. ^[c] The black dotted line indicates the point where substrate **28** starts reacting. Selectivity for ketone reduction 80% and for olefin reduction 20%.

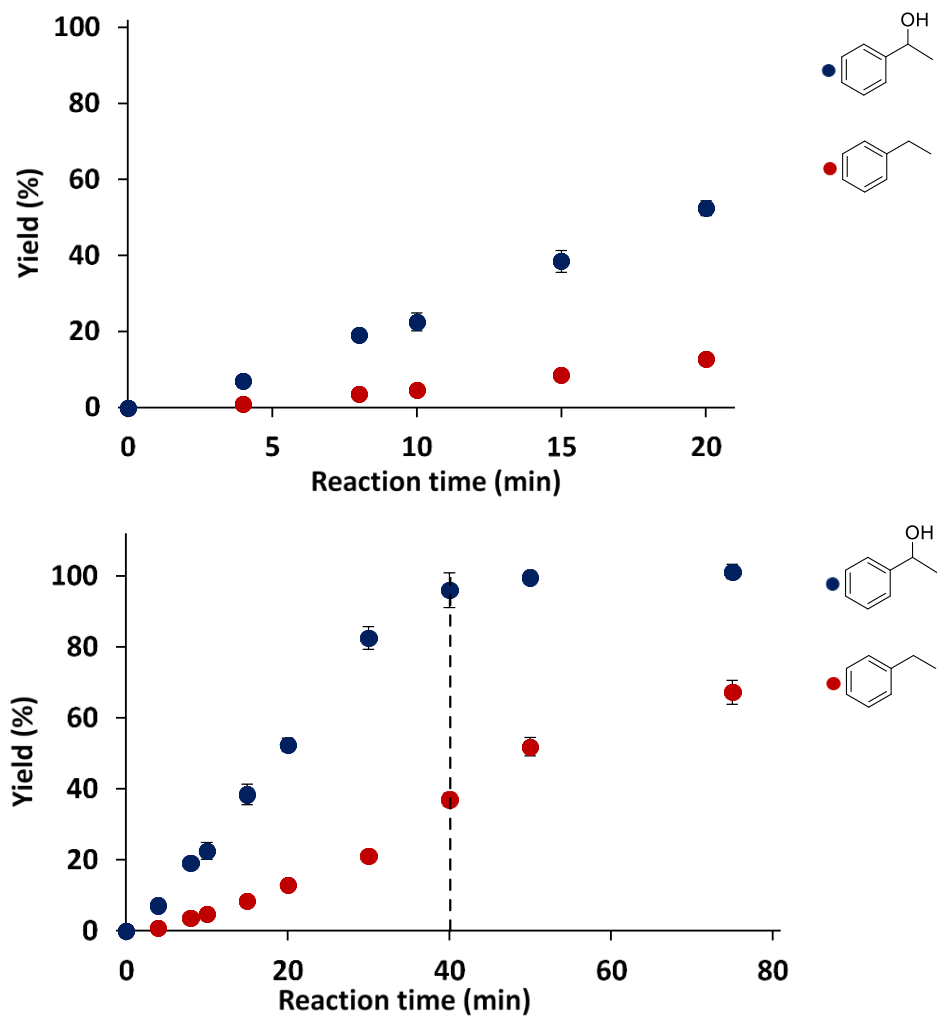
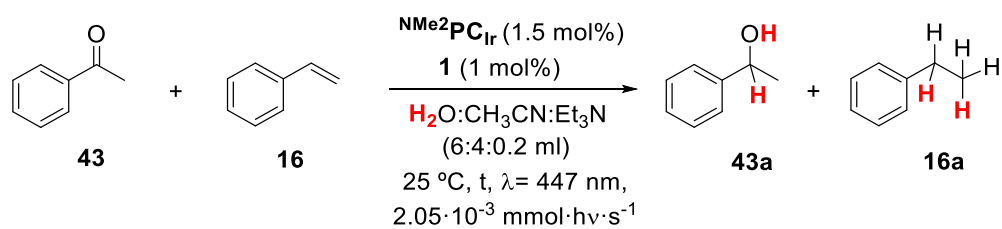


Figure S. 39. Monitoring of the competition between substrates **43** and **16**. Top: yield during the first 20 minutes of irradiation, it can be seen that the reduction of substrate **16** starts when **43** has not been totally reduced; bottom, all the reaction time monitoring (75 min). ^[a]Conditions: **1** (1 mol%), **NMe₂PCIr** (1.5 mol%), Substrate A + B (16.5 mM), A:B (1:1), in H₂O:CH₃CN:Et₃N (6:4:0.2 ml) irradiated (1 LED, 447 nm, 2.05 · 10⁻³ mmol · hv · s⁻¹ photons) for 75 min at 25 °C under N₂. ^[b] The plotted data is determined by GC analysis after workup and relative to a calibrated internal standard. ^[c] The black dotted line indicates the point where substrate **43** reaches full conversion. Selectivity: 72%.

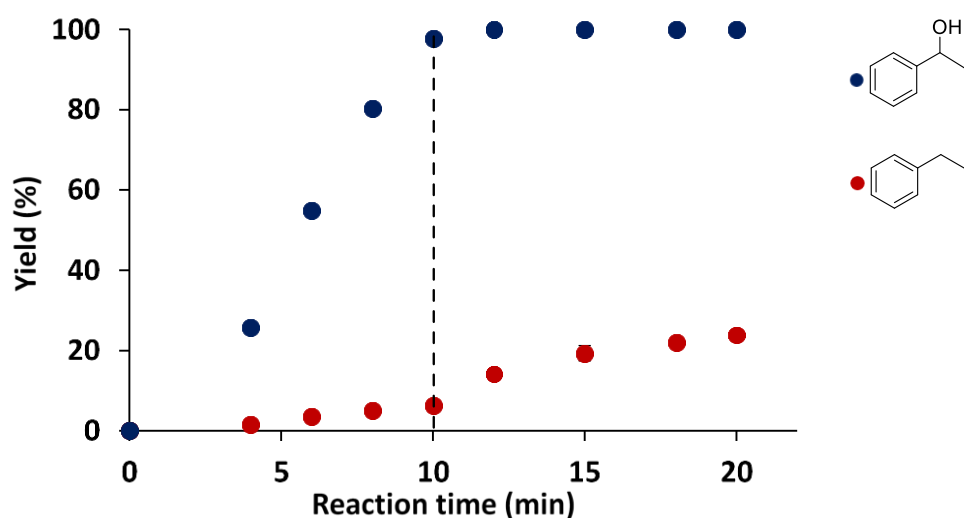
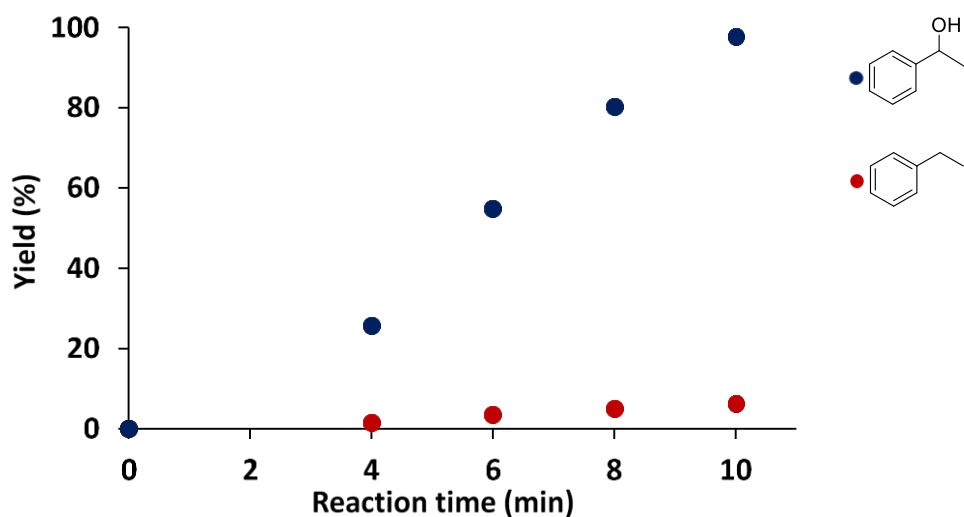
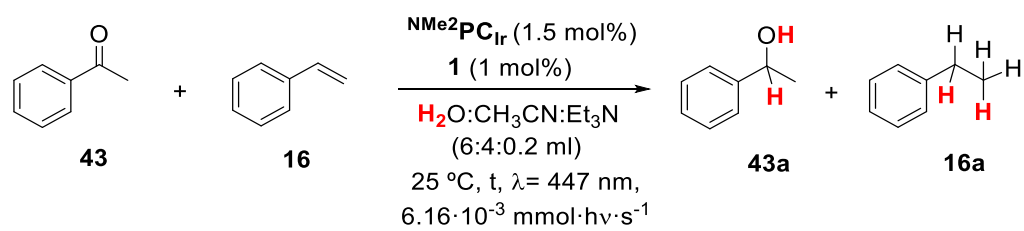


Figure S. 40. Monitoring of the competition between substrates **43** and **16**. Top: yield during the first 10 minutes of irradiation, it can be seen that the reduction of substrate **16** starts when **43** has not been totally reduced; bottom, all the reaction time monitoring (20 min) ^[a]Conditions: **1** (1 mol%), **NMe₂PCIr** (1.5 mol%), Substrate A + B (16.5 mM), A:B (1:1), in H₂O:CH₃CN:Et₃N (6:4:0.2 ml) irradiated (3 LEDs, 447 nm, 6.16 · 10⁻³ mmol · hv · s⁻¹ photons) for 20 min at 25 °C under N₂. ^[b] The plotted data is determined by GC analysis after workup and relative to a calibrated internal standard. ^[c]The black dotted line indicates the point where substrate **43** reaches full conversion. Selectivity: 88%.

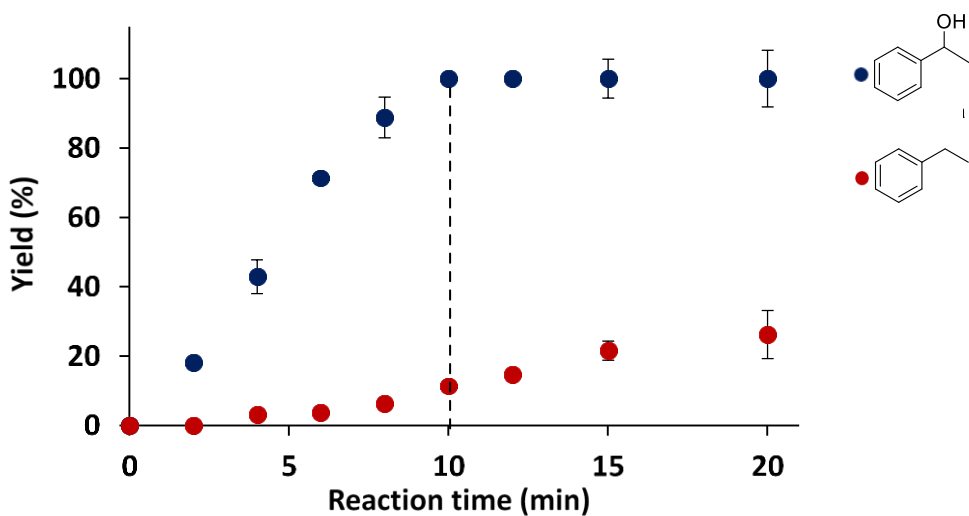
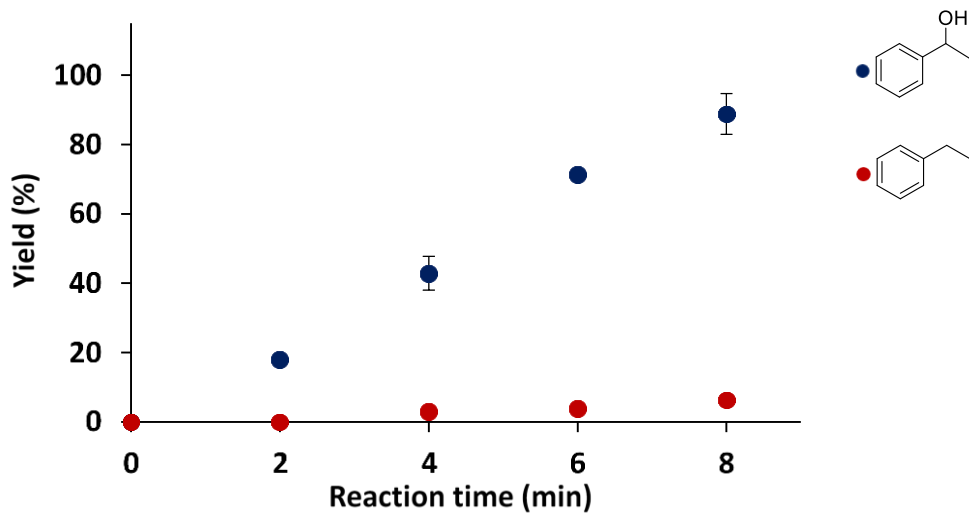
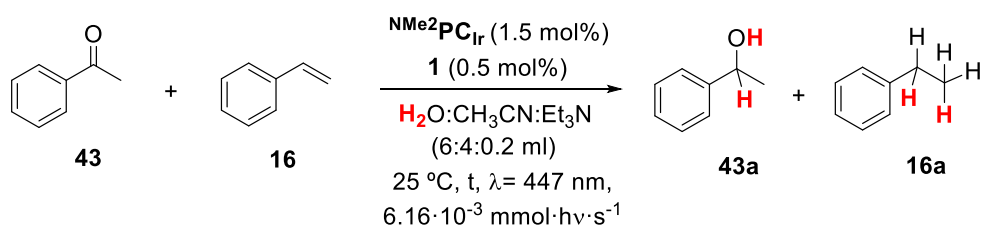


Figure S. 41. Monitoring of the competition between substrates **43** and **16**. Top: yield during the first 8 minutes of irradiation, it can be seen that the reduction of substrate **16** starts when **43** has not been totally reduced; bottom, all the reaction time monitorization (20 min). ^[a]Conditions: **1** (0.5 mol%), NMe_2PCIr (1.5 mol%), Substrate A + B (16.5 mM), A:B (1:1), in $\text{H}_2\text{O}:\text{CH}_3\text{CN}:\text{Et}_3\text{N}$ (6:4:0.2 ml) irradiated (3 LEDs, 447 nm, $6.16 \cdot 10^{-3} \text{ mmol} \cdot \text{hv} \cdot \text{s}^{-1}$ photons) for 20 min at 25 °C under N_2 . ^[b] The plotted data is determined by GC analysis after workup and relative to a calibrated internal standard. ^[c]The black dotted line indicates the point where substrate **43** reaches full conversion. Selectivity: 90%.

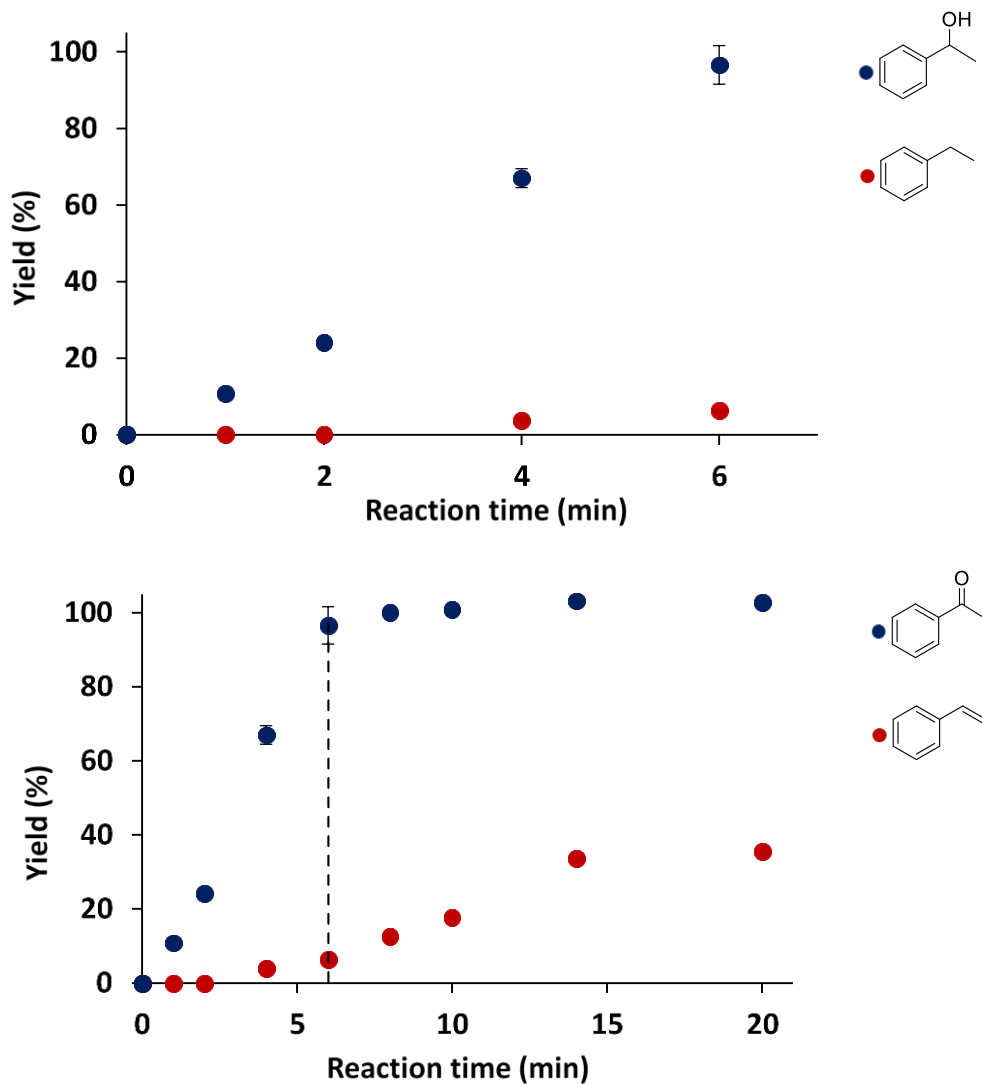
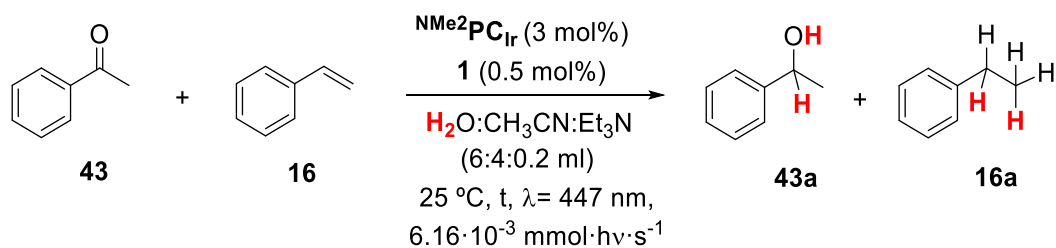


Figure S. 42. Monitoring of the competition between substrates **43** and **16**. Top: yield during the first 6 minutes of irradiation, it can be seen that the reduction of substrate **16** starts when **43** has not been totally reduced; bottom, all the reaction time monitoring (20 min).^[a] Conditions: **1** (0.5 mol%), **NMe₂PCIr** (3 mol%), Substrate A + B (16.5 mM), A:B (1:1), in H₂O:CH₃CN:Et₃N (6:4:0.2 ml) irradiated (3 LEDs, 447 nm, 6.16 · 10⁻³ mmol · hv · s⁻¹ photons) for 20 min at 25 °C under N₂.^[b] The plotted data is determined by GC analysis after workup and relative to a calibrated internal standard.^[c] The black dotted line indicates the point where substrate **43** reaches full conversion. Selectivity: 94%.

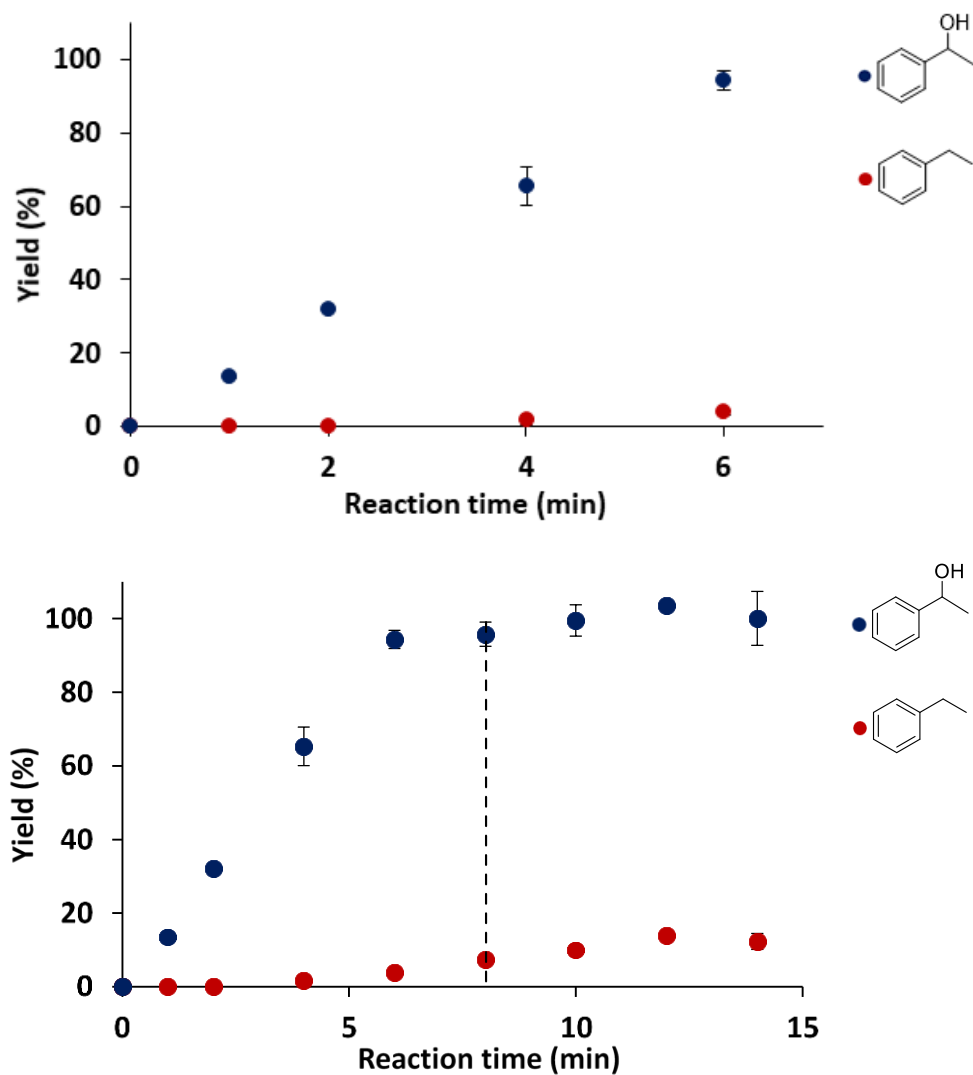
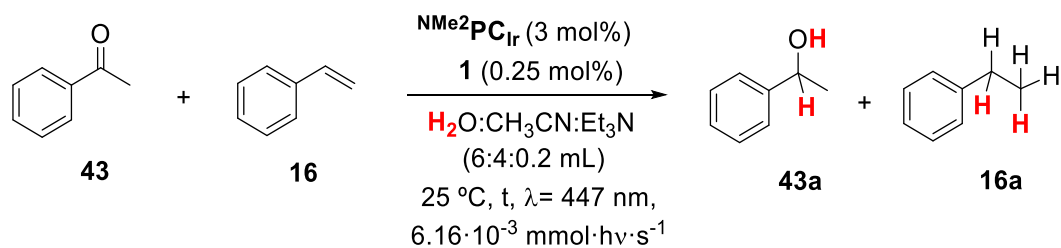


Figure S. 43. Monitoring of the competition between substrates **43** and **16**. Top: yield during the first 6 minutes of irradiation, it can be seen that the reduction of substrate **16** starts when **43** has not been totally reduced; bottom, all the reaction time monitoring (14 min) ^[a]Conditions: **1** (0.25 mol%), **NMe₂PCIr** (3 mol%), Substrate A + B (16.5 mM), A:B (1:1), in H₂O:CH₃CN:Et₃N (6:4:0.2 ml) irradiated (3 LEDs, 447 nm, 6.16 · 10⁻³ mmol · hv · s⁻¹ photons) for 14 min at 25 °C under N₂. ^[b] The plotted data is determined by GC analysis after workup and relative to a calibrated internal standard. ^[c]The black dotted line indicates the point where substrate **43** reaches full conversion. Selectivity: 96%.

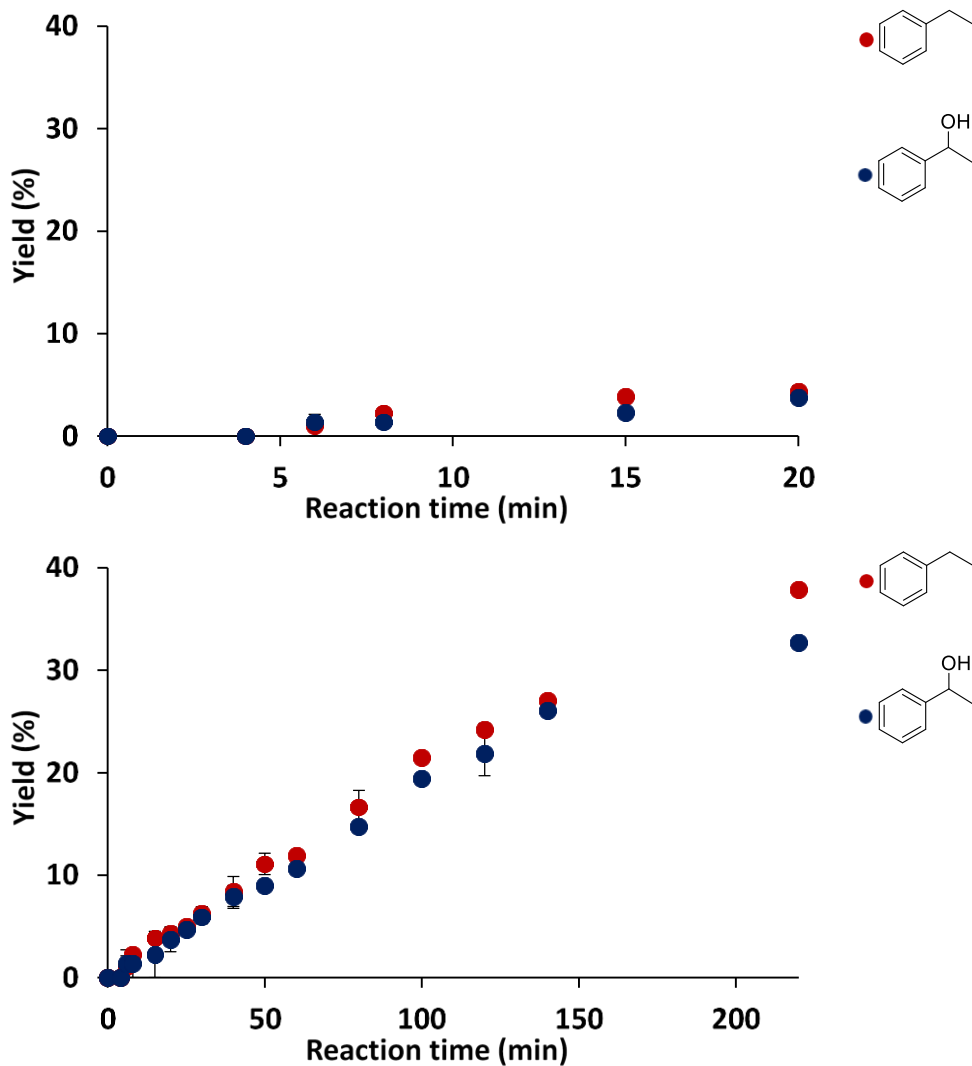
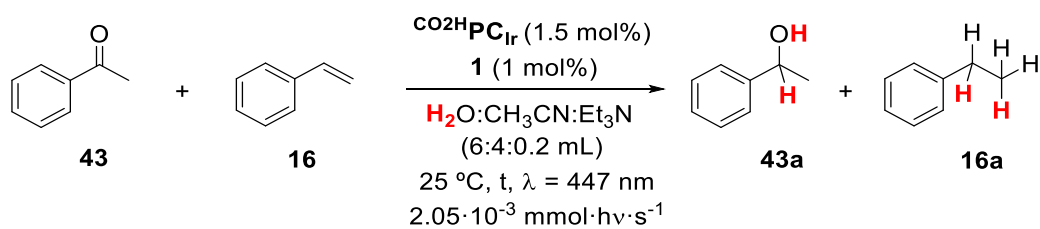


Figure S. 44. Monitoring of the competition between substrates **43** and **16**. Top: yield during the first 20 minutes of irradiation, it can be seen that the reduction of substrate **43** starts when **16** has not been totally reduced; bottom, all the reaction time monitoring (220 min). ^[a]Conditions: **1** (1 mol%), CO_2HPCIr (1.5 mol%), Substrate A + B (16.5 mM), A:B (1:1), in $\text{H}_2\text{O}:\text{CH}_3\text{CN}:\text{Et}_3\text{N}$ (6:4:0.2 ml) irradiated (1 LED, 447 nm, $2.05 \cdot 10^{-3} \text{ mmol} \cdot \text{h}\nu \cdot \text{s}^{-1}$ photons) for 220 min at 25 °C under N_2 . ^[b] The plotted data is determined by GC analysis after workup and relative to a calibrated internal standard. Selectivity (taken at the end): 54%.

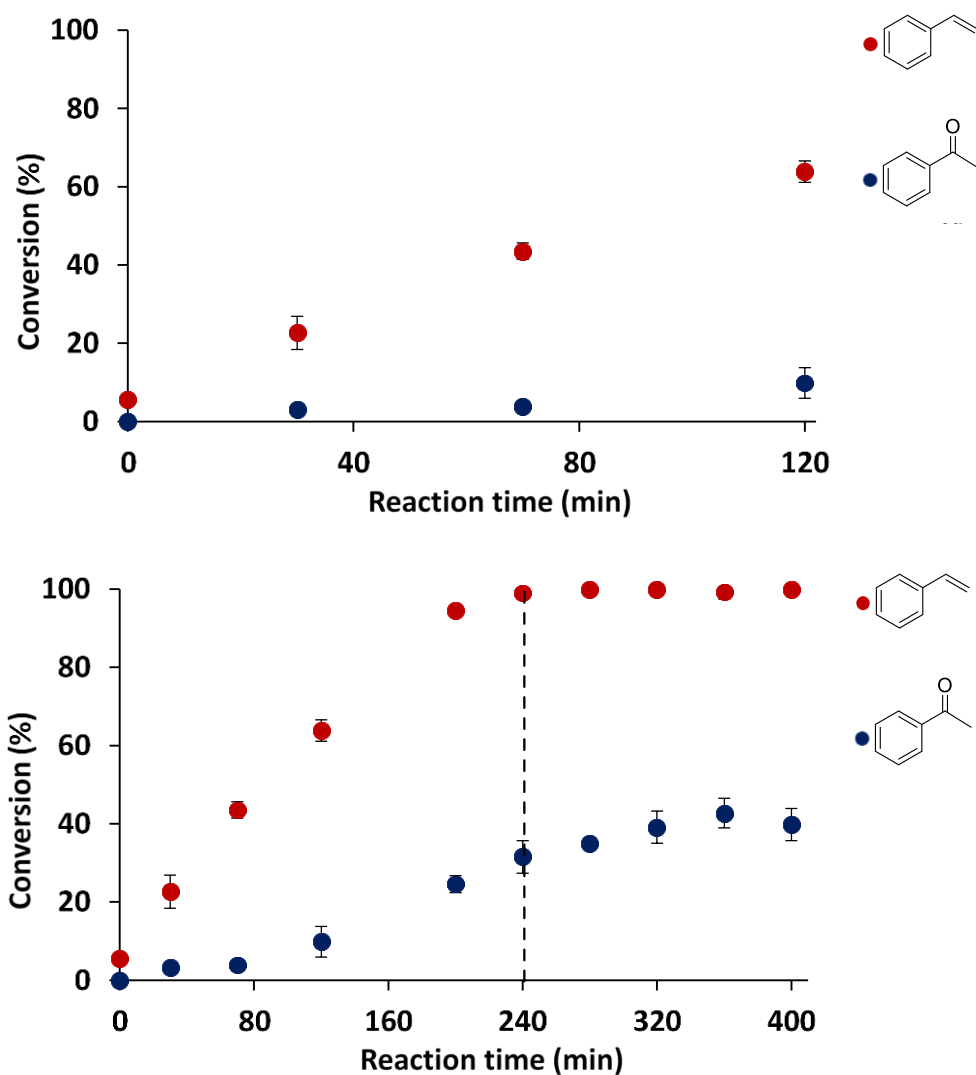
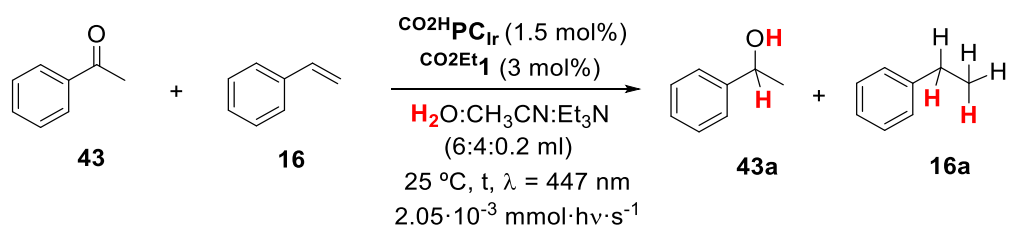


Figure S. 46. Monitoring of the competition between substrates **43** and **16**. Top: yield during the first 120 minutes of irradiation, it can be seen that the reduction of substrate **43** starts when **16** has not been totally reduced; bottom, all the reaction time monitorization (400 min). ^[a]Conditions: $\text{CO}_2\text{Et1}$ (3 mol%), CO_2HPCIr (1.5 mol%), Substrate A + B (16.5 mM), A:B (1:1), in $\text{H}_2\text{O}:\text{CH}_3\text{CN}:\text{Et}_3\text{N}$ (6:4:0.2 ml) irradiated (1 LED, 447 nm, $2.05 \cdot 10^{-3}$ mmol·hv·s⁻¹ photons) for 400 min at 25 °C under N_2 . ^[b] The plotted data is determined by GC analysis after workup and relative to a calibrated internal standard. ^[c] The black dotted line indicates the point where substrate **16** reaches full conversion. Selectivity: 76%.

15. Computational studies of the reduction potential of selected aromatic olefins

DFT calculations for the one electron reduction of selected aromatic olefins and the one electron reduction of their benzylic radicals generated by first HAT with the [Co-H] were calculated using the Gaussian09 program.^[26] Geometry optimizations were performed in the unrestricted spin formalism, with the B3LYP hybrid exchange-correlation functional^[27-29] and the standard 6-31G* 6d basis set for all atoms. An extra quadratic convergent SCF step was added when the first-order SCF did not converge (“scf=xqc” keyword). The solvation effect of water was introduced in geometry optimizations and energy through the SMD polarizable continuum model PCM-SMD.^[30-32] Dispersion effects were also included using the Grimme D₂ correction.^[33] The geometries have been edited with the Chemcraft program.

The located stationary points were characterized by analytical frequency calculations at the same level of theory than geometry optimizations. Gibbs energy values (G) were obtained by including thermal, solvation and Grimme corrections to the potential energy computed with the 6-311+G** 6d basis set on equilibrium geometries:

$$G = E_{6-311+G^{**}} + G_{\text{corr.}} + G_{\text{solv.}} + E_{\text{disp.}} \quad (1)$$

where the thermal correction ($G_{\text{corr.}}$) was obtained from gas phase analytical Hessians calculations at 298.15 K, the solvation energy ($G_{\text{solv.}}$) was calculated as the difference of the total free energy in gas phase and in water at the same level of theory and geometry and $E_{\text{disp.}}$ is the dispersion correction.

- Redox reactions

The standard one electron redox potentials relative to the SHE electrode were calculated by:

$$E^{\circ} = -\frac{\Delta G^{\circ} - \Delta G_{\text{SHE}}}{F} \quad (2)$$

where ΔG° is the standard free energy change associated with the reduction reaction, F is the Faraday constant (23.061 kcal·mol⁻¹·V⁻¹) and ΔG_{SHE} is the free energy change associated with the proton reduction to H₂ (-4.28 V). The ΔG_{SHE} value was derived using the Fermi-Dirac statistics for the treatment of electron thermodynamics.^[34]

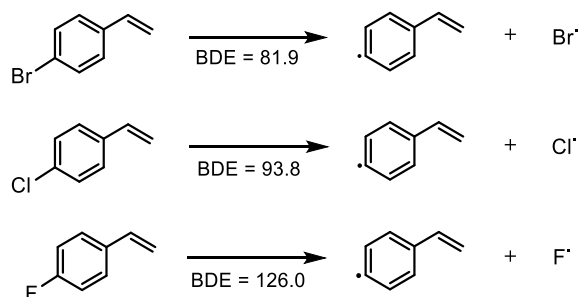


Figure S. 47. DFT bond dissociation energies for the selected substrates. All energies are in kcal·mol⁻¹.

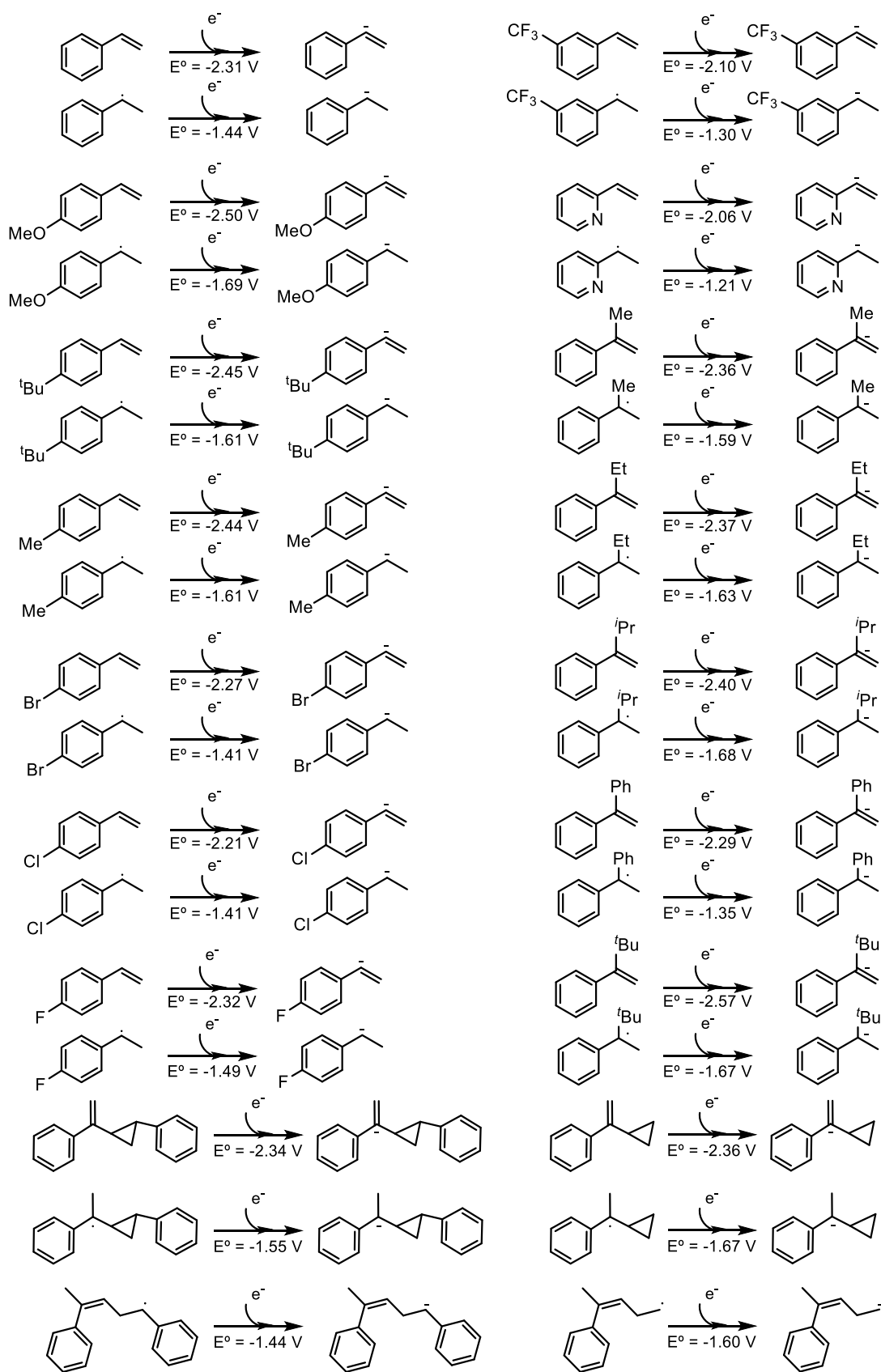


Figure S. 48. DFT calculated redox potentials for the above reduction processes derived from the selected substrates: one electron reduction of the olefin, and one electron reduction of the benzylic radical. All the potentials are referred to SCE.

Benzylic radicals derived from radical clocks

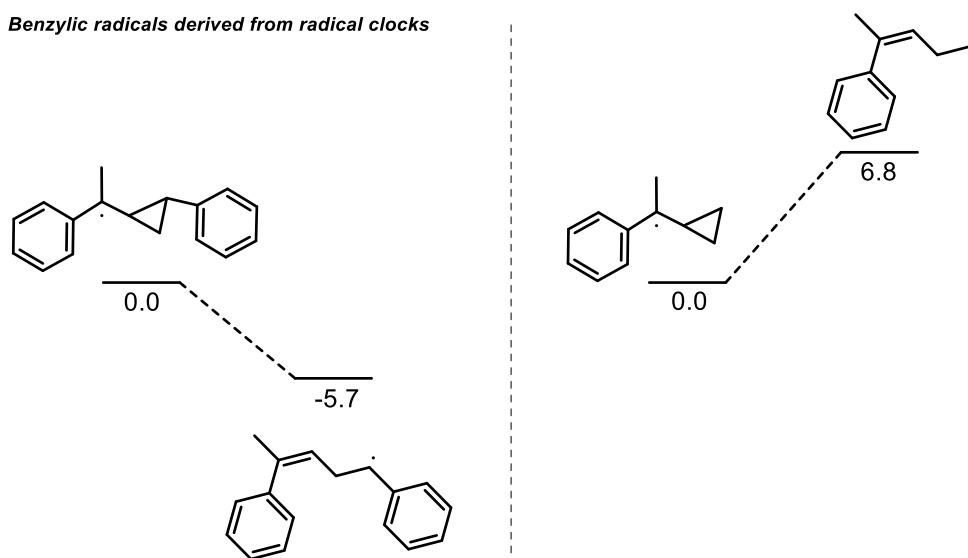


Figure S. 49. DFT calculated thermodynamic values for the reduced ring-opened and ring-retention products for the represented radical clocks.

16. NMR full characterization of the deuterium labelling mechanistic studies

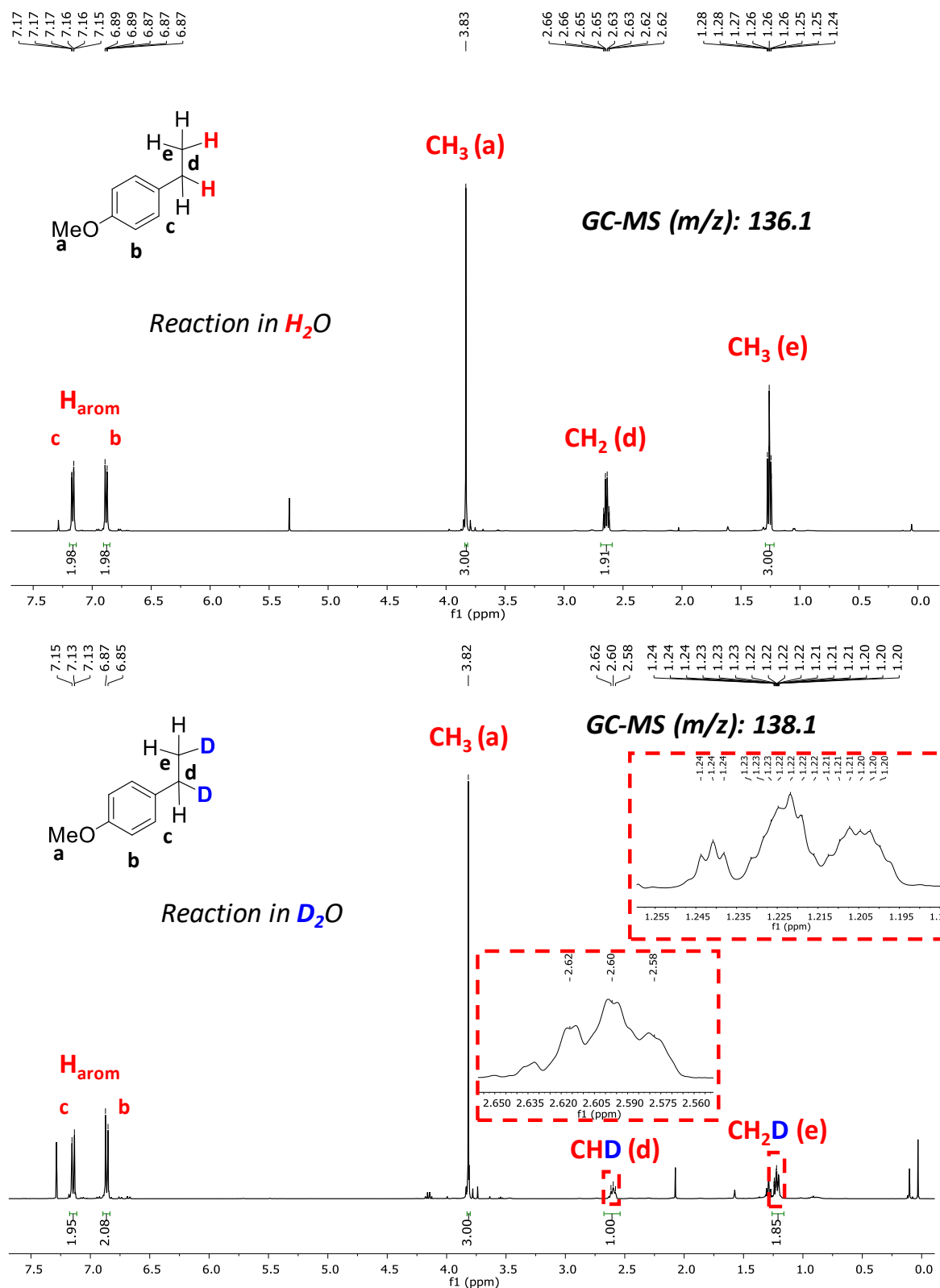


Figure S. 50. 1H -NMR spectrum ($CDCl_3$, 400 MHz, 300 K) of the isolated products **17a** and **[D]-17a** using H_2O (Top) or D_2O (99.9 % in deuterium) (Bottom) in the solvent mixture, respectively. Conditions: **1** (3 mol%), **PC_{Cu}** (3 mol%), substrate (0.087 mmol, 8.7 mM) in H_2O (or D_2O): CH_3CN : Et_3N (6:4:0.2 mL) irradiated at $\lambda = 447$ nm and 15 °C for 5h, under N_2 . Inset: amplification of the area of the $-CHD$ and the $-CH_2D$.

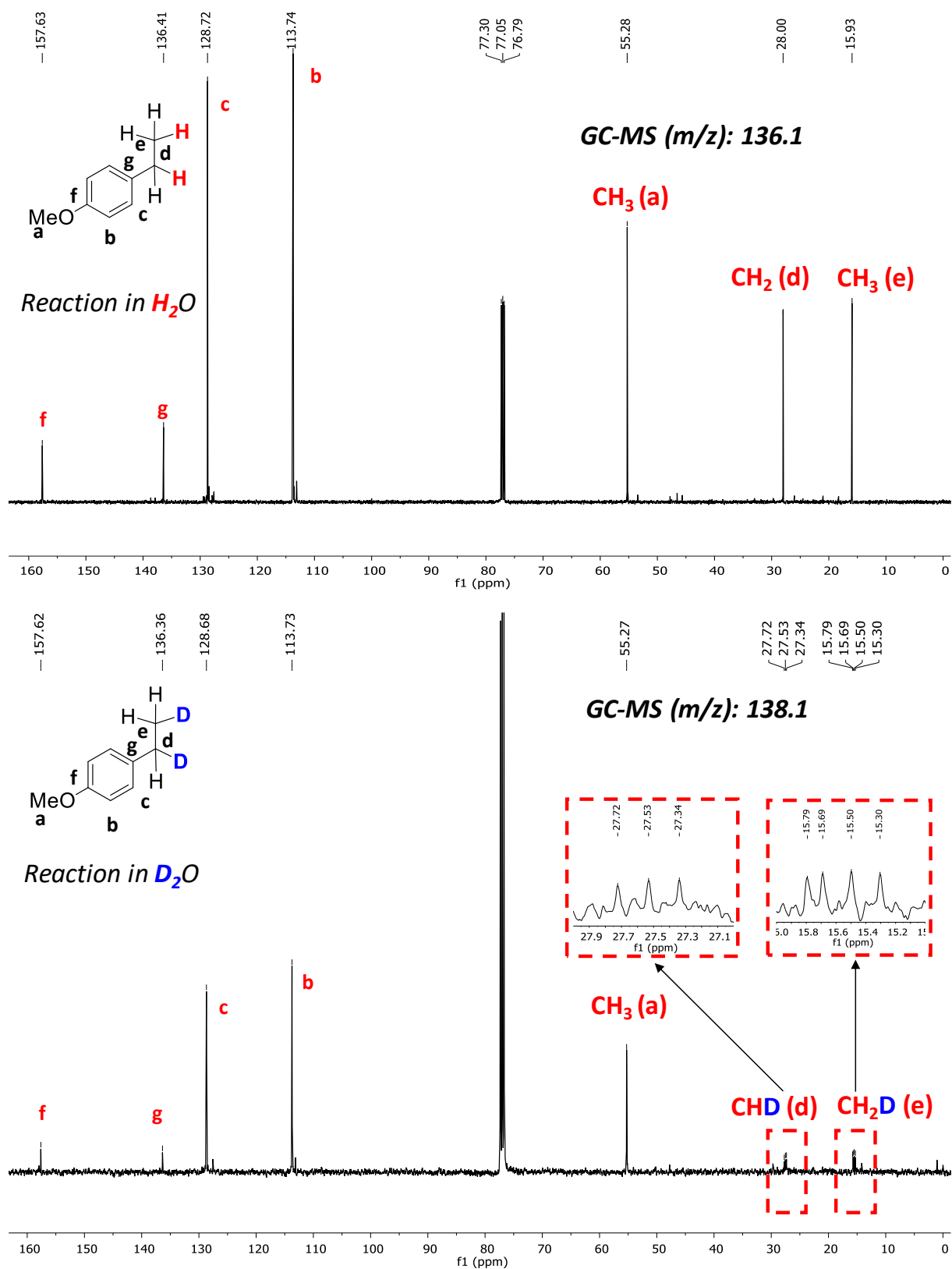


Figure S. 51. $^{13}C\{^1H\}$ -NMR spectrum (CDCl₃, 100.6 MHz, 300 K) of the isolated products **17a** and **[D]-17a** using H₂O (Top) or D₂O (99.9 % in deuterium) (Bottom) in the solvent mixture, respectively. Conditions: **1** (3 mol%), PCu (3 mol%), substrate (0.087 mmol, 8.7 mM) in H₂O (or D₂O):CH₃CN:Et₃N (6:4:0.2 mL) irradiated at $\lambda = 447$ nm and 15 °C for 5h, under N₂. Inset: amplification of the area of the –CHD and –CH₂D.

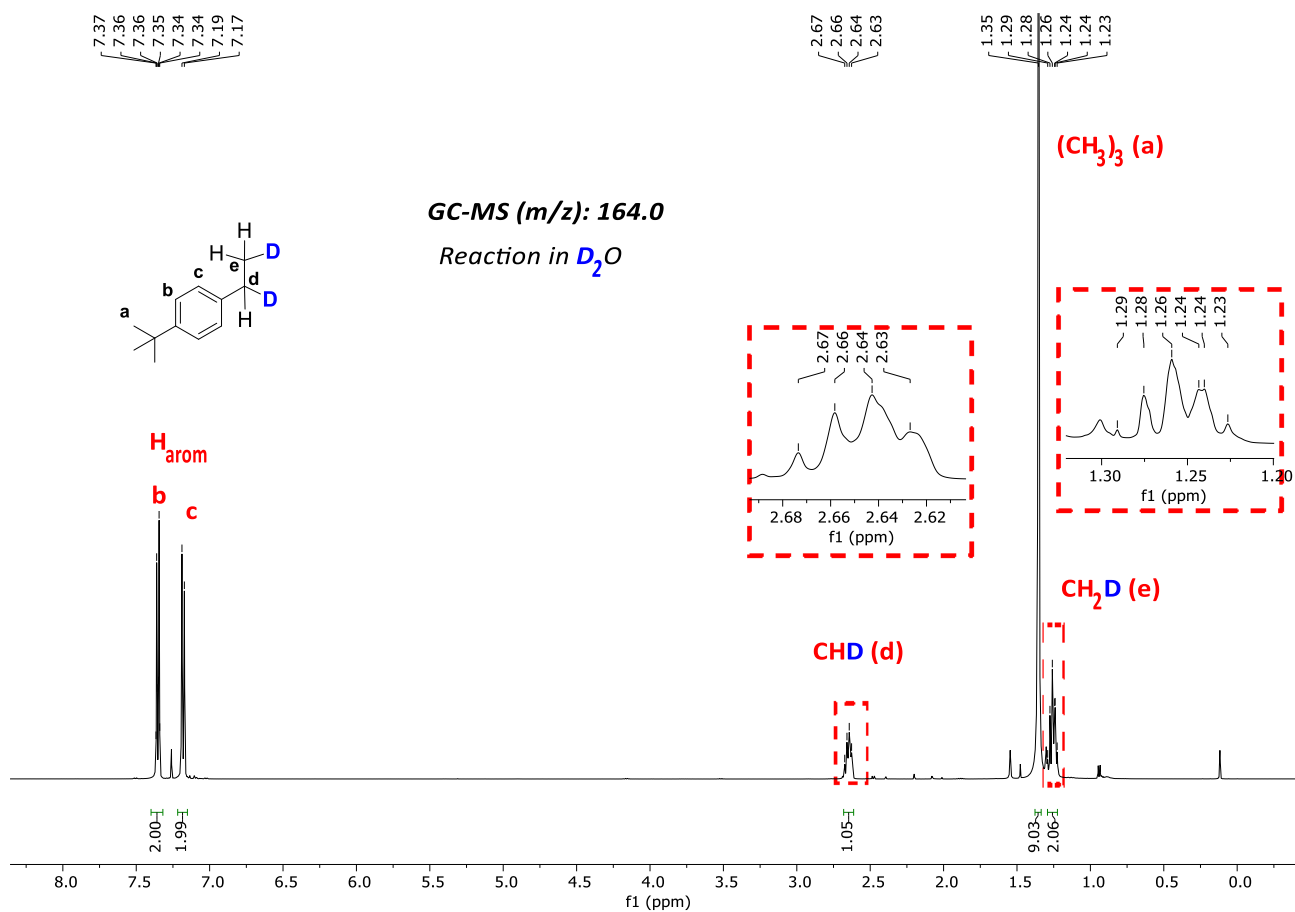


Figure S. 52. 1H -NMR spectra ($CDCl_3$, 400 MHz, 300 K) of the isolated products **18a** and **[D]-18a** using H_2O (top) or D_2O (99.9% in deuterium) (bottom) in the solvent mixture, respectively. Conditions: **1** (3 mol%), **PCu** (3 mol%), substrate (0.087 mmol, 8.7 mM) in H_2O (or D_2O): CH_3CN : Et_3N (6:4:0.2 ml) irradiated at $\lambda = 447$ nm and 15 °C for 5 h, under N_2 . Inset: amplification of the area of the $-CHD$ and the $-CH_2D$.

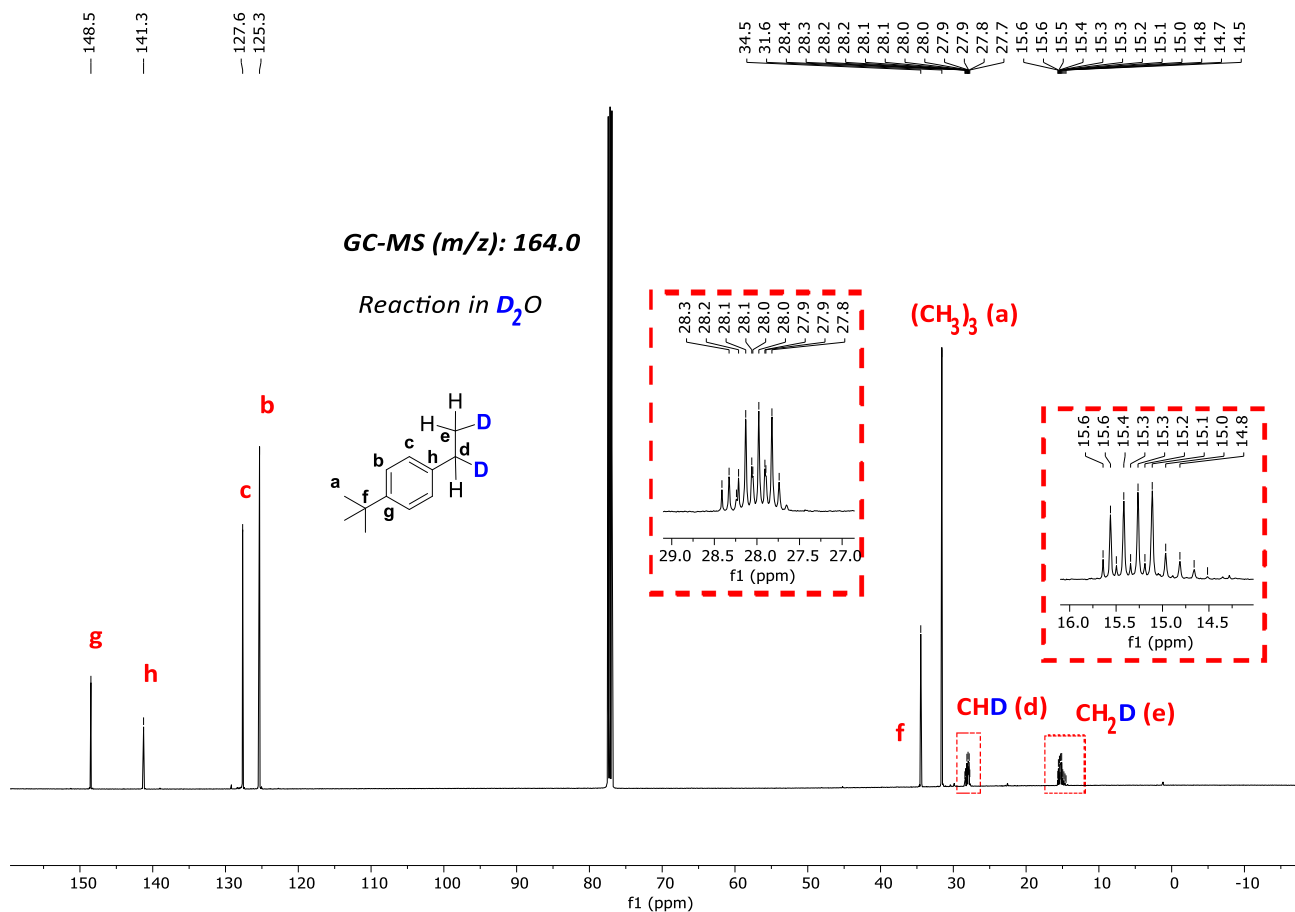


Figure S. 53. $^{13}C\{^1H\}$ -NMR spectra ($CDCl_3$, 100.6 MHz, 300 K) of the isolated products **18a** and **[D]-18a** using H_2O (Top) or D_2O (99.9 % in deuterium) (Bottom) in the solvent mixture, respectively. Conditions: **1** (3 mol%), PCu (3 mol%), substrate (0.087 mmol, 8.7 mM) in H_2O (or D_2O): CH_3CN : Et_3N (6:4:0.2 ml) irradiated at $\lambda = 447$ nm and 15 °C for 5 h, under N_2 . Inset: amplification of the area of the $-CH_2D$ and $-CHD$ with the insertion of deuterium showing the triplet due to the C–D coupling.

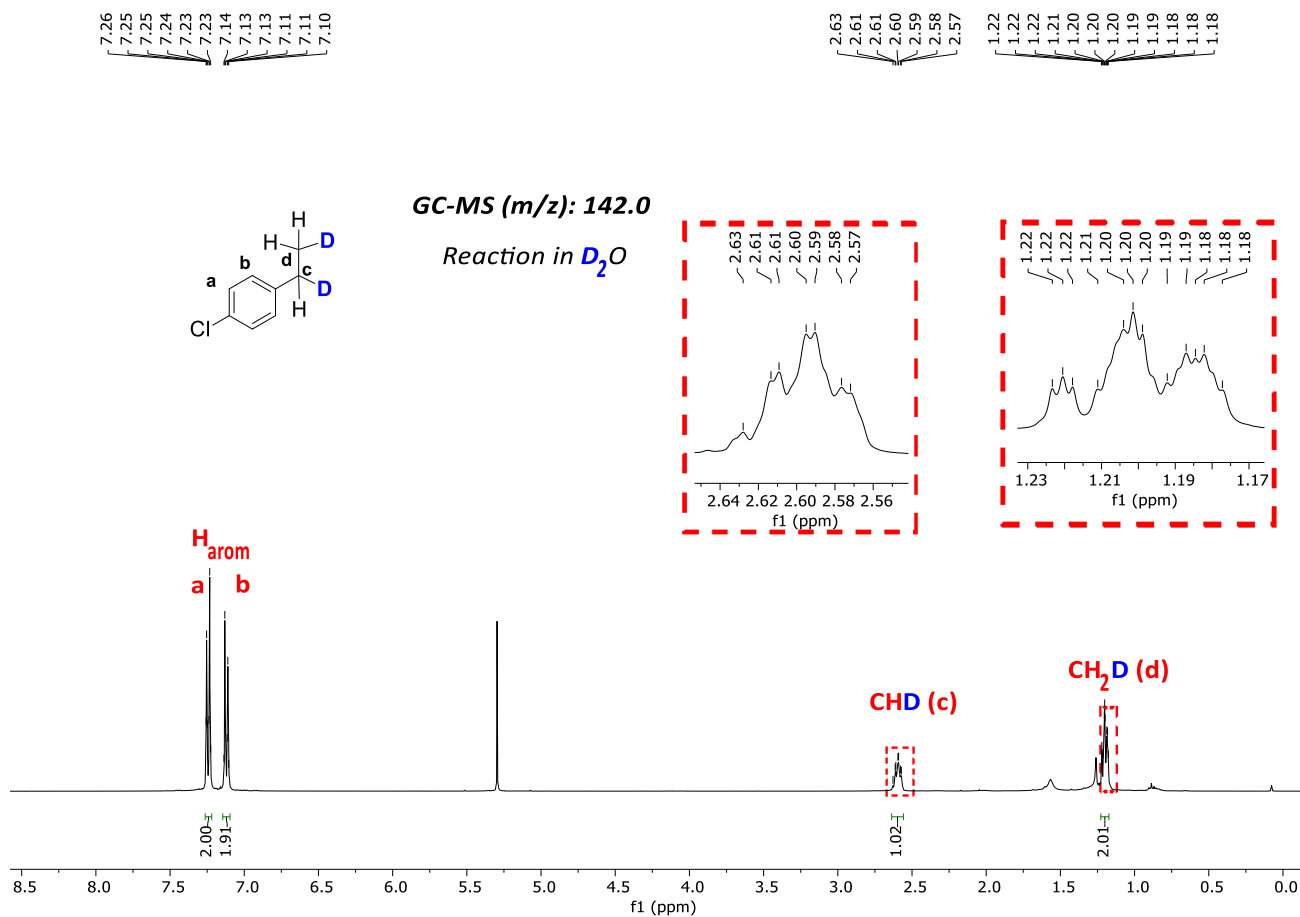


Figure S. 54. $^1\text{H-NMR}$ spectra (CDCl_3 , 400 MHz, 300 K) of the isolated products **23a** and **[D]-23a** using H_2O (top) or D_2O (99.9% in deuterium) (bottom) in the solvent mixture, respectively. Conditions: **1** (3 mol%), PCu (3 mol%), substrate (0.087 mmol, 8.7 mM) in H_2O (or D_2O): CH_3CN : Et_3N (6:4:0.2 ml) irradiated at $\lambda = 447$ nm and 15 °C for 5 h, under N_2 . Inset: amplification of the area of the $-\text{CHD}$ and the $-\text{CH}_2\text{D}$.

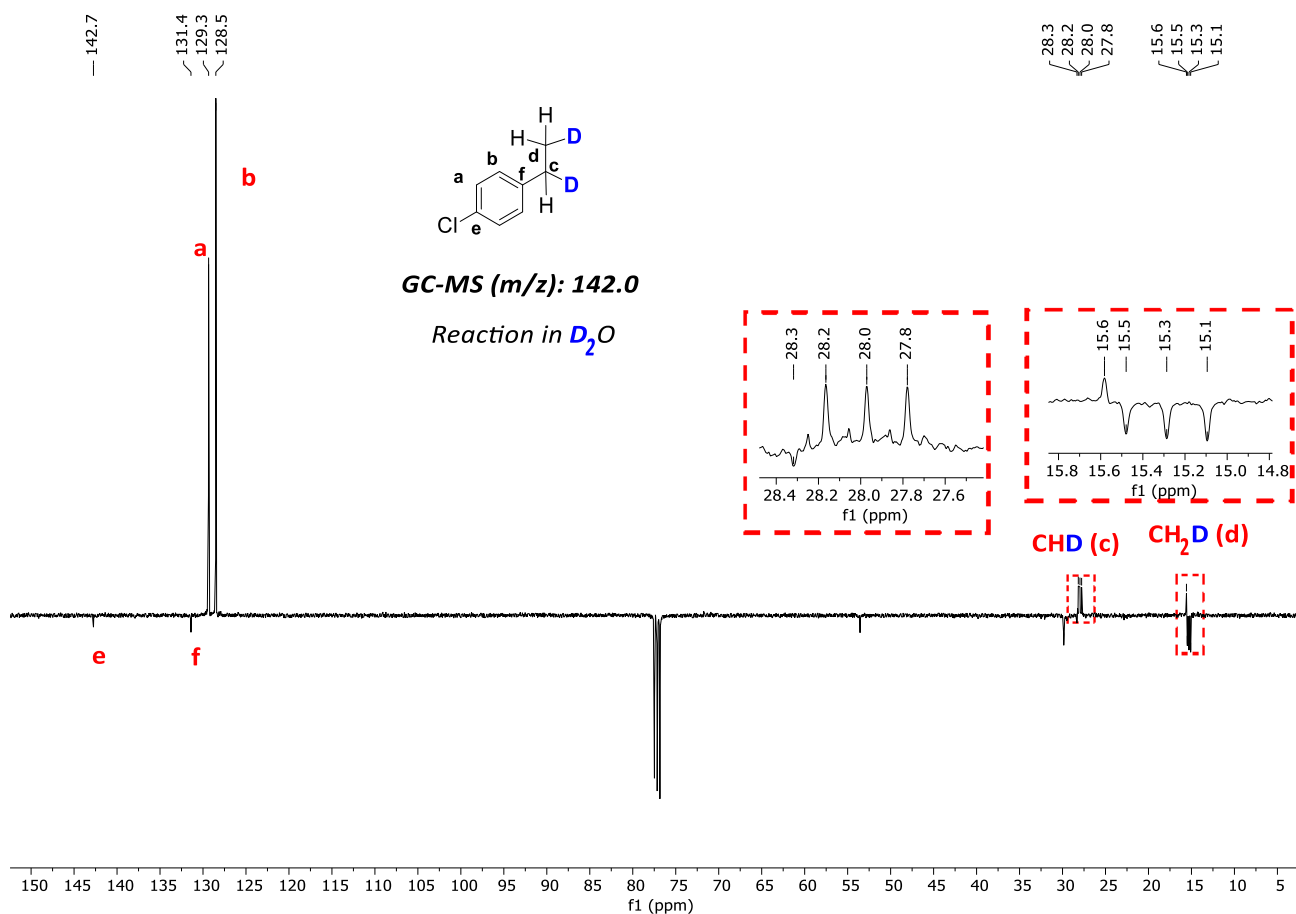


Figure S. 55. $^{13}C\{^1H\}$ -NMR and $^{13}C\{^1H\}$ -DEPTQ-135-NMR spectra ($CDCl_3$, 100.6 MHz, 300 K) of the isolated products **23a** and **[D]-23a** using H_2O (top) or D_2O (99.9 % in deuterium) (bottom) in the solvent mixture, respectively. Conditions: **1** (3 mol%), PCu (3 mol%), substrate (0.087 mmol, 8.7 mM) in H_2O (or D_2O): CH_3CN : Et_3N (6:4:0.2 ml) irradiated at $\lambda = 447$ nm and 15 °C for 5 h, under N_2 . Inset: amplification of the area of the $-CH_2D$ and $-CHD$ with the insertion of deuterium showing the triplet due to the C–D coupling.

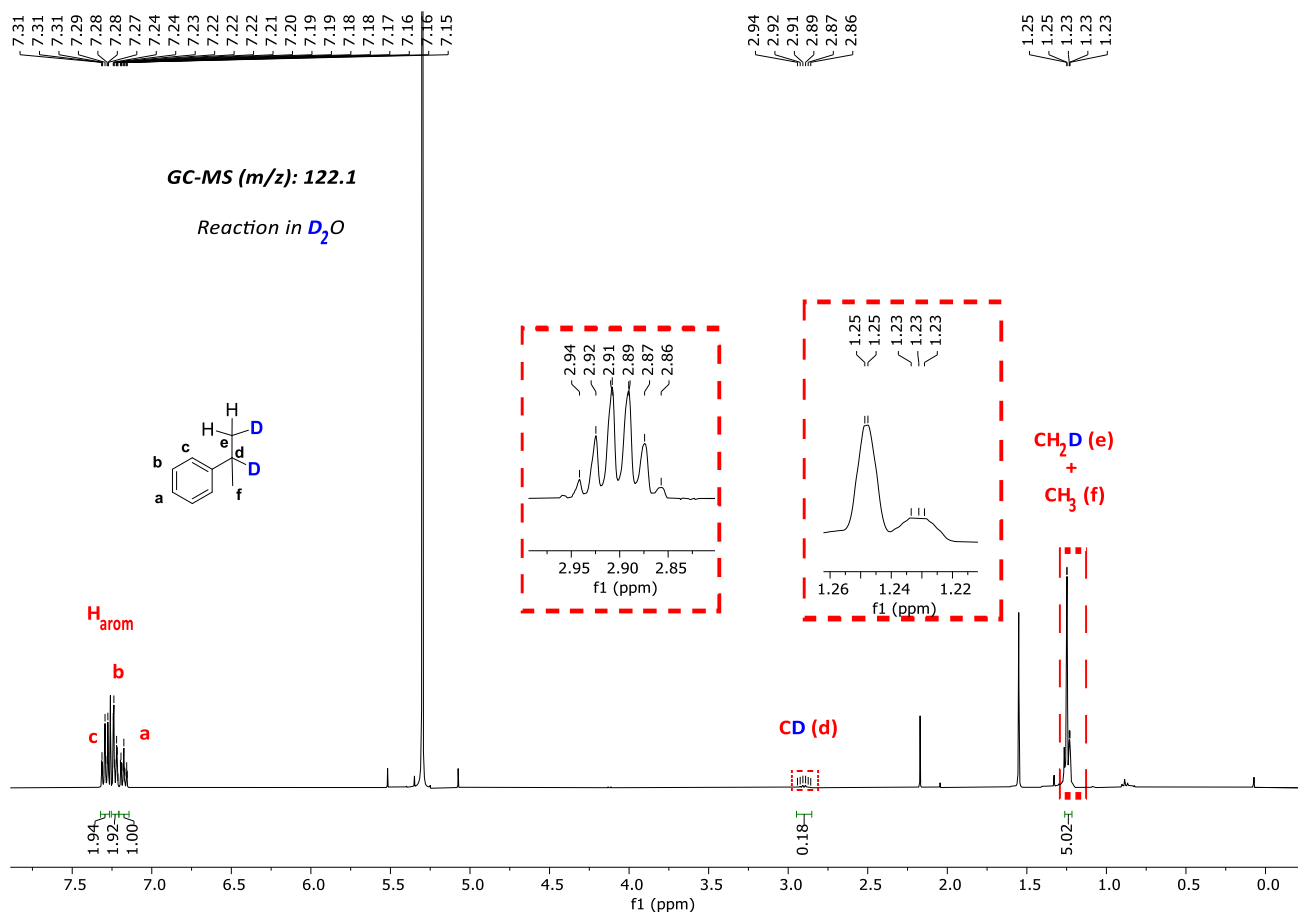


Figure S. 56. ¹H-NMR spectra (CDCl₃, 400 MHz, 300 K) of the isolated products **28a** and **[D]-28a** using H₂O (top) or D₂O (99.9 % in deuterium) (bottom) in the solvent mixture, respectively. Conditions: **1** (6 mol%), **PC**_{Cu} (6 mol%), substrate (0.044 mmol, 4.4 mM) in H₂O (or D₂O):CH₃CN:^tPr₂EtN (6:4:0.2 ml) irradiated at $\lambda = 447$ nm and -3 °C for 24 h, under N₂. Inset: amplification of the area of the -CD and the -CH₂D.

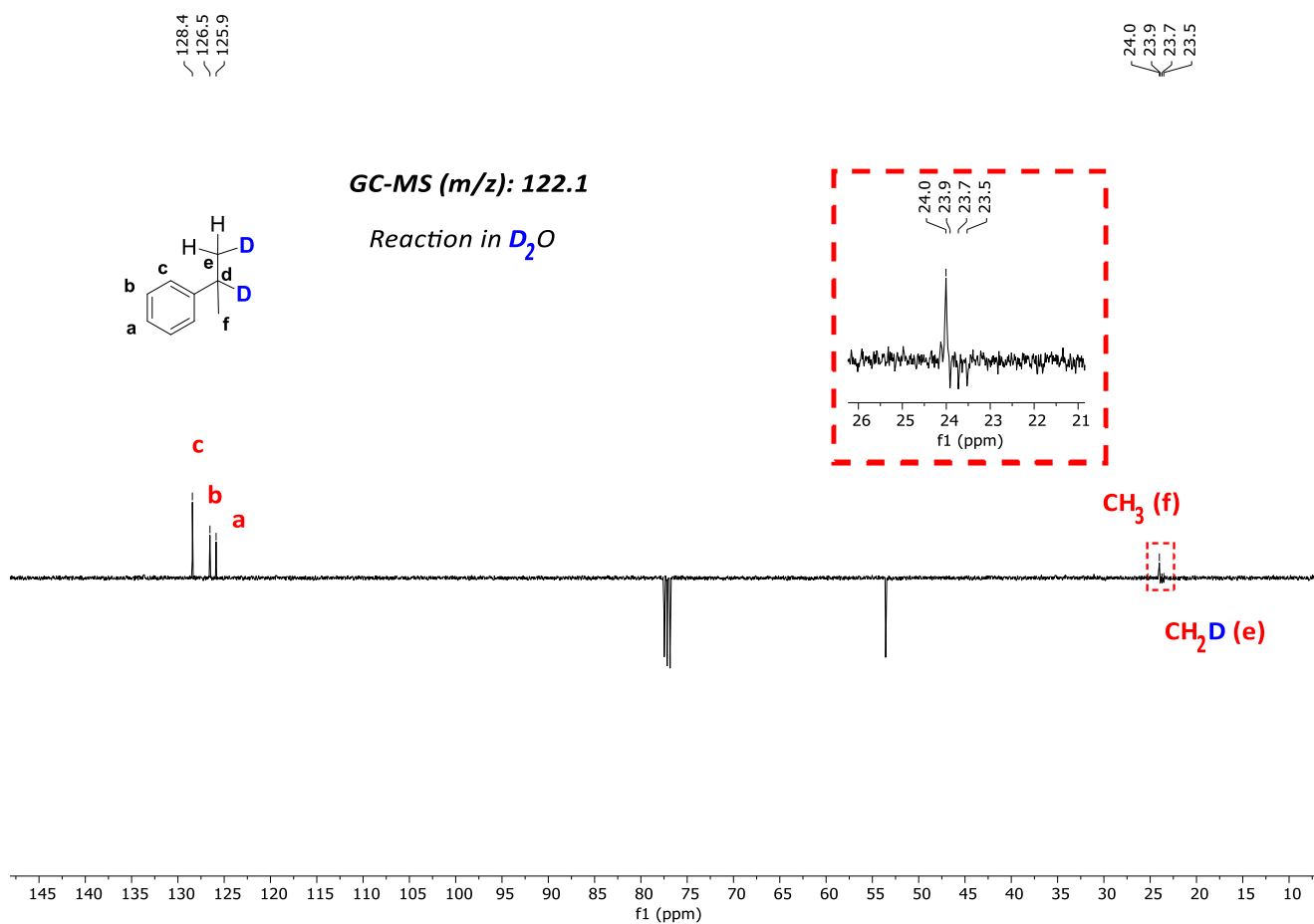


Figure S. 57. $^{13}C\{^1H\}$ -NMR and $^{13}C\{^1H\}$ -DEPT-135-NMR spectra ($CDCl_3$, 100.6 MHz, 300 K) of the isolated products **28a** and **[D]-28a** using H_2O (top) or D_2O (99.9 % in deuterium) (bottom) in the solvent mixture, respectively. Conditions: **1** (6 mol%), PCu (6 mol%), substrate (0.044 mmol, 4.4 mM) in H_2O (or D_2O): CH_3CN : iPr_2EtN (6:4:0.2 ml) irradiated at $\lambda = 447$ nm and -3 °C for 24 h, under N_2 . Inset: amplification of the area of the $-CH_2D$ with the insertion of deuterium showing the triplet due to the C–D coupling.

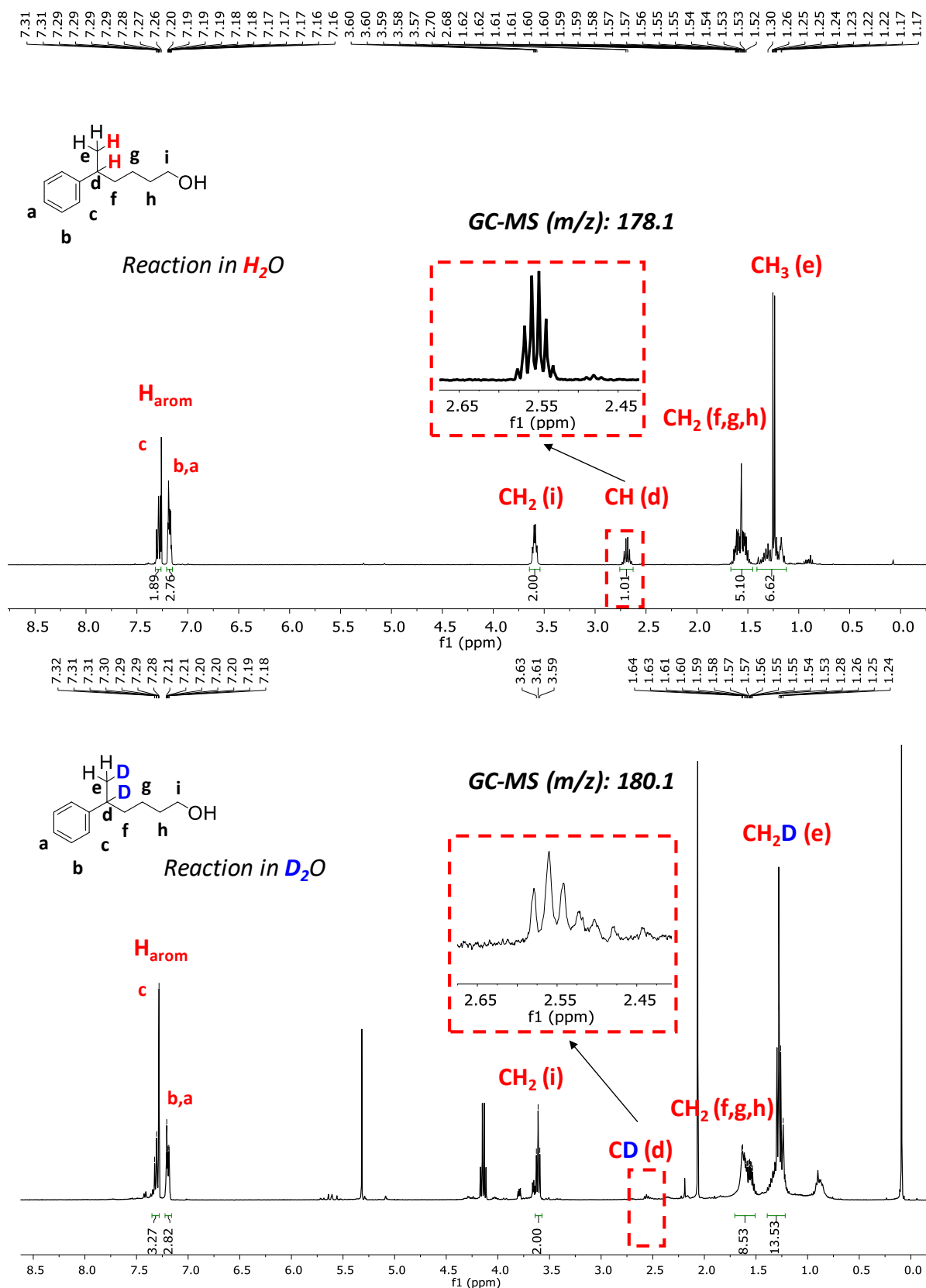


Figure S. 58. 1H -NMR spectrum ($CDCl_3$, 400 MHz, 300 K) of the isolated products **36a** and **[D]-36a** using H_2O (Top) or D_2O (99.9% in deuterium) (Bottom) in the solvent mixture, respectively. Conditions: **1** (6 mol%), **PCu** (6 mol%), substrate (0.044 mmol, 4.4 mM) in H_2O (or D_2O): CH_3CN : Pr_2EtN (6:4:0.2 mL) irradiated at $\lambda = 447$ nm and -3 °C for 24h, under N_2 . Inset: amplification of the area of the $-CH$ vs $-CD$.

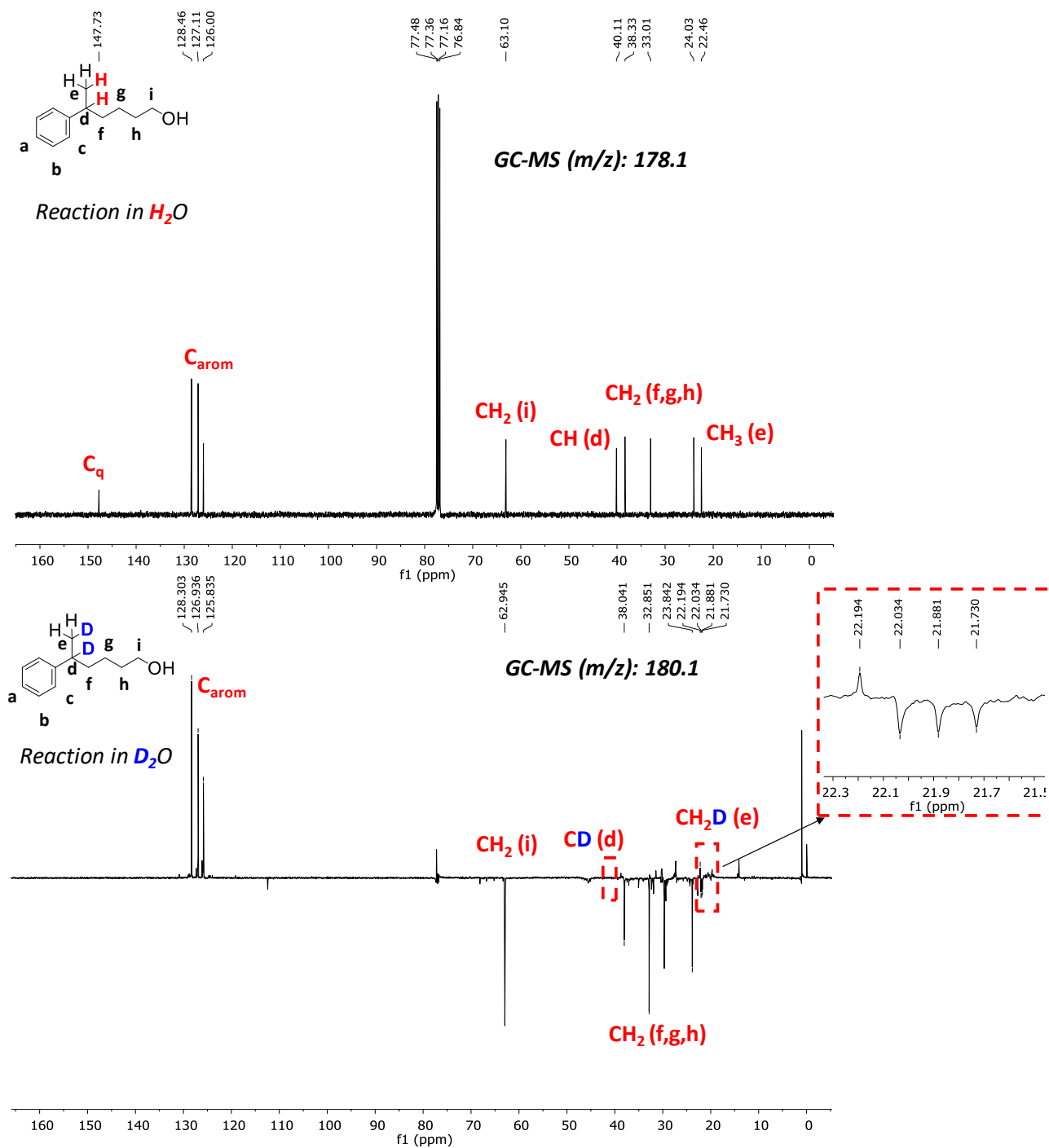


Figure S. 59. $^{13}\text{C}\{^1\text{H}\}$ -NMR and $^{13}\text{C}\{^1\text{H}\}$ -DEPT-135-NMR spectrum (CDCl_3 , 100.6 MHz, 300 K) of the isolated products **36a** and **[D]-36a**, using H_2O (Top) or D_2O (99.9 % in deuterium) (Bottom) in the solvent mixture, respectively. Conditions: **1** (6 mol%), PCu (6 mol%), substrate (0.044 mmol, 4.4 mM) in H_2O (or D_2O): CH_3CN : Pr_2EtN (6:4:0.2 mL) irradiated at $\lambda = 447$ nm and -3°C for 24h, under N_2 . Inset: amplification of the area of the $-\text{CH}_2\text{D}$ with the insertion of deuterium showing the triplet due to the C-D coupling.

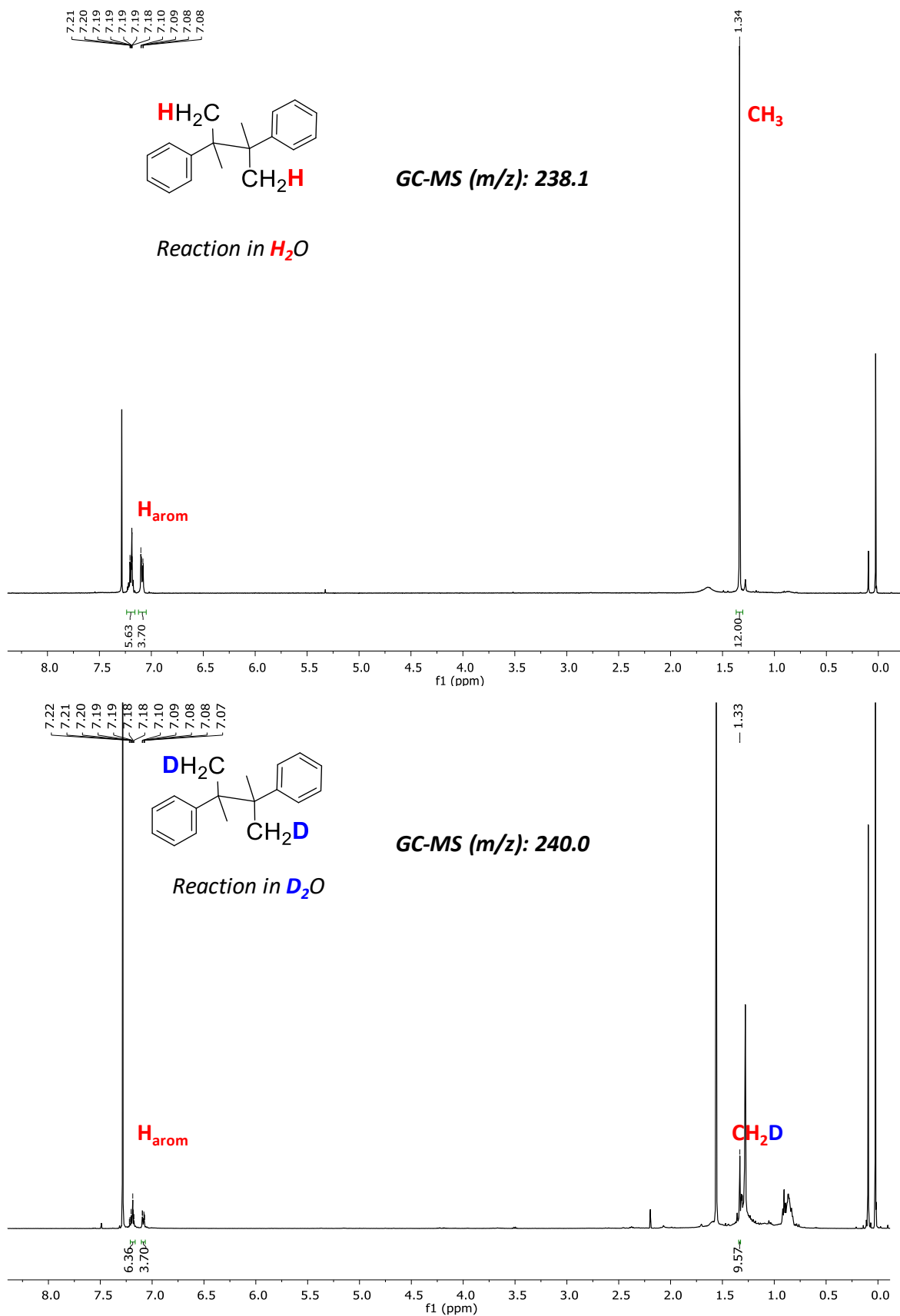


Figure S. 60. 1H -NMR spectrum ($CDCl_3$, 400 MHz, 300 K) of the isolated product **28b** and **[D]-28b** using H_2O (Top) or D_2O (99.9% in deuterium) (Bottom) in the solvent mixture, respectively. Conditions: **1** (6 mol%), **PCu** (6 mol%), substrate (0.165 mmol, 16.5 mM) in H_2O (or D_2O): CH_3CN : Pr_2EtN (6:4:0.2 mL) irradiated at $\lambda = 447$ nm and 30 °C for 5h, under N_2 .

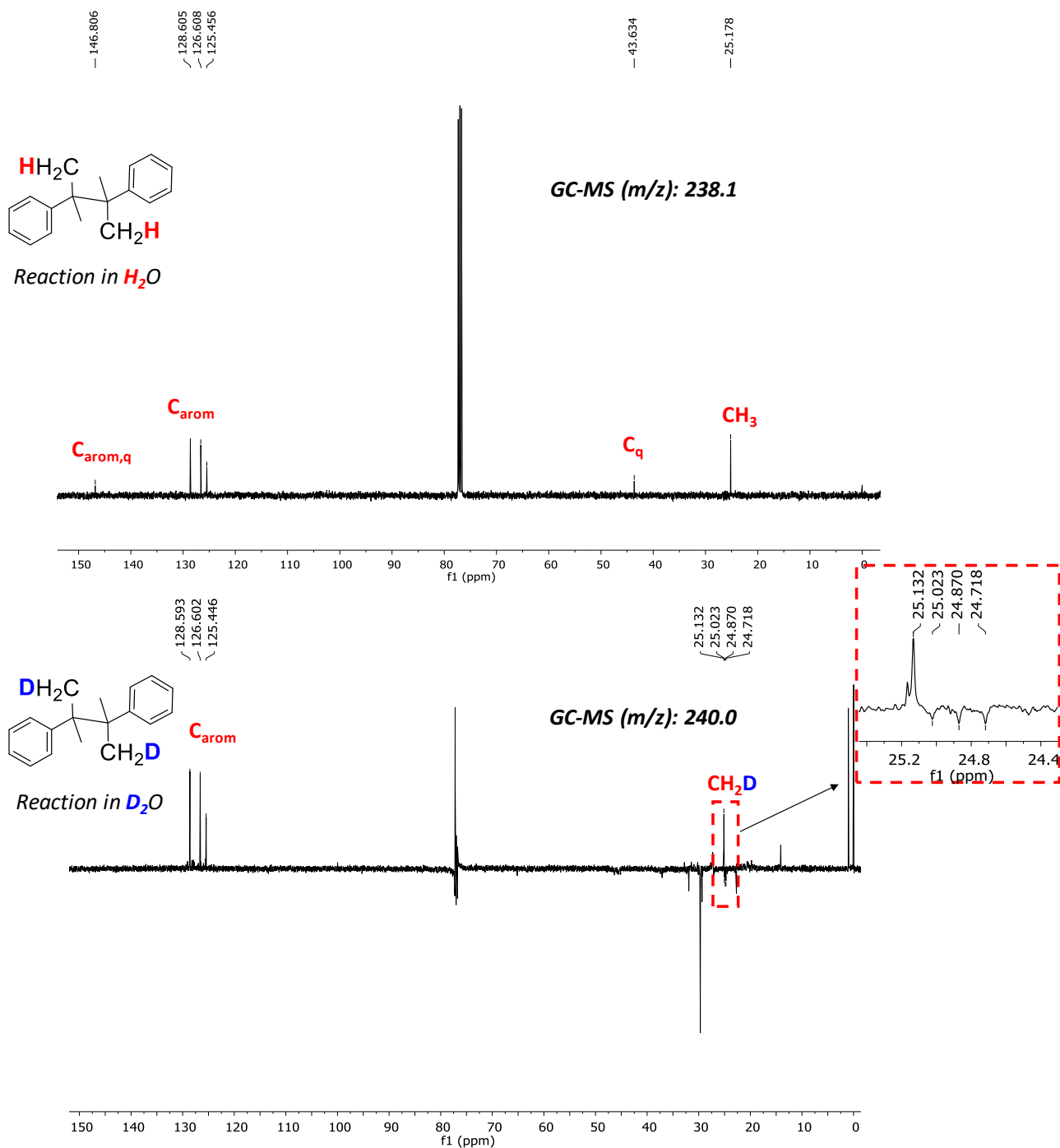


Figure S. 61. $^{13}C\{^1H\}$ -NMR and $^{13}C\{^1H\}$ -DEPT-135-NMR spectrum ($CDCl_3$, 125.8 MHz, 300 K) of the isolated product **28b** and **[D]-28b** using H_2O (Top) or D_2O (99.9 % in deuterium) (Bottom) in the solvent mixture, respectively. Conditions: **1** (6 mol%), PCu (6 mol%), substrate (0.165 mmol, 16.5 mM) in H_2O (or D_2O): CH_3CN : Pr_2EtN (6:4:0.2 mL) irradiated at $\lambda = 447$ nm and 30 °C for 5h, under N_2 . Inset: amplification of the area of the $-CH_2D$ showing the triplet due to the C-D coupling.

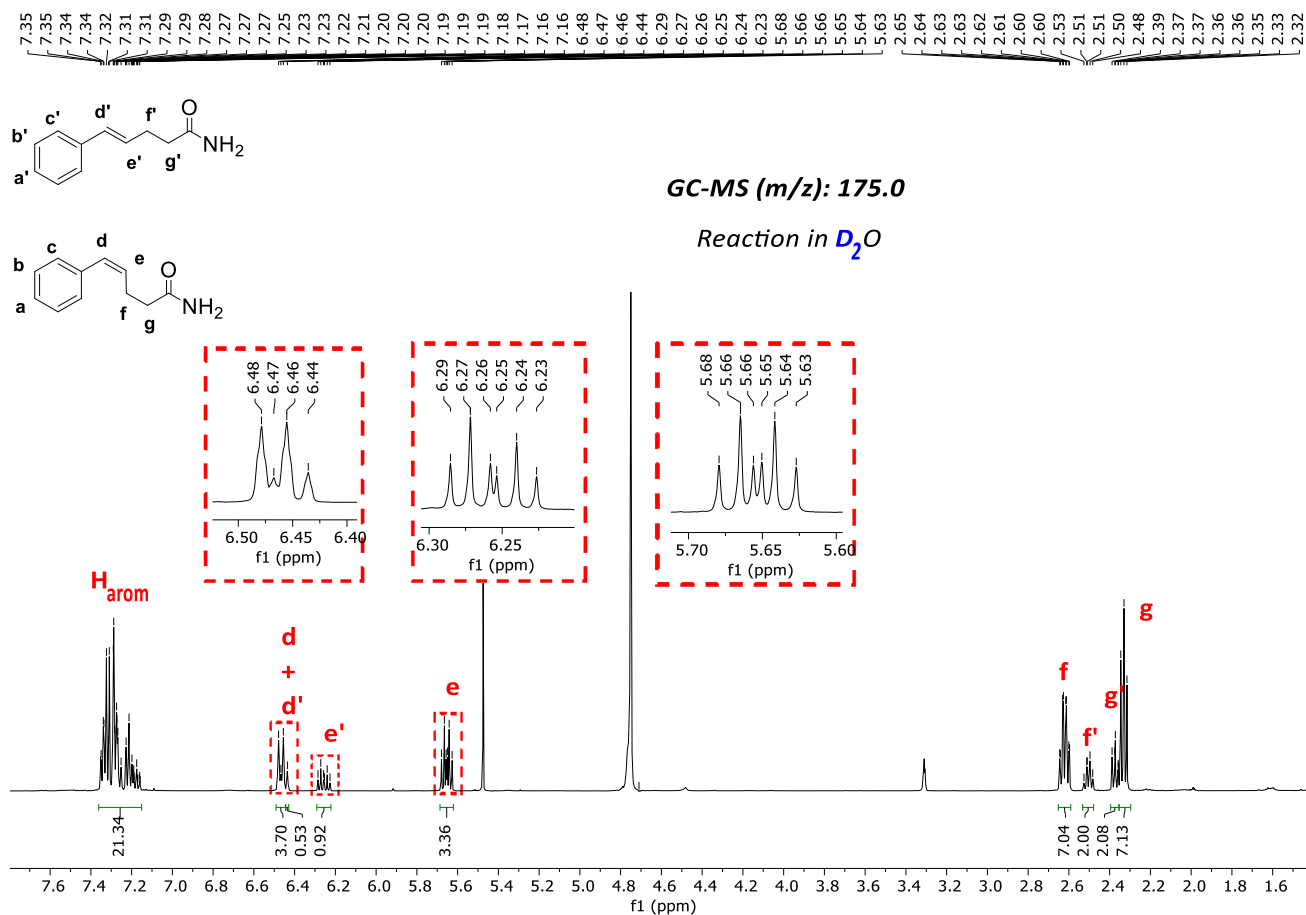


Figure S. 62. $^1\text{H-NMR}$ spectra (CD₃OD, 400 MHz, 300 K) of the mixture of products **41** and **41b** using D₂O (99.9 % in deuterium) in the solvent mixture, respectively. Conditions: **1** (3 mol%), PC_{Cu} (3 mol%), substrate (0.087 mmol, 8.7 mM) in D₂O:CH₃CN:Et₃N (6:4:0.2 ml) irradiated at $\lambda = 447$ nm and 25 °C for 5 h, under N₂. Inset: amplification of the area of the olefin characteristic signals.

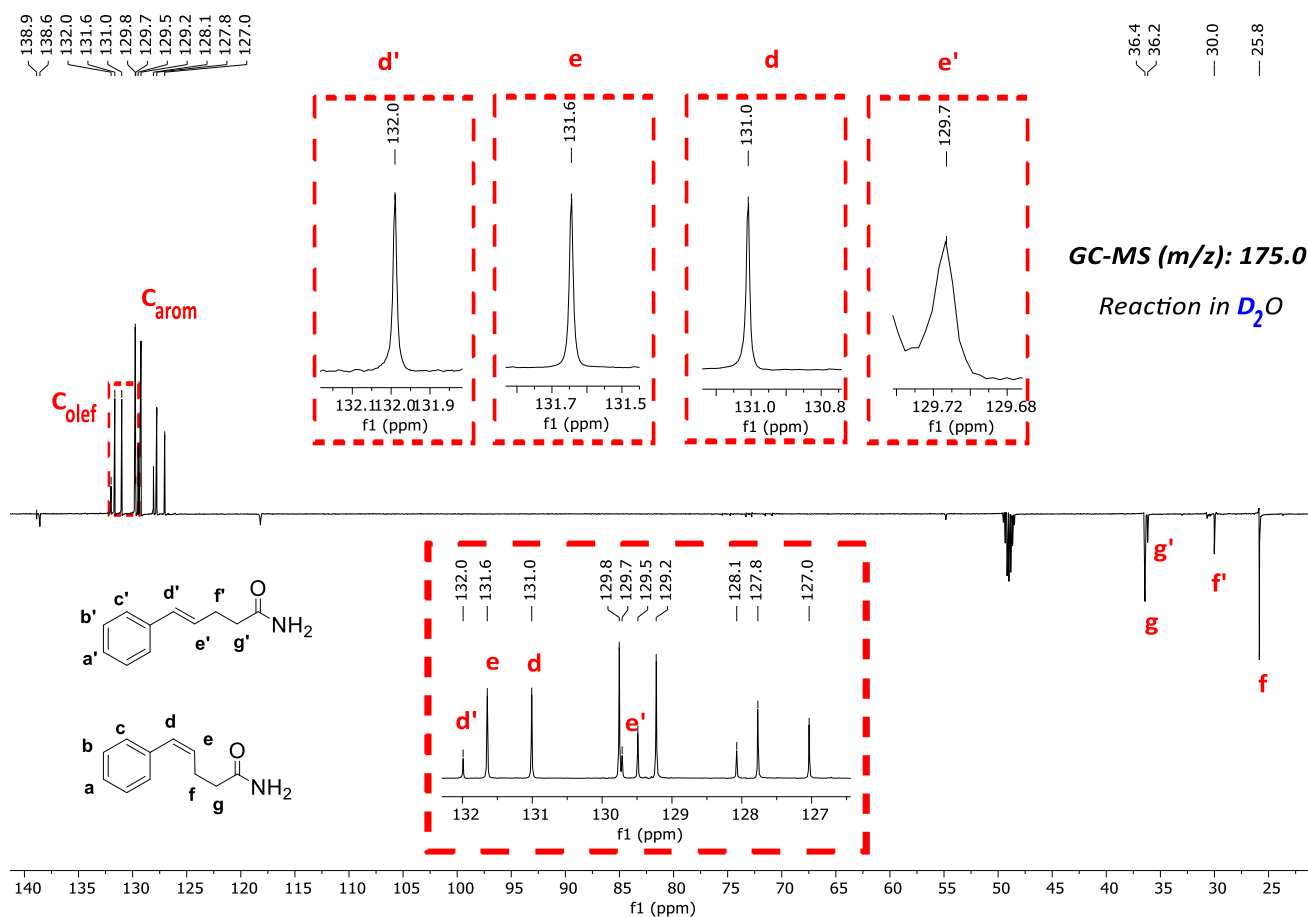
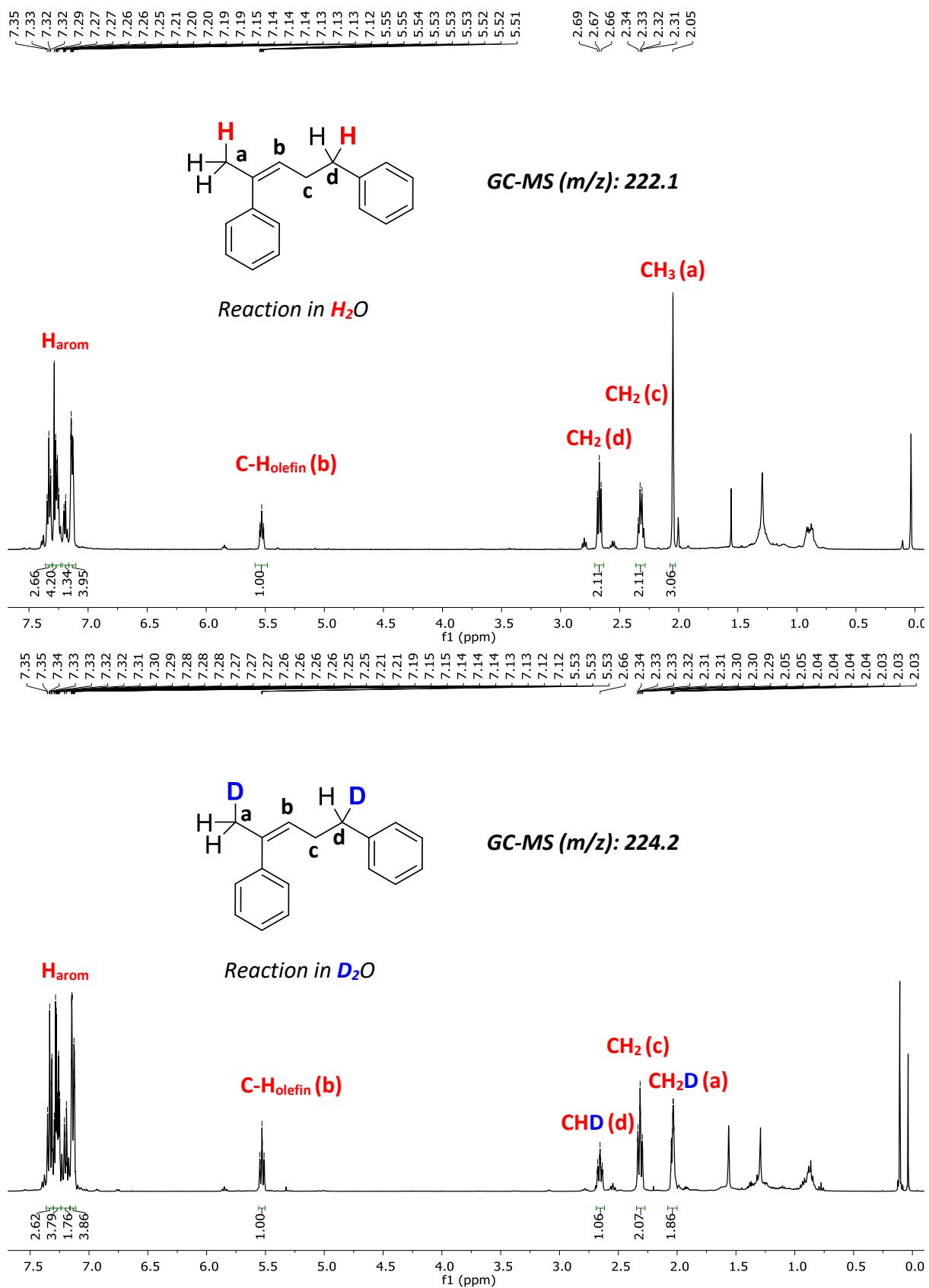


Figure S. 63. $^{13}\text{C}\{^1\text{H}\}$ -NMR and $^{13}\text{C}\{^1\text{H}\}$ -DEPTQ-135-NMR spectra (CD_3OD , 100.6 MHz, 300 K) of the mixture of products **41** and **41b** using D_2O (99.9 % in deuterium) in the solvent mixture, respectively. Conditions: **1** (3 mol%), PC_{Cu} (3 mol%), substrate (0.087 mmol, 8.7 mM) in $\text{D}_2\text{O}:\text{CH}_3\text{CN}:\text{Et}_3\text{N}$ (6:4:0.2 ml) irradiated at $\lambda = 447$ nm and 25 °C for 5 h, under N_2 . Inset: amplification of the area of the olefin characteristic signals (their appearance as singlets and not triplets correspond with no insertion of deuterium).



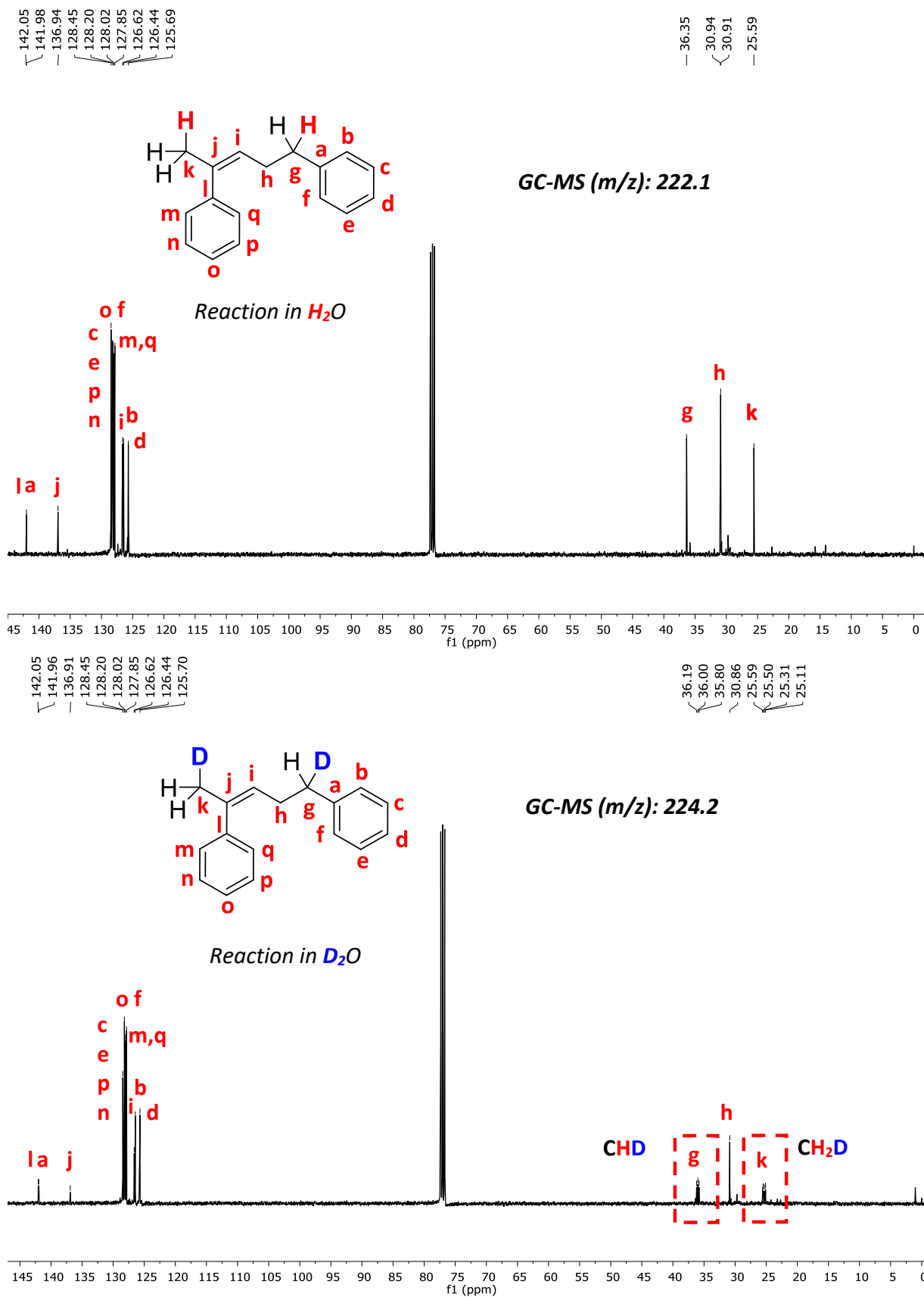


Figure S. 65. ¹³C-NMR spectrum (CDCl₃, 100.6 MHz, 300 K) of the isolated product **42b** and **[D]-42b** using H₂O (Top) or D₂O (99.9 % in deuterium) (Bottom) in the solvent mixture, respectively. Conditions: **1** (6 mol%), PC_{Cu} (6 mol%), substrate (0.044 mmol, 4.4 mM) in H₂O (or D₂O):CH₃CN:Pr₂EtN (6:4:0.2 mL) irradiated at λ = 447 nm and -3 °C for 24h, under N₂.

17. NMR of the radical clock ring-opening products
(1-(2-phenylcyclopropyl)vinyl)benzene

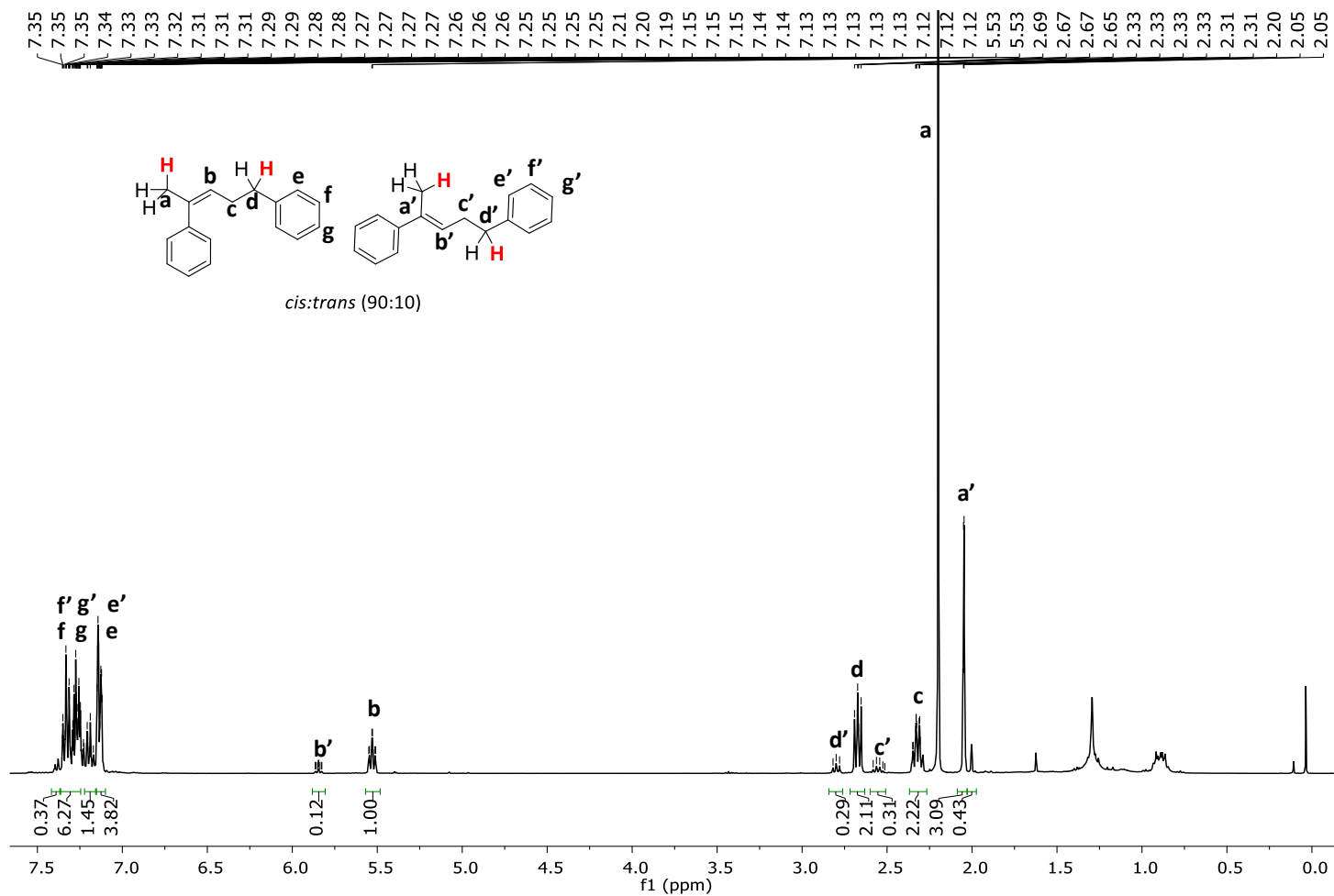


Figure S. 66. ¹H-NMR (CDCl₃, 400 MHz, 300 K) spectrum of the isolated product **42b** (in H₂O).

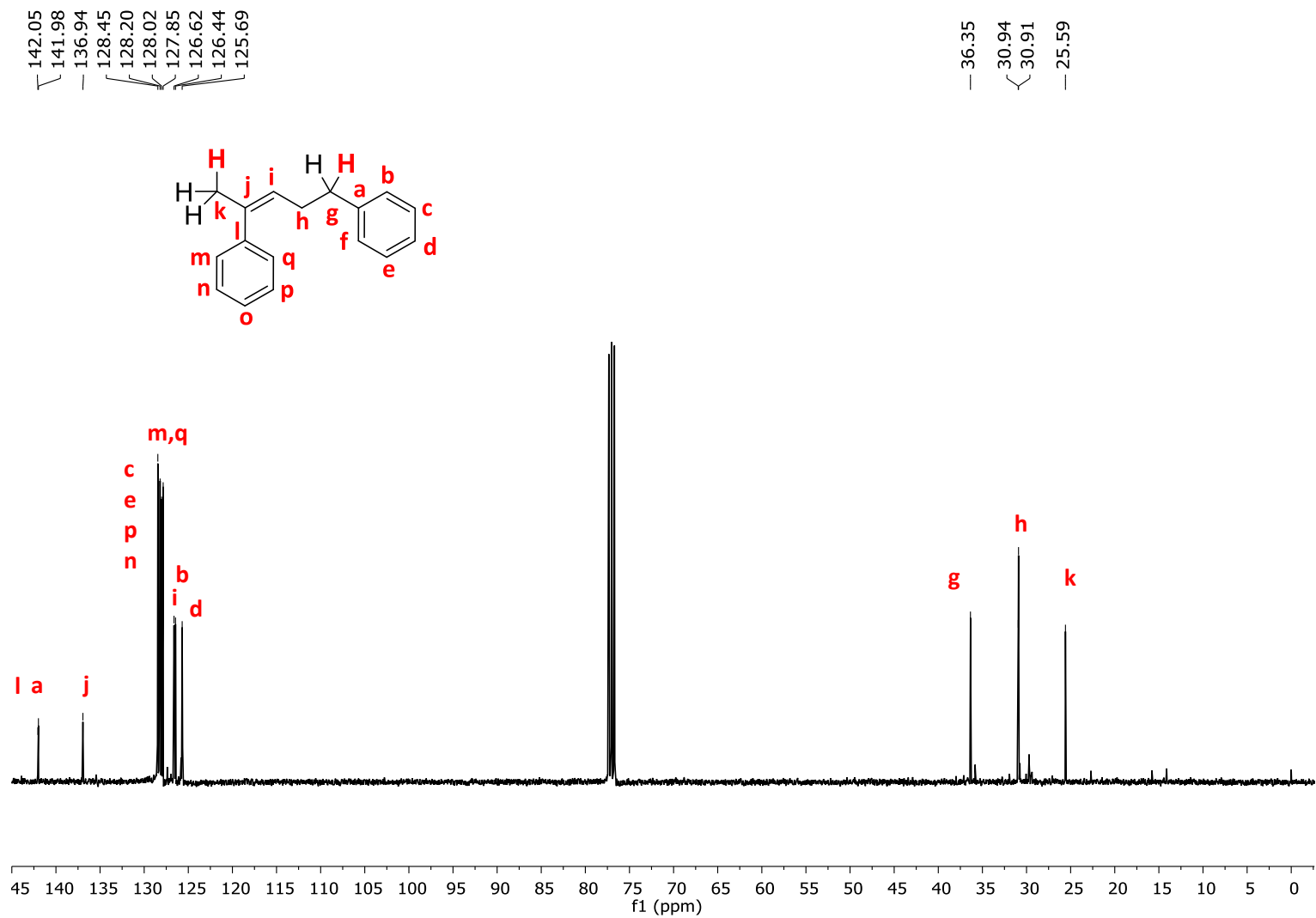


Figure S. 67. $^{13}\text{C}\{^1\text{H}\}$ -NMR (CDCl_3 , 100.6 MHz, 300 K) spectrum of the isolated product **42b** (in H_2O).

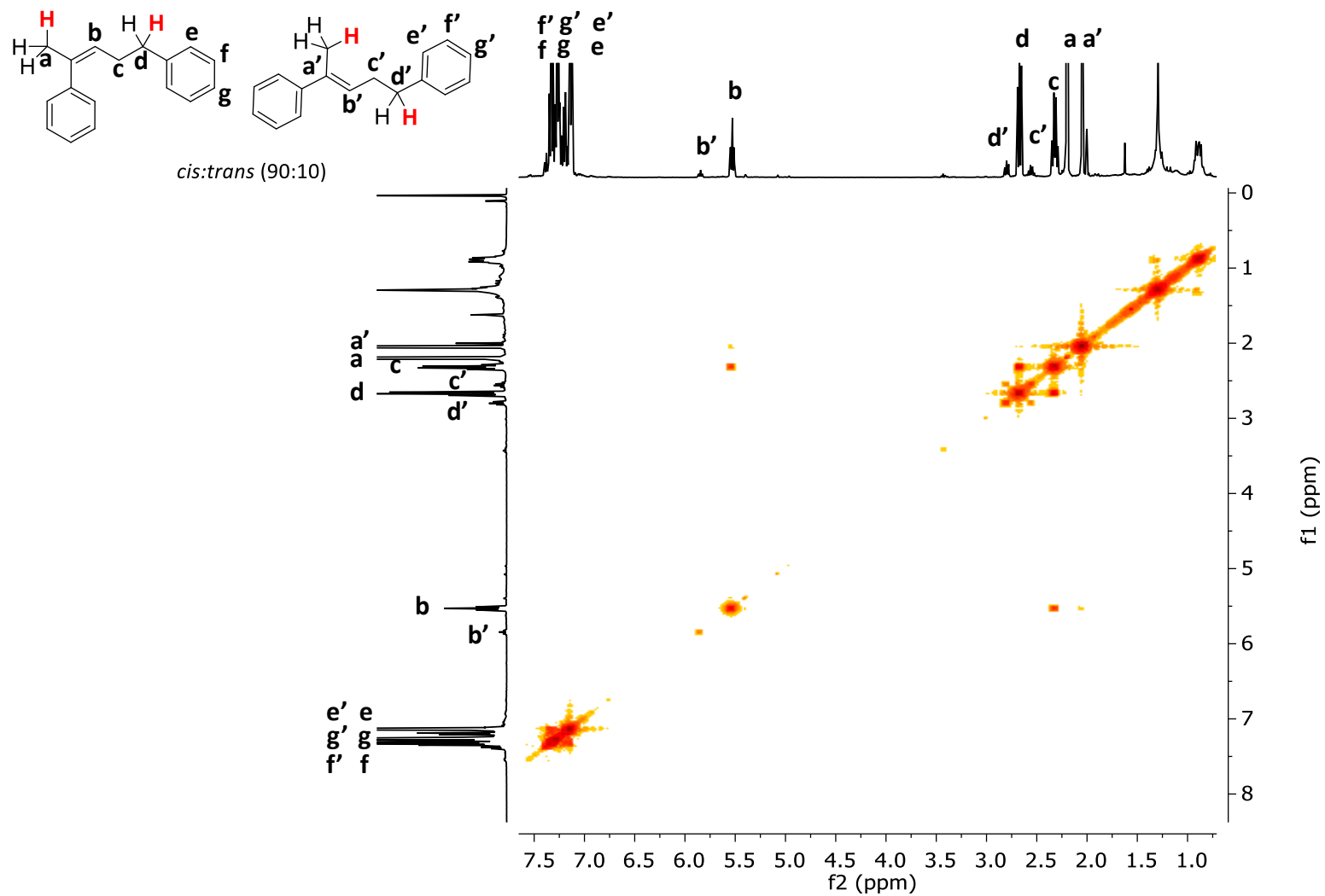
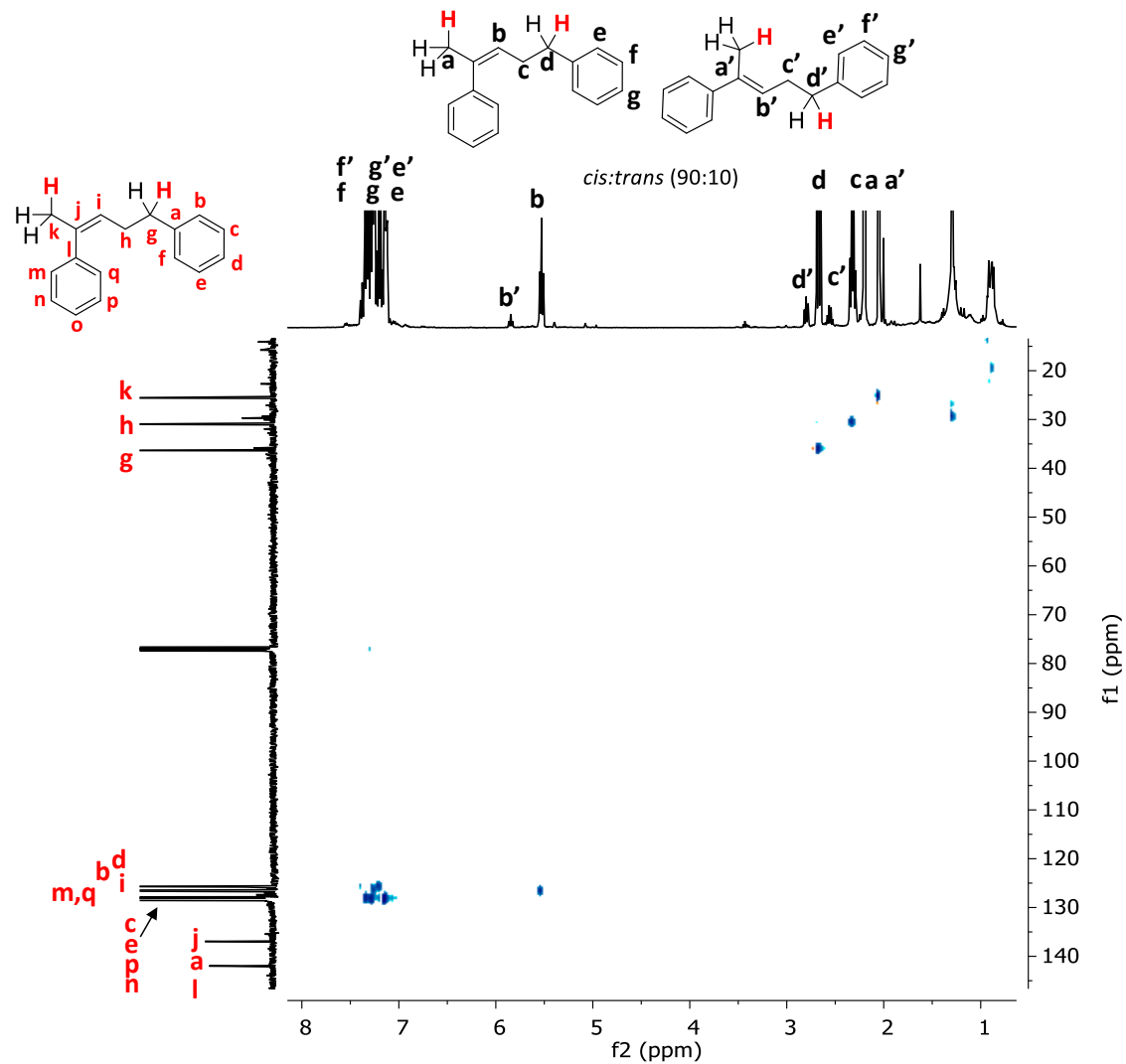


Figure S. 68. ^1H - ^1H COSY (CDCl₃, 400 MHz, 300 K) spectrum of the isolated of product **42b** (in H₂O).



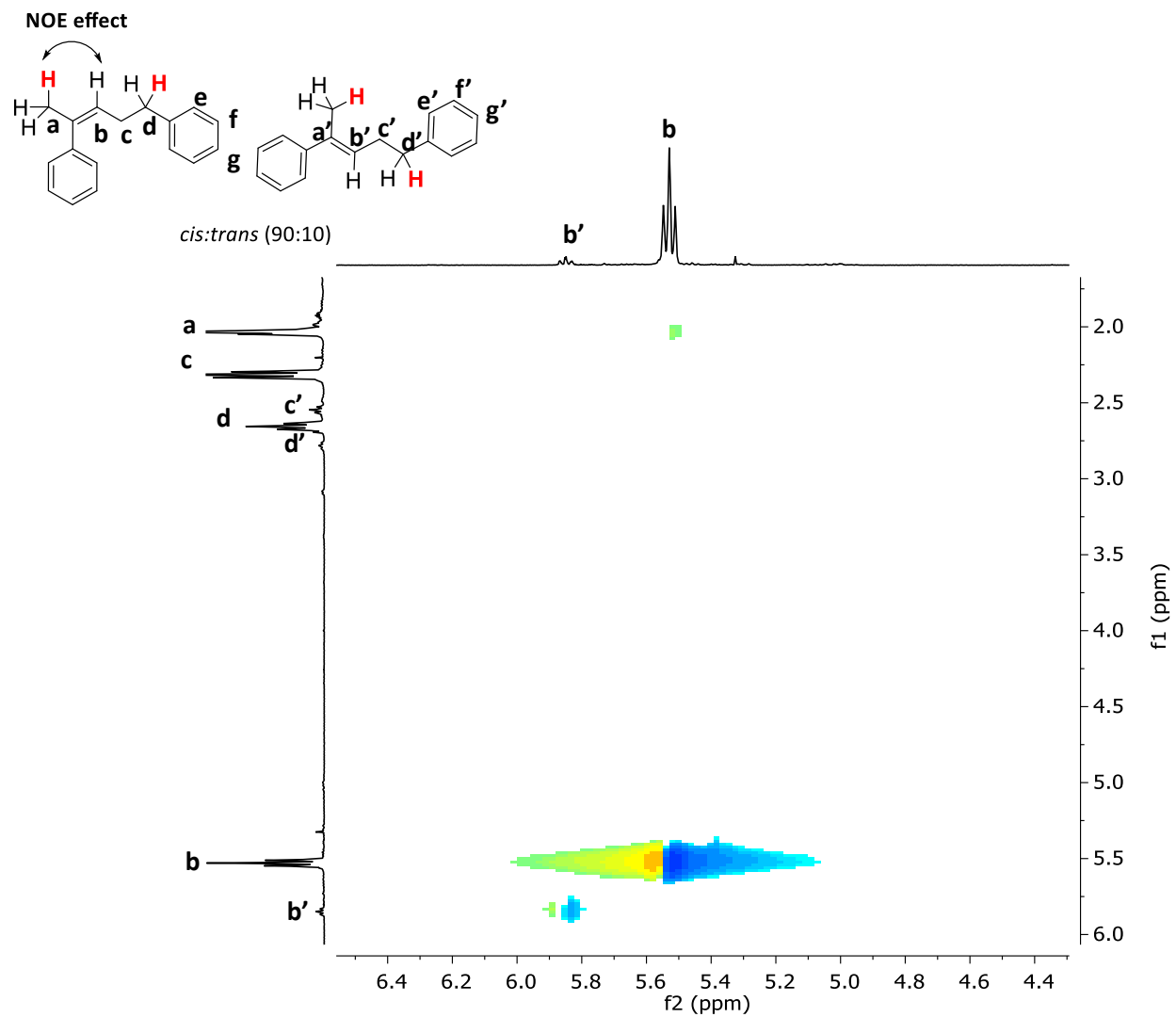


Figure S. 70. ^1H -NOESY (CDCl_3 , 400 MHz, 300 K) of the isolated product **42b** (in H_2O).

18. NMR spectra of synthesized substrates and isolated products

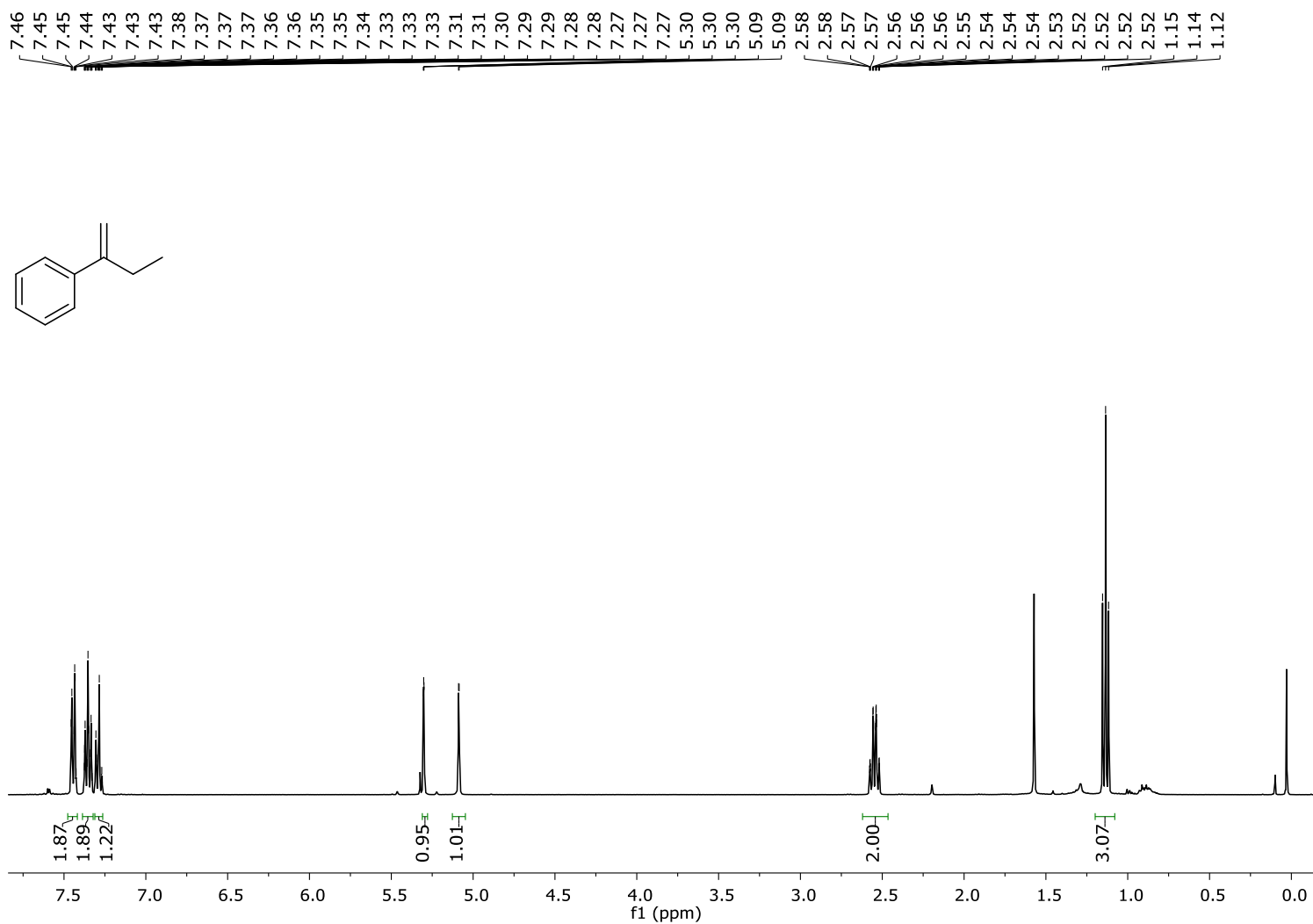


Figure S. 71. ¹H-NMR (CDCl₃, 400 MHz, 300 K) spectrum of substrate **29**.

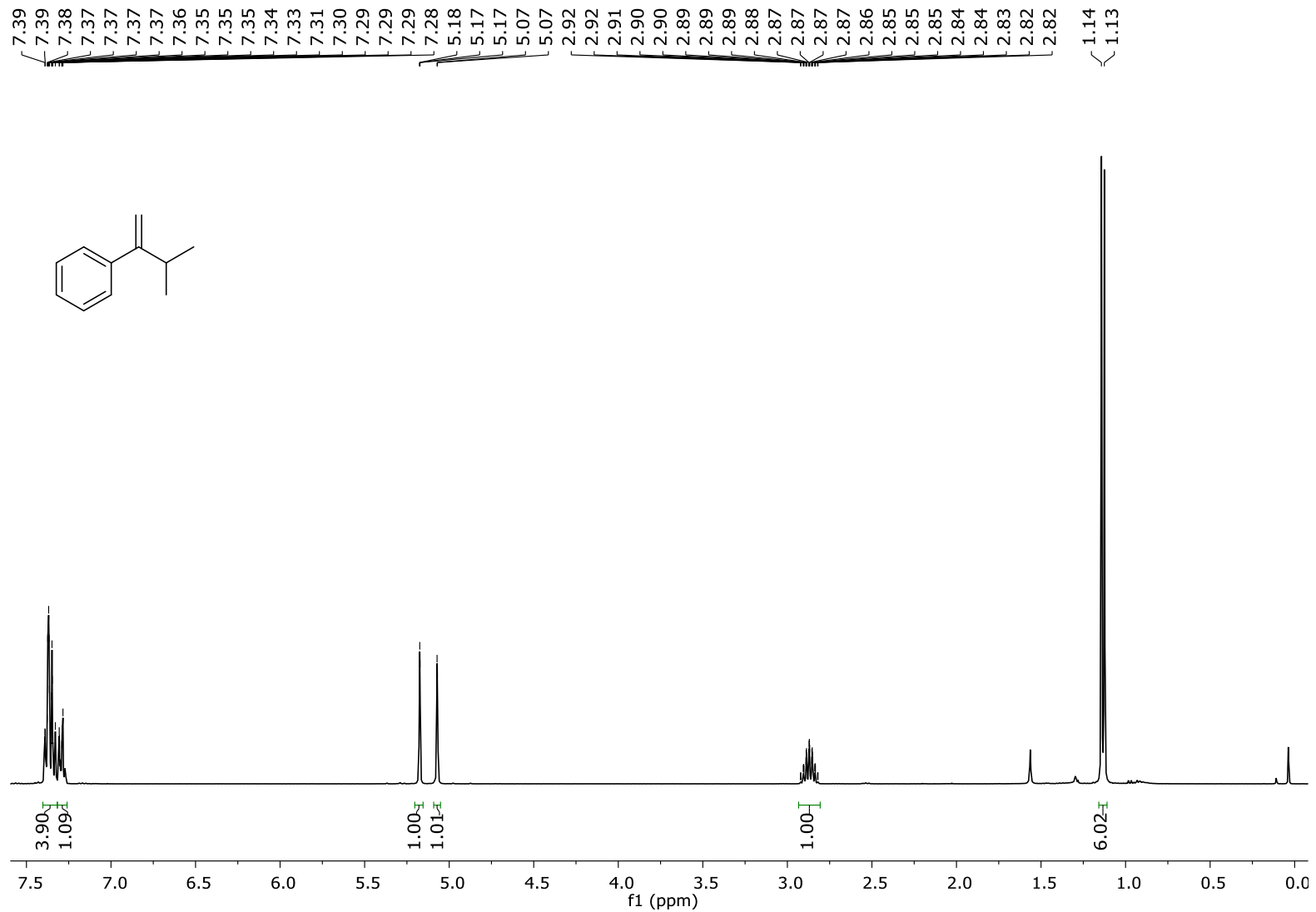


Figure S. 72. ¹H-NMR (CDCl₃, 400 MHz, 300 K) spectrum of substrate **30**.

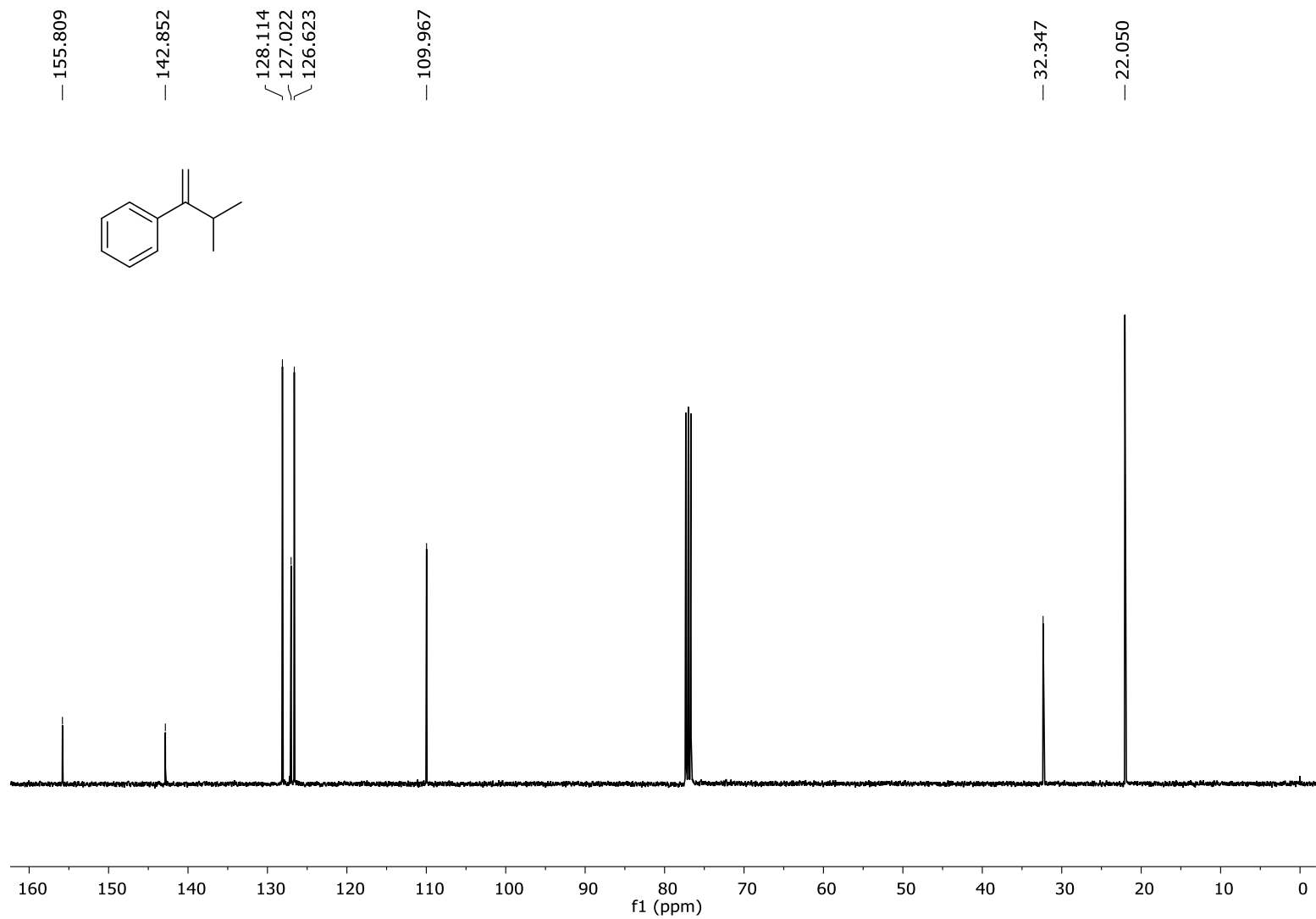


Figure S. 73. $^{13}\text{C}\{^1\text{H}\}$ -NMR (CDCl_3 , 100.6 MHz, 300 K) spectrum of substrate **30**.

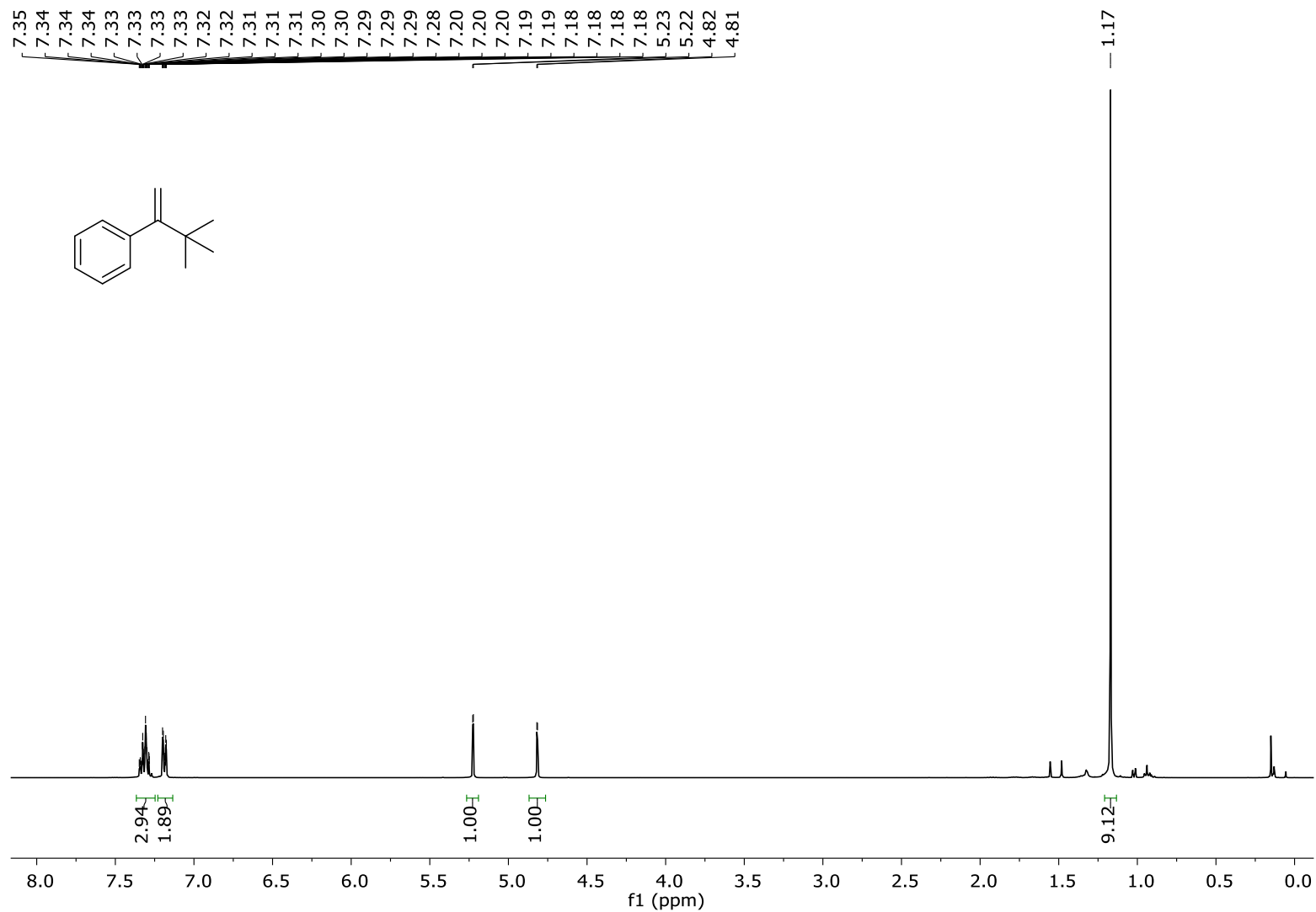


Figure S. 74. $^1\text{H-NMR}$ (CDCl_3 , 400 MHz, 300 K) spectrum of substrate **32**.

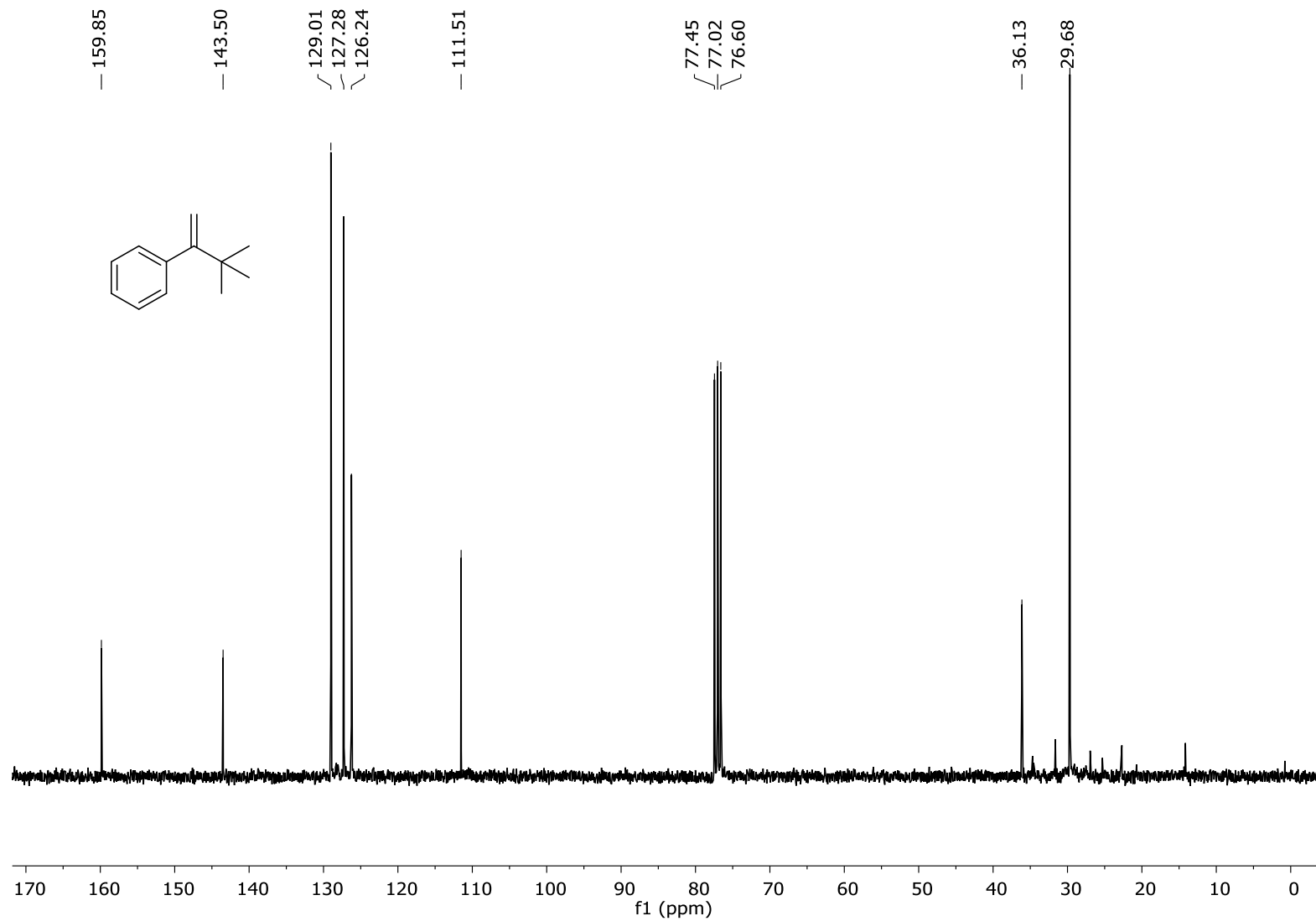


Figure S. 75. $^{13}\text{C}\{^1\text{H}\}$ -NMR (CDCl₃, 100.6 MHz, 300 K) spectrum of substrate **32**.

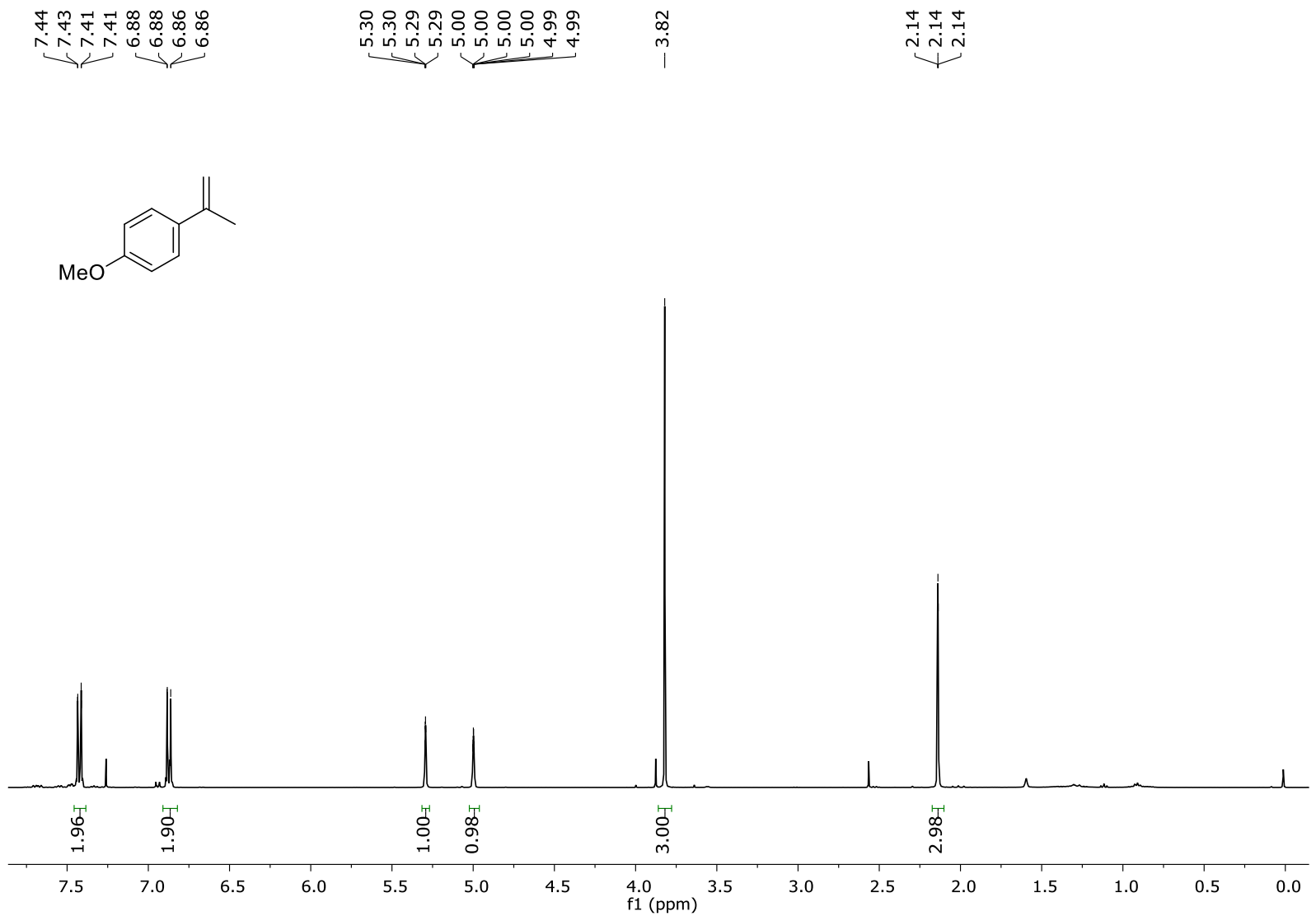


Figure S. 76. ¹H-NMR (CDCl₃, 400 MHz, 300 K) spectrum of substrate 33.

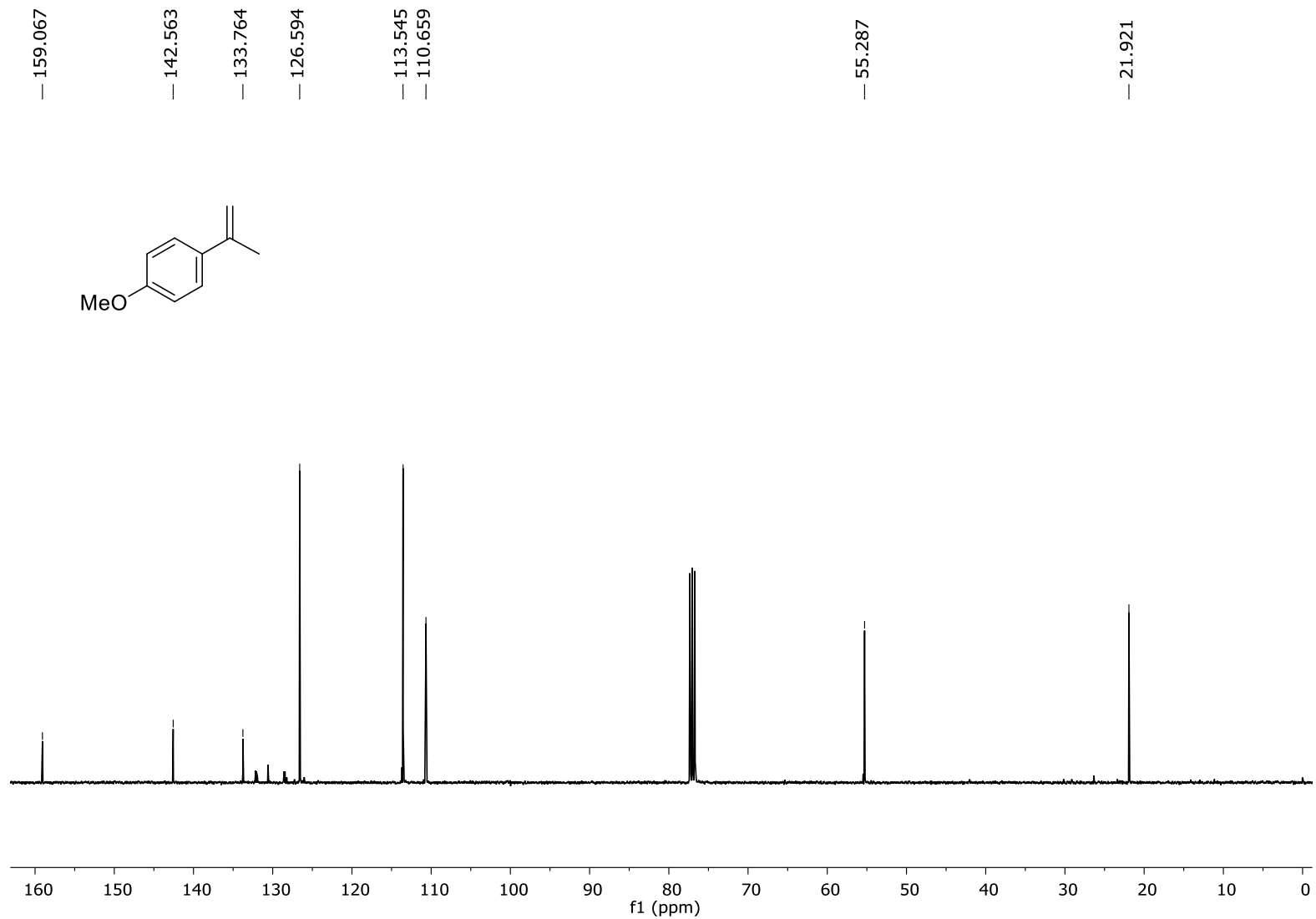


Figure S. 77. $^{13}\text{C}\{^1\text{H}\}$ -NMR (CDCl_3 , 100.6 MHz, 300 K) spectrum of substrate **33**.

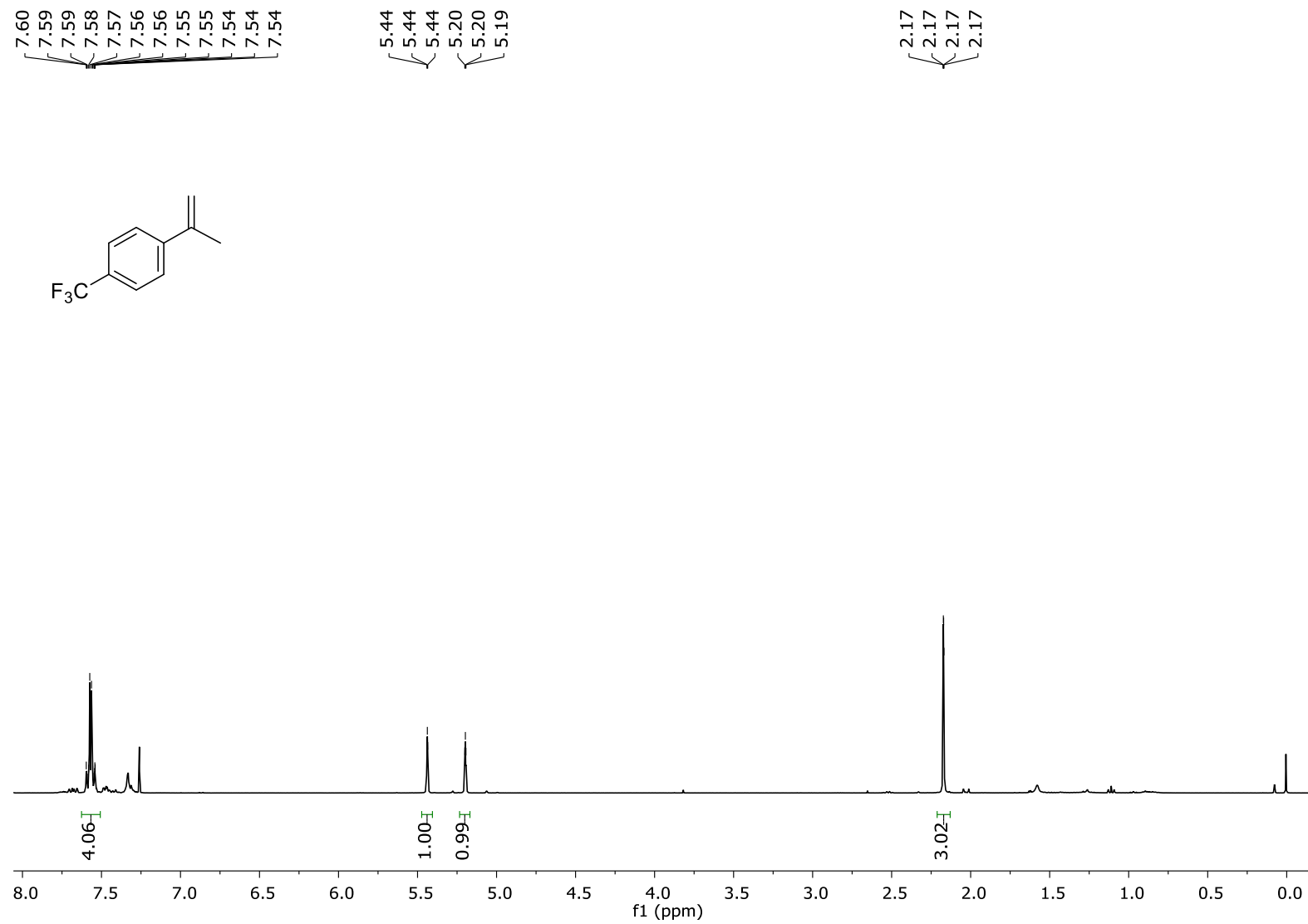


Figure S. 78. ¹H-NMR (CDCl₃, 400 MHz, 300 K) spectrum of substrate 34.

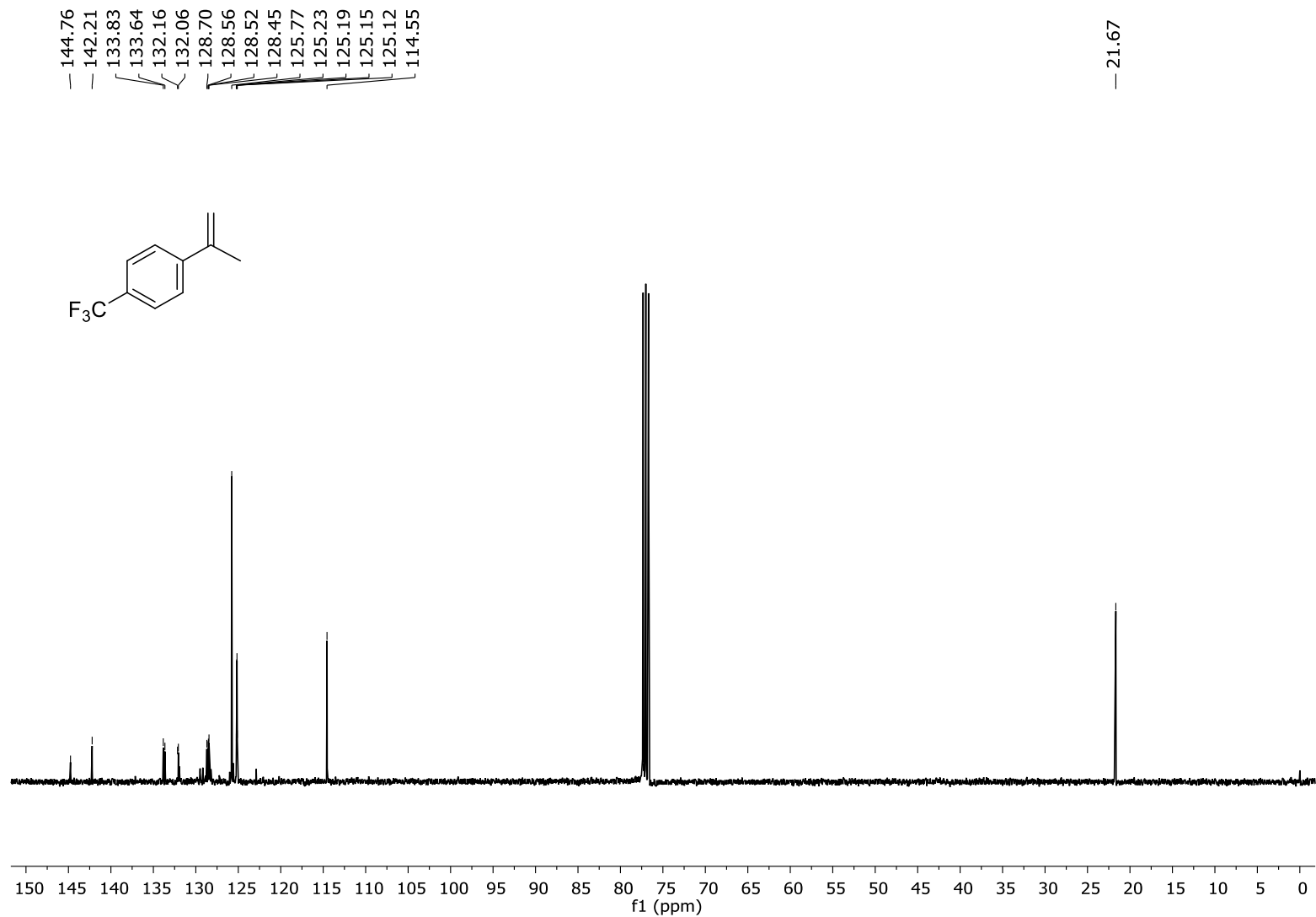


Figure S. 79. $^{13}\text{C}\{^1\text{H}\}$ -NMR (CDCl_3 , 100.6 MHz, 300 K) spectrum of substrate **34**.

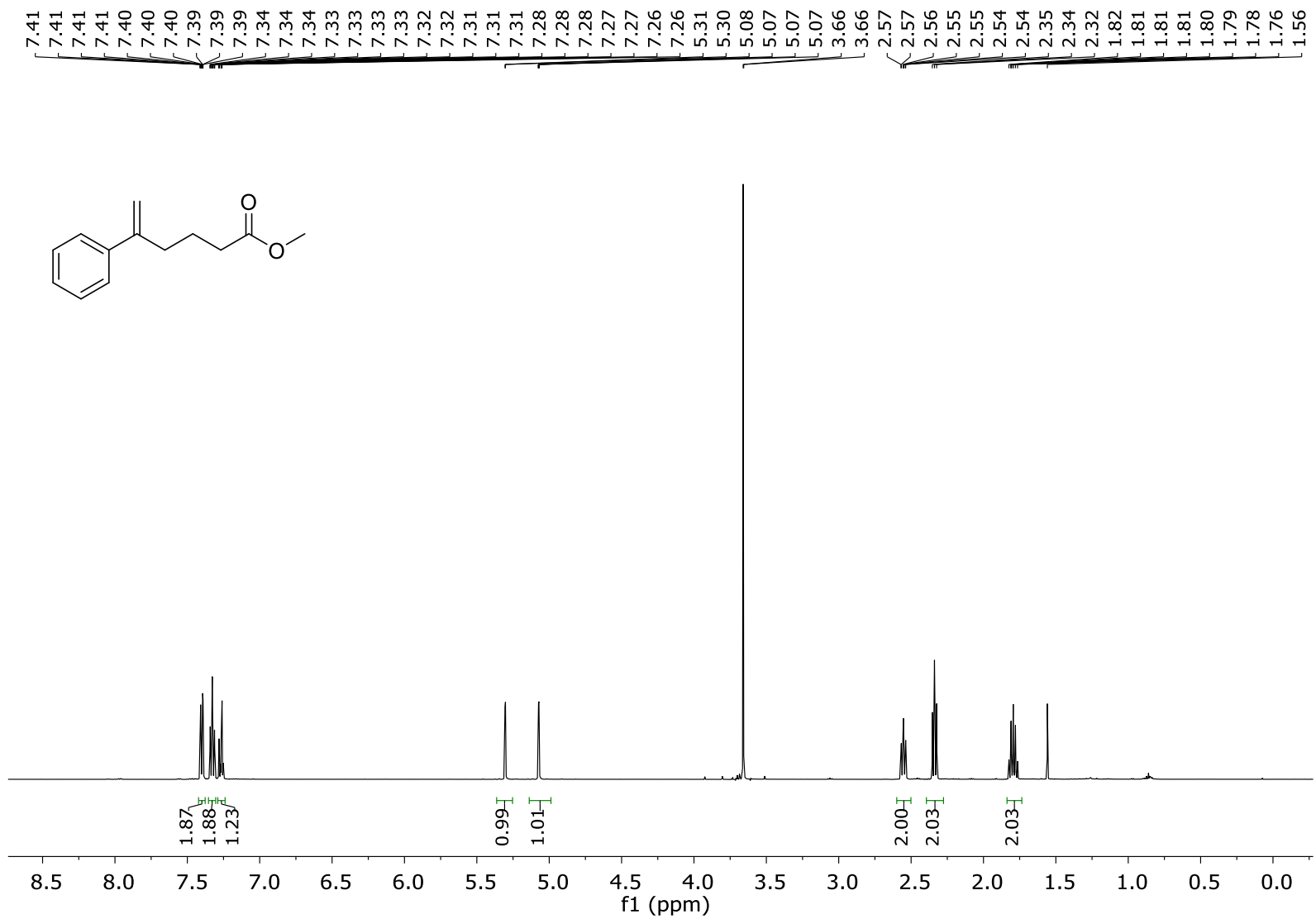


Figure S. 80. ¹H-NMR (CDCl₃, 500 MHz, 300 K) spectrum of substrate 35.

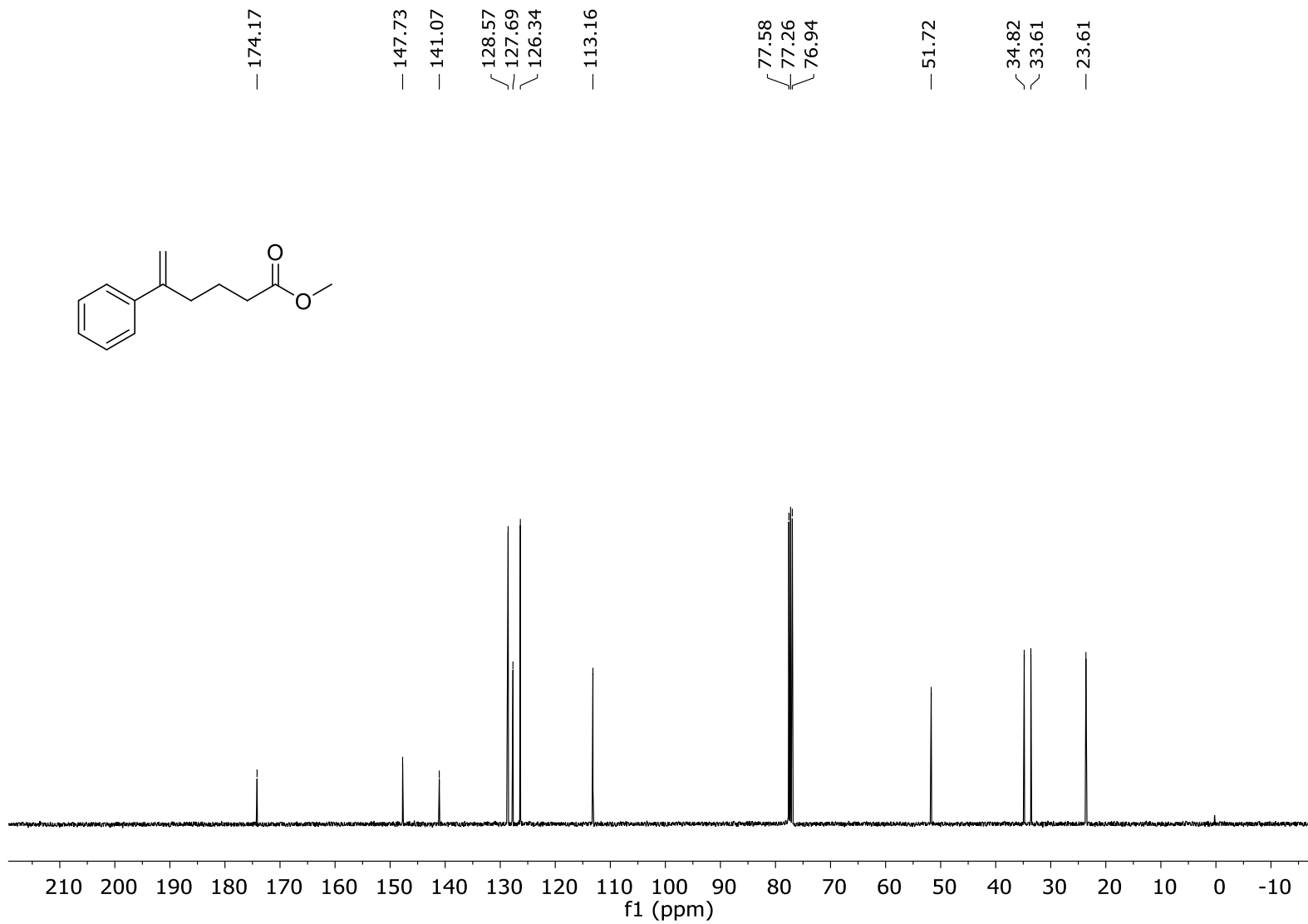


Figure S. 81. $^{13}\text{C}\{^1\text{H}\}$ -NMR (CDCl_3 , 100.6 MHz, 300 K) spectrum of substrate 35.

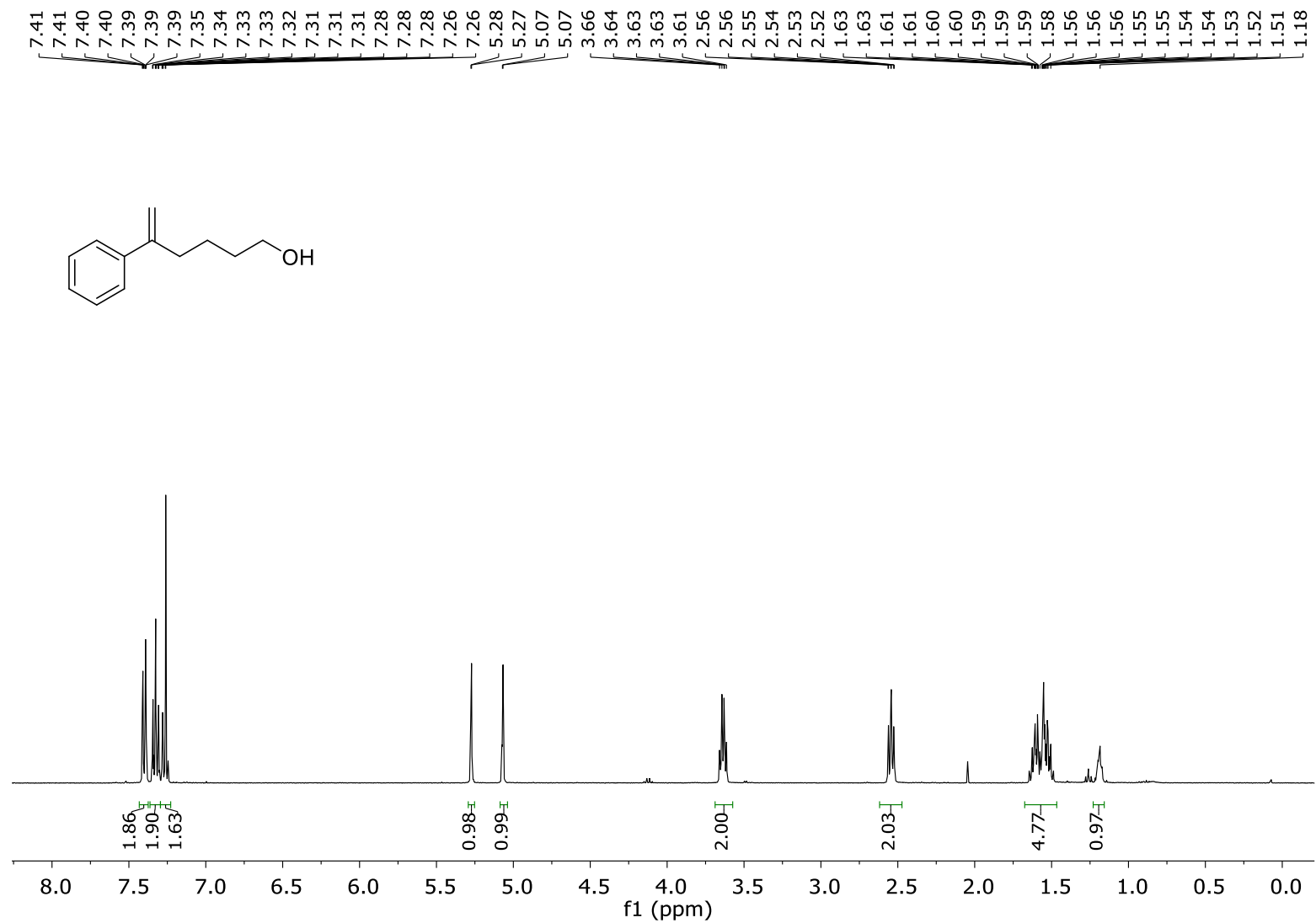


Figure S. 82. ¹H-NMR (CDCl₃, 400 MHz, 300 K) spectrum of substrate 36.

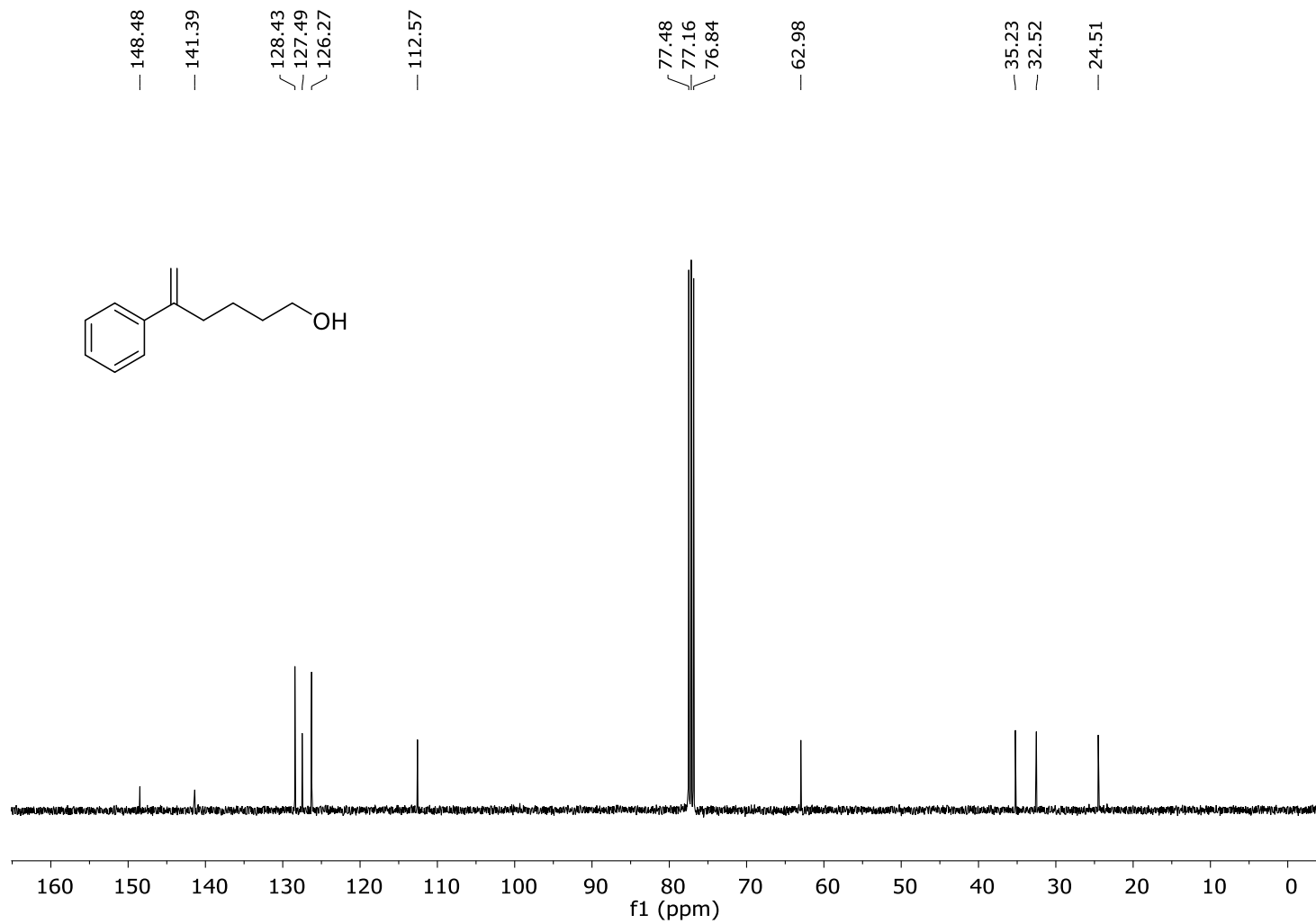


Figure S. 83. $^{13}\text{C}\{^1\text{H}\}$ -NMR (CDCl₃, 100.6 MHz, 300 K) spectrum of substrate **36**.

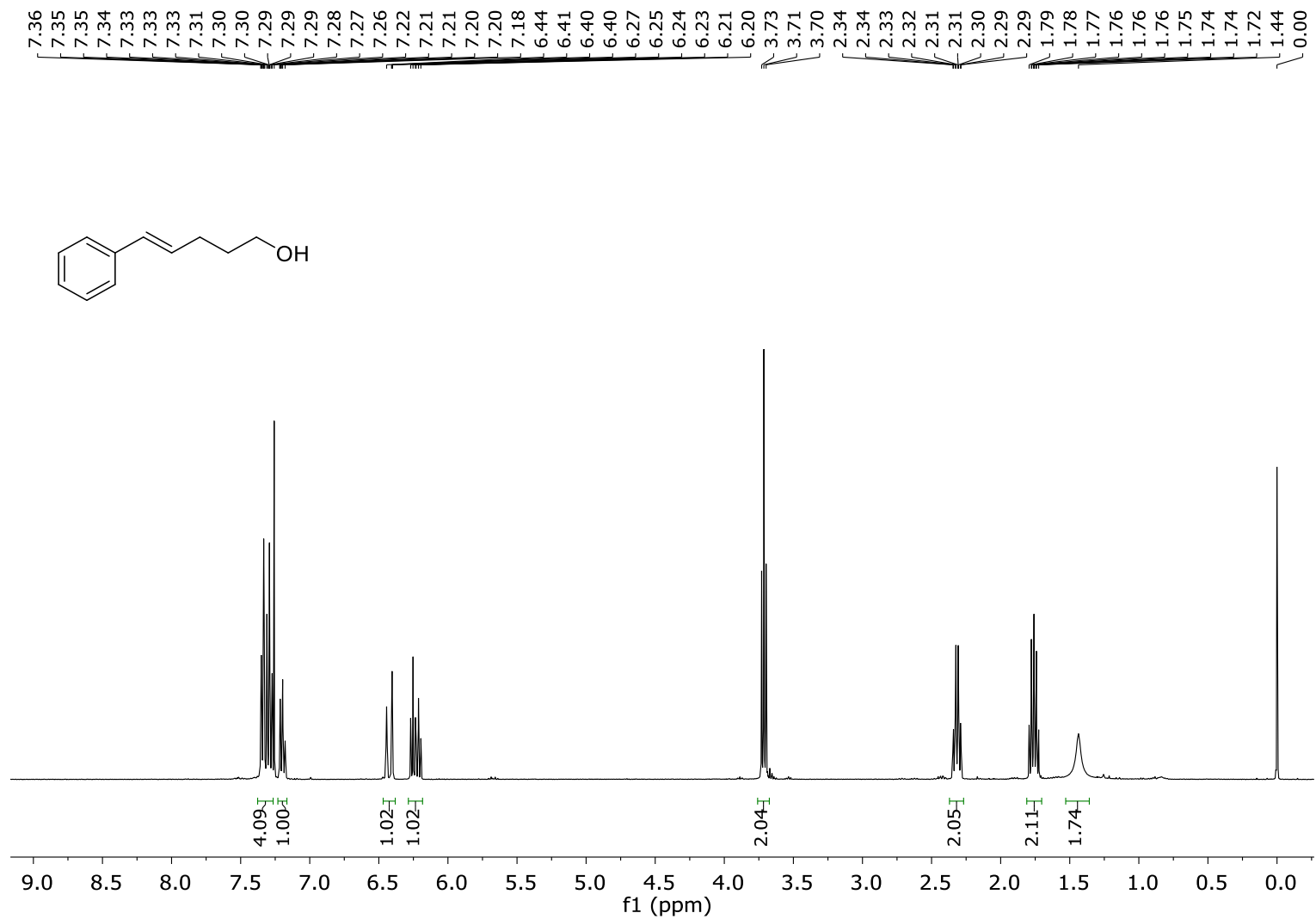


Figure S. 84. ¹H-NMR (CDCl₃, 400 MHz, 300 K) spectrum of substrate 39.

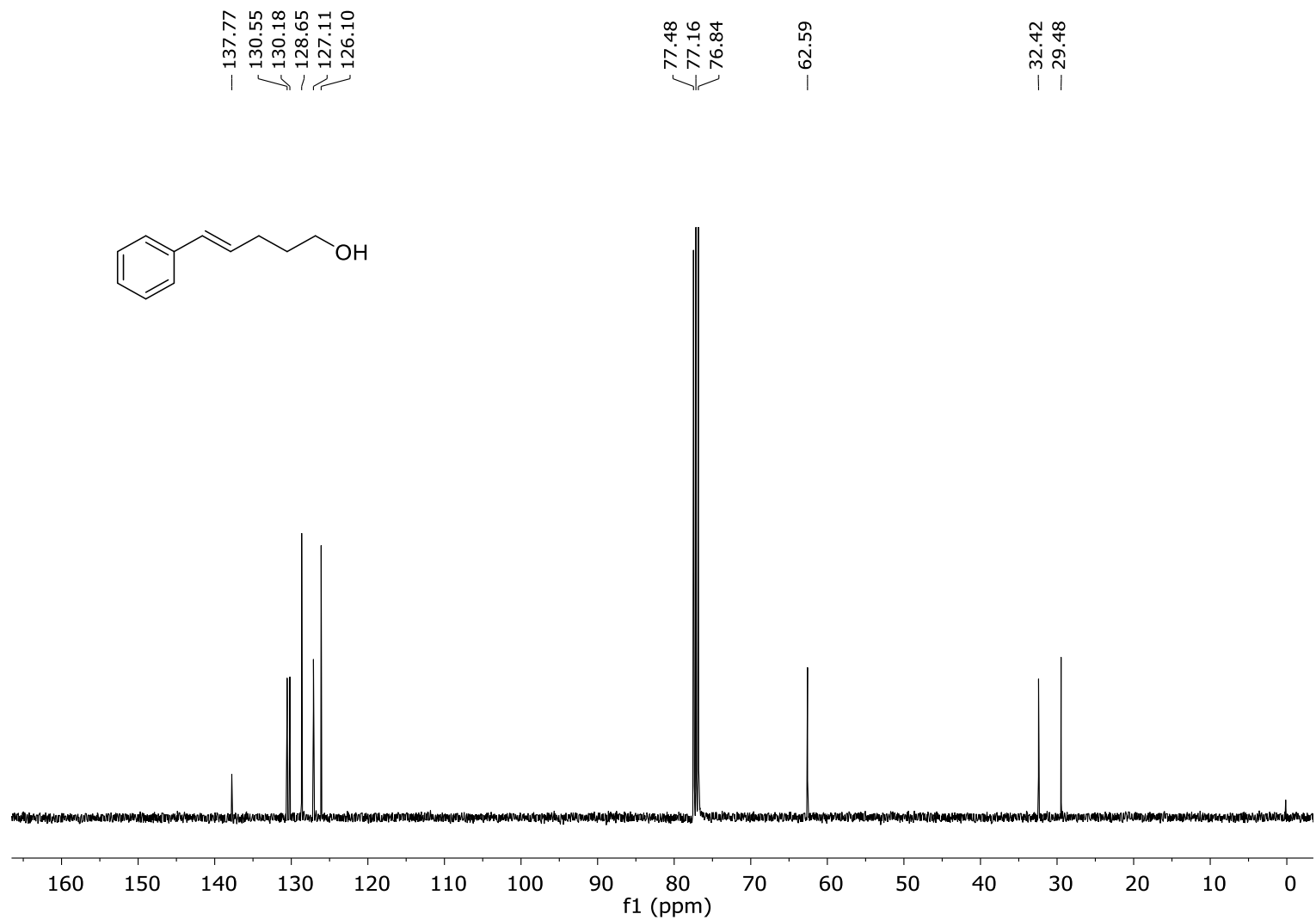


Figure S. 85. $^{13}\text{C}\{^1\text{H}\}$ -NMR (CDCl_3 , 100.6 MHz, 300 K) spectrum of substrate **39**.

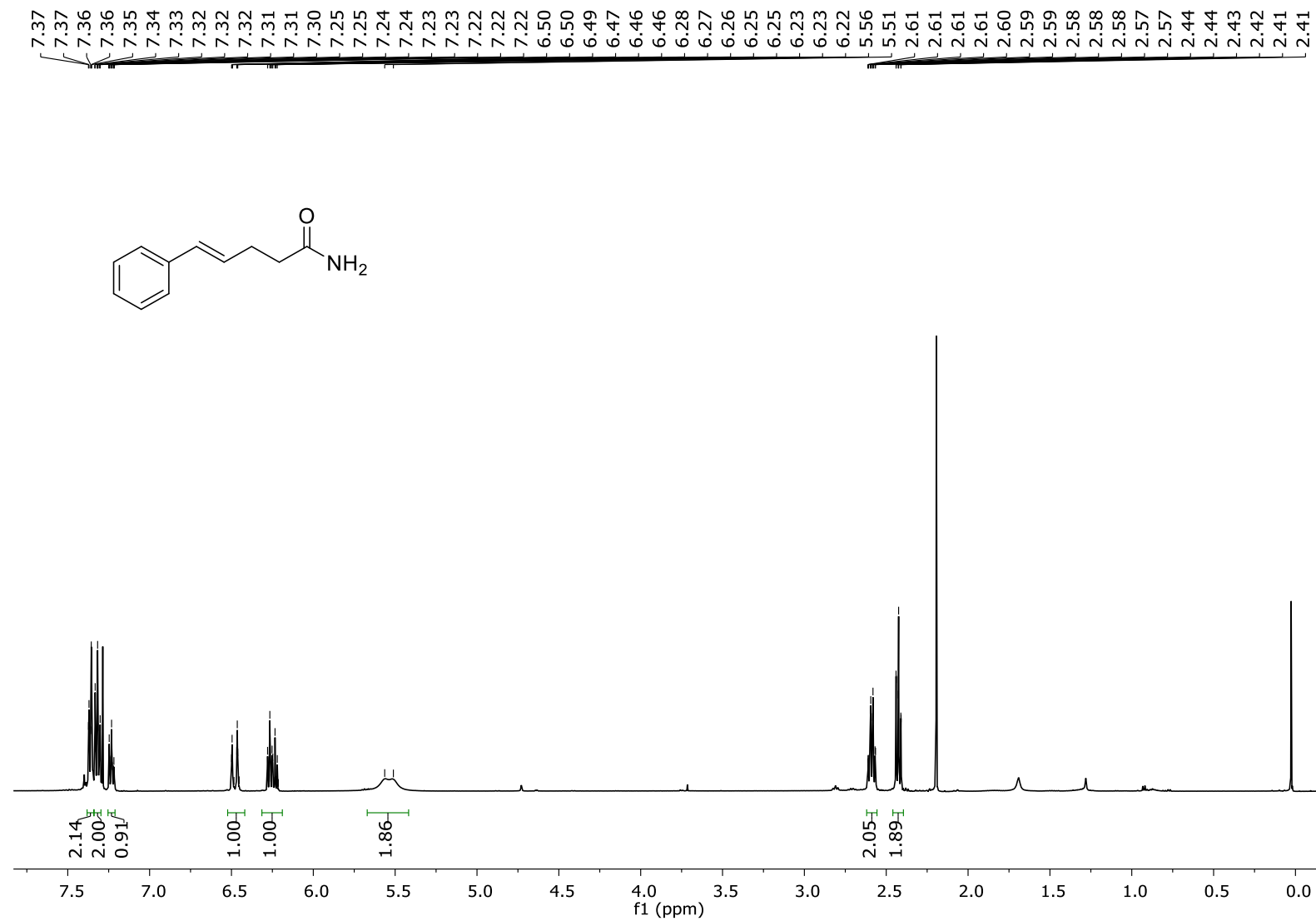


Figure S. 86. ¹H-NMR (CDCl₃, 400 MHz, 300 K) spectrum of substrate 41.

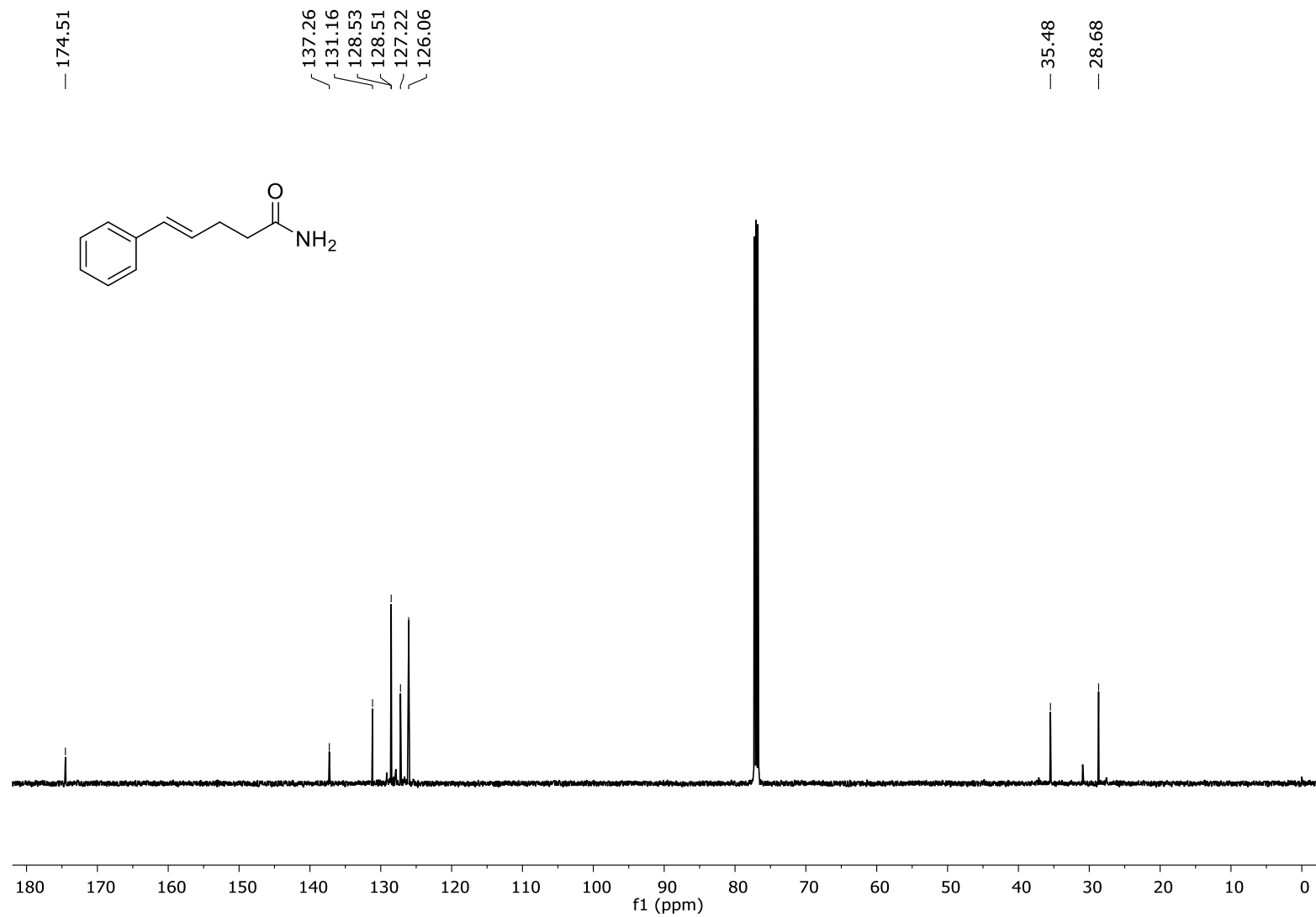


Figure S. 87. $^{13}\text{C}\{^1\text{H}\}$ -NMR (CDCl_3 , 100.6 MHz, 300 K) spectrum of substrate 41.

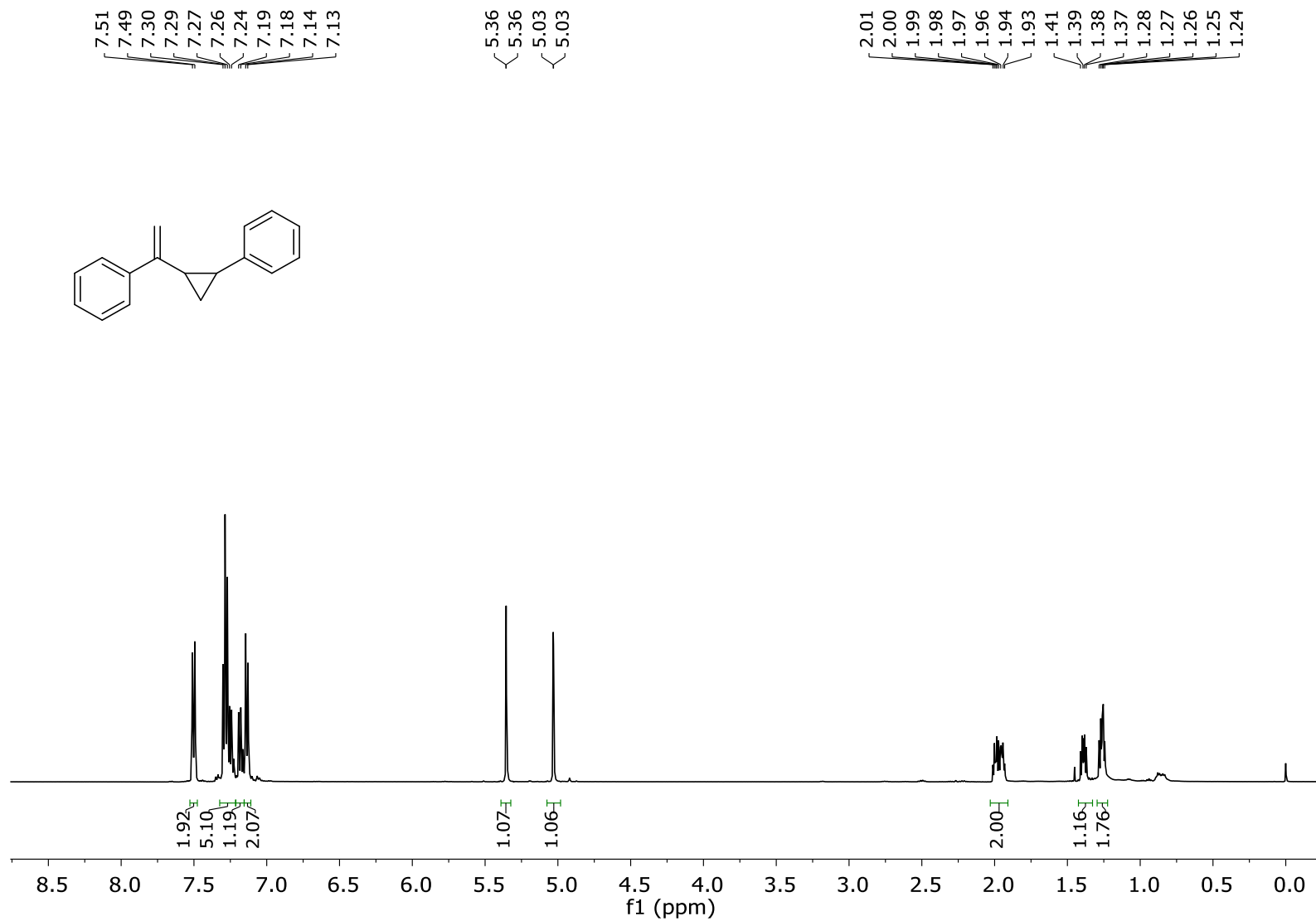


Figure S. 88. ¹H-NMR (CDCl₃, 500 MHz, 300 K) spectrum of substrate 42.

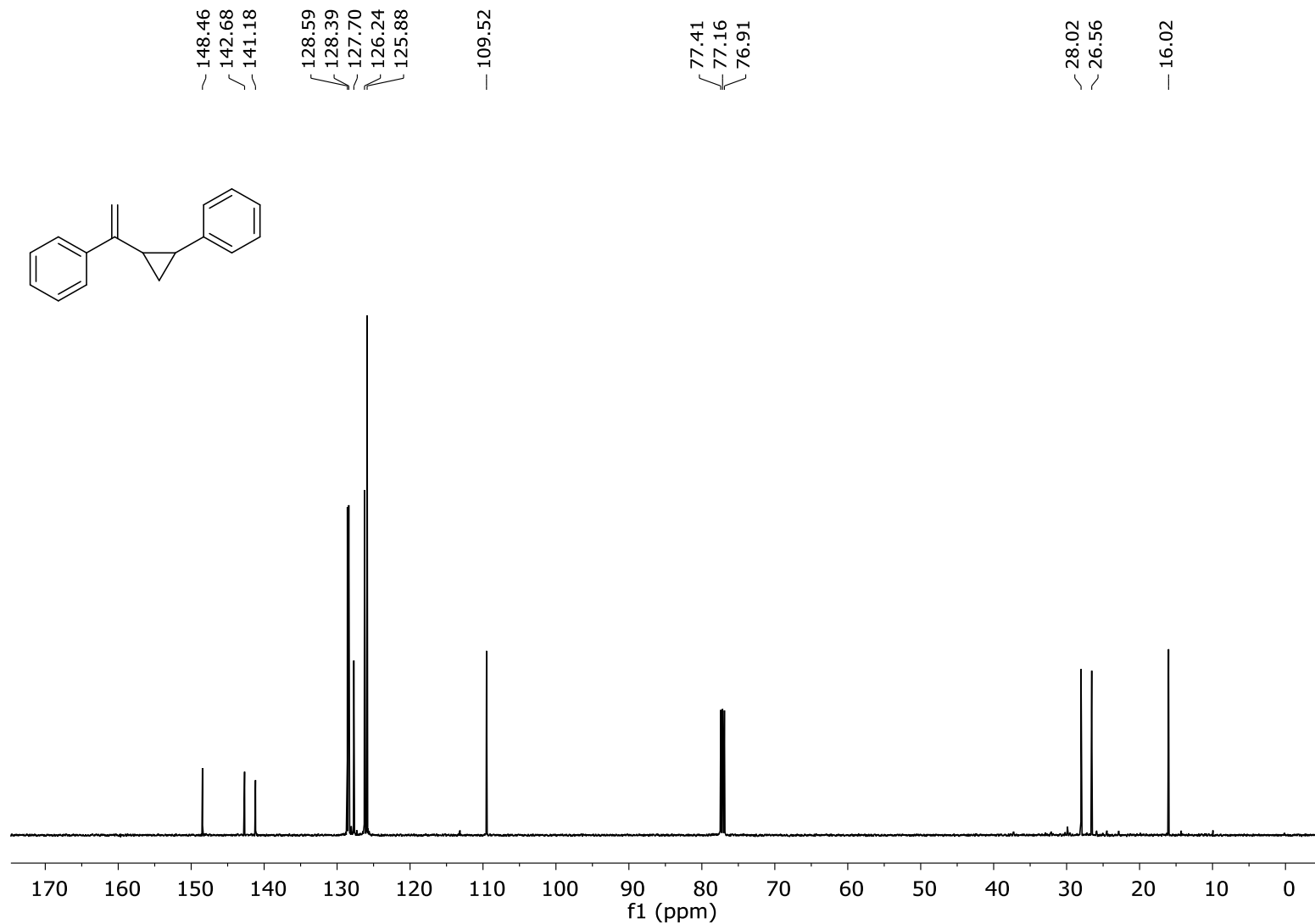


Figure S. 89. $^{13}\text{C}\{^1\text{H}\}$ -NMR (CDCl_3 , 125.75 MHz, 300 K) spectrum of substrate 42.

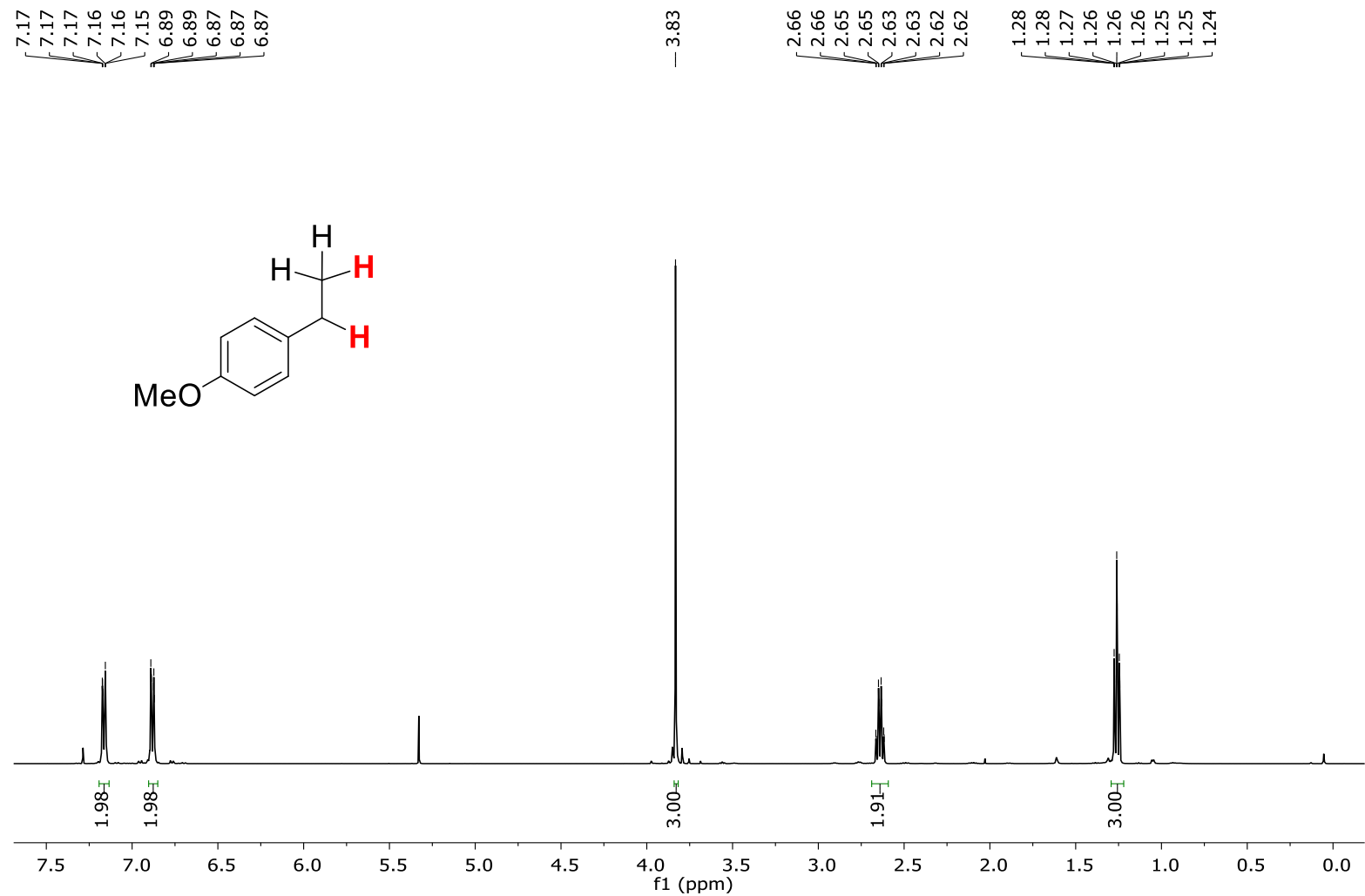


Figure S. 90. ¹H-NMR (CDCl₃, 400 MHz, 300 K) spectrum of product 17a.

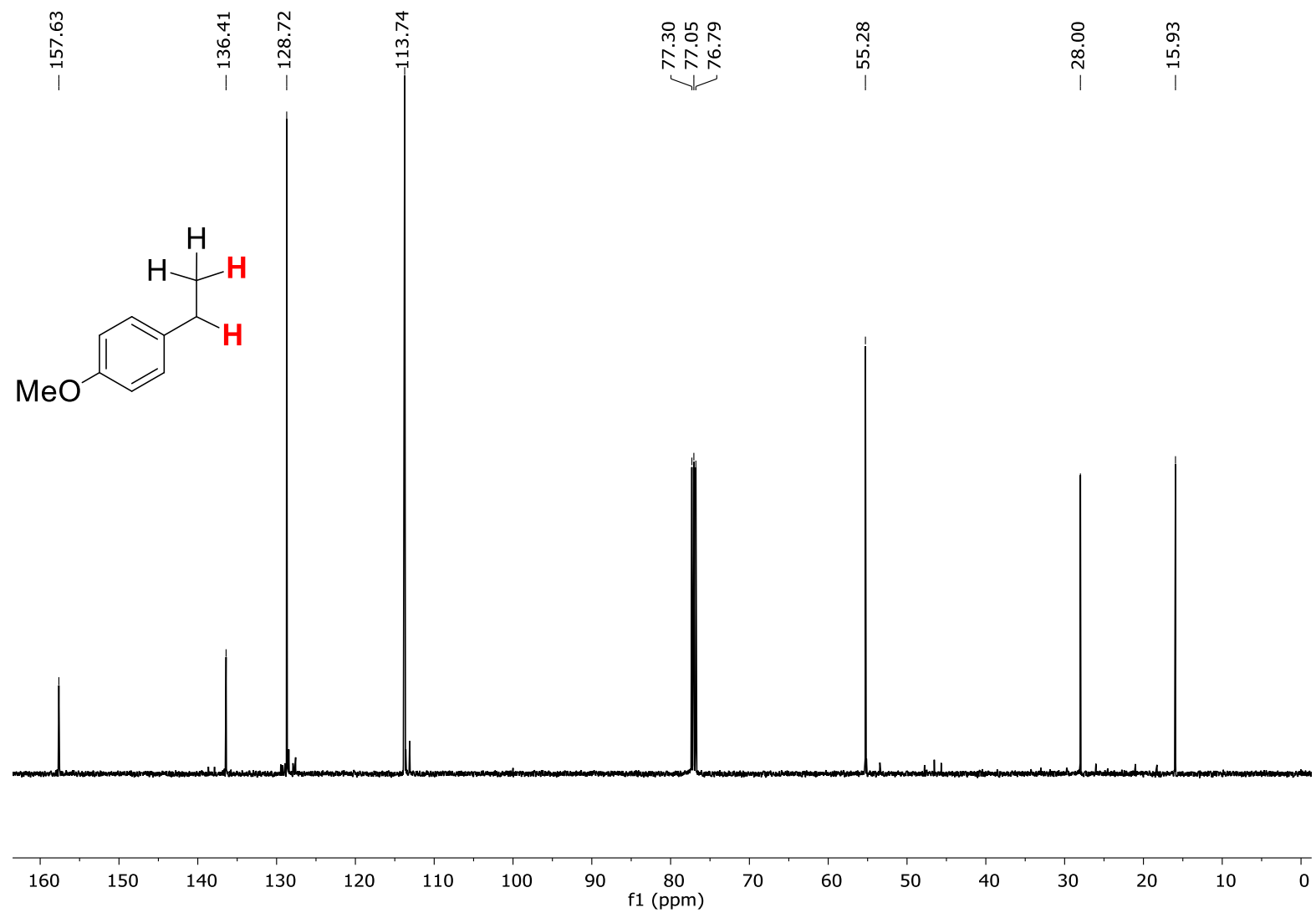


Figure S. 91. $^{13}\text{C}\{^1\text{H}\}$ -NMR (CDCl₃, 100.6 MHz, 300 K) spectrum of product 17a.

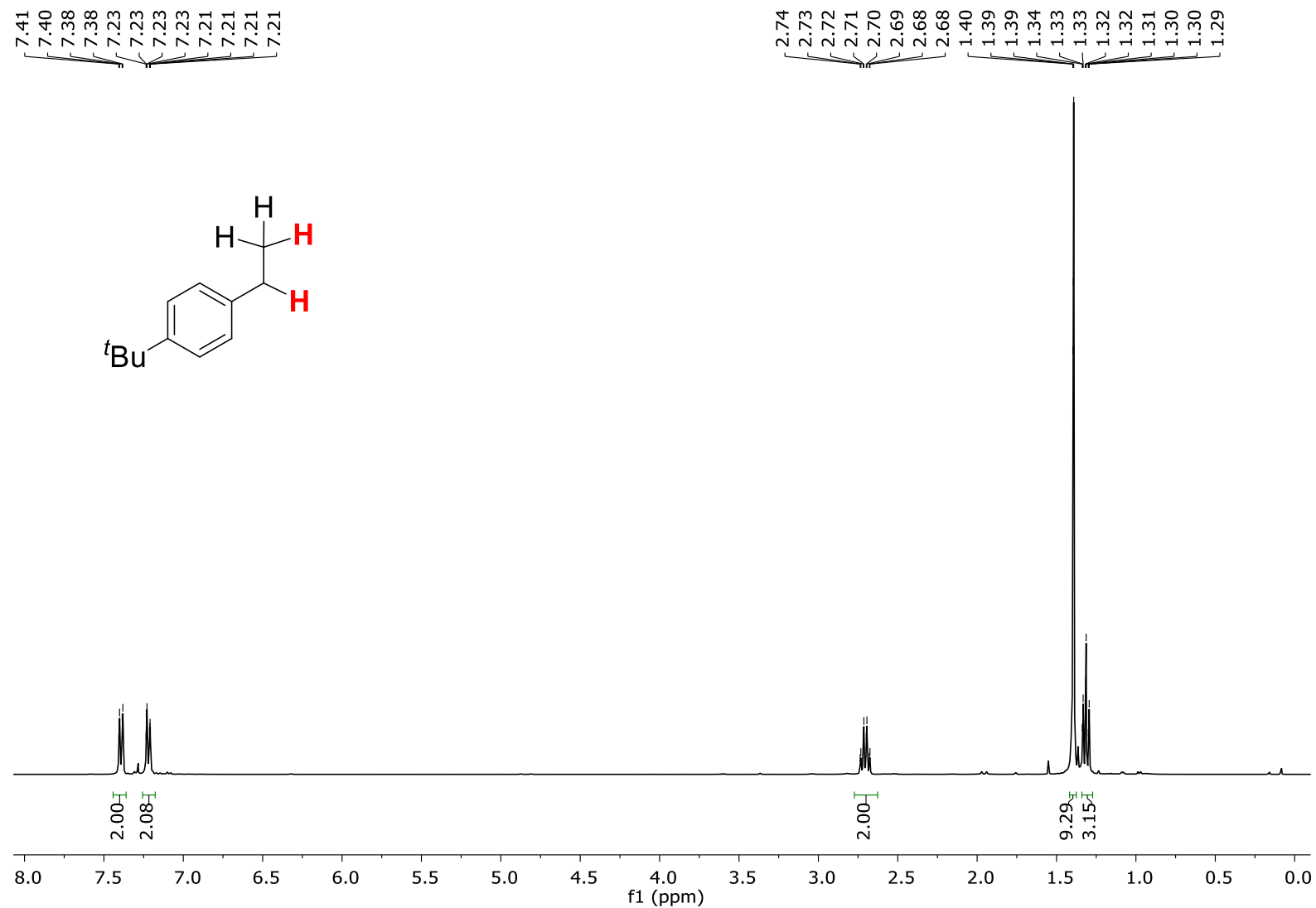


Figure S. 92. ¹H-NMR (CDCl₃, 400 MHz, 300 K) spectrum of product 18a.

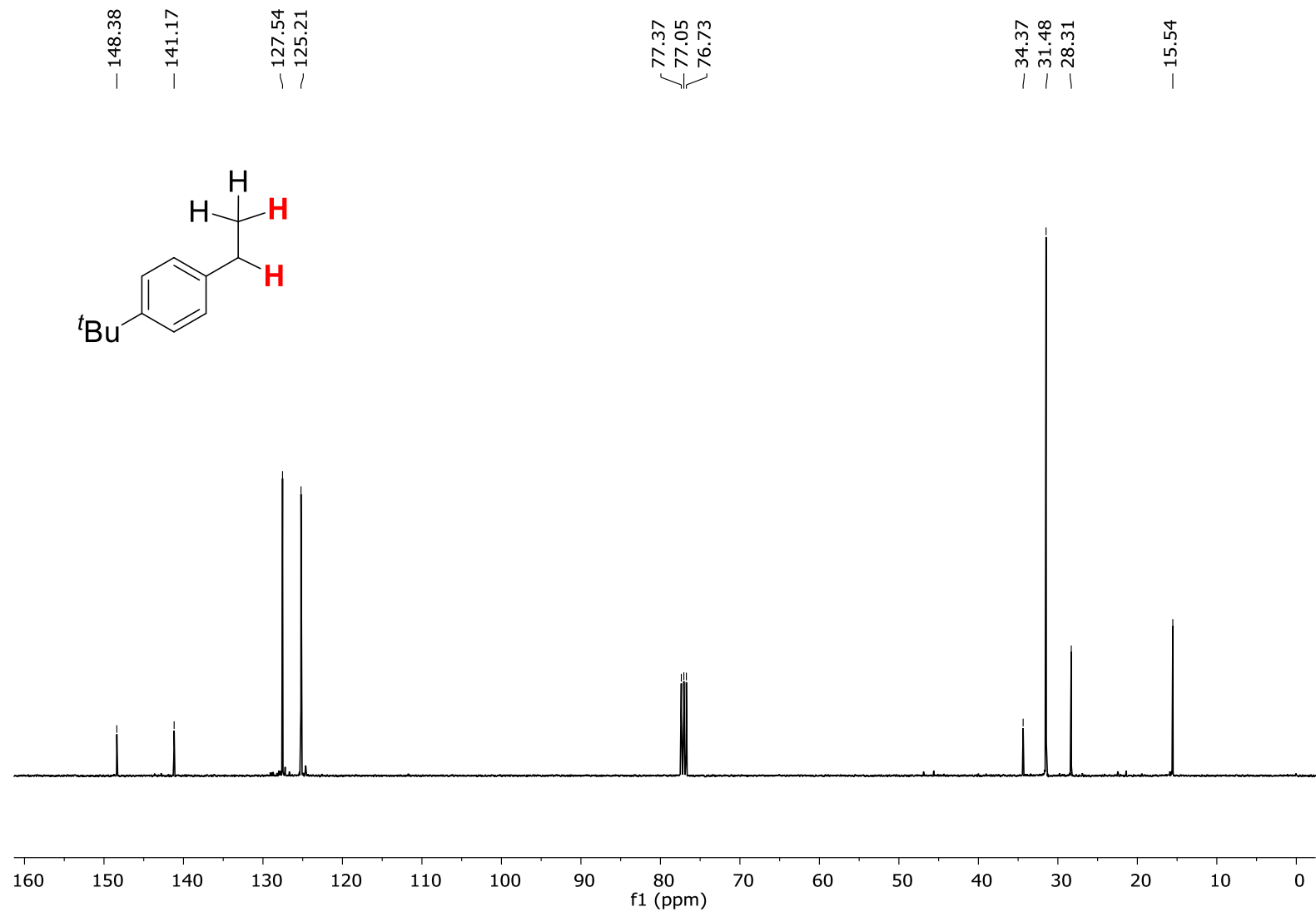


Figure S. 93. $^{13}\text{C}\{^1\text{H}\}$ -NMR (CDCl₃, 100.6 MHz, 300 K) spectrum of product **18a**.

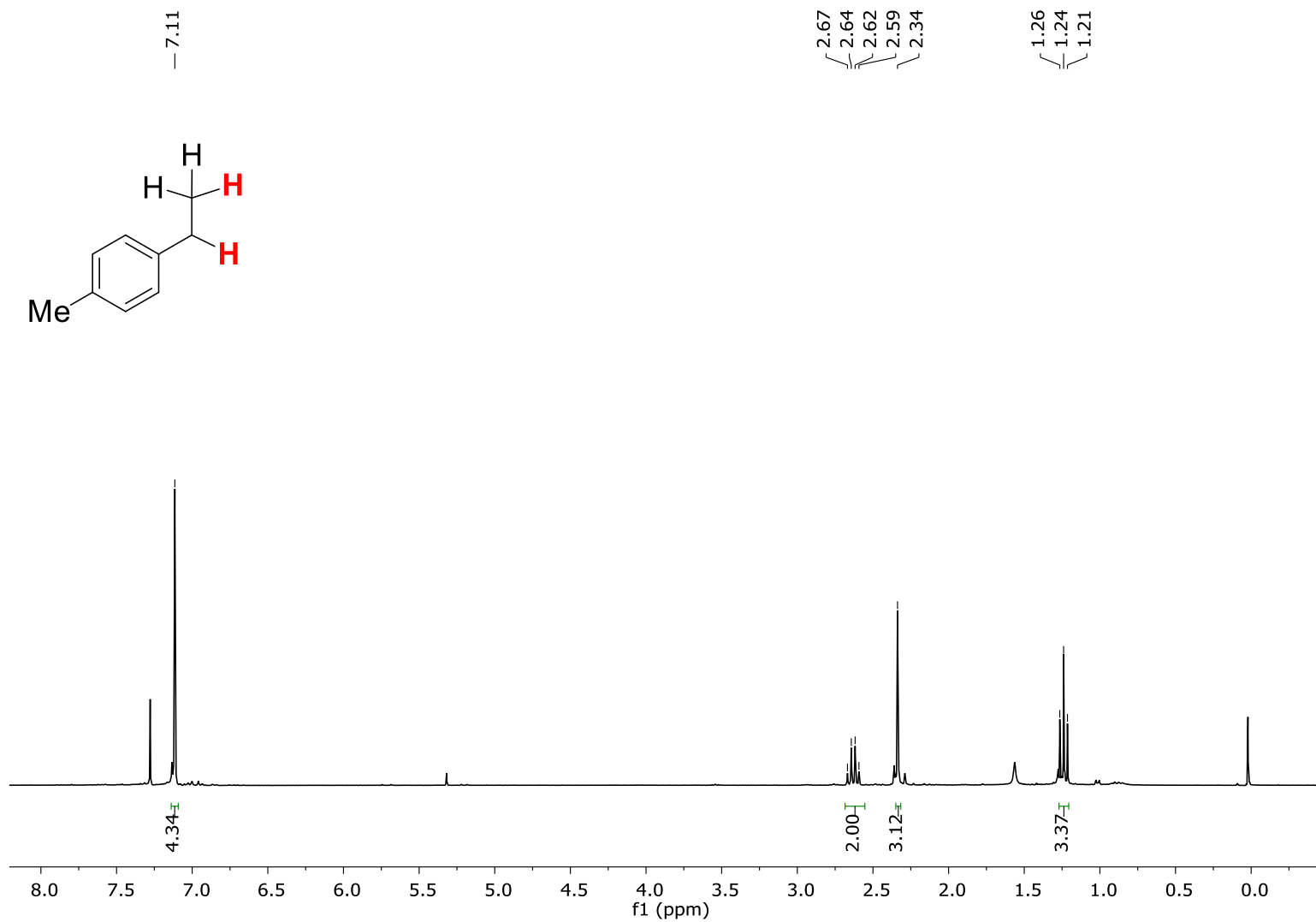


Figure S. 94. ¹H-NMR (CDCl₃, 400 MHz, 300 K) spectrum of product 19a.

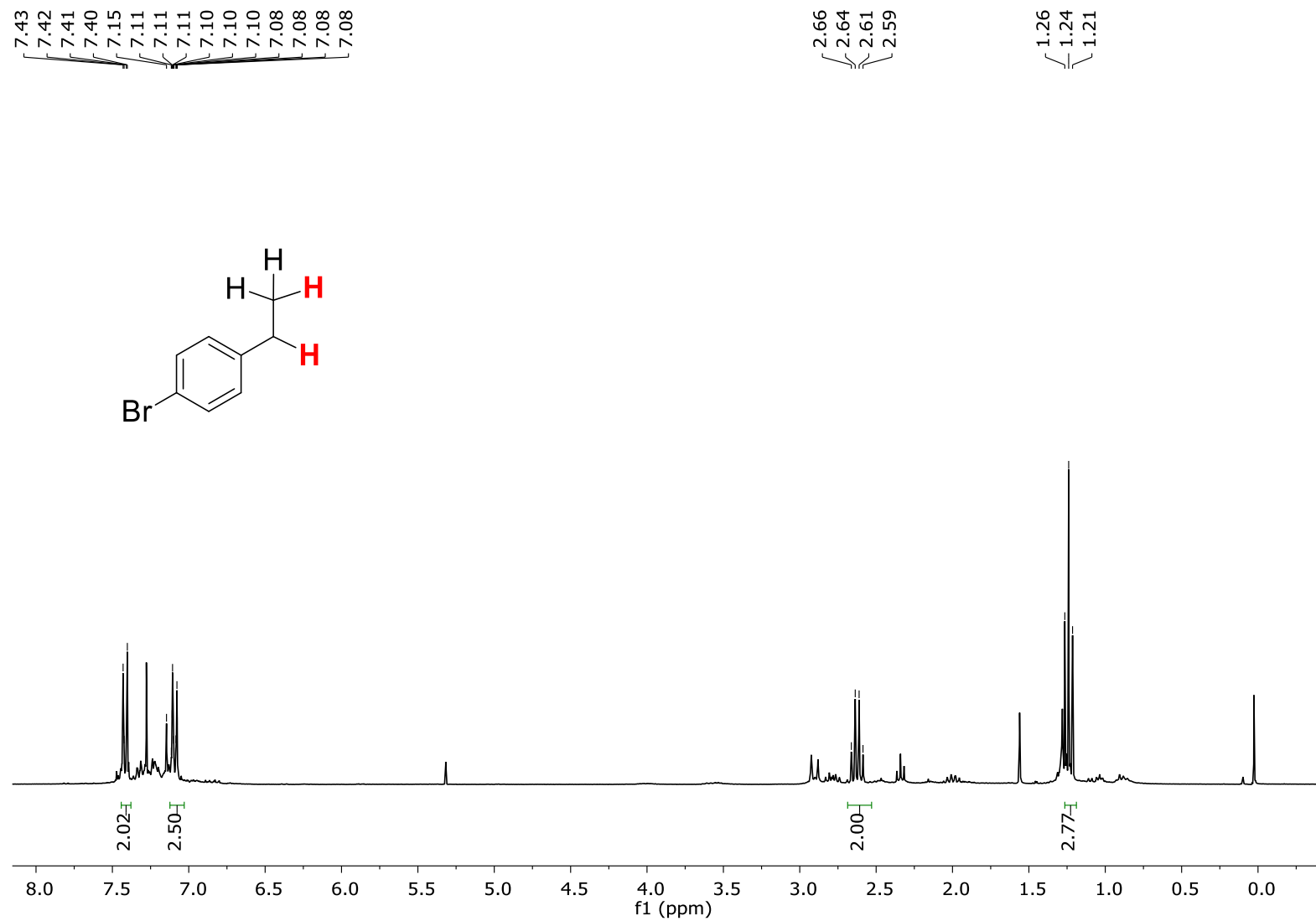


Figure S. 95. ¹H-NMR (CDCl₃, 400 MHz, 300 K) spectrum of product 22a.

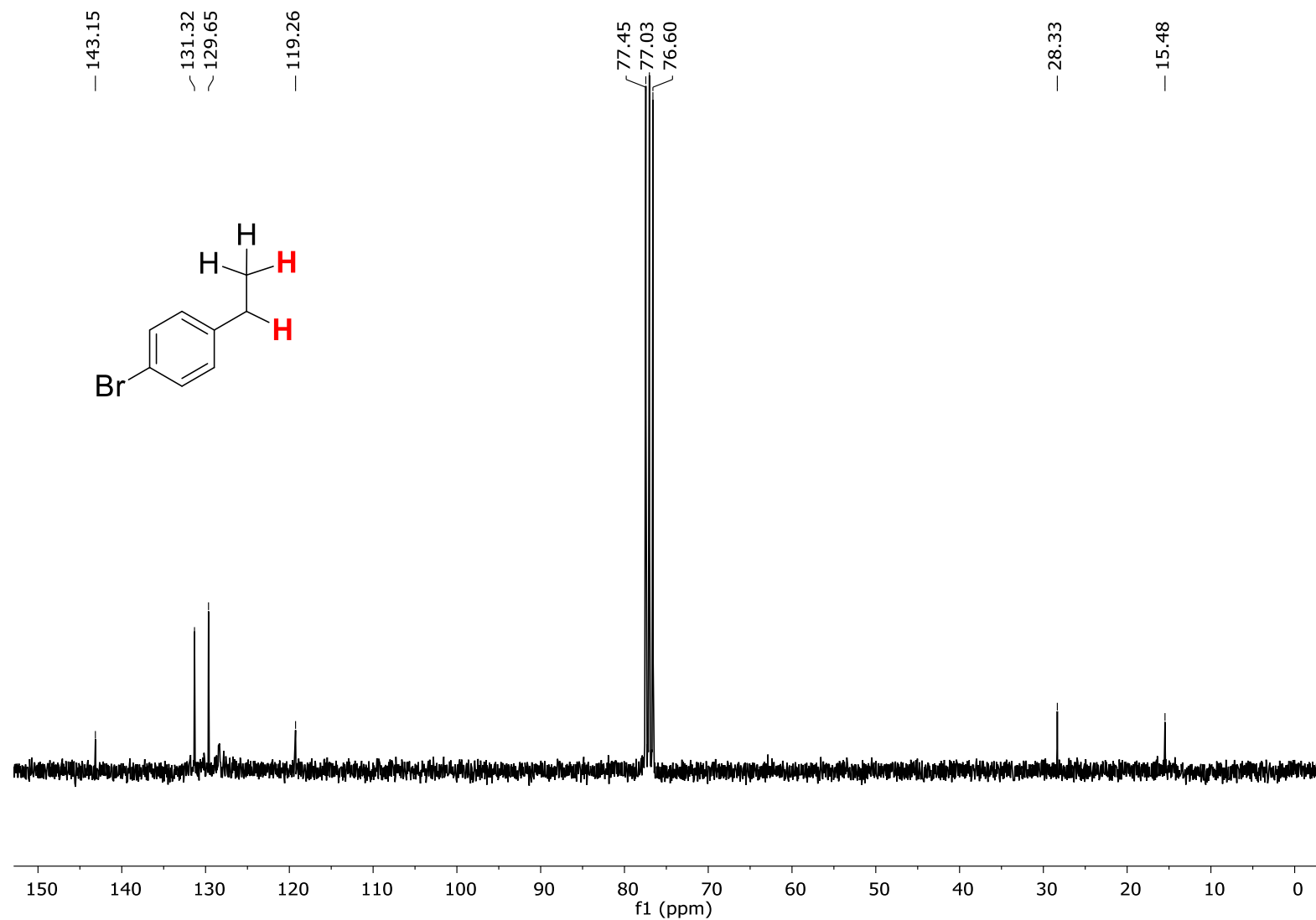


Figure S. 96. $^{13}\text{C}\{^1\text{H}\}$ -NMR (CDCl₃, 100.6 MHz, 300 K) spectrum of product **22a**.

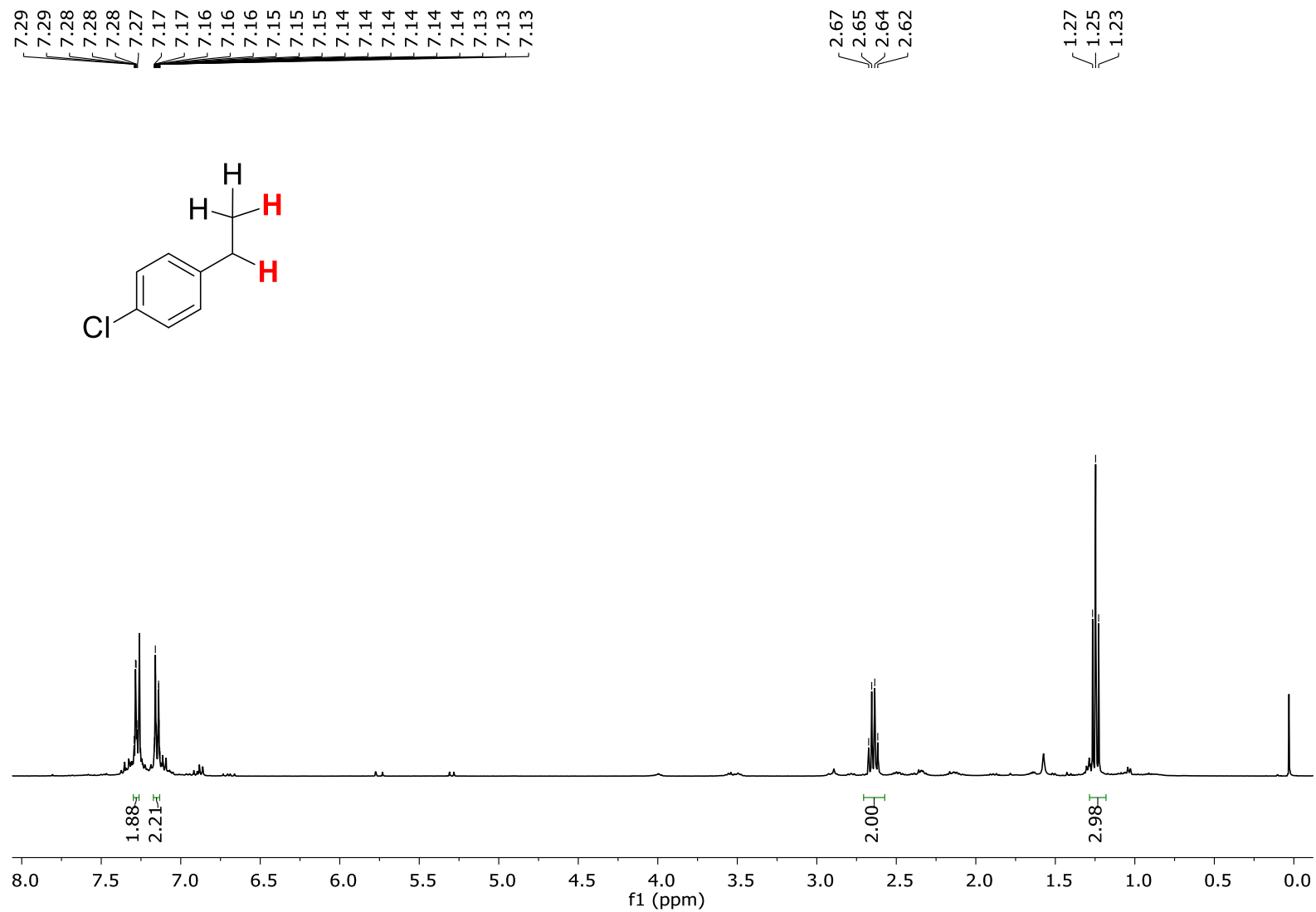


Figure S. 97. ¹H-NMR (CDCl₃, 400 MHz, 300 K) spectrum of product 23a.

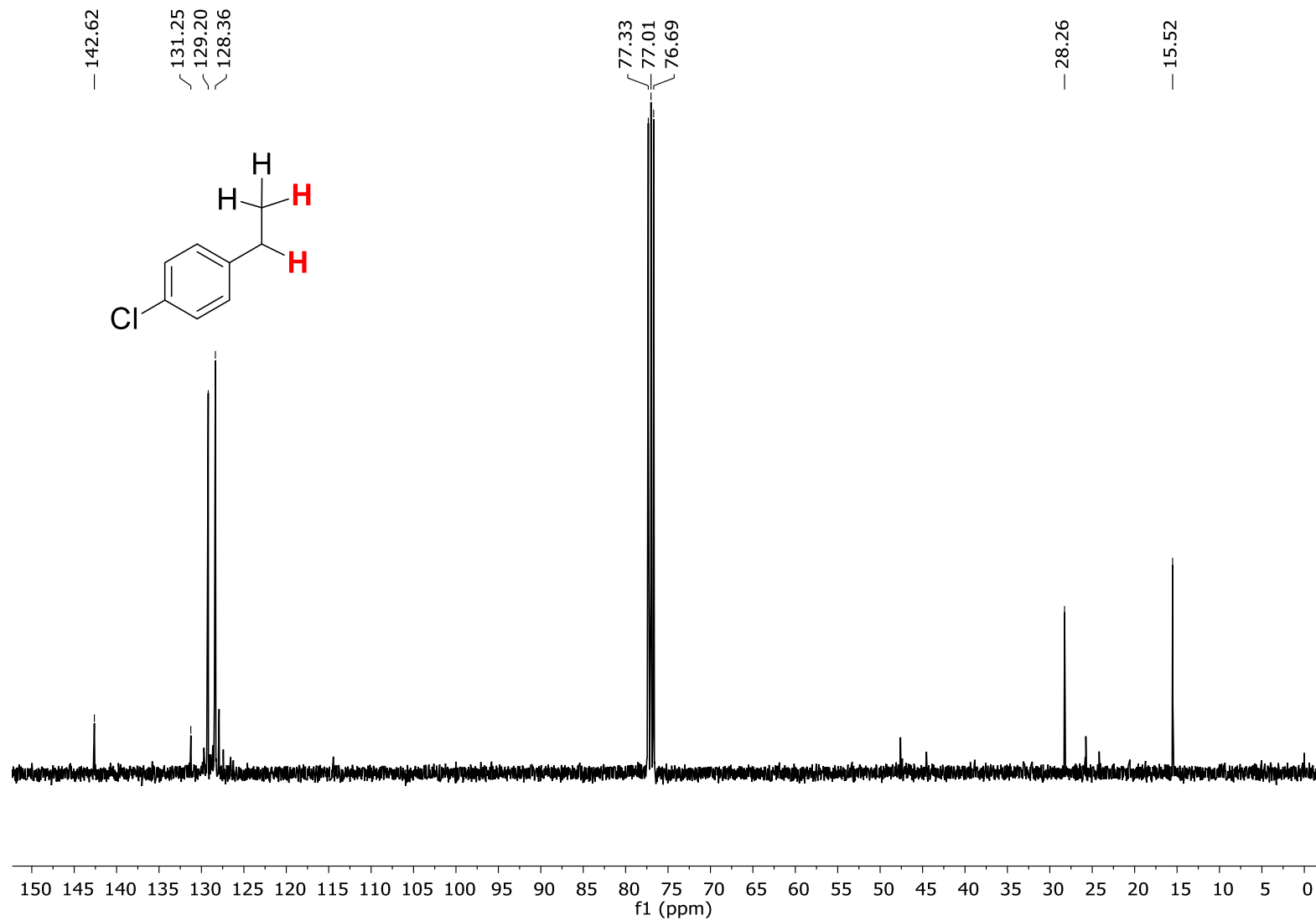


Figure S. 98. $^{13}\text{C}\{^1\text{H}\}$ -NMR (CDCl_3 , 100.6 MHz, 300 K) spectrum of product **23a**.

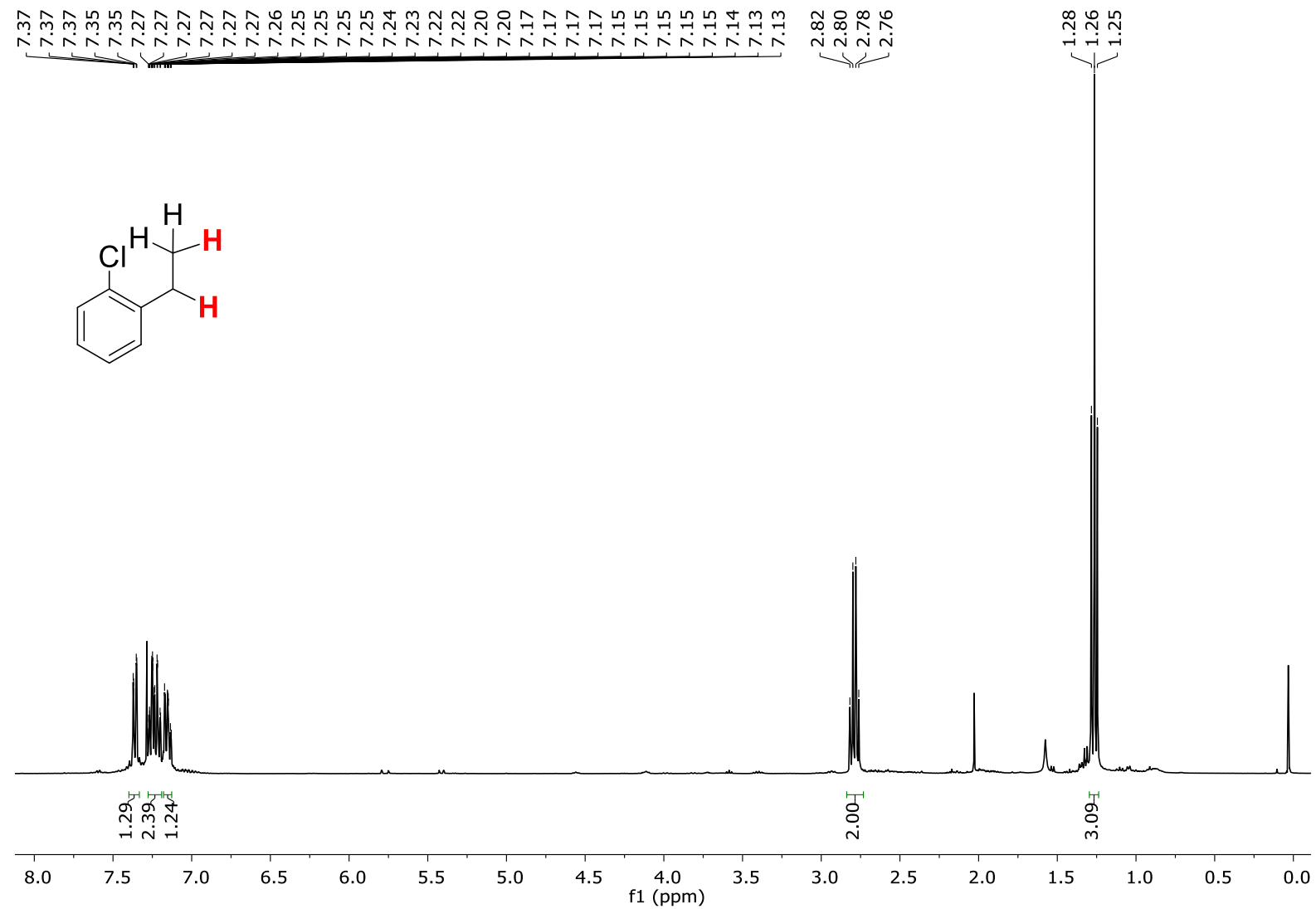


Figure S. 99. $^1\text{H-NMR}$ (CDCl_3 , 400 MHz, 300 K) spectrum of product **24a**.

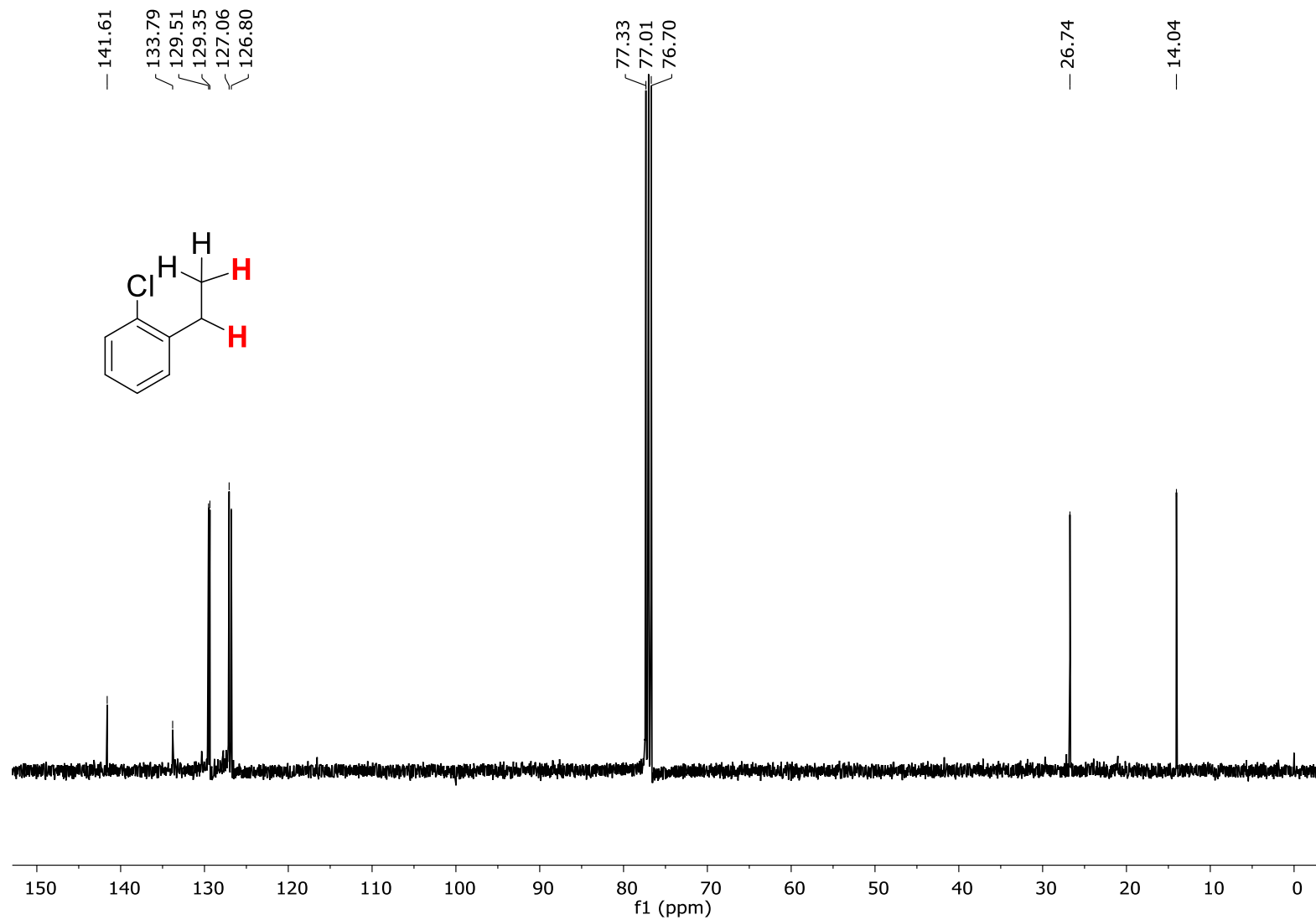


Figure S. 100. $^{13}\text{C}\{^1\text{H}\}$ -NMR (CDCl₃, 100.6 MHz, 300 K) spectrum of product **24a**.

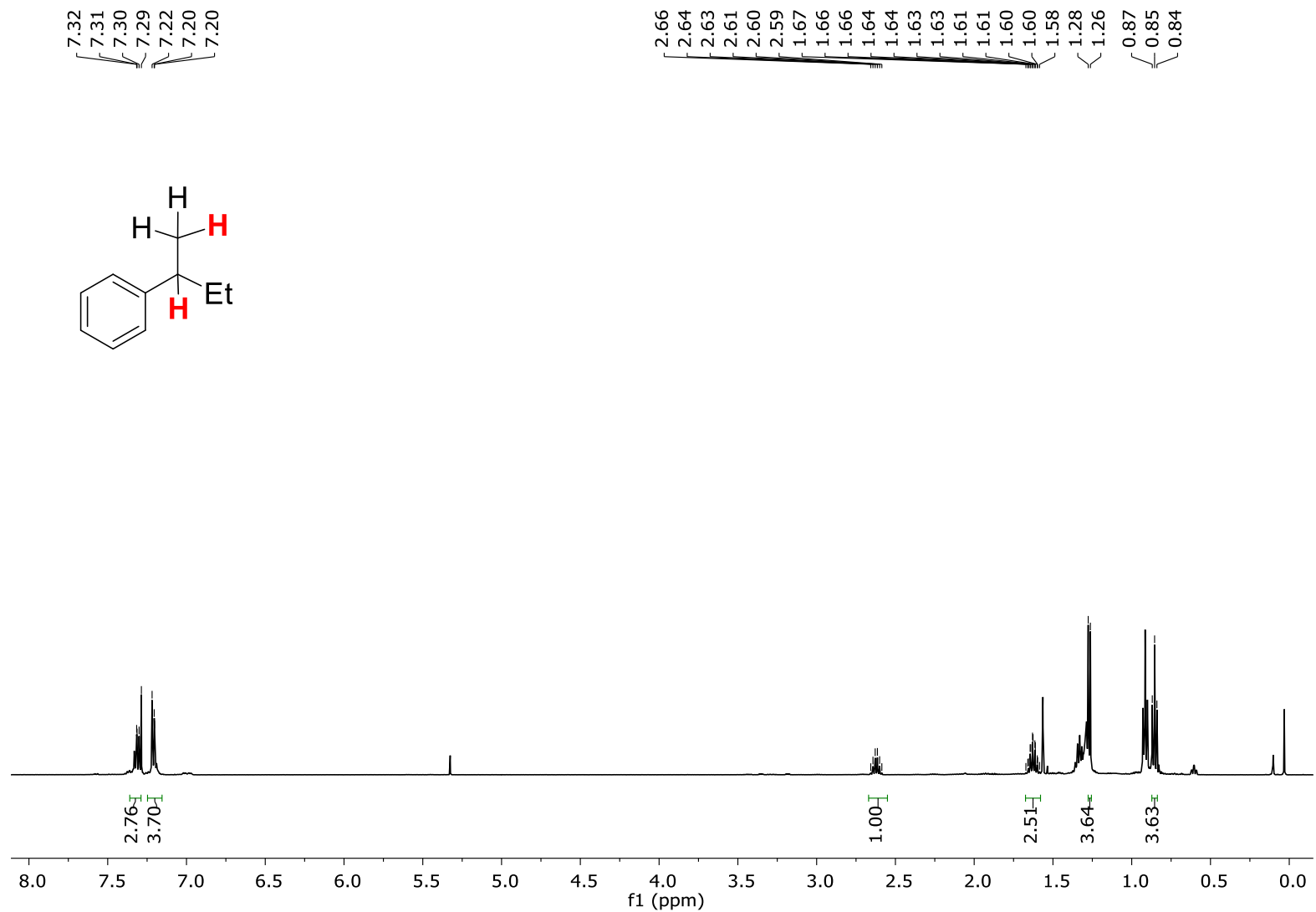


Figure S. 101. ¹H-NMR (CDCl₃, 400 MHz, 300 K) spectrum of product 29a.

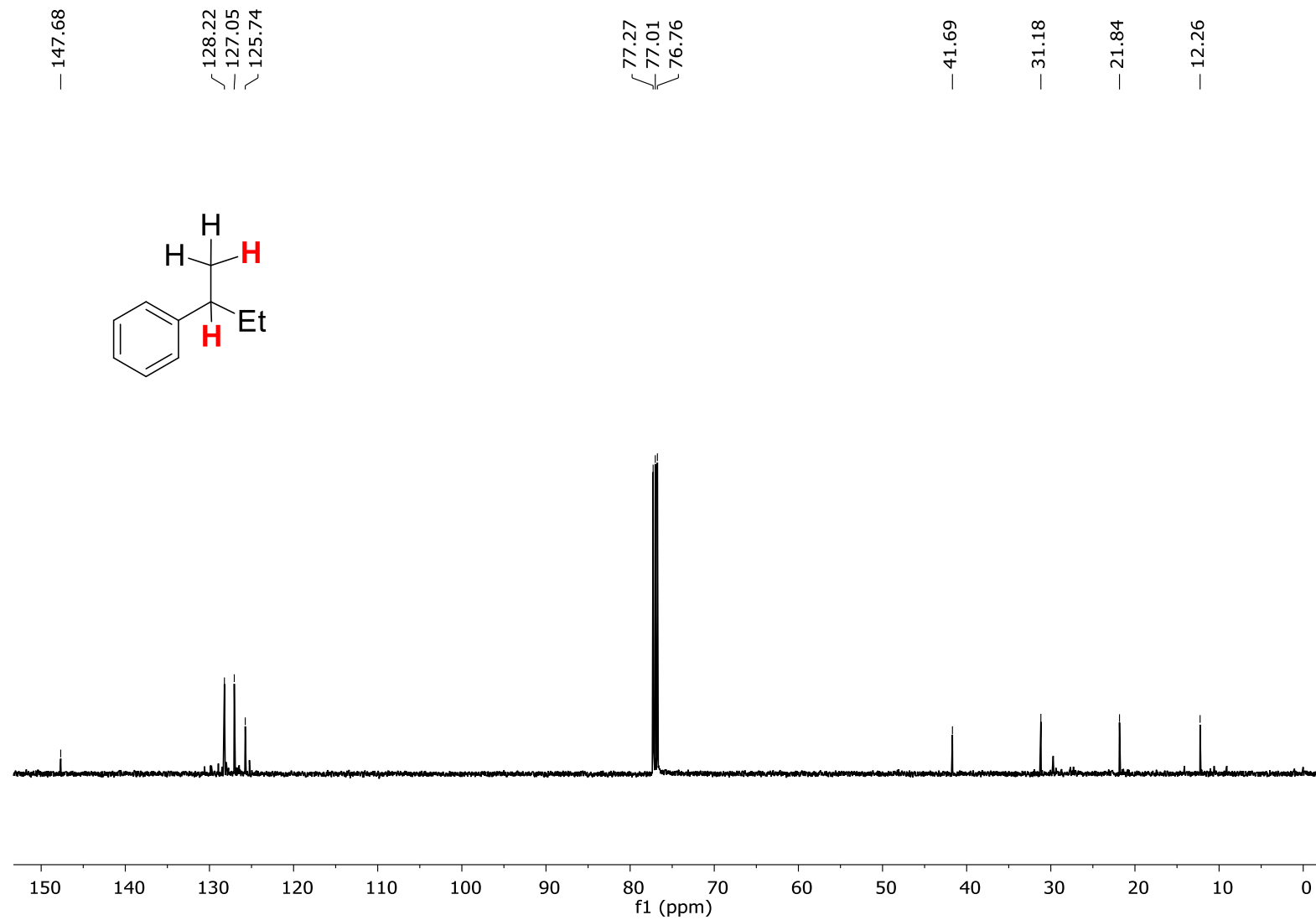


Figure S. 102. $^{13}\text{C}\{^1\text{H}\}$ -NMR (CDCl₃, 100.6 MHz, 300 K) spectrum of product 29a.

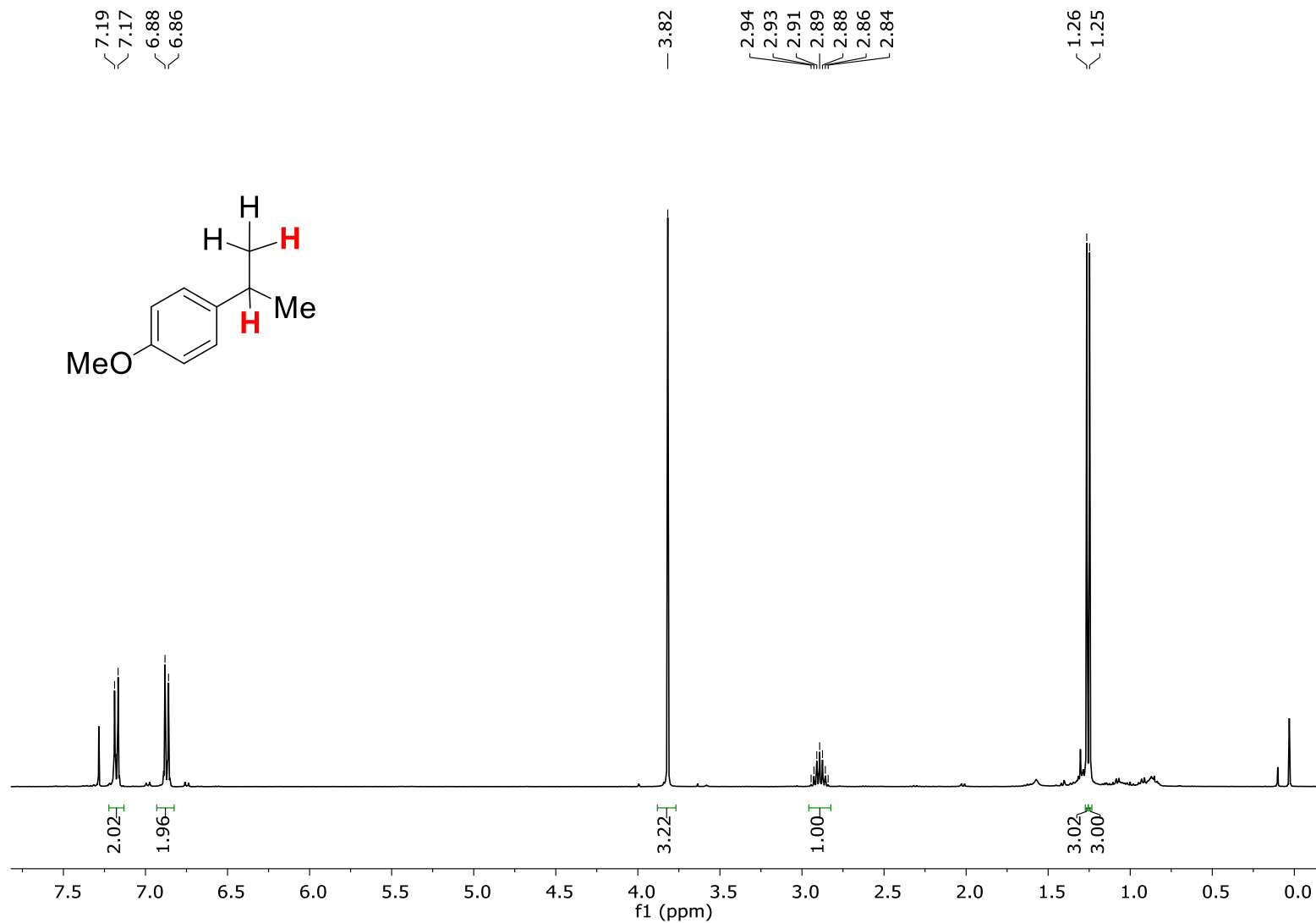


Figure S. 103. ¹H-NMR (CDCl₃, 400 MHz, 300 K) spectrum of product 33a.

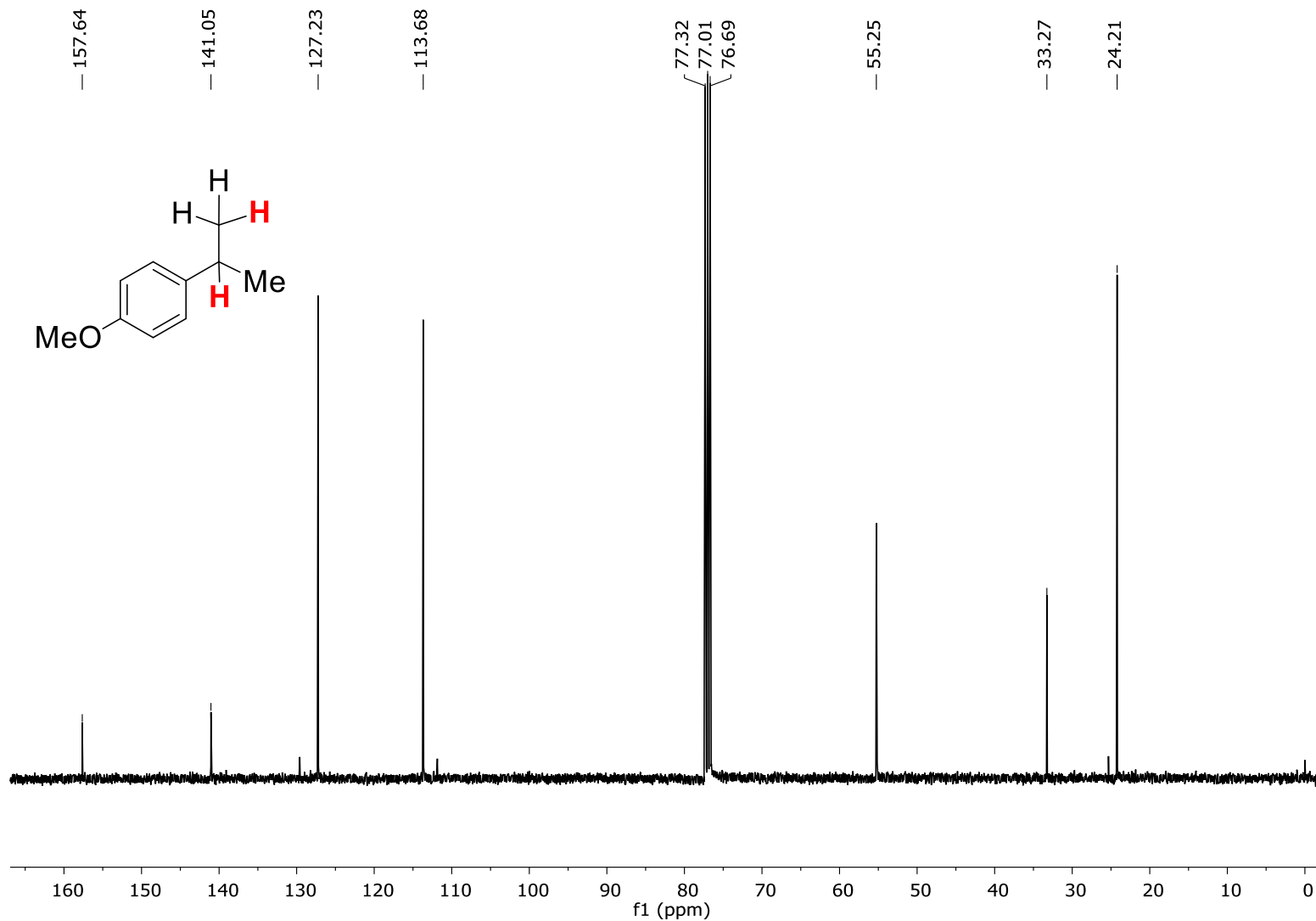


Figure S. 104. $^{13}\text{C}\{^1\text{H}\}$ -NMR (CDCl_3 , 100.6 MHz, 300 K) spectrum of product **33a**.

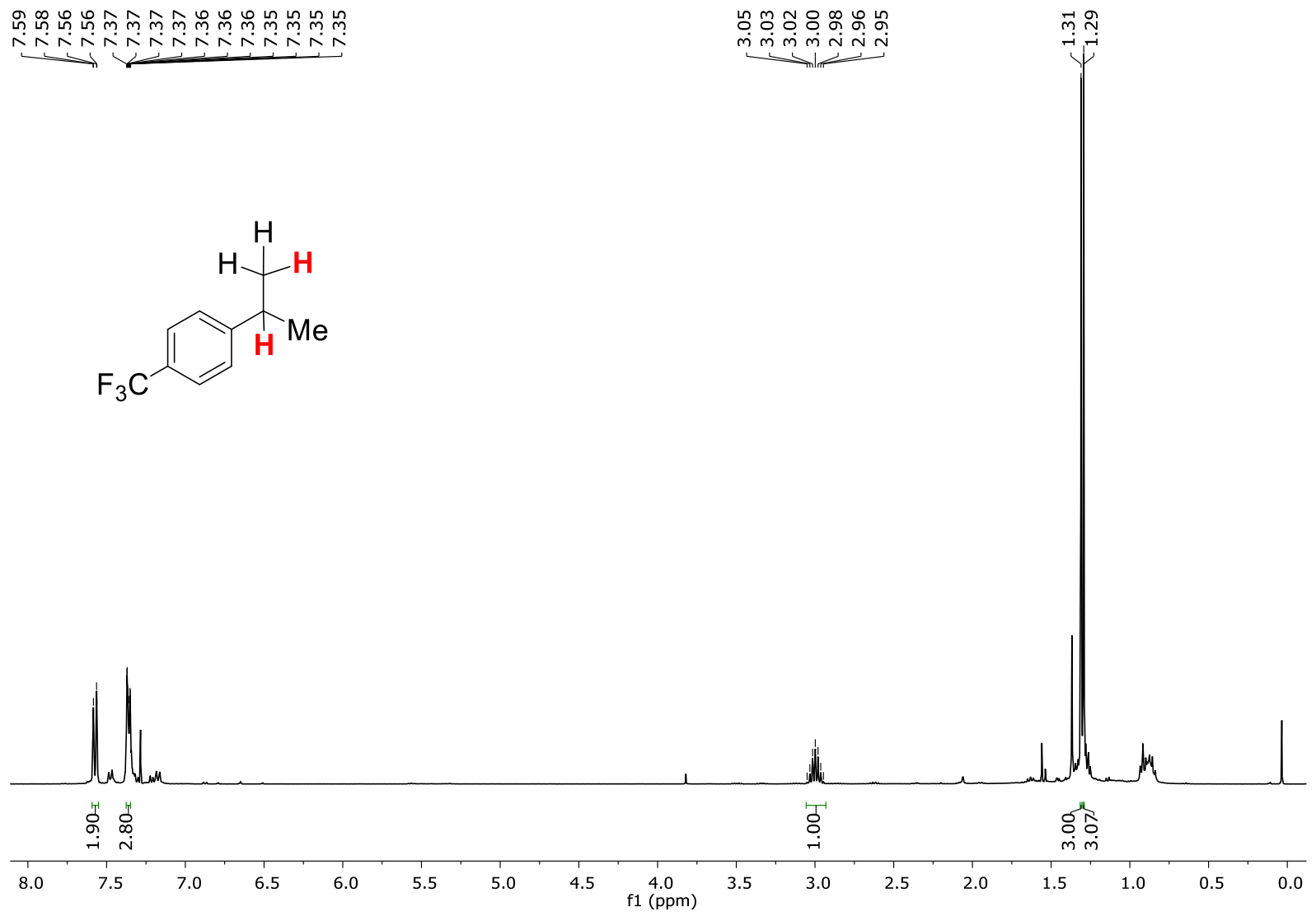


Figure S. 105. ¹H-NMR (CDCl₃, 400 MHz, 300 K) spectrum of product 34a.

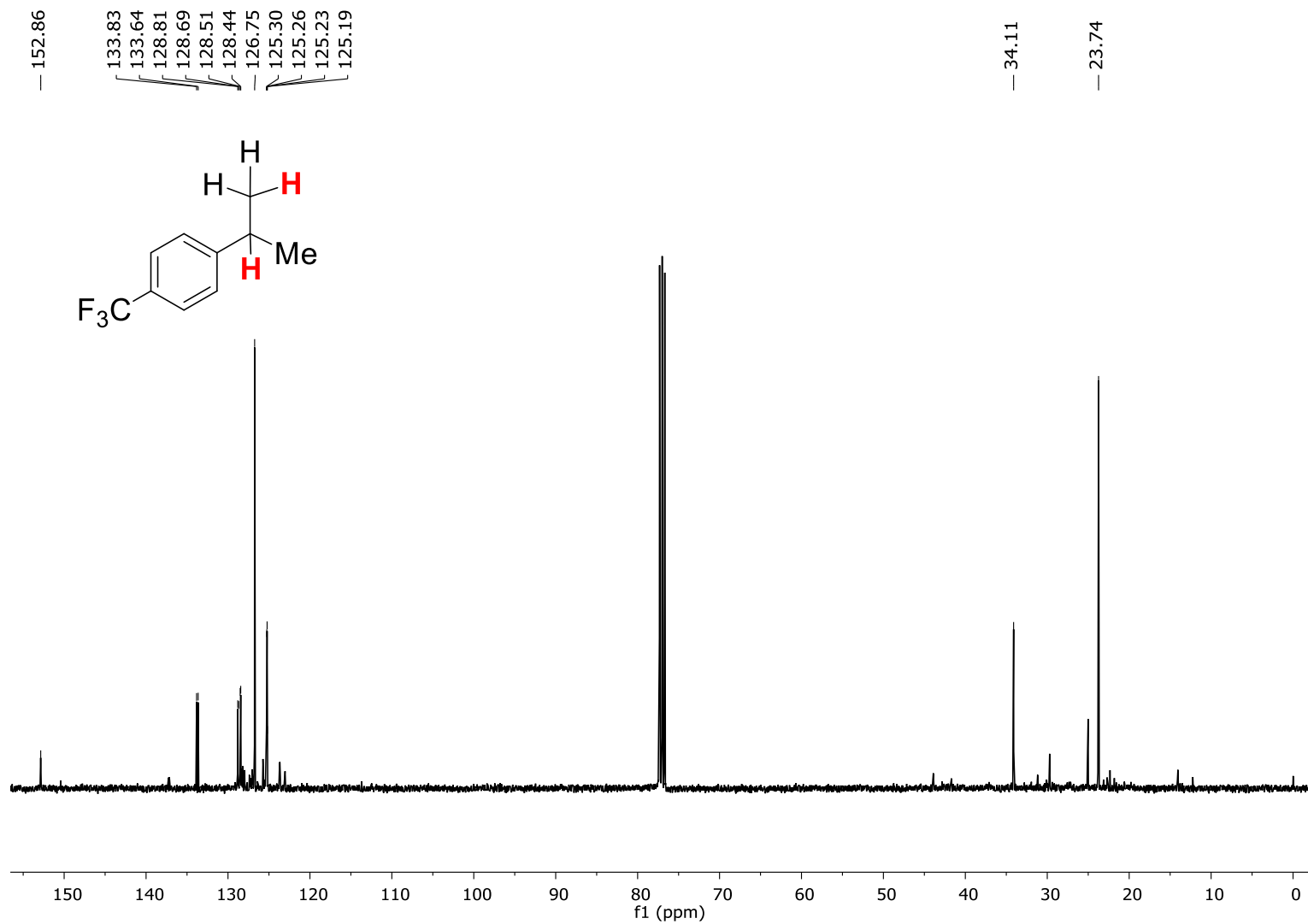


Figure S. 106. $^{13}\text{C}\{^1\text{H}\}$ -NMR (CDCl₃, 100.6 MHz, 300 K) spectrum of product **34a**.

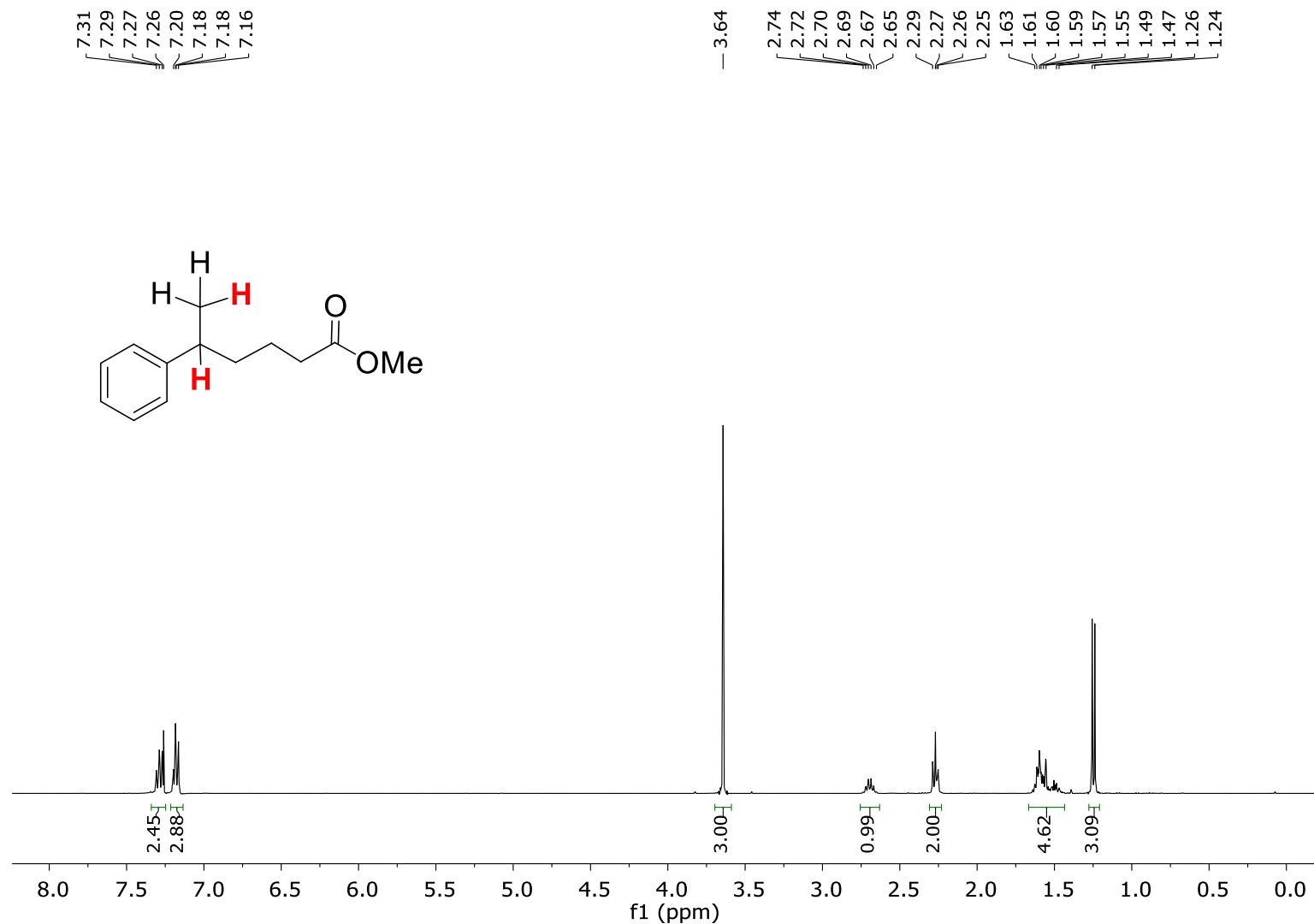


Figure S. 107. ¹H-NMR (CDCl₃, 400 MHz, 300 K) spectrum of product 35a.

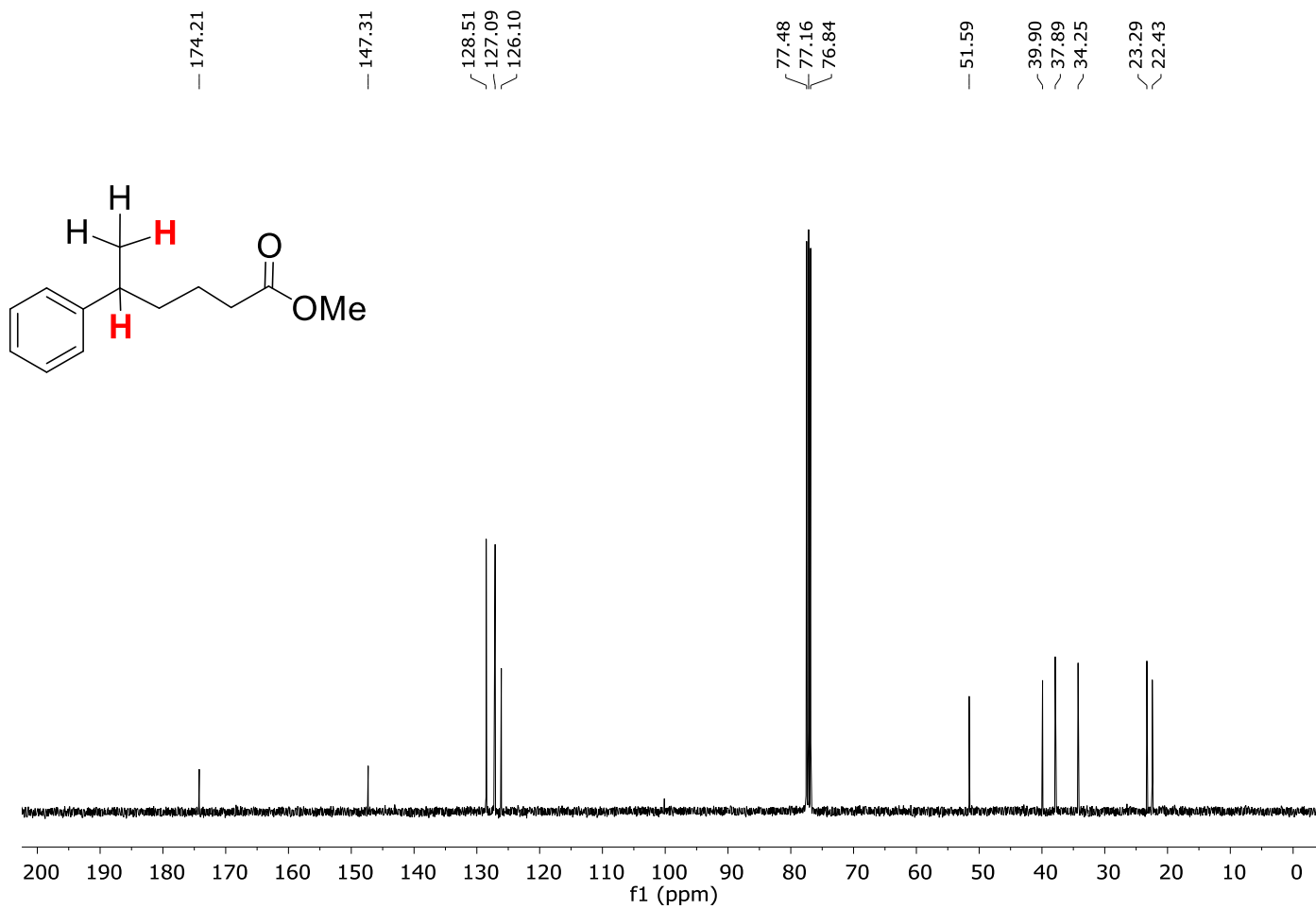


Figure S. 108. $^{13}\text{C}\{^1\text{H}\}$ -NMR (CDCl₃, 100.6 MHz, 300 K) spectrum of product 35a.

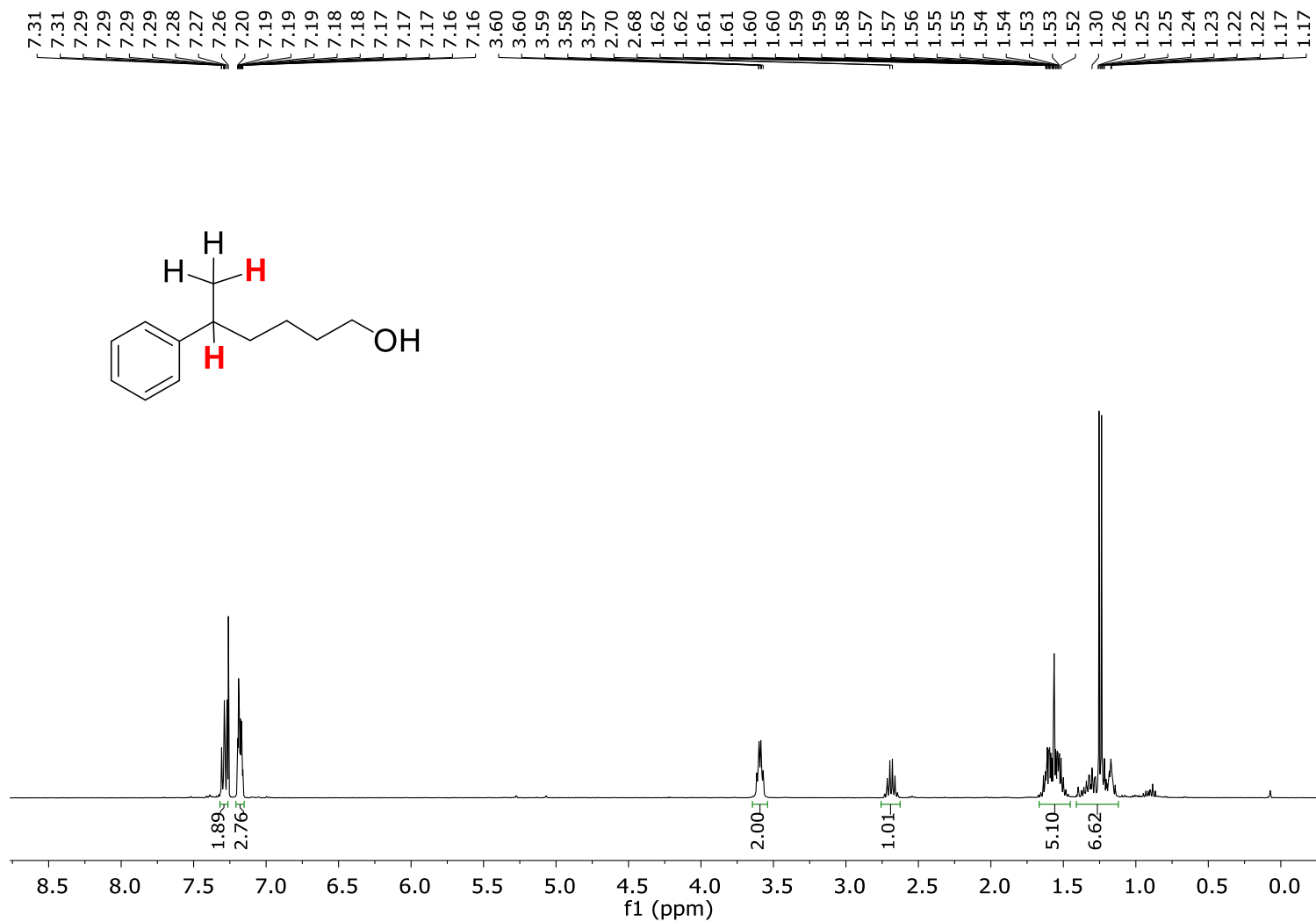


Figure S. 109. ¹H-NMR (CDCl₃, 400 MHz, 300 K) spectrum of product 36a.

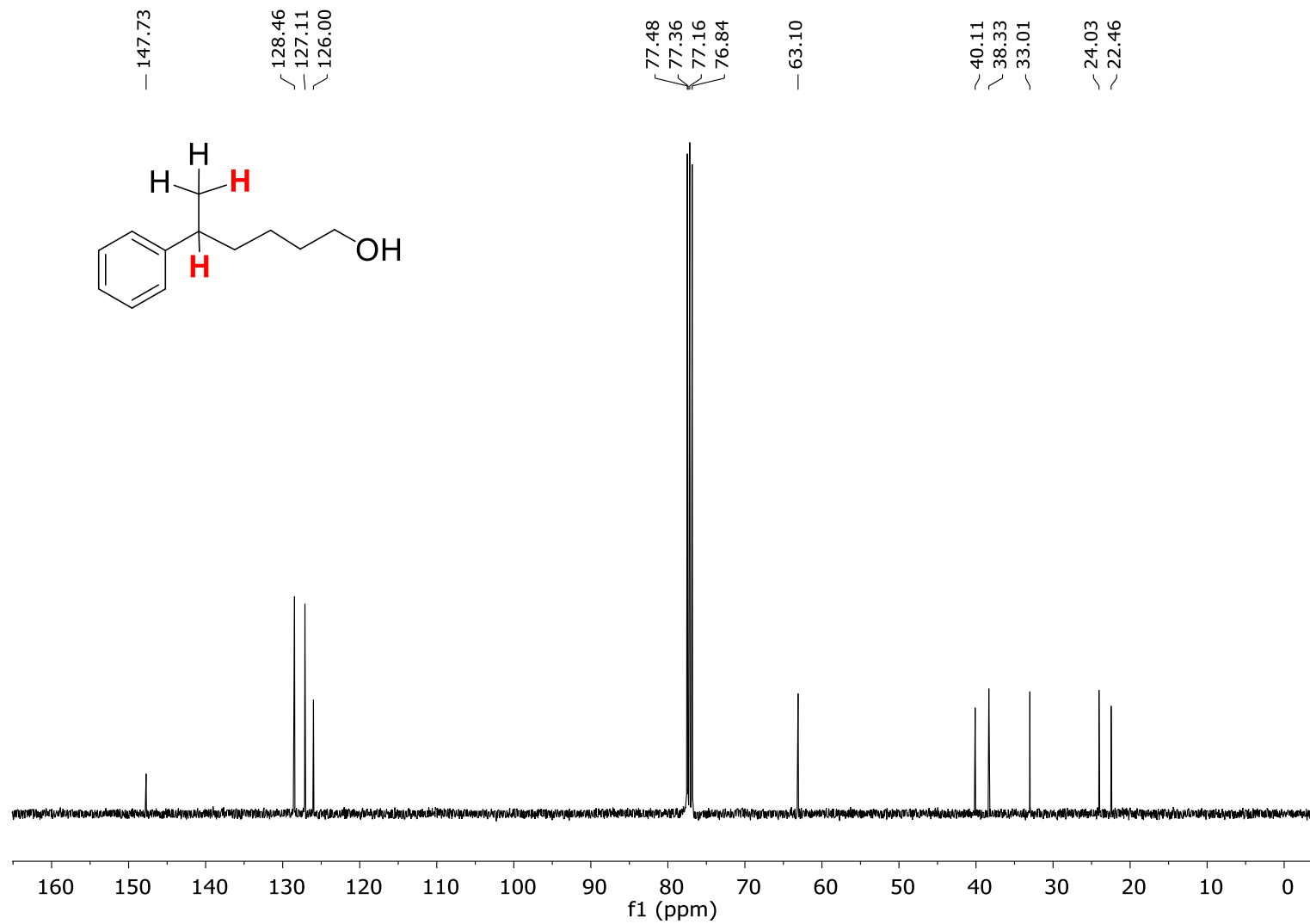


Figure S. 110. ¹³C{¹H}-NMR (CDCl₃, 100.6 MHz, 300 K) spectrum of product 36a.

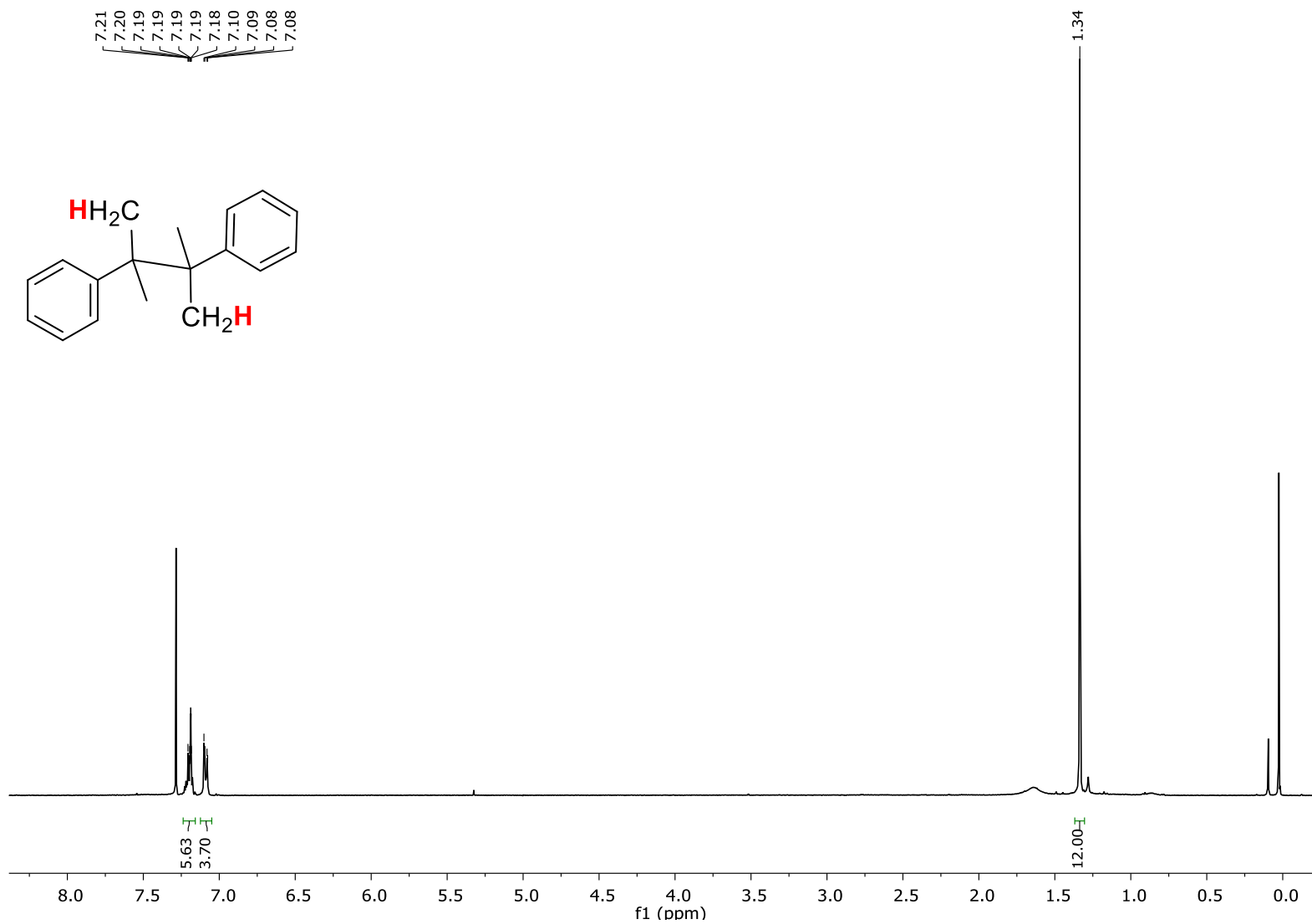


Figure S. 111. $^1\text{H-NMR}$ (CDCl₃, 500 MHz, 300 K) spectrum of product **28b**.

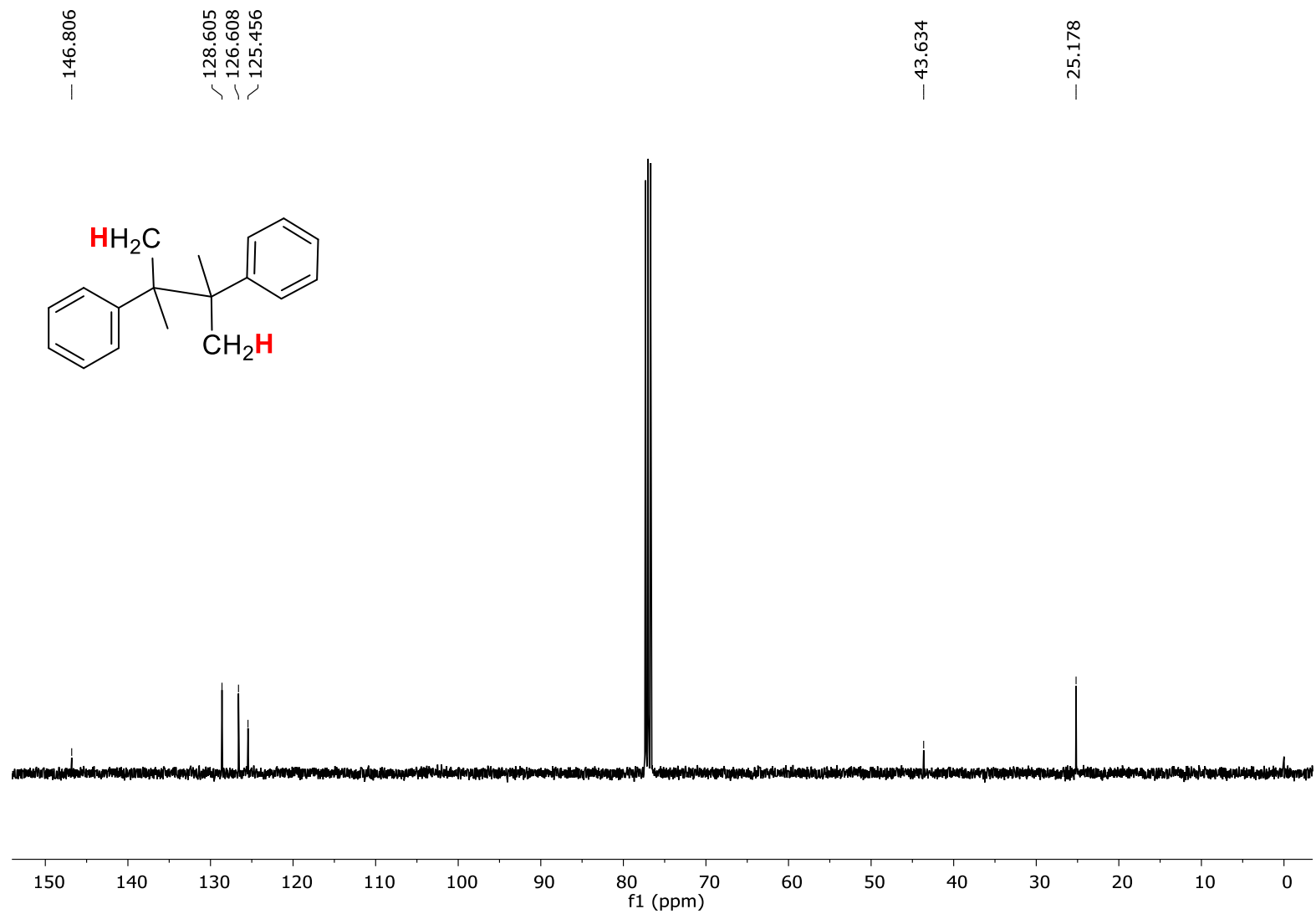
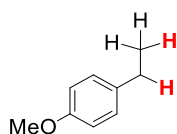


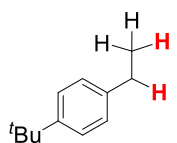
Figure S. 112. $^{13}\text{C}\{^1\text{H}\}$ -NMR (CDCl_3 , 125.75 MHz, 300 K) spectrum of product **28b**.

19. NMR data of the isolated products

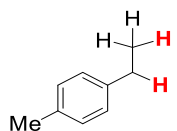
- Isolated alkanes



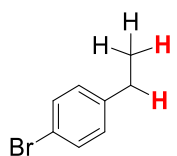
17a (92%) $^1\text{H-NMR}$ (CDCl_3 , 400 MHz, 300 K) δ , ppm: 7.17-7.15 (m, 2H), 6.89-6.87 (m, 2H), 3.83 (s, 3H), 2.66-2.62 (m, 2H), 1.28-1.24 (m, 3H). $^{13}\text{C}\{^1\text{H}\}$ -NMR (CDCl_3 , 100.6 MHz, 300 K) δ , ppm: 157.63, 136.41, 128.72, 113.74, 55.28, 28.00, 15.93. MS (GC): 136.1 [M].



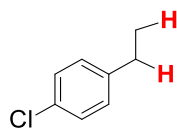
18a (81%) $^1\text{H-NMR}$ (CDCl_3 , 400 MHz, 300 K) δ , ppm: 7.41-7.38 (m, 2H), 7.23-7.21 (m, 2H), 2.74-2.68 (m, 2H), 1.39 (s, 9H), 1.34-1.29 (m, 3H). $^{13}\text{C}\{^1\text{H}\}$ -NMR (CDCl_3 , 100.6 MHz, 300 K) δ , ppm: 148.38, 141.17, 127.54, 125.21, 34.37, 31.48, 28.31, 15.54. MS (GC): 162.1 [M].



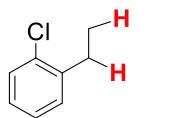
19a (92%) $^1\text{H-NMR}$ (CDCl_3 , 300 MHz, 300 K) δ , ppm: 7.12 (s, 4H), 2.63 (q, $J = 7.8$ Hz, 2H), 2.34 (s, 3H), 1.24 (t, $J = 7.8$ Hz, 3H). MS (GC): 120.1 [M].



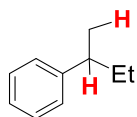
22a (53%) $^1\text{H-NMR}$ (CDCl_3 , 300 MHz, 300 K) δ , ppm: 7.43-7.40 (m, 2H), 7.15-7.08 (m, 2H), 2.62 (q, $J = 7.8$ Hz, 2H), 1.24 (t, $J = 7.8$ Hz, 3H). $^{13}\text{C}\{^1\text{H}\}$ -NMR (CDCl_3 , 75.45 MHz, 300 K) δ , ppm: 143.15, 131.32, 129.65, 119.26, 28.33, 15.48. MS (GC): 184.0 [M].



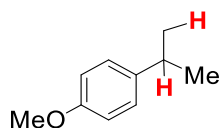
23a (66%) $^1\text{H-NMR}$ (CDCl_3 , 400 MHz, 300 K) δ , ppm: 7.29-7.27 (m, 2H), 7.17-7.13 (m, 2H), 2.64 (q, $J = 7.6$ Hz, 2H), 1.25 (t, $J = 7.6$ Hz, 3H). $^{13}\text{C}\{^1\text{H}\}$ -NMR (CDCl_3 , 100.6 MHz, 300 K) δ , ppm: 142.62, 131.25, 129.20, 128.36, 28.26, 15.52. MS (GC): 140.0 [M].



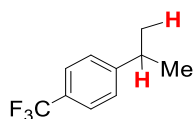
24a (61%) $^1\text{H-NMR}$ (CDCl_3 , 400 MHz, 300 K) δ , ppm: 7.37-7.35 (m, 1H), 7.27-7.20 (m, 2H), 7.17-7.13 (m, 1H), 2.79 (q, $J = 7.6$ Hz, 2H), 1.26 (t, $J = 7.6$ Hz, 3H). $^{13}\text{C}\{^1\text{H}\}$ -NMR (CDCl_3 , 100.6 MHz, 300 K) δ , ppm: 141.61, 133.79, 129.51, 129.35, 127.06, 126.80, 26.74, 14.04. MS (GC): 140.0 [M].



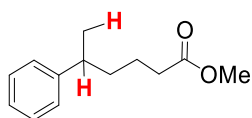
29a (57%) $^1\text{H-NMR}$ (CDCl_3 , 400 MHz, 300 K) δ , ppm: 7.32-7.29 (m, 2H), 7.22-7.20 (m, 2H), 2.62 (sext., $J = 6$ Hz, 1H), 1.67-1.58 (m, 2H), 1.27 (d, $J = 5.6$ Hz, 3H), 0.85 (t, $J = 5.6$ Hz, 3H). $^{13}\text{C}\{^1\text{H}\}$ -NMR (CDCl_3 , 100.6 MHz, 300 K) δ , ppm: 147.68, 128.22, 127.05, 125.74, 41.69, 31.18, 21.84, 12.26. MS (GC): 134.1 [M].



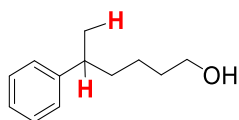
33a (74%) $^1\text{H-NMR}$ (CDCl_3 , 400 MHz, 300 K) δ , ppm: 7.19-7.17 (m, 2H), 6.88-6.86 (m, 2H), 3.22 (s, 3H), 2.89 (sept., $J = 6.8$ Hz, 1H), 1.26 (s, 3H), 1.25 (s, 3H). $^{13}\text{C}\{^1\text{H}\}$ -NMR (CDCl_3 , 100.6 MHz, 300 K) δ , ppm: 157.64, 141.05, 127.23, 113.68, 55.25, 33.27, 24.21. MS (GC): 150.1 [M].



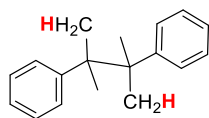
34a $^1\text{H-NMR}$ (CDCl_3 , 400 MHz, 300 K) δ , ppm: 7.59-7.56 (m, 2H), 7.37-7.35 (m, 2H), 2.99 (sept., $J = 6.8$ Hz, 1H), 1.31 (s, 3H), 1.29 (s, 3H). $^{13}\text{C}\{^1\text{H}\}$ -NMR (CDCl_3 , 100.6 MHz, 300 K) δ , ppm: 152.86, 133.74 (d, $J = 19.4$ Hz), 128.75 (d, $J = 11.57$ Hz), 128.48 (d, $J = 6.94$ Hz), 126.75, 125.24 (q, $J = 3.82$ Hz), 34.11, 23.74. MS (GC): 188.1 [M].



35a (66%). $^1\text{H-NMR}$ (CDCl_3 , 400 MHz, 300 K) δ , ppm: 7.33-7.25 (m, 2H), 7.22-7.15 (m, 3H), 3.64 (s, 3H), 2.69 (sext., $J = 6.9$ Hz, 1H), 2.30-2.24 (m, 2H), 1.65-1.46 (m, 4H), 1.25 (d, $J = 6.9$ Hz, 3H). $^{13}\text{C}\{^1\text{H}\}$ -NMR (CDCl_3 , 100.6 MHz, 300 K) δ , ppm: 174.2, 147.3, 128.5, 127.1, 126.1, 51.6, 39.9, 37.9, 34.3, 23.3, 22.4. GC (MS): 206.1 [M].

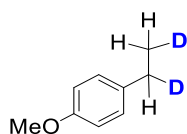


36a (83%). $^1\text{H-NMR}$ (CDCl_3 , 400 MHz, 300 K) δ , ppm: 7.32-7.25 (m, 2H), 7.21-7.16 (m, 3H), 3.59 (td, $J = 6.5$, 4.6 Hz, 2H), 2.69 (h, $J = 7.0$ Hz, 1H), 1.66-1.49 (m, 4H), 1.38-1.13 (m, 6H). $^{13}\text{C}\{^1\text{H}\}$ -NMR (CDCl_3 , 100.6 MHz, 300 K) δ , ppm: 147.7, 128.5, 127.1, 126.0, 63.1, 40.1, 38.3, 33.0, 24.0, 22.5. MS (GC): 178.1 [M].

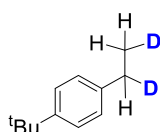


28b (45%). $^1\text{H-NMR}$ (CDCl_3 , 500 MHz, 300 K) δ , ppm: 7.21-7.18 (m, 6H), 7.10-7.08 (m, 4H), 1.34 (s, 12H). $^{13}\text{C}\{^1\text{H}\}$ -NMR (CDCl_3 , 125.75 MHz, 300 K) δ , ppm: 146.81, 128.61, 126.61, 125.46, 43.63, 25.18. MS (GC): 238.2 [M].

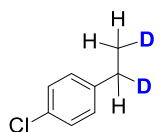
- Characterization of the deuterated alkanes



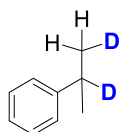
1-(ethyl-1,2- d_2)-4-methoxybenzene ([D]-17a). $^1\text{H-NMR}$ (CDCl_3 , 400 MHz, 300 K) δ , ppm: 7.15-7.13 (m, 2H, H_{arom}), 6.87-6.85 (m, 2H, H_{arom}), 3.82 (s, 3H, O- CH_3), 2.62-2.58 (m, 1H, CHD), 1.28-1.24 (m, 2H, CH_2D). $^{13}\text{C}\{^1\text{H}\}$ -NMR (CDCl_3 , 100.6 MHz, 300 K) δ , ppm: 157.62, 136.36, 128.68, 113.73, 55.27, 27.53 (t, $J = 19.1$ Hz, CHD), 15.79-15.30 (m, CH_2D).



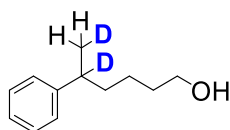
1-(tert-butyl)-4-(ethyl-1,2- d_2)benzene ([D]-18a). (54%, *this isolated yield was that low due to the volatility of the product) $^1\text{H-NMR}$ (CDCl_3 , 400 MHz, 300 K) δ , ppm: 7.37-7.34 (m, 2H, H_{arom}), 7.19-7.17 (m, 2H, H_{arom}), 2.67-2.63 (m, 1H, CHD), 1.35 (s, 9H, (CH_3) $_3$), 1.29-1.23 (m, 2H, CH_2D). $^{13}\text{C}\{^1\text{H}\}$ -NMR (CDCl_3 , 100.6 MHz, 300 K) δ , ppm: 148.5, 141.3, 127.6, 125.3, 34.5, 31.6, 28.0 (t, $J = 19.5$ Hz, CHD), 15.3 (t, $J = 19.3$ Hz, CH_2D). MS (GC): 164.0 [M].



1-chloro-4-(ethyl-1,2- d_2)benzene ([D]-23a). (33%, *this isolated yield was that low due to the volatility of the product) $^1\text{H-NMR}$ (CDCl_3 , 400 MHz, 300 K) δ , ppm: 7.26-7.23 (m, 2H), 7.14-7.10 (m, 2H), 2.63-2.57 (m, 1H, CHD), 1.22-1.18 (m, 2H, CH_2D). $^{13}\text{C}\{^1\text{H}\}$ -NMR (CDCl_3 , 100.6 MHz, 300 K) δ , ppm: 142.7, 131.4, 129.3, 128.5, 28.0 (t, $J = 19.4$ Hz, CHD), 15.3 (t, $J = 19.3$ Hz, CH_2D). MS (GC): 142.0 [M].

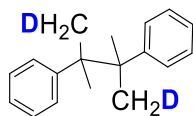


(1-methylethyl-1,2- d_2)benzene ([D]-28a). (38%, *this isolated yield was that low due to the volatility of the product) $^1\text{H-NMR}$ (CDCl_3 , 400 MHz, 300 K) δ , ppm: 7.31-7.27 (m, 2H), 7.24-7.21 (m, 2H), 7.20-7.15 (m, 2H), 1.27-1.23 (m, 2H, CH_2D). $^{13}\text{C}\{^1\text{H}\}$ -NMR (CDCl_3 , 100.6 MHz, 300 K) δ , ppm: 128.64, 126.74, 126.07, 23.93 (t, $J = 19.4$ Hz, CHD). MS (GC): 122.1 [M].

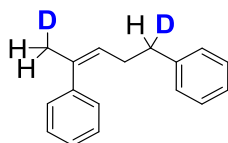


5-phenylhexan-5,6- d_2 -1-ol ([D]-36a). $^1\text{H-NMR}$ (CDCl_3 , 400 MHz, 300 K) δ , ppm: 7.32-7.28 (m, 2H, H_{arom}), 7.21-7.18 (m, 3H, H_{arom}), 3.63-3.59 (m, 2H, O- CH_2), 1.64-1.53 (m, 4H, (CH_2) $_2$), 1.28-1.24 (m, 4H, CH_2D and CH_2).

$^{13}\text{C}\{^1\text{H}\}$ -DEPT-135-NMR (CDCl_3 , 125.8 MHz, 300 K) δ , ppm: 128.30, 126.94, 125.84, 62.94, 38.04, 32.85, 23.84, 22.19, 21.88 (t, $J = 19.2$ Hz, CH_2D).



(2,3-dimethylbutane-2,3-diyl-1,4- d_2)dibenzene ([D]-28b). ^1H -NMR (CDCl_3 , 400 MHz, 300 K) δ , ppm: 7.20-7.18 (m, 6H, H_{arom}), 7.10-7.08 (m, 4H, H_{arom}), 1.33 (s, 10H, $(\text{CH}_3)_2$ and $(\text{CH}_2\text{D})_2$). $^{13}\text{C}\{^1\text{H}\}$ -DEPT-135-NMR (CDCl_3 , 125.8 MHz, 300 K) δ , ppm: 128.59, 126.60, 125.45, 25.13, 24.87 (t, $J = 19.2$ Hz, CH_2D).



(Z)-(pent-3-ene-1,4-diyl-1,5- d_2)dibenzene ([D]-42b). ^1H -NMR (CDCl_3 , 400 MHz, 300 K) δ , ppm: 7.35-7.31 (m, 2H, H_{arom}), 7.30-7.25 (m, 3H, H_{arom}), 7.21-7.19 (m, 2H, H_{arom}), 7.15-7.12 (m, 3H, H_{arom}), 5.53-5.52 (m, 1H, olefin-CH), 2.68-2.63 (m, 1H, CHD), 2.34-2.29 (m, 2H, CH_2), 2.05-2.02 (m, 2H, CH_2D). $^{13}\text{C}\{^1\text{H}\}$ -NMR (CDCl_3 , 100.6 MHz, 300 K) δ , ppm: 146.81, 128.61, 126.61, 125.46, 43.63, 25.18. MS (GC): 238.2 [M].

20. Selected chromatograms for the reduction reactions

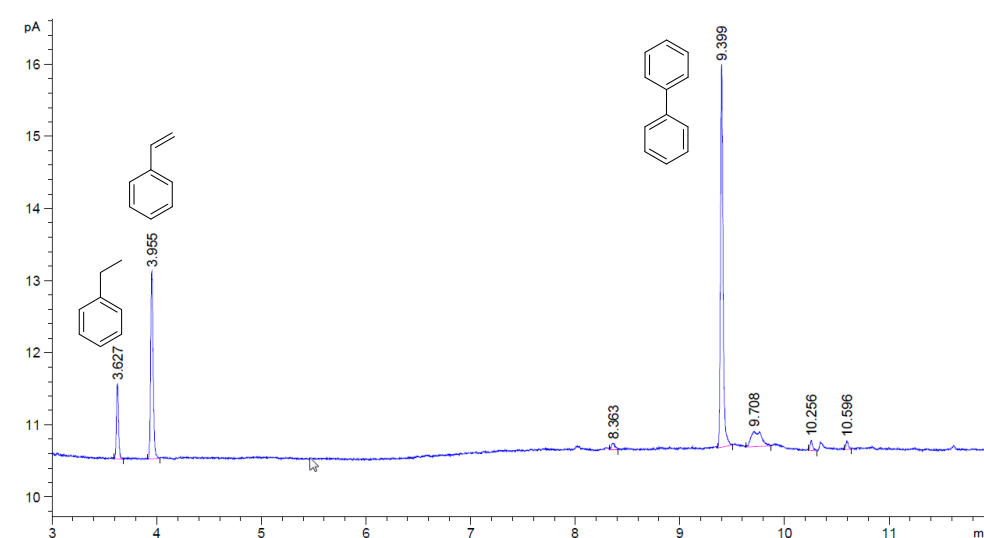


Figure S. 113. GC-FID chromatogram of the reaction mixture when using ^1PCu and **1** as dual catalytic system. Catalytic conditions **A**: **1** (261 μM , 3%), ^1PCu (261 μM , 3% mol), **16** (0.087 mmol, 8.7 mM) in $\text{H}_2\text{O}:\text{CH}_3\text{CN}:\text{Et}_3\text{N}$ (6:4:0.2 mL) irradiation at $\lambda = 447$ nm for 5 h at 15 $^\circ\text{C}$ under N_2 . Yields determined by GC analysis after workup relative to a calibrated internal standard. Values were average of triplicates.

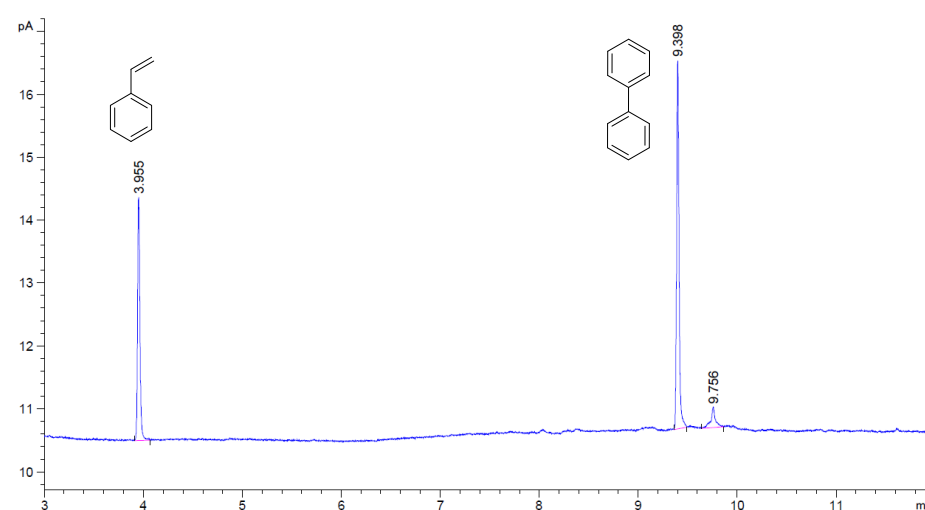


Figure S. 114. GC-FID chromatogram of the reaction mixture when using ^1PCu in the absence of **1**. Catalytic conditions **A**: ^1PCu (261 μM , 3% mol), **16** (0.087 mmol, 8.7 mM) in $\text{H}_2\text{O}:\text{CH}_3\text{CN}:\text{Et}_3\text{N}$ (6:4:0.2 mL) irradiation at $\lambda = 447$ nm for 5 h at 15 $^\circ\text{C}$ under N_2 . Yields determined by GC analysis after workup relative to a calibrated internal standard. Values were average of triplicates.

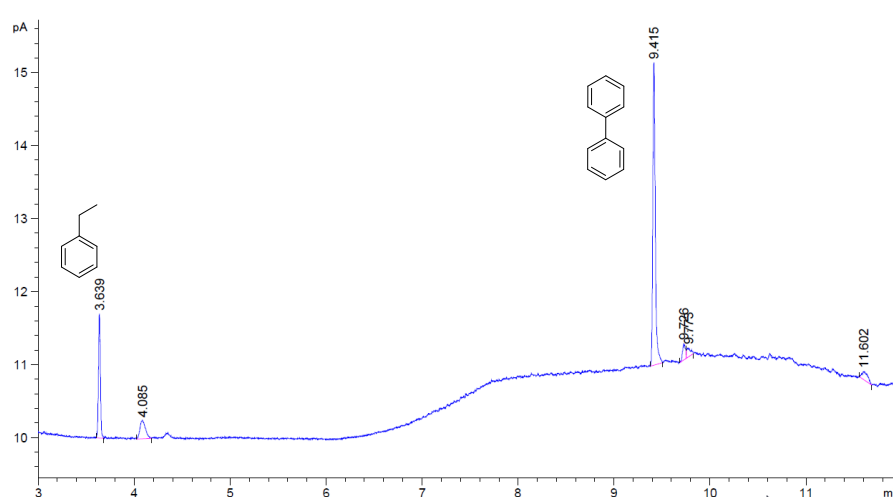


Figure S. 115. GC-FID chromatogram of the reaction mixture when using $^{\text{SO}_3}\text{PCu}$ and **1** as dual catalytic system. Catalytic conditions **A**: **1** (261 μM , 3%), $^{\text{SO}_3}\text{PCu}$ (261 μM , 3% mol), **16** (0.087 mmol, 8.7 mM) in $\text{H}_2\text{O}:\text{CH}_3\text{CN}:\text{Et}_3\text{N}$ (6:4:0.2 mL) irradiation at $\lambda = 447$ nm for 5 h at 15 $^\circ\text{C}$ under N_2 . Yields determined by GC analysis after workup relative to a calibrated internal standard. Values were average of triplicates.

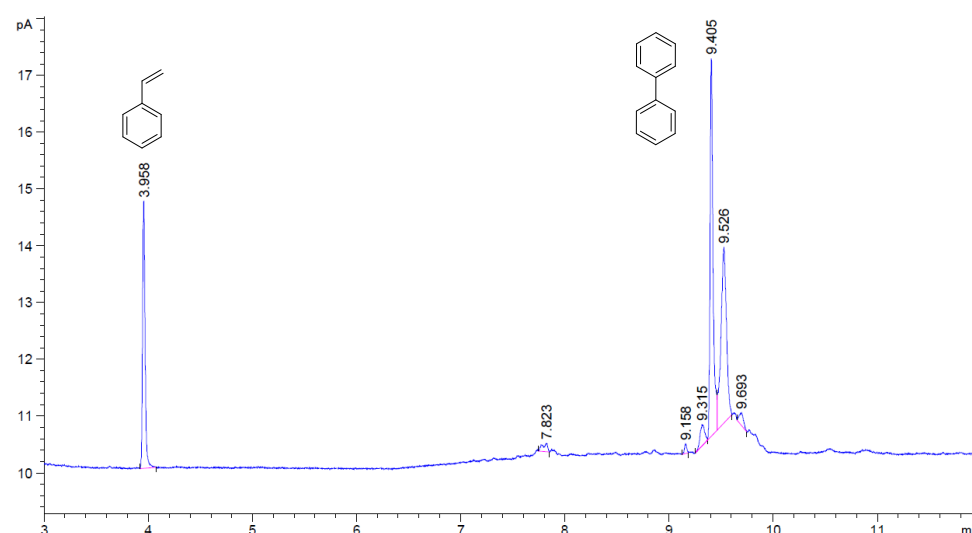


Figure S. 116. GC-FID chromatogram of the reaction mixture when using SO_3PCu in the absence of **1**. Catalytic conditions **A**: SO_3PCu (261 μM , 3% mol), **16** (0.087 mmol, 8.7 mM) in $\text{H}_2\text{O}:\text{CH}_3\text{CN}:\text{Et}_3\text{N}$ (6:4:0.2 mL) irradiation at $\lambda = 447$ nm for 5 h at 15 $^\circ\text{C}$ under N_2 . Yields determined by GC analysis after workup relative to a calibrated internal standard. Values were average of triplicates.

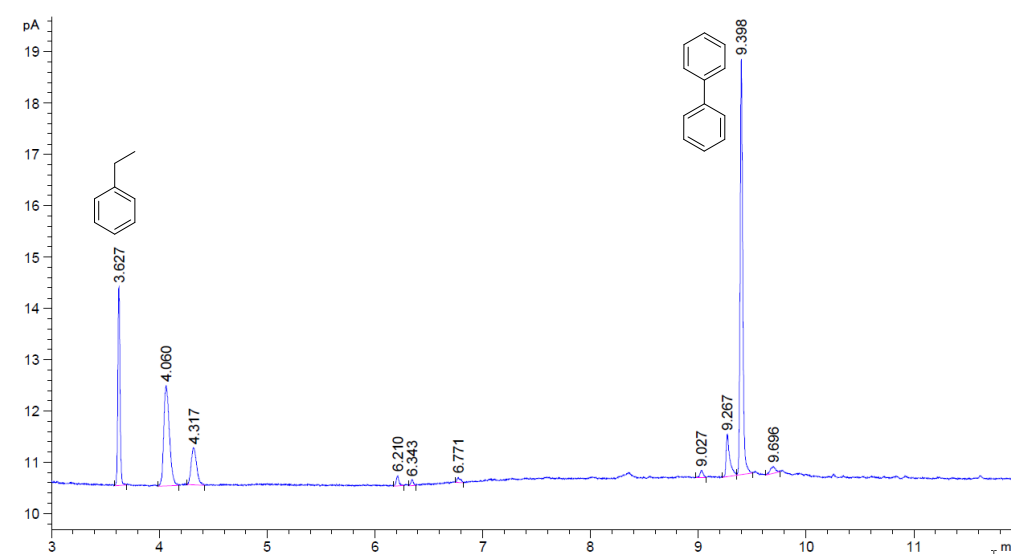


Figure S. 117. GC-FID chromatogram of the reaction mixture when using NMe_2PCIr and **1** as dual catalytic system. Catalytic conditions **A**: **1** (261 μM , 3%), NMe_2PCIr (261 μM , 3% mol), **16** (0.087 mmol, 8.7 mM) in $\text{H}_2\text{O}:\text{CH}_3\text{CN}:\text{Et}_3\text{N}$ (6:4:0.2 mL) irradiation at $\lambda = 447$ nm for 5 h at 15 $^\circ\text{C}$ under N_2 . Yields determined by GC analysis after workup relative to a calibrated internal standard. Values were average of triplicates.

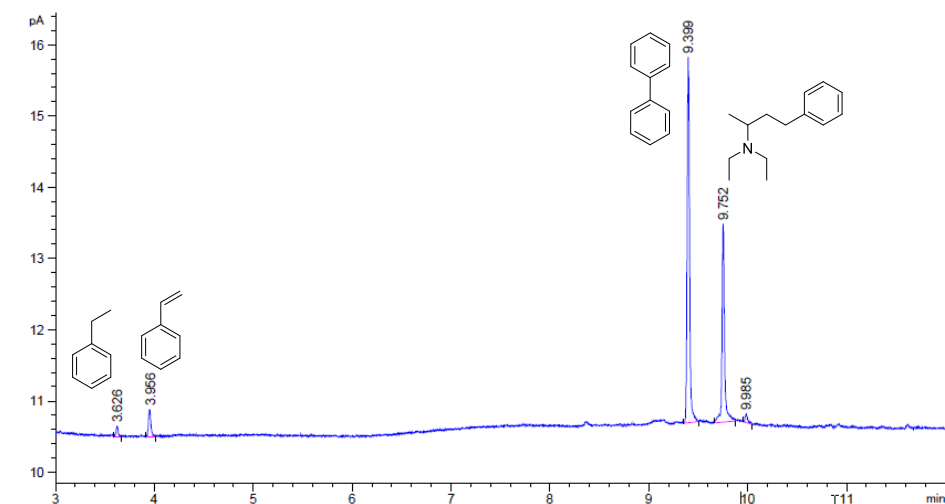


Figure S. 118. GC-FID chromatogram of the reaction mixture when using NMe_2PCIr in the absence of **1**. Catalytic conditions **A**: NMe_2PCIr (261 μM , 3% mol), **16** (0.087 mmol, 8.7 mM) in $\text{H}_2\text{O}:\text{CH}_3\text{CN}:\text{Et}_3\text{N}$ (6:4:0.2 mL) irradiation at $\lambda = 447$ nm for 5 h at 15 $^\circ\text{C}$ under N_2 . Yields determined by GC analysis after workup relative to a calibrated internal standard. Values were average of triplicates.

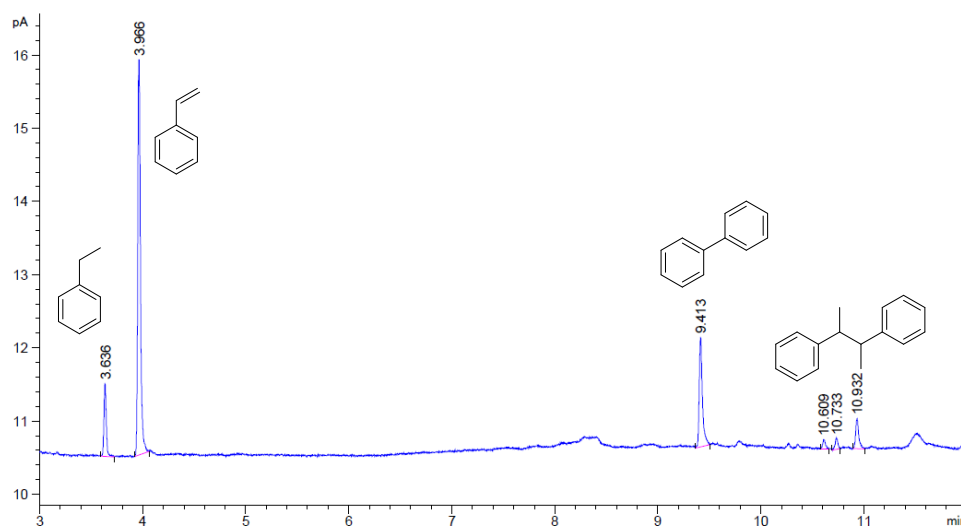


Figure S. 119. GC-FID chromatogram of the reaction mixture when using HPCIr and **1** as dual catalytic system. Catalytic conditions **A**: **1** (261 μM , 3% mol), HPCIr (261 μM , 3% mol), **16** (0.087 mmol, 8.7 mM) in $\text{H}_2\text{O}:\text{CH}_3\text{CN}:\text{Et}_3\text{N}$ (6:4:0.2 mL) irradiation at $\lambda = 447$ nm for 5 h at 15 $^\circ\text{C}$ under N_2 . Yields determined by GC analysis after workup relative to a calibrated internal standard. Values were average of triplicates.

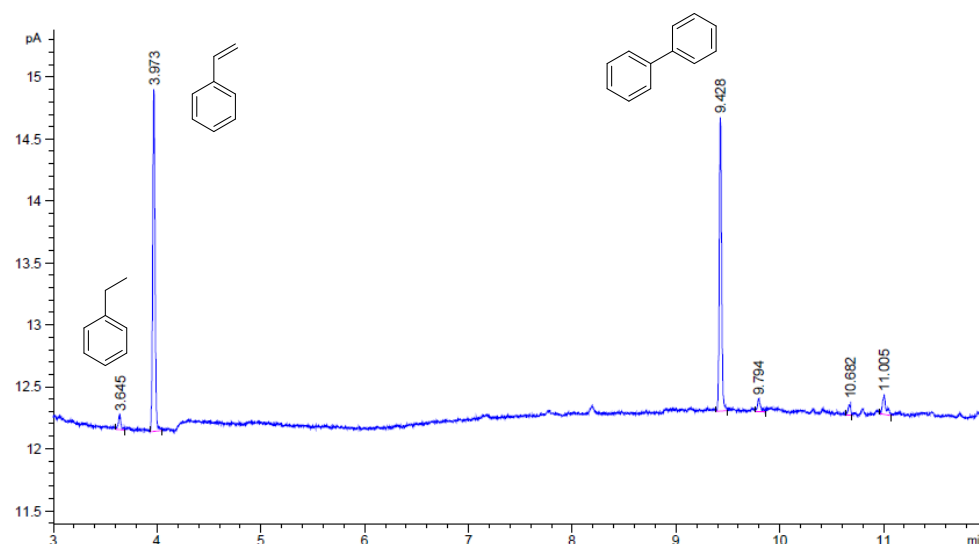


Figure S. 120. GC-FID chromatogram of the reaction mixture when using HPCr in the absence of **1**. Catalytic conditions **A**: HPCr (261 μM , 3% mol), **16** (0.087 mmol, 8.7 mM) in $\text{H}_2\text{O}:\text{CH}_3\text{CN}:\text{Et}_3\text{N}$ (6:4:0.2 mL) irradiation at $\lambda = 447$ nm for 5 h at 15 $^\circ\text{C}$ under N_2 . Yields determined by GC analysis after workup relative to a calibrated internal standard. Values were average of triplicates.

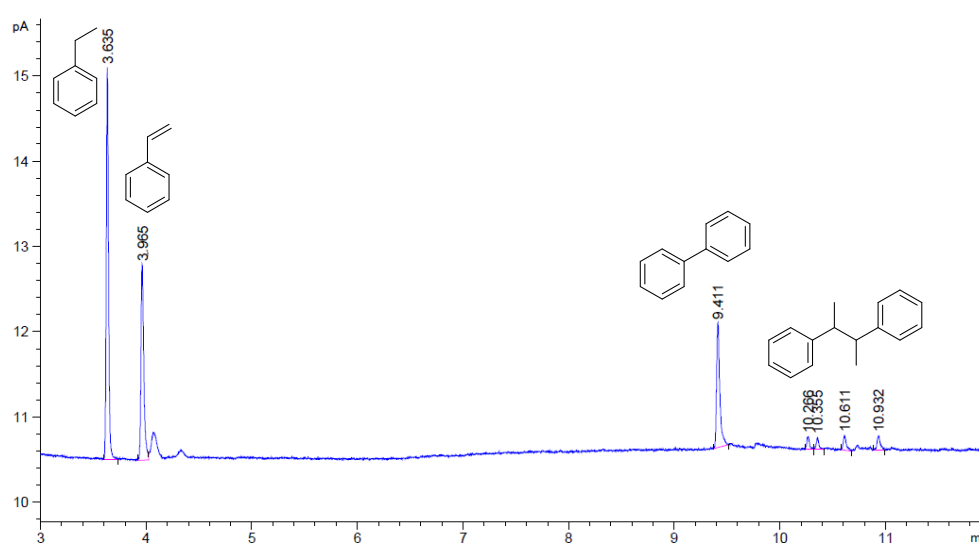


Figure S. 121. GC-FID chromatogram of the reaction mixture when using CO_2HPCr and **1** as dual catalytic system. Catalytic conditions **A**: **1** (261 μM , 3%), CO_2HPCr (261 μM , 3% mol), **16** (0.087 mmol, 8.7 mM) in $\text{H}_2\text{O}:\text{CH}_3\text{CN}:\text{Et}_3\text{N}$ (6:4:0.2 mL) irradiation at $\lambda = 447$ nm for 5 h at 15 $^\circ\text{C}$ under N_2 . Yields determined by GC analysis after workup relative to a calibrated internal standard. Values were average of triplicates.

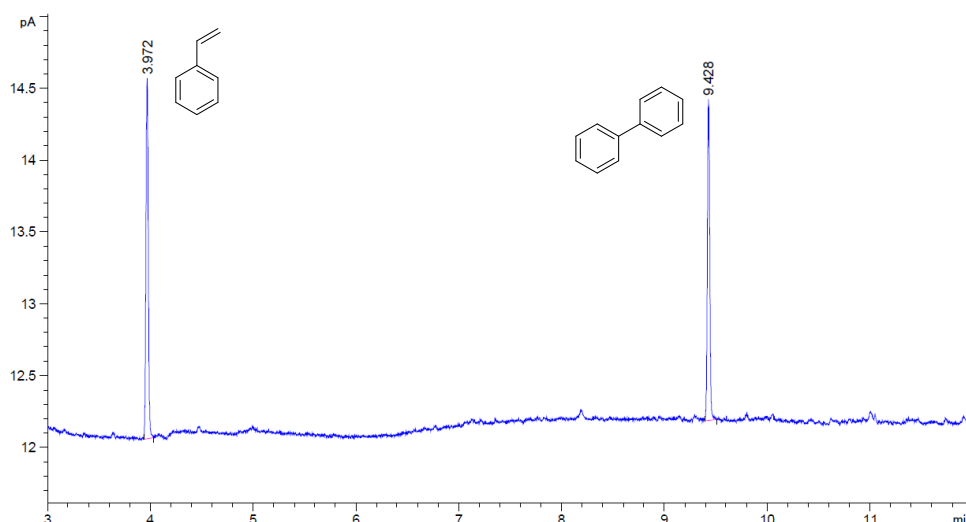


Figure S. 122. GC-FID chromatogram of the reaction mixture when using $\text{CO}_2\text{HPC}_{\text{Ir}}$ in the absence of **1**. Catalytic conditions **A**: $\text{CO}_2\text{HPC}_{\text{Ir}}$ (261 μM , 3% mol), **16** (0.087 mmol, 8.7 mM) in $\text{H}_2\text{O}:\text{CH}_3\text{CN}:\text{Et}_3\text{N}$ (6:4:0.2 mL) irradiation at $\lambda = 447$ nm for 5 h at 15 $^\circ\text{C}$ under N_2 . Yields determined by GC analysis after workup relative to a calibrated internal standard. Values were average of triplicates.

21. References

1. Luo, S. P., *et al.*, Photocatalytic water reduction with copper-based photosensitizers: a noble-metal-free system. *Angew. Chem. Int. Ed.* **2013**, *52* (1), 419-23.
2. Cline, E. D.; Adamson, S. E.; Bernhard, S., Homogeneous Catalytic System for Photoinduced Hydrogen Production Utilizing Iridium and Rhodium Complexes. *Inorg. Chem.* **2008**, *47*, 10378-10388.
3. Call, A.; Codolà, Z.; Acuña-Parés, F.; Lloret-Fillol, J., Photo- and electrocatalytic H_2 production by new first-row transition-metal complexes based on an aminopyridine pentadentate ligand. *Chem. Eur. J.* **2014**, *20* (20), 6171-83.
4. Lee, S. H.; Kim, J. H.; Park, C. B., Coupling Photocatalysis and Redox Biocatalysis Toward Biocatalyzed Artificial Photosynthesis. *Chem. Eur. J.* **2013**, *19*, 4392 – 4406.
5. Roefles, G.; Lubben, M.; Hage, R.; Jr., L. Q.; Feringa, B. L., *Chem. Eur. J.* **2000**, *6*, 2152-2159.
6. Radaram, B.; Ivie, J. A.; Singh, W. M.; Grudzien, R. M.; Reibenspies, J. H.; Webster, C. E.; Zhao, X., Water oxidation by mononuclear ruthenium complexes with TPA-based ligands. *Inorg. Chem.* **2011**, *50* (21), 10564-71.
7. Maity, N. C., *et al.*, Manganese complexes with non-porphyrin N4ligands as recyclable catalyst for the asymmetric epoxidation of olefins. *Catal. Sci. Technol.* **2014**, *4* (1), 208-217.
8. Chen, M. S.; White, M. C., *Science* **2007**, *318*, 783-787.
9. Monos, T. M.; Sun, A. C.; McAtee, R. C.; Devery, J. J., 3rd; Stephenson, C. R., Microwave-Assisted Synthesis of Heteroleptic Ir(III)(+) Polypyridyl Complexes. *J. Org. Chem.* **2016**, *81* (16), 6988-94.
10. Wu, X.; Li, X.; Hems, W.; King, F.; Xiao, J., *Org. Biomol. Chem.* **2004**, *2*, 1818–1821.
11. Lloret-Fillol, J.; Codolà, Z.; Garcia-Bosch, I.; Gómez, L.; Pla, J. J.; Costas, M., Efficient water oxidation catalysts based on readilyavailable iron coordination complexes. *Nat. Chem.* **2011**, *3*, 807 –813.
12. Call, A.; Casadevall, C.; Acuna-Pares, F.; Casitas, A.; Lloret-Fillol, J., Dual cobalt-copper light-driven catalytic reduction of aldehydes and aromatic ketones in aqueous media. *Chemical Science* **2017**, *8* (7), 4739-4749.
13. Call, A., *et al.*, Understanding light-driven H_2 evolution through the electronic tuning of aminopyridine cobalt complexes. *Chemical Science* **2018**, *9* (9), 2609-2619.

14. Lloret-Fillol, J. C., C.; León, J.; Call, A.; Casitas, A.; Pla, J. J.; Hernández, P. J.; Caldentey, X. F. Photoreactor. **2017**.
15. De Angelis, F., *et al.*, Controlling Phosphorescence Color and Quantum Yields in Cationic Iridium Complexes: A Combined Experimental and Theoretical Study. *Inorganic Chemistry* **2007**, *46* (15), 5989-6001.
16. Waern, J. B., *et al.*, Luminescent Cyclometalated RhIII, IrIII, and (DIP)2RuII Complexes with Carboxylated Bipyridyl Ligands: Synthesis, X-ray Molecular Structure, and Photophysical Properties. *Inorganic Chemistry* **2008**, *47* (8), 3340-3348.
17. Goldsmith, J. I.; Hudson, W. R.; Lowry, M. S.; Anderson, T. H.; Bernhard, S., Discovery and High-Throughput Screening of Heteroleptic Iridium Complexes for Photoinduced Hydrogen Production. *Journal of the American Chemical Society* **2005**, *127* (20), 7502-7510.
18. Jones, W. E.; Fox, M. A., Determination of Excited-State Redox Potentials by Phase-Modulated Voltammetry. *The Journal of Physical Chemistry* **1994**, *98* (19), 5095-5099.
19. Larsen, A. F.; Ulven, T., Efficient Synthesis of 4,7-Diamino Substituted 1,10-Phenanthroline-2,9-dicarboxamides. *Organic Letters* **2011**, *13* (13), 3546-3548.
20. Wolf, C.; Tumambac, G. E.; Villalobos, C. N., Acid-Mediated Halogen Exchange in Heterocyclic Arenes: A Highly Effective Iodination Method. *Synlett* **2003**, *2003* (12), 1801-1804.
21. McIntyre, S.; Hörmann, E.; Menges, F.; Smidt, S. P.; Pfaltz, A., Iridium-Catalyzed Enantioselective Hydrogenation of Terminal Alkenes. *Advanced Synthesis & Catalysis* **2005**, *347* (2-3), 282-288.
22. Murai, K.; Matsushita, T.; Nakamura, A.; Fukushima, S.; Shimura, M.; Fujioka, H., Asymmetric Bromolactonization Catalyzed by a C3-Symmetric Chiral Trisimidazoline. *Angew. Chem. Int. Ed.* **2010**, *49*, 9174-9177.
23. Musacchio, A. J.; Nguyen, L. Q.; Beard, G. H.; Knowles, R. R., Catalytic Olefin Hydroamination with Aminium Radical Cations: A Photoredox Method for Direct C–N Bond Formation. *J. Am. Chem. Soc.* **2014**, *136* (35), 12217-12220.
24. Denmark, S. E.; Chi, H. M., Lewis Base Catalyzed, Enantioselective, Intramolecular Sulfenoamination of Olefins. *Journal of the American Chemical Society* **2014**, *136* (25), 8915-8918.
25. Concellón, J. M.; Rodríguez-Solla, H.; Méjica, C.; Blanco, E. G., Stereospecific Cyclopropanation of Highly Substituted C–C Double Bonds Promoted by CrCl₂. Stereoselective Synthesis of Cyclopropanecarboxamides and Cyclopropyl Ketones. *J. Org. Chem.* **2007**, *9*, 2981-2984.
26. Ahneman, D. T.; Doyle, A. G., C-H functionalization of amines with aryl halides by nickel-photoredox catalysis. *Chemical Science* **2016**, *7* (12), 7002-7006.
27. Becke, A. D., *J. Chem. Phys.* **1993**, *98*, 1372-1377.
28. Becke, A. D., *J. Chem. Phys.* **1993**, *98*, 5648.
29. Lee, C. T.; Yang, W. T.; Parr, R. G., *Phys. Rev. B* **1988**, *37*, 785.
30. P. C. Hariharan, J. A. P., *Theoret. Chimica Acta* **1973**, *28*, 213.
31. W. J. Hehre, R. D., J. A. Pople *J. Chem. Phys.* **1972**, *56*, 2257.
32. M. Suensson, S. H., R. D. J. Froese, T. Matsubara, S. Sieber, K. Morokuma, *J. Phys. Chem.* **1996**, *100*, 19357.
33. Schwabe, T.; Grimme, S., *Phys. Chem. Chem. Phys.* **2007**, *9*, 3397-3406.
34. Winget, P.; Cramer, C. J.; Truhlar, D. G., *Theor. Chem. Acc.* **2004**, *112*, 217-227.